A process-based crop growth model for assessing Global Change effects on biomass production and water demand

A component of the integrative Global Change decision support system DANUBIA

Inaugural-Dissertation

zur

Erlangung des Doktorgrades

der Mathematisch-Naturwissenschaftlichen Fakultät

der Universität zu Köln

vorgelegt von

Victoria Ilse Shamim Lenz

aus Kiel

Köln, 2007

Berichterstatter:	Prof. Dr. Karl Schneider
	Prof. Dr. Georg Bareth
Tag der mündlichen Prüfung:	29. Juni 2007

Dedicated to my parents

Abstract

Spatial and temporal changes in crop water demand are of fundamental significance when examining potential impacts of Global Change on water resources on the regional scale. Carried out within the project GLOWA-Danube, this study investigates the response of crops to changing environmental conditions as well as to agricultural management. As a component of the integrative Global Change decision support system DANUBIA, a process-based crop growth model was developed by combining the models GECROS and CERES. The object-oriented, generic model comprises sugar beet, spring barley, maize, winter wheat and potato. The modelled processes are valid for all crops and mainly comprise phenological development, photosynthesis, transpiration, respiration, nitrogen demand, root growth, soil layer-specific water and nitrogen uptake, allocation of carbon and nitrogen as well as leaf area development and senescence. Attention is given to crop-specific differences through assignment to crop categories (e.g. C_4 photosynthesis type) and a set of crop-specific parameters. The model was validated by comparing simulated data with several sets of field measurements, covering a wide range of meteorological and pedological conditions in Germany. Furthermore, the responsiveness of the model to Global Change effects was examined in terms of increased air temperatures and atmospheric carbon dioxide concentrations. The results show that the model efficiently simulates crop development and growth and adequately responds to Global Change effects. The crop growth model is therefore a suitable tool for numerically assessing the consequences of Global Change on biomass production and water demand, taking into account the complex interplay of water, carbon and nitrogen fluxes in agro-ecosystems. Within DANUBIA, the model will contribute to the development of effective strategies for a sustainable management of water resources in the Upper Danube Basin.

Kurzzusammenfassung

Räumliche und zeitliche Veränderungen des Wasserbedarfs von Nutzpflanzen sind von entscheidender Bedeutung, um auf der regionalen Skala die Auswirkungen des Globalen Wandels auf die Wasserverfügbarkeit zu erfassen. Im Rahmen des Projektes GLOWA-Danube untersucht diese Arbeit die Reaktion von Nutzpflanzen auf sich ändernde Umweltbedingungen und Bewirtschaftungsmaßnahmen. Als Teil des integrativen Entscheidungsunterstützungssystems DANUBIA wurde ein Wachstumsmodell für Nutzpflanzen entwickelt, welches die Modelle GECROS und CERES kombiniert. Das objekt-orientierte, generische Modell ist für Zuckerrüben, Sommergerste, Mais, Winterweizen und Kartoffeln anwendbar. Die modellierten Prozesse gelten für alle Nutzpflanzen und sind im Wesentlichen: phänologische Entwicklung, Photosynthese, Transpiration, Respiration, Stickstoffbedarf, Wurzelwachstum, bodenschichtspezifische Wasser- und Stickstoffaufnahme, Allokation von Kohlen- und Stickstoff sowie Blattflächenentwicklung und Seneszenz. Die Differenzierung in die einzelnen Nutzpflanzen wird durch die Zuweisung einer Kategorie wie z.B. C_4-Pflanzen und durch eine Anzahl nutzpflanzenspezifischer Parameter erreicht. Für die Validierung des Modells wurden simulierte Daten mit Reihen von Feldmessungen verglichen. Diese Messungen repräsentieren ein breites Spektrum an meteorologischen und pedologischen Bedingungen in Deutschland. Zudem wurde die Reaktivität des Modells auf Effekte des Globalen Wandels untersucht. Diese Analyse wurde mittels erhöhter Lufttemperaturen und atmosphärischer Kohlendioxidkonzentrationen durchgeführt. Die Ergebnisse zeigen die Fähigkeit des Modells, Entwicklung und Wachstum der Nutzpflanzen abzubilden und treffend auf Effekte des Globalen Wandels zu reagieren. Daher stellt das Pflanzenwachstumsmodell ein geeignetes Instrument dar, die Auswirkungen des Globalen Wandels auf die Biomasseproduktion und den Wasserbedarf von Nutzpflanzen numerisch zu erfassen. Die Modellierung berücksichtigt das vielschichtige Wirkungsgefüge zwischen Wasser-, Kohlenstoff- und Stickstoffflüssen in Agrarökosystemen. Als Teil von DANUBIA wird das Modell dazu beitragen, wirkungsvolle Strategien für einen nachhaltigen Umgang mit den Wasserressourcen im Oberen Donaueinzugsgebiet zu entwickeln.

Acknowledgements

The present thesis was prepared during the second phase of the project GLOWA-Danube, funded by the German Federal Ministry of Education and Research. I gratefully acknowledge this financial support.

The thesis was supervised by Prof. Dr. Karl Schneider, to whom I wish to express my gratitude not only for introducing me to a fascinating field of research, but also for his guidance throughout and for invaluable directives and suggestions for improving this work.

I also sincerely thank Prof. Dr. Georg Bareth for consenting to act as second examiner.

I warmly thank my colleagues Christian Klar, Peter Neuhaus, Marius Schmidt and Hanno Wendt for the excellent teamwork in a stimulating atmosphere. I greatly appreciated their competence and their fruitful ideas, likewise their ever-undaunted optimism.

Thanks are also due to Dahlia Strecker and Christian Koyama for their assistance during the field campaigns. A very special thank-you to Christian Koyama for his reliable laboratory analyses. I am also indebted to farm proprietors Müllenbach, Schulte-Eickhoff and Trimborn for their kindness in allowing me to carry out measurements on their fields.

I am grateful to all colleagues within the GLOWA-Danube project for their friendly collaboration.

My thanks also go to my friend Doris for comforting exchanges over thesis-writing and her readiness to help me whenever needed.

I specially thank my friend Guido for the sympathy with which he encouraged my work and for never failing to brighten my spirits.

My wholehearted thanks to my parents not only for their constant loving care of me but also for the assurance of their staunch support at all times.

Table of contents

List of figures

List of tables

List of abbreviations

ATP	adenosine triphosphate
BBCH	Biologische Bundesanstalt, Bundessortenamt and Chemical Industry
BMBF	Bundesministerium für Bildung und Forschung
CERES	Crop Environment Resource Synthesis
DSSAT	Decision Support System for Agrotechnology Transfer
FACE	free-air CO_2 enrichment
GECROS	Genotype-by-Environment interaction on crop growth Simulator
GIS	Geographic Information Systems
GLOWA	Globaler Wandel des Wasserkreislaufes
HASL	height above mean sea level
IA	index of agreement
IPCC	Intergovernmental Panel on Climate Change
LAI	leaf area index
LED	light-emitting diode
MAE	mean absolute error
MEF	modelling efficiency index
NADP	nicotinamide adenine dinucleotide phosphate
NADP+	oxidized form of NADPH
NADPH	reduced form of NADP+
NIR	near infrared radiation
PAR	photosynthetically active radiation
PEP	phosphoenolpyruvate
PROMET-V	Process Oriented Modular Environment and Vegetation model
PS I (II)	photosystem I (II)
RMSE	root mean squared error
RRMSE	relative root mean squared error
Rubisco	Ribulose-1,5-biphosphate carboxylase-oxygenase
RuBP	Ribulose-1,5-biphosphate
TM	Thematic Mapper
UML	Unified Modeling Language
UNEP	United Nations Environment Programme
WMO	World Meteorological Organisation

1 Introduction

1.1 Background

Crop production is highly sensitive to meteorological and environmental conditions and is affected by Climate Change in manifold ways. Plants function as an interface for the exchange of water and carbon between atmosphere and terrestrial biosphere. Since stomatal control of water vapour and carbon dioxide fluxes governs the processes of transpiration and photosynthesis, vegetation plays a vital role in the water cycle. Here crops occupy a special position because, being selected and sown by farmers, water budgets in agricultural regions are controllable through crop management options.

Development and growth of crops are influenced both directly by increased carbon dioxide concentration in the atmosphere as well as indirectly by associated climate changes caused by the enhanced greenhouse effect, such as increased temperature.

The *Intergovernmental Panel on Climate Change* (IPCC), founded by the *World Meteorological Organisation* (WMO) and the *United Nations Environment Programme* (UNEP), has published a comprehensive synopsis of the latest findings in Global Climate Change research. The Fourth Assessment Report *Climate Change 2007* (IPCC 2007) states that "*Warming of the climate system is unequivocal, as is now evident from observations of increases in global average air and ocean temperatures, widespread melting of snow and ice, and rising global average sea level*".

According to the record of global surface temperatures documented since 1850, the last twelve years from 1995 to 2006 have with one exception been the twelve warmest. Observations over the last hundred years have revealed that the linear trend of rising global temperatures has almost doubled its rate in the past half-century (0.13 °C per decade). This steeper gradient over the last five decades is very likely (>90 % probability of occurrence) caused by the mounting concentrations of anthropogenic greenhouse gases. Of these gases carbon dioxide is pre-eminent, its global atmospheric concentration reaching 379 ppm in 2005. This value marks the highest ever concentration reached in the last 650 000 years and represents a 35 percent increase over the pre-industrial value (approx. 280 ppm). Chiefly responsible for this steady increase are fossil fuel emissions. (IPCC 2007)

Even at present-day levels, a global warming of approx. 0.2 °C in the next 20 years is expected from irreversible long-term effects on the climate system. The frequency of extreme weather phenomena such as heavy precipitation and heat waves, as well as unprecedented heat records will further rise during the 21st century. (IPCC 2007)

To mitigate the adverse effects of these projected changes, effective strategies for an adaptive resource management are required. Climate Change affects nature and the life of human beings in both local and global contexts in multiple ways. The broad domain of Global Change Research comprises examination of human impact on the environment, investigation into the effects on mutually dependent processes in the biosphere, implications for socio-economic structures, adaptation strategies as well as prediction of changes to come.

One of the foremost challenges for this interdisciplinary field of research is the management of water resources to secure sustainable water availability. The global water cycle is influenced by both nature and society and exhibits complex feedback mechanisms.

In 2000, the *German Federal Ministry of Education and Research* (*Bundesministerium für Bildung und Forschung*, BMBF) launched the research programme GLOWA* (*Globaler Wandel des Wasserkreislaufes*): "Global Change of the Hydrological Cycle - an example of integrative interdisciplinary and application-oriented Global Change Research". It is the objective of the GLOWA programme with its worldwide perspectives to develop strategies for a sustainable management of water resources on the regional scale, taking into account global environmental changes as well as socio-economic factors. In order to fulfil the complex claims of an interdisciplinary approach, new methods and techniques are developed and tested.

Cooperation between diverse natural and social sciences in cross-boundary integrative research implies linking numerous and divergent spatial and temporal scales. Involving stakeholders from politics, industry and society ensures that applicable tools are devised for supporting decisions in the interest of sustainable water management. (RIELAND 2004)

The GLOWA programme is a pilot project with this conceptual background and comprises several case studies carried out in river basins covering approx. 100 000 km² each (Africa: Drâa, Ouémé, Volta; Asia: Jordan; Europe: Elbe, Danube).

* www.glowa.org

The present study is embedded in the project GLOWA-Danube: "Integrative Techniques, Scenarios and Strategies for the Future of Water in the Upper Danube Basin", coordinated by Prof. Dr. Wolfram Mauser, *Department of Earth and Environmental Sciences, University of Munich.* The project is planned for nine years from 2001 to 2010. The work presented here was carried out in the second project phase (2004 to 2007).

A team of experts from diverse disciplines are collaborating with water resources stakeholders to develop integrative strategies and tools to secure a sustainable water use in the catchment area of the Upper Danube. The test site represents a typical mountain-foreland region in temperate mid-latitudes and covers approx. 77 000 km². The participating scientists are experts in the fields of geography, meteorology, hydrology, glaciology, plant ecology, remote sensing, water resources engineering, environmental economics, agricultural economics, environmental psychology, tourism research and computer science.

It is the central objective of GLOWA-Danube to identify, analyse and develop innovative techniques for coupled and spatially explicit modelling so as to integrate expert knowledge from the numerous disciplines involved. These new techniques are realized in the decision support system DANUBIA. Interaction between the coupled models embraces all important environmental and socio-economic processes for simulating water fluxes in the Upper Danube Basin as well as in other mountain-foreland regions. (MAUSER & LUDWIG 2002, LUDWIG *et al.* 2003)

The modelling platform DANUBIA is based on object-oriented software engineering with Java as implementation language. One of the advantages of object-oriented model design is the explicit and restricted data exchange. To standardize the construction and documentation of each model singly as well as in its interactions with other models, the Unified Modeling Language (UML) (BOOCH *et al.* 1999) serves as a common tool.

The agreement on a uniform set of tools, the integration of the disciplinary expertises via clearly defined interfaces and the development of interdisciplinary methods for considering and analyzing the interactions between the involved models characterize the innovative approach of DANUBIA. The integration of more than a dozen models in DANUBIA allows for the interaction of a multitude of processes on different spatial and temporal scales, taking into account the latest scientific and methodological advances in the disciplines involved.

1.2 Objectives of the study

In view of the vast area covered by crops, agro-ecosystems are of fundamental significance when examining Global Change effects on the water cycle.

This study investigates the response of crops to Climate Change as well as to agricultural management. The reaction of various crops to environmental factors and cultivation practices is examined in terms of biomass production and water demand. Through quantifying the amount of water transpired, it is sought to find out how crops influence water fluxes at the landsurface.

The only method for comprehensively assessing the effects of Global Change on crops is the utilization of process-based crop growth models. These simulation models allow extrapolation to the future by modelling crop growth as a function of crop physiological responses to altered meteorological conditions and management decisions. By considering site-specific influencing factors, the model can be used to predict spatially explicit patterns of Global Change effects.

With the chief aim in mind of investigating the sensitivity of crops to Climate Change as well as to agricultural management, it was necessary to take the following steps. The research presented in this thesis therefore comprises:

- the choice of adequate modelling approaches for the crop growth model
- model development
- model validation
- the analysis of its responsiveness to Global Change effects

In the following two sub-chapters an outline of the modelling approaches and an overview of the state-of-the-art in terms of crop growth modelling are given.

Chapter 2 describes the crop growth model including model design, algorithms as well as selection and derivation of crop-specific parameters. The validation analysis for various crops, carried out by comparing field measurements with model results, is presented in chapter 3. Additionally, the responsiveness of the model to Global Change effects is examined on the field scale and is exemplarily illustrated on the regional scale. In chapter 4, the efficiency of the model in simulating crop growth under varying environmental conditions and with different farming practices is discussed. The conclusions of the study are presented in chapter 5. Future challenges are outlined in chapter 6.

1.3 Modelling approach

The choice of modelling approach results from the requirements which the crop growth model has to fulfil. To define these requirements, the function and the relevance of crops within the water cycle are first illustrated.

Plants are dependent on water supply and influence the water balance in manifold ways on all temporal and spatial scales. Part of the precipitation is intercepted by plants, thereby decreasing the amount of water for infiltration. A dense vegetation cover diminishes surface and subsurface runoff as well as evaporation. Via water uptake and transpiration, vegetation transports water from the soil to the atmosphere (Fig. 1). Transpiration is an essential component of the water balance, representing about 43 % of the total precipitation and nearly 70 % of the total evaporated water in Germany (BAUMGARTNER & LIEBSCHER 1996).

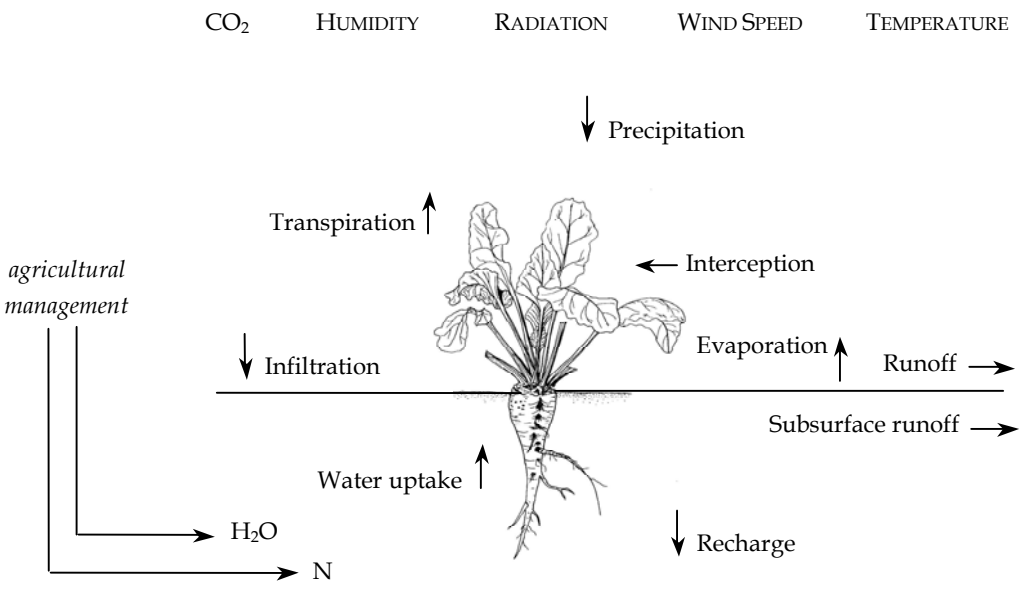

Fig. 1: Schematic presentation of the hydrological processes (small arrows), abiotic factors (small capitals) and management in an agro-ecosystem (plant drawing taken from KÖRBER-GROHNE 1987).

For a thorough understanding of the feedback processes between vegetation and water, links between hydrological, biogeochemical, and ecological processes must be considered in an ecohydrological approach (NEWMAN *et al.* 2006). The cycles of water, carbon and nitrogen as well as energy fluxes in the soil-plant-atmosphere system are most intricately entwined. This multifaceted interaction is further complicated in agro-ecosystems through the interference of human activity. Tillage, irrigation and fertilizer application manipulate site-specific factors like soil water and nutrient availability to

improve plant growth. Economic interests prescribing the use of fertilizers and pesticides to ensure profitability are in conflict with farming practices fostering conservation of resources. Adaptive management strategies provide an instrument for promoting the sustainable use of water resources under Global Change conditions.

Farmers are key stakeholders in terms of water resources management. The choice of crop and the specific management procedures involved have profound and large-scale ecohydrological impacts.

Agricultural land use is strongly influenced by abiotic factors (e.g. water availability), all of these being sensitive to climate change, as well as by immediate economic interests and higher-level decisions by policy-makers. One such decision was the European Union´s sugar market reform, which came into force in 2006 and will directly affect the extent of the area under sugar beet cultivation and consequently the spatial and temporal patterns of water demand. Another example is the increasing cultivation of crops for renewable energy production.

Assessing the effects of Climate Change and management options (including the choice of crop) on the ecohydrological processes in a landscape is enabled by utilizing complex simulation models like the decision support system DANUBIA which allows for the application of alternative scenarios associated with Global Change. Analyzing the results enables the development of strategies to secure future water resources.

Examples of the manifold questions for the definition as well as the analysis of these scenarios are: Which crops are least vulnerable to climate change and which suffer most from scarcity of water? Which crops will yield poorer harvests? Will C_4 crops like maize prosper at the expense of C_3 crops under climate change conditions? How will exotic plants such as *Miscanthus giganteus* (a fast-growing, perennial C_4 grass) grown for biofuel production alter water, carbon and nitrogen fluxes in agro-ecosystems?

To find answers to questions of this kind using the Global Change decision support system DANUBIA, a crop growth model is needed which is responsive to Climate Change and managerial options, taking into account the dynamic interplay of water, carbon and nitrogen fluxes in agro-ecosystems.

Key requirements of this crop growth model are defined by both scientific demands and technical guidelines.

Integrative requirements, arising from the interaction of the different disciplines within the GLOWA-Danube project, are:

- Sensitivity to Global Change and transferability to other regions
- Dynamic interaction between crop-water-nitrogen and agricultural management

Disciplinary requirements, arising from the task of modelling crop growth in the context of Global Change research, are:

- Coupling and interaction of photosynthesis and transpiration
- Consideration of hourly micrometeorological drivers for simulating the relevant fluxes of energy, water und carbon dioxide
- Incorporation of the most relevant crops and extensibility in terms of additional crops

Methodological requirements are:

- Provision of modelled data for export to other DANUBIA models during run-time
- Technical compliance with interfaces in DANUBIA
- Object-oriented design using the programming language Java

The described criteria and the application in the Global Change context require a process-based modelling approach for the DANUBIA crop growth model. In contrast to an empirical approach which derives model equations from observed data, a process-based approach considers the underlying biological, chemical, physical and physiological processes governing plant growth and development. This methodology enables extrapolation to future years as well as spatial transferability since there is potentially no need for site-specific calibration. As early as 1981, J.L. Monteith in his annual presidential speak to the *Royal Meteorological Society* declared: "*The statistical blunderbuss is a very clumsy weapon for attacking the problem of crop-weather relations; but it is also very uninstructive because it ignores the interaction of physical and physiological mechanisms*" (cited by JAME & CUTFORTH 1996).

One of the main processes of plant growth is photosynthesis. To capture the effect of increased atmospheric carbon dioxide concentration and air temperature, photosynthesis modelling needs to be based on a biochemical approach (FARQUHAR *et al.* 1980). Here temperature effects at the leaf level and temperature response functions for biochemical parameters are taken into consideration. The modelled processes of photosynthesis and transpiration are linked via stomatal control. The dynamic interaction between crops, water and nitrogen is ensured by various feedback mechanisms.

Processes of transpiration, photosynthesis, water and nitrogen uptake are modelled in hourly time-steps based on hourly input data so as to capture the highly non-linear response of these processes to fluctuations in environmental conditions. Using daily input data, short-time effects of environmental factors (e.g. high air temperature or low soil moisture) on plant growth may be ignored.

The DANUBIA crop growth model includes the process-based growth simulation of winter wheat, spring barley, maize (including grain and silage maize), sugar beet and potato. To enable other crops to be integrated without difficulty, a generic model design is imperative. The simulated processes of plant development and growth are valid for all crops. Attention is given to crop-specific differences through assignment to crop categories (e.g. C_4 plant, winter crop or long-day plant) and a set of crop-specific parameters.

To simulate water and nitrogen uptake, influenced by root length density, and to assure consistency with the concept of modelling soil nitrogen transformation by the DANUBIA soil model, root length density in different soil layers is simulated.

The mentioned modelling concepts are realized in the DANUBIA crop growth model by combining the models GECROS (YIN & VAN LAAR 2005) and CERES (JONES & KINIRY, eds, 1986, RITCHIE & GODWIN 2000).

GECROS (**G**enotype-by-**E**nvironment interaction on **cro**p growth **S**imulator) is the most recent of the Wageningen crop growth models. It is a generic model and incorporates the current knowledge of interacting ecophysiological processes. CERES (**C**rop **E**nvironment **Re**source **S**ynthesis) comprises well established, widely used and extensively validated models for different crops.

The choice of this hybrid modelling approach combines the advantages of the GECROS and CERES models in an ideal manner.

1.4 State-of-the-art

The first crop growth models date from as early as the mid-1960s (SINCLAIR & SELIGMAN 1996). These authors define crop modelling as "*the simulation of crop growth by numerical integration of constituent processes with the aid of computers*" and call it a "*technology used to construct a relatively transparent surrogate (or substitute) for a real crop,*

one that can be analyzed and manipulated with far greater ease than the complex and cumbersome original".

In the last 40 years, the evolution of crop models has been supported by scientific progress in many different research fields, advances in computer technology as well as further development of measurement techniques and devices for use in laboratory and in field. Increasing concern about the sustainable management of environmental resources and Global Change effects on crop production and agro-ecosystems has triggered the development of sophisticated crop models. Empirically based models are being gradually replaced by process-based models of varying degrees of complexity.

Applications of crop models span a wide range, e.g. prediction (especially yield forecasting), determination of optimal management strategies, suitability for use on large spatial scales, characterization of plant varieties or use as educational tools (JONES *et al.* 2006). Today, a multitude of crop growth models exists. Each is characterized by a combination of diverse scientific as well as technical features. These concern the intended application and target group, the spatial as well as temporal scale, the crops considered, the simulated processes accounted for, the modelling approaches employed, the degree of validation, the input data required, the validity of parameters used, the coupling to other sub-models, the embedding in a modelling framework, the availability of scientific and technical documentation, the accessibility of source code, the choice of programming language, software design etc..

Numerous publications about models for one specific crop are found in the literature (e.g. GAYLER *et al.* 2002, QI *et al.* 2005, YANG *et al.* 2004). Additionally, a plethora of studies exist focussing on a single aspect (e.g. GASTAL & LEMAIRE 2002, JAME & CUTFORTH 2004) or on one modelled process (e.g. FLEISHER *et al.* 2006, MIRSCHEL *et al.* 2005, THORNLEY & CANNELL 2000, WU *et al.* 1999).

The DSSAT (**D**ecision **S**upport **S**ystem for **A**grotechnology **T**ransfer) cropping system model (HOOGENBOOM *et al.* 2003) includes models of 17 different crops, among these the CERES-Maize, -Wheat and -Barley models (JONES & KINIRY, eds, 1986, RITCHIE & GODWIN 2000). DSSAT is based on a modular structure, incorporating all crops as modules as well as providing databases and several support software components for use with the crop models. Over the last 20 years, the DSSAT suite of models have been widely validated and used (JONES *et al.* 2003).

Examples for other models embracing a set of crops are: AGROSIM (**Agro**-ecosystem **Sim**ulation, WENKEL & MIRSCHEL, eds, 1995), APSIM (**A**gricultural **P**roduction **S**ystems S**im**ulator, KEATING *et al.* 2003), CropSyst (STÖCKLE *et al.* 2003) and STICS (**S**imulateur mul**TI**disciplinaire pour les **C**ultures **S**tandard, BRISSON *et al.* 2003) as well as LINTUL (**L**ight **Int**erception and **U**tili**z**ation Simulator) and SUCROS (**S**imple and **U**niversal **Cro**p Growth **S**imulator), both developed by the Wageningen modelling group (e.g. VAN ITTERSUM *et al.* 2003). These are all generic crop models.

Linking crop growth models with Geographic Information Systems (GIS) permits their application on regional or even global scales. Examples for regional applications of models considering various crops as well as crop-soil-water interactions are e.g. PROMET-V (**Pr**ocess **O**riented **M**odular **E**nvironmen**t** and **V**egetation model, SCHNEIDER 1999, 2003) and SWIM (**S**oil and **W**ater **I**ntegrated **M**odel, KRYSANOVA *et al.* 1998, 2000). Some of the models coupled to GIS allow the use of remote sensing data not only for the validation of model results but for the adjustment of parameters during run-time (e.g. JONGSCHAAP 2006, LAUNAY & GUERIF 2005, SCHNEIDER 1999, 2003). An overview of crop growth simulation using remote sensing data and GIS is given by DADHWAL (2004). The increasing availability of input data, derived from meteorological measurements or models, or land use classifications by remote sensing data, soil maps, digital elevation models, etc. will further improve the applicability of crop models on large scales.

None of the so far mentioned models is suitable for comprehensively assessing Global Change effects, the reason being the lack of a biochemically based modelling approach for photosynthesis. If the direct effect of atmospheric carbon dioxide is at all accounted for in these models, simple approaches are used. Exceptions are specific versions of the LINTUL and SUCROS models (VAN ITTERSUM *et al.* 2003). Regardless of this deficiency, manifold studies on the impact of Global Change on biomass production have been published (e.g. ALEXANDROV *et al.* 2002, KRYSANOVA *et al.* 2007, OLESEN *et al.* 2000, WESSOLEK & ASSENG 2006, WOLF 2002).

Models for gas exchange based on the biochemical approach by FARQUHAR *et al.* (1980) are published e.g. by FRIEND (1995) and HUMPHRIES & LONG (1995). This biochemical approach is widely employed in studies of natural ecosystems, presented e.g. by FALGE (1997), FRIEND *et al.* (1997), GARCIA-QUIJANO & BARROS (2005), LUCHT *et al.* (2006), REICHSTEIN (2001) and WHITE *et al.* (1999). WANG *et al.* (2005) modified the BIOME-BGC

(**B**io**G**eochemical **C**ycles, e.g. WHITE *et al.* 2000) model to account for winter wheat and maize crops, presenting a study for the North China Plain.

However, to the knowledge of the author, only two models considering several crops include the biochemical approach of modelling photosynthesis: *ecosys* (GRANT 2001) and GECROS (YIN & VAN LAAR 2005). Both use the "functional balance" theory (BROUWER 1962) for the allocation of carbon and nitrogen, which is also one prerequisite for comprehensively simulating the effects of Global Change. None of the other above mentioned crop growth models simulates partitioning of carbon and nitrogen dynamically and interrelatedly.

MATTHEWS & STEPHENS (2002) identify two focal points towards which crop modelling research is at present directed: applicability to large spatial scales (whole farm, catchment or region) and incorporation of genotypes. Crop models should include genotype-specific parameters for incorporating the latest findings offered by the rapid advances in functional genomics (YIN *et al.* 2004a). The model GECROS (YIN & VAN LAAR 2005) satisfies this requirement by giving due regard to various genotype-specific parameters. In view of the numerous models available and their abilities, crop models are found to be rarely used for decision support (STEPHENS & MIDDLETON 2002). HOOGENBOOM (2000) points to the need for improving crop models to this end.

In the last few years, object-oriented software design for crop models is becoming increasingly popular. Adopting the object-oriented paradigm facilitates code modification and reusability (PAPAJORGJI *et al.* 2004). One example for an object-oriented crop model is CropSyst (STÖCKLE *et al.* 2003).

The incorporation of the generic model GECROS, which is based on sound physiological principles, into the DANUBIA crop growth model ensures that current knowledge of individual physiological processes as well as their interactions and feedback mechanisms are considered. The object-oriented DANUBIA crop growth model not only achieves state-of-the-art standards in terms of both scientific and technical criteria, but is also applicable on the regional scale as part of a Global Change decision support system.

2 Description of the crop growth model

In the following chapter the process-based and object-oriented DANUBIA crop growth model, developed in this study, will be documented. The model builds on the strength of existing models by combining GECROS (YIN & VAN LAAR 2005) and CERES (JONES & KINIRY, eds, 1986, RITCHIE & GODWIN 2000). The generic model comprises the simulation of sugar beet (*Beta vulgaris* L.), spring barley (*Hordeum vulgare* L.), maize (*Zea mays* L.), winter wheat (*Triticum aestivum* L.) and potato (*Solanum tuberosum* L.).

First of all, the technical structure and software implementation of the modelling framework and the crop model itself is presented. Whereas GECROS is implemented in the FORTRAN Simulation Translator (VAN KRAALINGEN *et al.* 2003) and CERES in the FORTRAN computer language, the object-oriented DANUBIA crop growth model is implemented in Java.

Secondly, the simulated processes of crop development and growth are described in detail, providing the model algorithms. Following a specification of the required input data, the various crop-specific parameters are dealt with in the last sub-chapter.

2.1 Structure and software implementation

The DANUBIA crop growth model is one of many models integrated in the simulation and decision support system DANUBIA. Following an overview of the DANUBIA modelling framework, the design of the DANUBIA crop growth model is presented.

2.1.1 Modelling framework

Within the project GLOWA-Danube, the integrative simulation and decision support system DANUBIA was developed by the *Computer Science* group at the *Ludwig-Maximilians-University* in Munich. In the present study, only a brief overview of the modelling framework is presented. A comprehensive and detailed presentation of DANUBIA is given by LUDWIG (2007).

According to BARTH *et al.* (2004), the objectives of DANUBIA are

- to perform and supervise integrative simulations,

- to examine cross-disciplinary effects of interactive processes,
- to support decision-making for sustainable management of water resources.

The development of the network-based modelling platform DANUBIA is based on object-oriented software engineering with Java as implementation language (BARTH *et al.* 2004).

At present DANUBIA couples 16 simulation models, each representing the expertise of the various disciplines collaborating in the project GLOWA-Danube. These single models are dynamically coupled and mutually exchange information during an integrative simulation run. This exchange of data between the models is realized via defined interfaces. Each model serves as a provider (export of data) as well as a client (import of data) of information (BARTH *et al.* 2004).

Within DANUBIA, the individual simulation models are grouped into five key components according to their function. Whereas e.g. the component *Actor* comprises socio-economic models, the component *Landsurface* includes the models for the simulation of the energy, water and matter fluxes at the landsurface. Fig. 2 shows the interrelations between these five major DANUBIA components, illustrated using the Unified Modeling Language (UML) (BOOCH *et al.* 1999). This UML diagram shows only the interfaces between the key components, ignoring the interfaces between the single models within a component. The data exchange between these five components is handled by component controllers (BARTH *et al.* 2004).

The *Landsurface* component is presented in more detail in the UML diagram, showing the included single process-based models (subcomponents). The model *Soil* simulates water and nitrate fluxes, heat transfer and nitrogen transformation processes in the rooted soil zone. Energy and water fluxes at the landsurface are simulated by the model *Surface,* while processes of snow accumulation and melting are quantified by the model *Snow*. The radiation balance and the radiation distribution in vegetation canopies are computed by *Radiation Balance*. The subcomponent *Biological* simulates the water, carbon and nitrogen fluxes within the vegetation as well as the energy balance at the leaf level. To duly account for the differences between modelling natural and agricultural ecosystems, this subcomponent is further split in *Natural Ecosystems* and *Agricultural Ecosystems*. The latter is responsible for simulating crop growth and is named "DANUBIA crop growth model" in the present study.

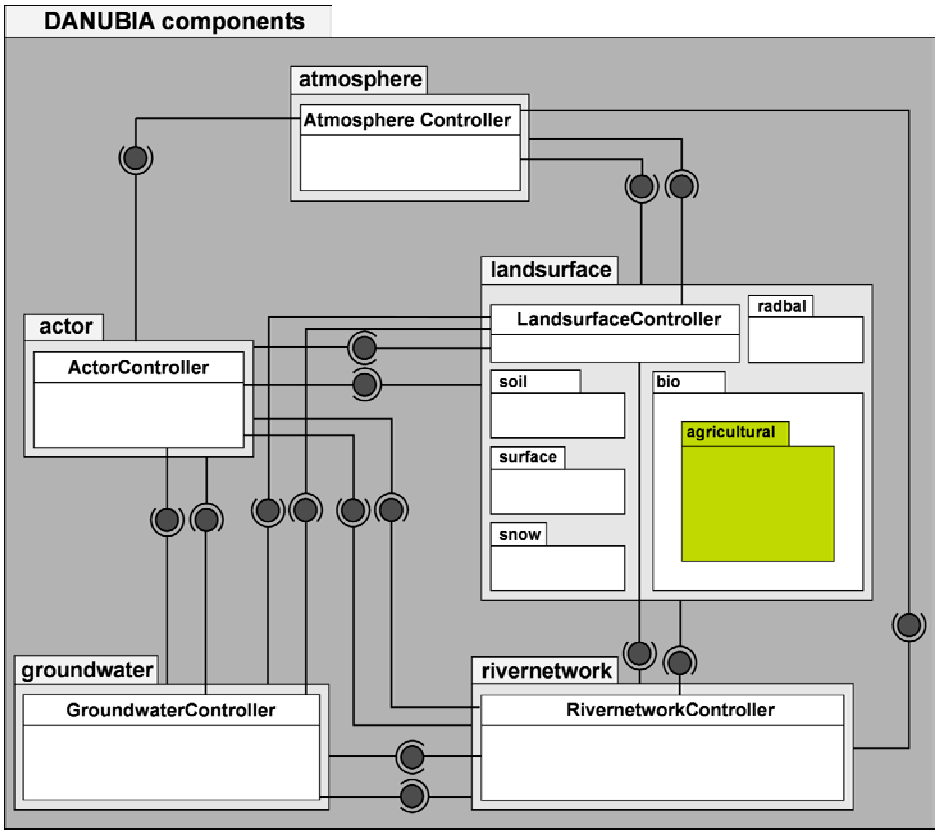

Fig. 2: UML package diagram of DANUBIA components.
Interfaces are shown as sockets (import) and balls (export).

The following example illustrates data-exchange within DANUBIA: Information on farming practices (choice of crop, dates of sowing and fertilizer applications) are provided by the *Actor Controller* and used by the *Landsurface Controller*. Whereas the information on sowing dates is utilized by the DANUBIA crop growth model, information on fertilizer applications is utilized by the DANUBIA soil model. In turn, the agricultural yield (simulated by the crop growth model) is exported to the *Landsurface Controller* and imported by the *Farming* model via the *Actor Controller* to determine future agricultural land use plans.

Within the *Landsurface* component, a large number of data are dynamically exchanged between the models. Fig. 3 shows the complex interrelations between the *Landsurface* subcomponents. In the following, an example of the communication between the subcomponents is given: The leaf area is simulated by *Biological* and exported to *Surface*. Based on the projected leaf area, the latter calculates the interception of rainfall and exports the resulting effective precipitation to *Soil.* The model *Soil* simulates and exports the soil moisture of different soil layers to *Biological,* which in turn computes the root water uptake and exports the uptake rates to *Soil*.

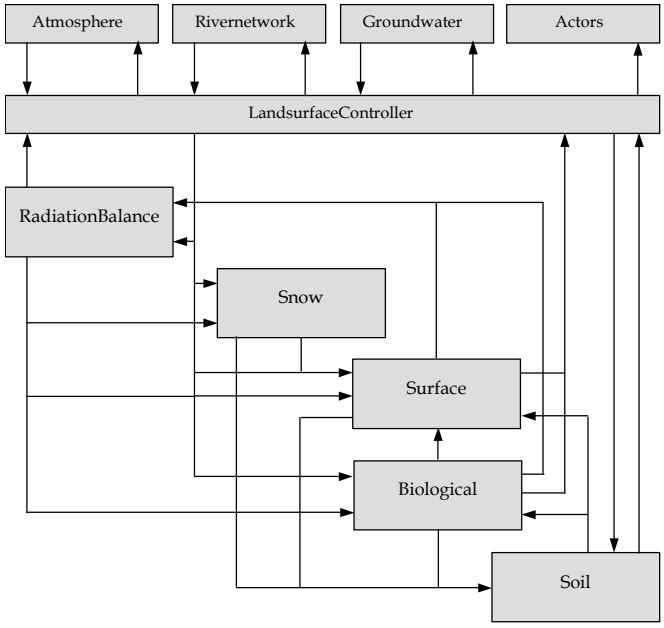

Fig. 3: Interrelations of the models within the DANUBIA *Landsurface* component (based on LUDWIG *et al.* 2003).

The main import parameters of the DANUBIA crop growth model are:

- meteorological drivers (provided by the model *Radiation Balance* and the component *Atmosphere*)
- soil data (provided by the model *Soil*)
- farming practices (provided by the component *Actors*)

The main export parameters of the DANUBIA crop growth model are:

- root characteristics including uptake rates (used by the model *Soil*)
- amounts of crop carbon and nitrogen recirculated to soil (used by the model *Soil*)
- canopy characteristics (used by the models *Radiation Balance* and *Surface*)
- agricultural yield (used by the component *Actors*)

The external time step of the simulated processes within the *Landsurface* component is one hour. The complex interactions between the *Landsurface* subcomponents are taken into account by a higher internal temporal resolution of 15 minutes (LUDWIG *et al.* 2003).

DANUBIA is raster-based and uses the concept of process pixels (abbreviated to "proxels"). For mesoscale modelling, a grid spacing of 1 km² is chosen. Depending on

the spatial resolution of for instance soil and land use data, the spatial resolution of a proxel can be further refined. Each proxel is characterized by a defined set of constant attributes e.g. geographical location, elevation, soil texture as well as dynamic properties like agricultural land use.

2.1.2 Model design

In the following, the design of the object-oriented DANUBIA crop growth model is illustrated.

Object-oriented programming rests on a few fundamental concepts. Objects are entities with specific characteristics, comprising attributes (encapsulated data) and operations (methods to access or manipulate these attributes). Objects interact with or contain other objects. Classes are the units of source code which define these properties and from which individual objects are instantiated (generated). Inheritance is a technique by which subclasses can be derived from a superclass, sharing some or all of the superclass features. In the subclasses, supplementary characteristics can be defined.

For generic crop growth models, object-oriented design represents an ideal paradigm. General processes of growth and development that are common to all crops can be defined in superclasses. Further specialization into different functional types (e.g. C_3 or C_4 photosynthesis type) and single crops is implemented in a hierarchy of subclasses. In the DANUBIA crop growth model, general plant attributes (e.g. leaf area index) and operations (e.g. calculation of transpiration) are implemented or declared in the superclass (parent class) *Plant*. A specialization into subclasses (child classes), representing specific crops, is derived from the inheritance hierarchy as illustrated in the UML diagram (Fig. 4). *Plant* is the superclass at the highest level of hierarchy for all kinds of plants. *Crop* is the superclass for all crops, providing the additional operations "sowing" and "harvesting".

Specification into the various crops is based on their assignment to a functional group (e.g. C_3 or C_4 photosynthesis type) and a set of crop-specific parameters (e.g. biochemical leaf photosynthesis parameters). This structure allows the model to be easily expanded to include more crops.

In ecosystem modelling, object-oriented programming emphasizes the existent or imaginary objects, their states and the actions they are capable of carrying out (ACOCK

& REDDY 1997). At the sowing date, an object of the type *Plant* is generated. Until harvesting, all processes of crop development and growth are either calculated by this *Plant* object or are delegated to further specialized objects for complex functionalities, which are organized in packages (collections of related classes).

In one of these packages *("leafGasExchange")* the calculations of the photosynthesis and transpiration rates at the leaf level are implemented. Included are the superclass *LeafGasFlux* as well as the two subclasses *LeafGasFluxC3* and *LeafGasFluxC4*, on account of the differences in modelling C_3 and C_4 photosynthesis. The subclasses of *Crop* implement marker-interfaces to assign the specific type of photosynthesis.

Diverse physical constants and calculations used for simulating crop growth are provided by the package *utility*.

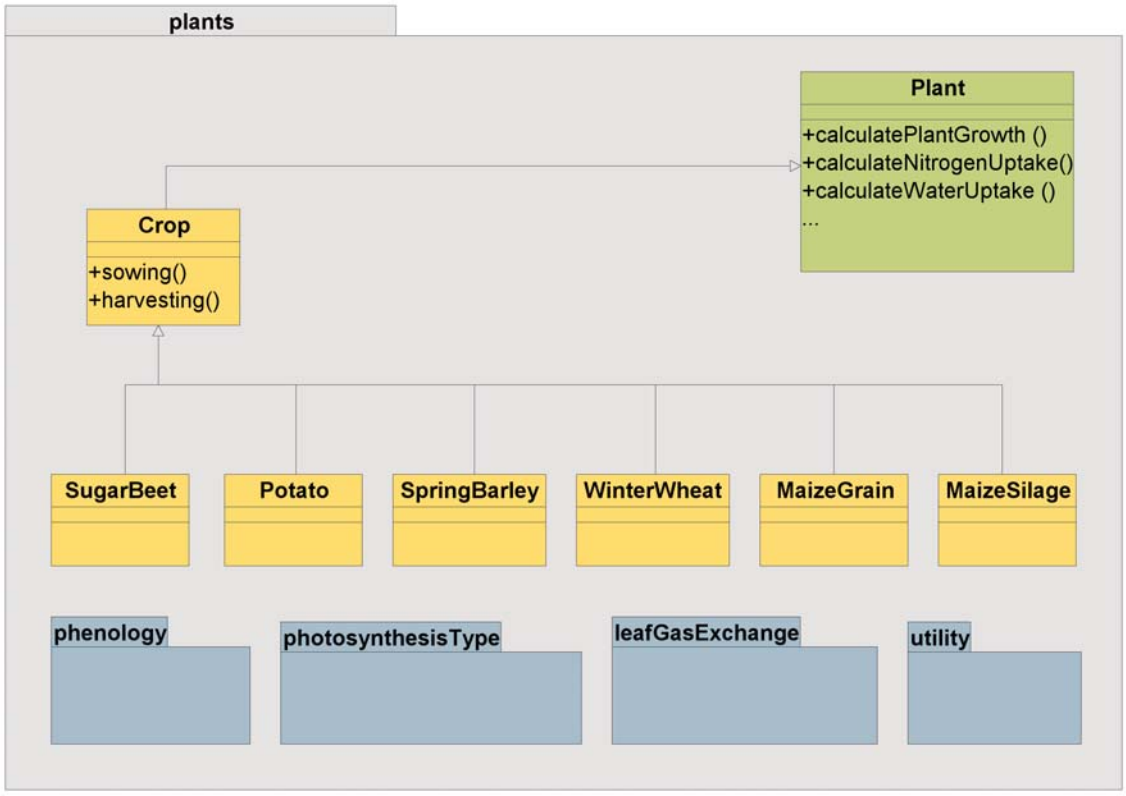

Fig. 4: The inheritance hierarchy of the class *Plant*.
Arrows pointing from the subclasses to the superclass indicate the inheritance ("is child of") relation.

The package *phenology* comprises the functionalities for simulating the phenological development of crops and is depicted in Fig. 5.

The consecutive phenological phases (subclasses of the class *Phase*) form a chain of states connected by defined conditions of transition. An object *Phase* consists of a

phase- as well as crop-specific implementation for calculating phenological development and an assigned consecutive phase. The latter is reached as soon as the condition for transition is met.

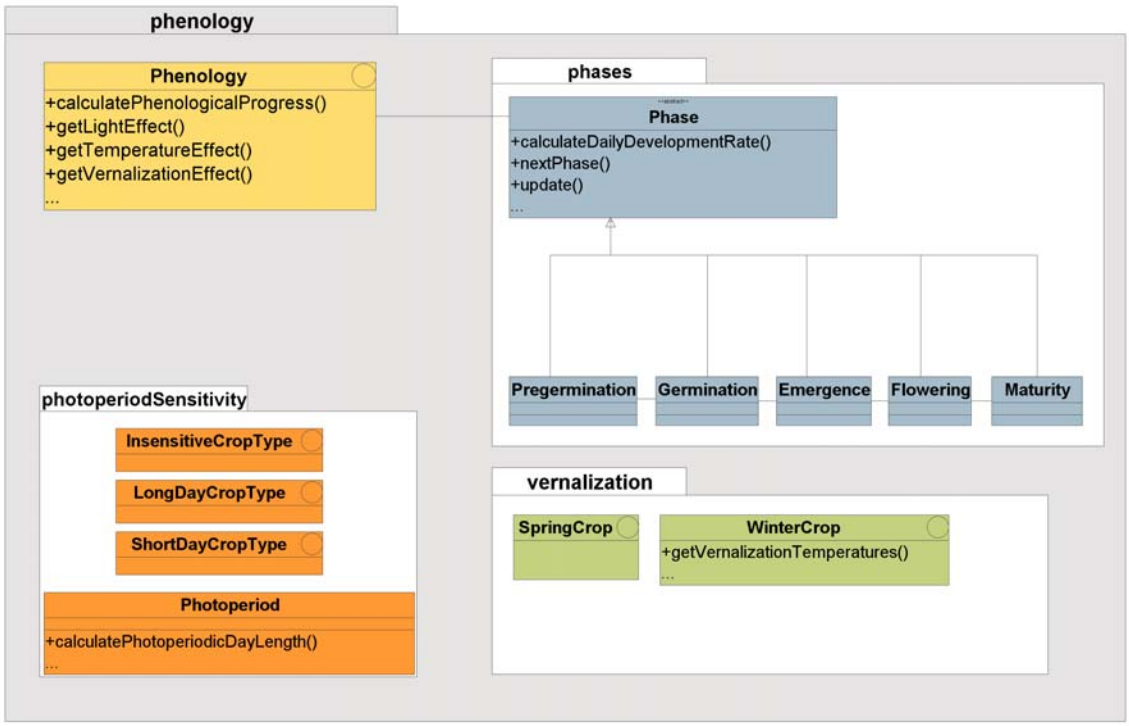

Fig. 5: The structure of the phenology model.
The depicted classes of phenological development can be further refined.

As is shown in Fig. 5, crops are categorized into three different classes in terms of their photoperiod sensitivity. Additionally, crops are grouped in spring and winter crops depending on their vernalization requirement. The subclasses of *Crop* implement marker-interfaces to indicate the types of photoperiod sensitivity and vernalization requirement.

2.2 Simulated processes

In the following sub-chapters, the processes modelled by the DANUBIA crop growth model are described, including the model algorithms. Fig. 6 shows the processes that are dynamically modelled from sowing till harvesting. The concepts and algorithms are adopted from two models: CERES (JONES & KINIRY, eds, 1986, RITCHIE & GODWIN 2000) and GECROS (YIN & VAN LAAR 2005). The processes related to the soil compartment (water and nitrogen uptake) are adopted from CERES. For simulating root growth and phenological development, a hybrid approach combining advantages of both models is chosen. All other processes are realized according to GECROS.

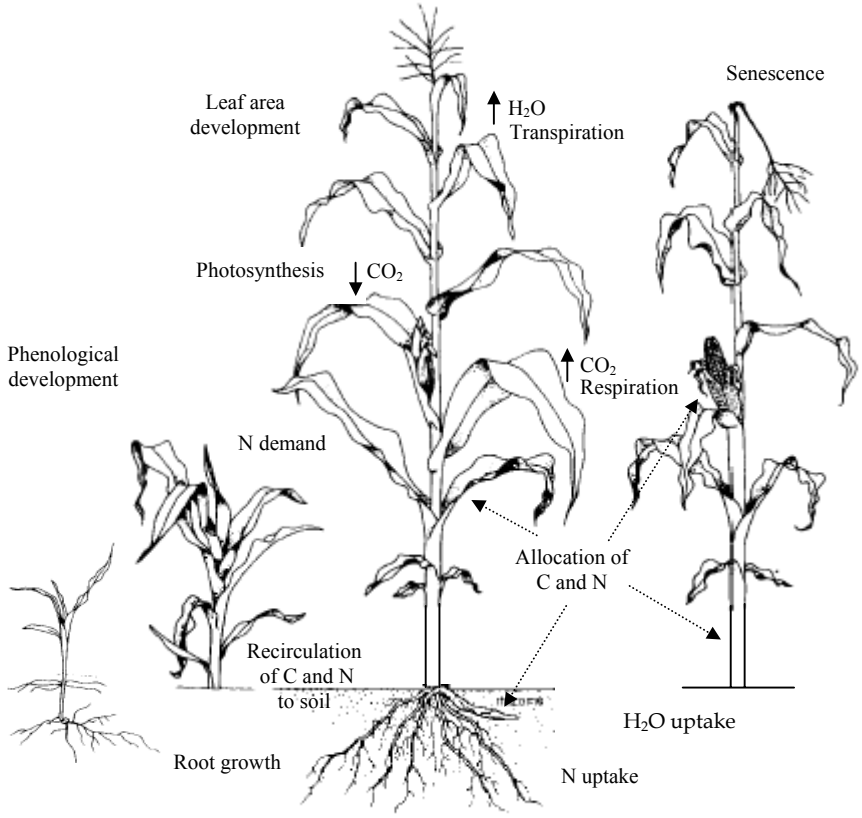

Fig. 6: Modelled processes in the DANUBIA crop growth model (drawings taken from MEIER, ed., 2001).

The model works with two different temporal scales. In order to capture non-linear responses to microclimatic conditions, the processes photosynthesis, transpiration, water and nitrogen uptake are calculated in an hourly time-step. Hourly model results of photosynthesis and nitrogen uptake fluxes are aggregated to daily values. These serve as a base for modelling processes associated with biomass formation on a daily

time-step (root growth, respiration, allocation of carbon and nitrogen to different plant organs, leaf area development, nitrogen demand, senescence, recirculation of carbon and nitrogen from crop to soil). For modelling phenological development, hourly meteorological input data are used but phenological progress is computed on a daily base.

The conceptual scheme of the DANUBIA crop growth model is presented in Fig. 7. It is based on the relational diagram of the model GECROS (YIN & VAN LAAR 2005). Extensions and modifications concern root length density, water and nitrogen uptake, as well as the environmental variables soil temperature and air pressure.

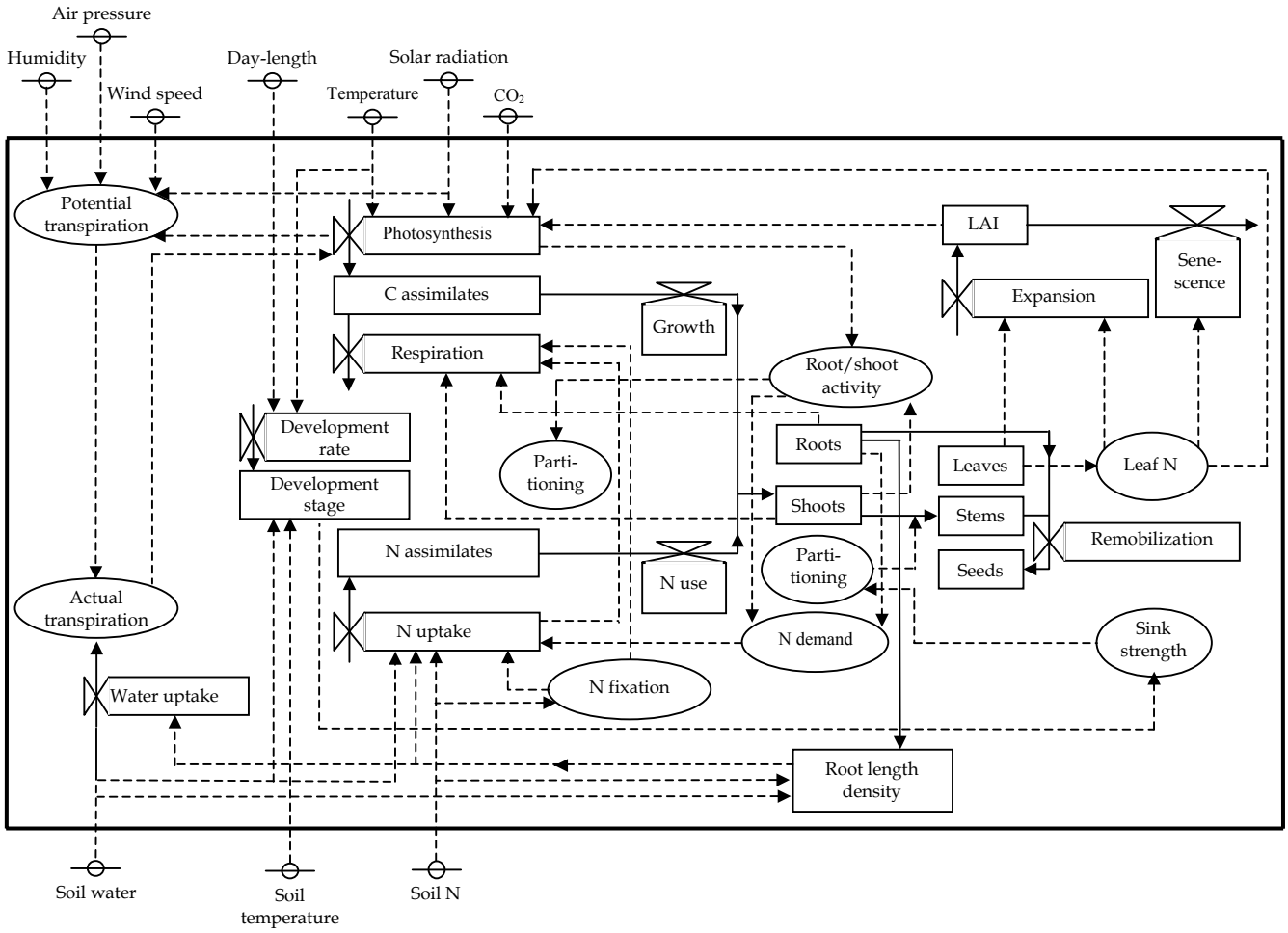

Fig. 7: Relational diagram of the DANUBIA crop growth model, based on the diagram of the model GECROS (YIN & VAN LAAR 2005). Symbols introduced by FORRESTER (1961) are used: boxes for state variables, valves for rate variables, ellipses for intermediate variables, small crossed circles for environmental variables, full-line arrows for material flows and dashed-line arrows for information flows.

Parameters used in the description of the model are listed in tables in the specific sub-chapters, showing the corresponding symbols, descriptions and units. In these tables, crop-specific input parameters are marked with an asterisk. The values of the crop-

specific input parameters are tabulated in Appendix D. A complete list of the symbols used for the parameters in this chapter is given in Appendix B, providing the descriptions and units. Unless declared otherwise, weight in g refers to weight of dry matter (biomass) and m² denotes ground area. Some of the model algorithms as well as the derivation of algorithms are described in Appendix A.

2.2.1 Phenological development

While plant growth can be defined as an increase in weight or in height, phenology describes the timing of developmental stages. Plants pass through a species-specific life cycle which is characterized by sequential phases of development, e.g. the formation of leaves or the initiation of flowering. Phenology influences growth, but accumulation of biomass can take place without any progress in the development stage (GOUDRIAAN & VAN LAAR 1994).

Predicting crop phenology is essential for the simulation of agricultural ecosystems. Besides playing an important role in leaf area and yield formation, phenology determines the timing of fertilizer application and other cultivation practices. Because of significant genotypic variation within a species, phenological traits are crucial for selecting optimal crop varieties for different environments.

Approach

The concept of modelling phenology in the model GECROS (YIN & VAN LAAR 2005) serves as a base and is amplified. In GECROS, phenology is expressed as development stage φ, a unitless variable. Fig. 8 lists the key phenological events related to the development stage. According to GECROS, the storage organ of the different crops is refered to as "seed", making no distinction between seed, grain or tuber. "Start of seed fill" is related to about two days after anthesis for cereals, to tuber formation in case of potato and to start of development of beet root for sugar beet.

The development stage φ equals the accumulated daily development rate ω_i (d^{-1}) over the growing season, which is calculated based on a multiplicative approach:

$$\omega_i = R_{max} \; f(T) \; f(P) \; f(V) \qquad (2.2.1\text{–}1)$$

The maximum daily development rate (R_{max}) is the reciprocal of the minimum number of days of a phenological phase under optimal environmental conditions (XUE *et al.* 2004).

In addition to temperature *f(T)* and photoperiod response *f(P),* the GECROS phenology model is refined by taking account of the vernalization response *f(V).* These three response functions (each restricted to a range of 0 to 1) represent the most important environmental factors controlling phenology. Each affects the developmental progress, e.g. non-optimal temperatures or day-lengths decrease the development rate. The multiplicative relationship accounts for the interactions of temperature, photoperiod and vernalization on phenology.

The maximum daily development rate is a phase- as well as a cultivar-specific parameter. According to GECROS, different values for the pre-seed fill period ($\varphi < 1$) and for the seed fill period ($\varphi \geqq 1$) are considered ($R_{max,v}$ and $R_{max,r}$). For winter wheat, STRECK *et al.* (2003b) propose a further subdivision of $R_{max,v}$ based on the key stage of terminal spikelet initiation. The maximum daily development rate is lower before this stage than after. Therefore, $R_{max,v1}$ (φ int the emergence till terminal spikelet initiation phase) and $R_{max,v2}$ (φ in the subsequent phase until start of seed fill) are accounted for in case of winter wheat.

Not all three response factors influence phenology during the whole development cycle (see Fig. 8).

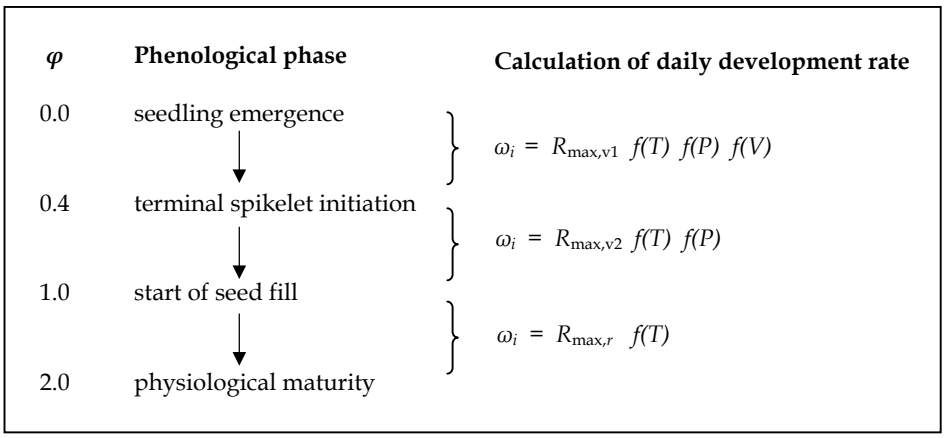

Fig. 8: Assignment of development stage to phenological phase and calculation of daily development rate. The phase of terminal spikelet initiation is only valid for winter wheat.

The phase-specific maximum rates of development are genetically determined for each cultivar and can be defined in experiments (YIN & VAN LAAR 2005). Default crop-specific values are given in Appendix D.

Temperature response

Development rate is primarily affected by temperature (e.g. YAN & HUNT 1999). A widely used approach for quantifying the influence of temperature on phenology is the "growing degree-day" concept, which uses temperature sums to predict the duration of different development stages. Numerous variants on the subject of temperature sums based on linear functions are published. MCMASTER & WILHELM (1997) point at the need for clear definitions regarding the concept of growing degree-days. Different methods of calculating growing degree-days implemented in crop models can easily cause errors when relying on parameters from literature.

In consideration of the impact of global warming and the non-linearity of temperature response functions in biological systems, many studies have been published during the last decade using a non-linear representation of the temperature effect on phenology (e.g. JAME *et al.* 1998, STEWART *et al.* 1998, YAN & HUNT 1999, JAME & CUTFORTH 2004, KIM *et al.* 2004, FLEISHER *et al.* 2006).

YIN *et al.* (1995) introduced the Beta model, a flexible bell-shaped non-linear function, to describe the relationship between development rate and temperature:

$$f(T) = \left[\left(\frac{T_c - T_a}{T_c - T_o} \right) \left(\frac{T_a - T_b}{T_o - T_b} \right)^{\frac{T_o - T_b}{T_c - T_o}} \right]^{c_t} \qquad (2.2.1\text{–}2)$$

The temperature effect function *f(T)* ranges between 0 and 1. Besides air temperature (T_a), plant-specific values for the base (T_b), the optimum (T_o) and the ceiling temperature (T_c) for phenological development are influencing variables. The temperature response curvature coefficient c_t determines the shape of the curve and allows flexibility for diverse asymmetric response functions. In case of missing data, c_t can be set to 1. For instance, Fig. 9 shows the temperature effect curve for summer barley (with $T_b = 0$ °C, $T_o = 25$ °C, $T_c = 37$ °C, $c_t = 1$) (YIN & VAN LAAR 2005). At air temperatures lower than T_b or higher than T_c, the temperature effect is zero and development ceases. T_o is the temperature at which development proceeds most rapidly. Hourly values of air temperature serve as input data for calculating *f(T)*, and the daily average value for *f(T)* is used for eq. (2.2.1–2).

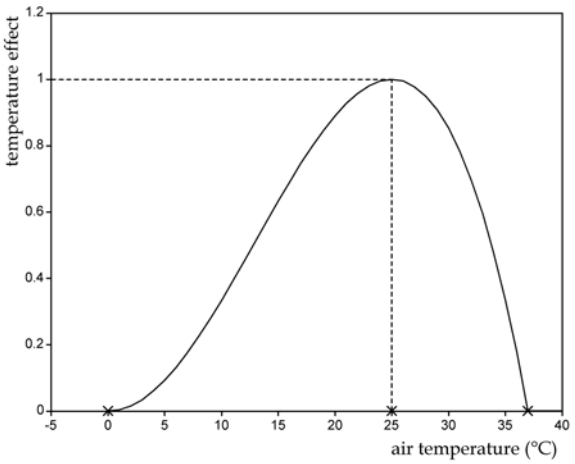

Fig. 9: Temperature effect for spring barley (after YIN & VAN LAAR 2005). Critical temperatures (T_b, T_o, T_c) are marked with a cross.

During the seed-fill phase, supra-optimum temperatures are restricted to the optimum temperature to avoid a decreased development at high temperatures. Hence, a shortened seed-fill period due to exposure to high temperatures is accounted for (YIN & VAN LAAR 2005). Critical temperatures for the considered plant species are listed in Appendix D. According to STRECK *et al.* (2003b), for winter wheat increasing critical temperatures for each sub-phase are assumed.

Photoperiodic response

Besides temperature, another important environmental factor for phenological development is photoperiod. The seasonal change in the duration of daylight and night periods influences floral initiation. Long-day plants flower only when the day-length exceeds a critical value, whereas short-day plants need a day-length less than a defined value. Photoperiod-neutral plants are insensitive to day-length.

In general, the effect of photoperiod is considered to influence phenology only in the pre-flowering phase (e.g. HODGES & RITCHIE 1991, WANG & ENGEL 1998). Recently, HAN *et al.* (2005) showed that many crops are sensitive to post-flowering photoperiod as well. However, following the concept of GECROS, photoperiodism is considered during a plant-specific defined period in the vegetative phase only. Between the start (φ_1) and the end (φ_2) of the photoperiod-sensitive phase, the photoperiod effect *f(P)* is calculated as:

$$f(P) = 1 - p_{sen}\,(D_{lp} - M_{op}) \qquad (2.2.1\text{–}3)$$

The photoperiod response *f(P)* varies from 0 to 1. The factor p_{sen} accounts for the photoperiod-sensitivity, being zero for insensitive crops, positive for short-day crops and negative for long-day crops. The parameters p_{sen} as well as φ_1 and φ_2 are genotype-specific. In GECROS, default values for the last two parameters are given: 0.2, and 0.7, respectively. D_{lp} is the photoperiodic day-length, calculated using eq. (A-1) (Appendix A). In GECROS, standard values for the optimum photoperiod M_{op} are 11 h for short-day crops and 18 h for long-day crops.

Winter wheat and spring barley are typical long-day plants, whereas maize as a tropical plant originally is a short-day plant. However, in the DANUBIA crop growth model, maize is assumed to be photoperiod-insensitive, because maize grown in temperate regions is adapted to its environment (HAN *et al.* 2005). Sugar beet is a long-day crop, but because its flowering in the second year is not related to yield formation, it is considered to be also photoperiod-insensitive. Potato plants originally require short days for tuberization, but the effect of photoperiod on modern cultivars in Europe is almost not perceptible (MACKERRAN 2004). Therefore potato is assumed to be a photoperiod-insensitive crop.

The genotype-specific parameters p_{sen} as well as φ_1 and φ_2 for a given cultivar can be accurately estimated from experiments performed in controlled environments (e.g. ADAMS *et al.* 2001, YIN *et al.* 2005). General values are presented in Appendix D.

Vernalization response

In addition to photoperiodic requirements some plant species need a prolonged period of exposure to low temperatures before floral initiation. Amongst others, temperate cereal crops like winter wheat require this process of vernalization for entering the reproductive development stage.

Since in GECROS the process of vernalization is not considered, the approach of STRECK *et al.* (2003a) is integrated for modelling the phenological development of winter wheat. The authors present a nonlinear, generalized vernalization response function for winter wheat and prove its supremacy over the three-stage linear function used in widely recognized wheat crop growth models like e.g. ARCWHEAT (WEIR *et al.* 1984) and CERES-Wheat (RITCHIE 1991).

The nonlinear function simulates the vernalization response as a smooth and continuous effect. This gives a more realistic description of the reaction of biological

systems to environmental factors than the abrupt changes when using linear functions. Several studies show that the phenological response to vernalization has a sigmoidal shape (e.g. BROOKING 1996, RAWSON *et al.* 1998). Another advantage is the generality because no genotype-specific coefficients are used.

Two combined factors influence the response to vernalization: temperatures as well as duration of the vernalization period. The effect of cold temperatures is accumulated until the plant is fully vernalized. The extent of vernalization is quantified in number of "effective vernalization days" (*VD*), following the concept in the CERES-Wheat model (HODGES & RITCHIE 1991). An exposure to the optimum vernalization temperature for a period of 24 h results in 1 *VD*. Under non-optimal conditions, only a fraction of 1 *VD* per day is reached.

The temperature effect during the vernalization period is calculated hourly as described above (eq. (2.2.1–3)), using cardinal temperatures (minimum, optimum, and maximum) of -1.3 °C, 4.9 °C, and 15.7 °C, respectively (PORTER & GAWITH 1999). The hourly values are averaged to obtain daily values of *VD* which are accumulated and serve as input for calculating the daily vernalization response *f(V)*. This response varies from 0 (unvernalized) to 1 (fully vernalized plants) and is expressed by the formula (STRECK *et al.* 2003a):

$$f(V) = \frac{VD^5}{VD_{0.5}{}^5 + VD^5} \qquad (2.2.1\text{–}4)$$

Analysis of literature data indicated that the number of effective vernalization days needed for full vernalization is 50. The coefficient $VD_{0.5}$ represents the effective vernalization days when plants show one-half of the response of fully vernalized plants ($f(V) = 0.5$); it has a value of 22.5. The exponent 5 determines the sigmoidal shape of the response to *VD*. Details for the derivation of eq. (2.2.1–4) are given by STRECK *et al.* (2003a).

Following STRECK *et al.* (2003a) the vernalization effect influences the phenological development between emergence and terminal spikelet initiation (Fig. 8).

Table 1: Symbols, definitions and units used for modelling phenology.
Crop-specific input parameters are marked with an asterisk.

Symbol		Definition	Unit
c_t	*	curvature factor for temperature response	-
D_{lp}		photoperiodic day-length	h
D_s	*	sowing depth	cm
$E_{m,a}$	*	coefficient for determining threshold for emergence	-
$E_{m,b}$	*	factor for determining threshold for emergence	-
$E_{m,th}$		threshold for emergence	-
$f(P)$		photoperiod response	-
$f(T)$		temperature response	-
$f(V)$		vernalization response	-
M_{op}		optimum photoperiod	h
p_{sen}	*	photoperiod sensitivity	h^{-1}
R_{max}		maximum daily development rate	d^{-1}
$R_{max,r}$	*	R_{max} in the reproductive (seed fill) phase	d^{-1}
$R_{max,v}$	*	R_{max} in the vegetative phase	d^{-1}
$R_{max,v1}$	*	R_{max} in the emergence till terminal spikelet initiation phase	d^{-1}
$R_{max,v2}$	*	R_{max} in the terminal spikelet initiation till start of seed fill phase	d^{-1}
T_a		air temperature	°C
T_b	*	base temperature	°C
$T_{b,em}$	*	base temperature for emergence	°C
T_c	*	ceiling temperature	°C
T_o	*	optimum temperature	°C
T_{sm}		daily mean soil temperature	°C
TT_{em}		daily thermal time for emergence	°C day
VD		effective vernalization days	d
$VD_{0.5}$		VD when plants are 50 % vernalized	d
φ		development stage	-
φ_1	*	development stage at which photoperiod sensitivity starts	-
φ_2	*	development stage at which photoperiod sensitivity ends	-
ω_i		daily development rate	d^{-1}

Germination and emergence

To simulate phenology not only from the date of emergence but from sowing, two additional stages adapted from the CERES-Wheat and CERES-Maize models (JONES & KINIRY, eds, 1986, HODGES & RITCHIE 1991, WILKENS & SINGH 2003) are integrated.

After sowing, germination occurs except where the soil temperature is below 0 °C or the soil water content in the top soil layer is near wilting point (lower limit of plant extractable water). Subsequent seedling emergence is affected by soil temperature and depth of sowing. Taking into account a plant-specific base temperature for the period before above-ground plant development ($T_{b,em}$) at which development stops, the daily thermal time for emergence (TT_{em}) is calculated:

$$TT_{em} = T_{sm} - T_{b,em} \quad (2.2.1\text{–}5)$$

where T_{sm} is daily mean soil temperature. If T_{sm} is below $T_{b,em}$, daily thermal time is zero (HODGES & RITCHIE 1991). If the accumulated daily values of TT_{em} equal a crop-

specific value ($E_{m,th}$), the transition from germination to emergence takes place. The threshold for emergence ($E_{m,th}$) is linearly related to sowing depth (D_s):

$$E_{m,th} = E_{m,a} + E_{m,b}\ D_s \qquad (2.2.1\text{–}6)$$

where, $E_{m,a}$ and $E_{m,b}$ are plant-specific coefficients.

Phenological scales

Different phenological scales exist for the description of the plant´s developmental cycle. In the past few years, the use of an uniform coding system (BBCH-scale, BBCH = **B**iologische Bundesanstalt, **B**undessortenamt and **CH**emische Industrie, Germany) of phenologically similar stages both for mono- and dicotyledonous plants is recommended (MEIER, ed., 2001).

For comparisons of modelled data with measurements, a transformation of the model´s internal scale to the BBCH-scale is needed. The BBCH-code is based on the well-known system by ZADOKS *et al.* (1974). WANG & ENGEL (1998) have presented an overview of corresponding stages by ZADOKS *et al.* (1974) and their model´s internal scale ranging from 0 to 2 for winter wheat. These data, together with the development stages in CERES-Maize, -Wheat and -Barley models (HOOGENBOOM *et al.* 2003) and the BBCH-code, provide the base for a transformation of the development rate into the BBCH-scale (Appendix E) for wheat, barley and maize. Because of missing data for potato and sugar beet, the assignment of development rate to phenological stage is not carried out more precisely than in GECROS.

Water and nitrogen stress

Because of the absence of a comprehensive, process-based concept, phenology response to water and nitrogen stress is not considered. Crop phenological reaction to water stress is a complex subject. MCMASTER *et al.* (2005) take first steps towards gaining an understanding in presenting developmental sequences observed under water-limited conditions. MIRSCHEL *et al.* (2005) state that water and nitrogen scarcity can notably accelerate phenological development and simulate the influence of the two stress factors in a dynamic semi-empirical approach for winter barley and winter rye. However, a process-based approach suitable for the five considered crops is not yet obtainable.

Future prospects

Phenology is essential for the selection of appropriate cultivars for an environment. Genotype-specific parameters allow flexibility in simulating development of different cultivars.

A comprehensive understanding of the underlying physiological processes controlling phenology has yet to be achieved. Advances in molecular biology and functional genomics offer possibilities for better understanding of mechanisms governing phenology (MCMASTER 2005). Identifying genes associated with phenology will lead to a complete process-based understanding and an improved mechanistic modelling.

2.2.2 Photosynthesis and transpiration

The processes of CO_2 exchange and transpiration are tightly coupled. Diffusion of CO_2 and water vapour between the atmosphere and leaf interior is controlled by the stomata. Responses of both processes to environmental factors like atmospheric CO_2 concentration, air temperature, relative humidity and water supply are interrelated. For example, in case of water shortage partially closed stomata inhibit the loss of water vapour. This in turn has a direct effect on the assimilation rate. Leaf temperature is influenced by transpiration and affects various biochemical processes in photosynthesis. The flux of CO_2 inside the leaf is governed by the demand of photosynthesis and limited by the diffusion capacity.

The approach of modelling gas exchange in GECROS (YIN & VAN LAAR 2005) is adopted in the DANUBIA crop growth model. Photosynthesis is the largest-scale synthetic process on earth (NOBEL 2005). Although the process of photosynthesis implies immensely complex mechanisms, it can be modelled using relatively few algorithms. GECROS uses the concept of modelling photosynthesis first described by FARQUHAR *et al.* (1980), which is widely used in gas exchange studies but has scarcely been implemented into crop growth models (YIN & VAN LAAR 2005). One of the few exceptions is the model *ecosys* (GRANT 2001).

Photosynthesis and transpiration are modelled at the leaf level and subsequently integrated for the whole canopy (see chapter 2.2.3: *Scaling of canopy parameters*).

Rubisco carboxylation rates

The detailed mechanistic photosynthesis model by FARQUHAR *et al.* (1980) relates the biochemistry of CO_2 assimilation to gas exchange. It is based on the kinetic properties of the enzyme ribulose-1,5-biphosphate carboxylase-oxygenase (Rubisco) and depicts responses of photosynthesis to light, CO_2, O_2 and temperature. Ribulose-1,5-biphosphate (RuBP) is the substrate used by Rubisco to fix CO_2. Rubisco catalyzes the competing reactions of the carboxylation or the oxygenation of RuBP in the chloroplast stroma. The carboxylation is the first major step of CO_2 fixation (VON CAEMMERER 2000).

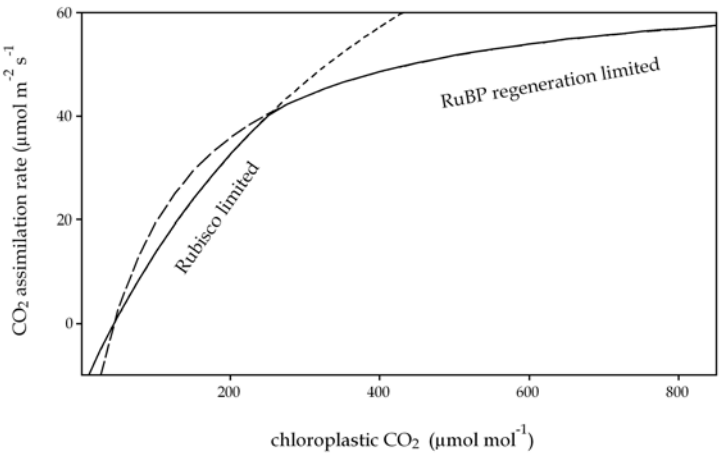

Fig. 10: Modelled rate of CO_2 assimilation as a function of chloroplastic CO_2 concentration (after VON CAEMMERER 2000). The Rubisco-limited rate has a short-dashed line extension at high CO_2, the RuBP-limited rate has a long-dashed line extension at low CO_2. The solid line curve, being the minimum rate of both, shows the rate of CO_2 assimilation.

Rubisco carboxylation rate is described by either its Rubisco-limited rate (V_c) or by the RuBP-limited rate (V_j). Thus, gross leaf photosynthesis rate (P_p in g CO_2 m^{-2} leaf s^{-1}) is calculated as:

$$P_p = \left(1 - \Gamma_* / C_c\right) \min\left(V_c, V_j\right) \quad 44 \times 10^{-6} \qquad (2.2.2\text{–}1)$$

where min ( ) denotes "minimum of", Γ_* is the CO_2 compensation point in the absence of dark respiration and C_c is the CO_2 concentration at the carboxylation site. The first term quantifies CO_2 released due to photorespiration. Multiplying by the molar mass of CO_2 (44 g) and 10^{-6} converts units of (µmol CO_2 m^{-2} leaf s^{-1}) to (g CO_2 m^{-2} leaf s^{-1}).

The RuBP-saturated rate of CO_2 assimilation is calculated as:

$$V_c = V_{cmax} \; C_c \; / \left[C_c + K_{mC}\left(1 + O_i / K_{mO}\right)\right] \qquad (2.2.2\text{–}2)$$

where O_i is the intercellular oxygen concentration (assumed to be constant). The Michaelis-Menten constants for CO_2 and O_2 are represented by K_{mC} and K_{mO} respectively and describe the kinetics of Rubisco.

Because V_c is dependent on the maximum Rubisco activity, V_{cmax}, it is also often called the Rubisco-limited rate of CO_2 assimilation (VON CAEMMERER 2000).

At high intercellular CO_2 partial pressure, the rate of RuBP regeneration controlled by electron transport (V_j) declines and CO_2 assimilation rate is limited by the supply of RuBP (VON CAEMMERER 2000). V_j is also referred to as electron transport-limited rate.

To introduce the terminology used for calculating V_j, the following section contains a few remarks on the light reaction of photosynthesis.

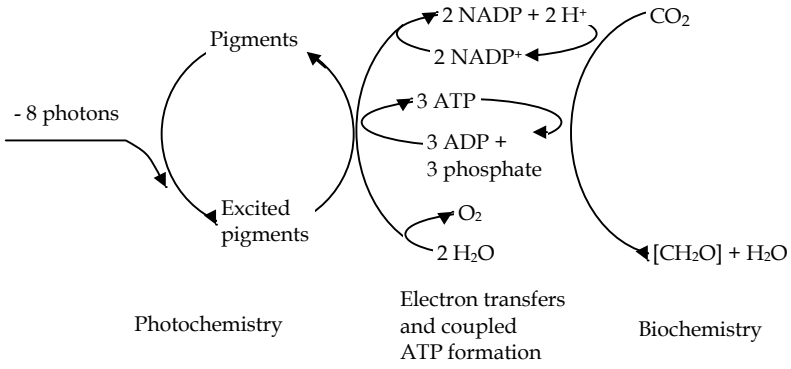

Fig. 11: Schematic representation of the three stages of photosynthesis (redrawn from NOBEL 2005). $[CH_2O]$ represents a general carbohydrate.

Light is absorbed by a photosystem in the leaf´s chloroplast. A photosystem includes a variety of protein subunits that are associated with specific pigments. Depending on the light-absorbing wavelengths of the pigments, two different types of photosystems are distinguished: PS I and PS II (NOBEL 2005).

Fig. 11 schematically shows the three stages of photosynthesis. The absorption of light can excite photosynthetic pigments, leading to the photochemical reactions in which electrons are donated by special chlorophylls. A series of electron transfers begins, leading to the reduction of the oxydized form of nicotinamide adenine dinucleotide phosphate ($NADP^+$) to the reduced form (NADPH). The formation of the other biochemical energy compound ATP (adenosine triphosphate) is coupled to the electron transfer steps. The electron flow pathways can either be cyclic, non-cyclic or pseudocyclic. The biochemical reactions involve the integration of CO_2 into carbohydrates (NOBEL 2005).

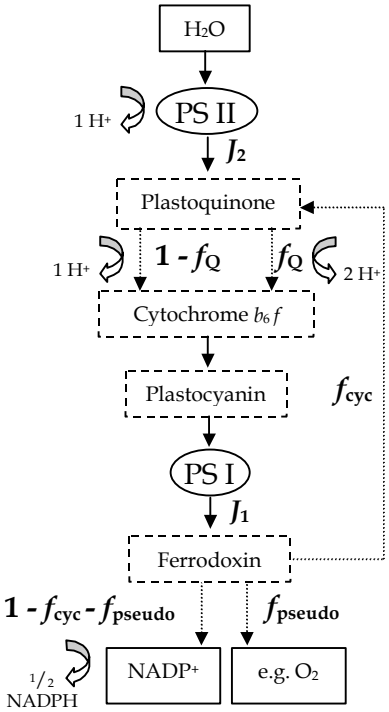

Fig. 12: Various pathways of electron transport in the light reaction. Solid arrows show the flux of electron flow, dotted arrows show the fraction of relevant pathway, and the curved arrows show the number of protons (H+) or NADPH produced per electron transported. Marked by a dashed frame are specific molecules that act as electron acceptors or donors in chloroplasts. Redrawn from YIN & VAN LAAR (2005).

YIN *et al.* (2004b) modified the original calculation of V_j (FARQUHAR *et al.* 1980) to capture the co-limitation of NADPH and ATP on electron transport. Whereas the original calculation is based on linear whole-chain (non-cyclic) electron transport, YIN *et al.* (2004b) also incorporate the non-linear pathways of electron transport (Fig. 12). Their concept is based on the generalized stoichiometry for the ratio of NADPH and ATP as needed by C_3 metabolic reactions. The electron transport-limited rate of photosynthesis is given by:

$$V_j = J_2 \frac{\left(2 + f_Q - f_{cyc}\right) C_C}{h\left[3C_C + 7\Gamma_*\right]\left(1 - f_{cyc}\right)} \qquad (2.2.2\text{–}3)$$

where h denotes the number of protons required to produce 1 mol ATP, and J_2 is the rate of electron transport through PS II. The term in squared brackets describes the ATP consumption rate per carboxylation. The relationship between the different types of electron transport pathways is expressed as:

$$1 - f_{cyc} - f_{pseudo} = \frac{\left(4C_C + 8\Gamma_*\right)\left(2 + f_Q - f_{cyc}\right)}{h\left(3C_C + 7\Gamma_*\right)} \qquad (2.2.2\text{–}4)$$

where f_{cyc} denotes the fraction of electron transport which is cyclic around PS I, f_{pseudo} is the pseudocyclic fraction, and f_Q is the fraction involved in the Q-cycle.

The dependency between J_2 and absorbed irradiance of the chloroplasts (I) is formulated as:

$$\theta J_2^2 - \left(\alpha_2 I + J_{max} \right) J_2 + \alpha_2 I J_{max} = 0 \qquad (2.2.2\text{–}5)$$

with

$$\alpha_2 = J_2 \frac{1 - f_{cyc}}{1 + \left(1 - f_{cyc} \right) / \Phi_{2m}} \qquad (2.2.2\text{–}6)$$

where Θ describes the convexity of the response curve, and J_{max} is the upper limit to J_2 (equivalent to the maximum rate of whole chain transport while cyclic flow takes place concurrently). The electron transport efficiency of PS II on the basis of light absorbed by both photosystems is represented by a_2, and Φ_{2m} is the maximum electron transport efficiency of PS II on the basis of light absorbed by PS II alone.

Pseudo-cyclic electron transport is linked to non-stomatal effects on photosynthesis which are not considered. Thus, f_{pseudo} is set to zero. For C_3 plants, f_Q is assumed to be zero whereas it equals f_{cyc} in case of C_4 plants. Derivation of equations (2.2.2–3) to (2.2.2–6) as well as more details are given by YIN *et al.* (2004b).

The CO_2 compensation point equals the CO_2 concentration in the chloroplast when no assimilation occurs. YIN *et al.* (2004b) modified the original equation for the CO_2 compensation point in the absence of dark respiration (Γ_*):

$$\Gamma_* = 0.5 \left\{ \exp\left(-3.3801 + 5220 / \left[298 R \left(T_l + 273 \right) \right] \right) \right\} O_i K_{mC} / K_{mO} \qquad (2.2.2\text{–}7)$$

where the exponential part corresponds to the ratio of the maximum oxygenation rate to the maximum carboxylation rate of Rubisco. The ratio is established from functions presented by BERNACCHI *et al.* (2001). The factor 0.5 accounts for the fact that 0.5 mol CO_2 is released when Rubisco catalyzes the reaction with one mol O_2 in photorespiration.

The CO_2 compensation point in the presence of dark respiration (Γ) is given by (FARQUHAR *et al.* 1980):

$$\left(\Gamma - \Gamma_* \right) / \left[\Gamma + K_{mC} \left(1 + O_i / K_{mO} \right) \right] = R_d \times 10^6 / \left(44 V_{cmax} \right) \qquad (2.2.2\text{–}8)$$

Table 2: Symbols, definitions and units for modelling photosynthesis and transpiration. Crop-specific input parameters are marked with an asterisk.

Symbol	Definition	Unit
A	net assimilation rate	g CO_2 m^{-2} leaf s^{-1}
c_0	empirical coefficient in eq. (2.2.2–9)	-
c_1	empirical coefficient in eq. (2.2.2–9)	kPa^{-1}
C_a	CO_2 concentration in the air	µmol mol^{-1}
C_c	CO_2 concentration at carboxylation site of chloroplasts	µmol mol^{-1}
C_i	intercellular CO_2 concentration	µmol mol^{-1}
D_a	water vapour pressure saturation deficit of air	kPa
D_{al}	air-to-leaf vapour pressure deficit	kPa
E_a	actual leaf transpiration	mm s^{-1}
E_{Jmax} *	activation energy for J_{max}	J mol^{-1}
E_p	potential leaf transpiration	mm s^{-1}
$E_{Rub,k}$	proxy for activation energies E_{KmC}, E_{KmO}, E_{Rd} and E_{Vcmax} in eq. (2.2.2–10)	J mol^{-1}
$e_{s(Ta)}$	saturated vapour pressure of air	kPa
$e_{s(Tl)}$	saturated vapour pressure of leaf	kPa
f_{cyc}	fraction of cyclic electron transport around photosystem I	-
f_{pseudo}	fraction of pseudocyclic electron transport	-
f_Q	fraction of electron transport that follows the Q-cycle	-
$g_{c,p}$	potential conductance for CO_2	m s^{-1}
I	leaf chloroplasts-absorbed PAR	µmol m^{-2} leaf s^{-1}
J_2	rate of linear electron transport through photosystem II	µmol electron m^{-2} leaf s^{-1}
J_{max}	maximum rate of J_2	µmol electron m^{-2} leaf s^{-1}
J_{max25}	J_{max} at 25 °C	µmol electron m^{-2} leaf s^{-1}
K_{mC}	Michaelis-Menten constant for CO_2	µmol mol^{-1}
K_{mO}	Michaelis-Menten constant for O_2	mmol mol^{-1}
n	leaf N content	g N m^{-2} leaf
n_b *	minimum leaf N for photosynthesis	g N m^{-2} leaf
P_a	actual gross leaf photosynthesis	g CO_2 m^{-2} leaf s^{-1}
P_p	potential gross leaf photosynthesis	g CO_2 m^{-2} leaf s^{-1}
r_{bh}	leaf boundary layer resistance to heat	s m^{-1}
r_{bw}	leaf boundary layer resistance to water vapour	s m^{-1}
R_d	leaf dark respiration	g CO_2 m^{-2} leaf s^{-1}
R_{d25}	R_d at 25 °C	g CO_2 m^{-2} leaf s^{-1}
R_k	proxy for K_{mC}, K_{mO}, R_d and V_{cmax} in eq. (2.2.2–10)	various
R_n	net leaf absorbed radiation	J m^{-2} leaf s^{-1}
$r_{sw,a}$	leaf stomatal resistance to water in the presence of water stress	s m^{-1}
$r_{sw,p}$	leaf stomatal resistance to water in the absence of water stress	s m^{-1}
r_t	turbulence resistance	s m^{-1}
s	slope of the curve relating saturation vapour pressure to temperature	kPa $°C^{-1}$
s^*	proxy for s (eq. (2.2.2–21)	kPa $°C^{-1}$
T_a	air temperature	°C
T_l	leaf temperature	°C
V	vapour pressure	kPa
V_c	rate of carboxylation limited by Rubisco activity	µmol CO_2 m^{-2} leaf s^{-1}
V_{cmax}	maximum rate of carboxylation limited by Rubisco activity	µmol CO_2 m^{-2} leaf s^{-1}
V_{cmax25}	V_{cmax} at 25 °C	µmol CO_2 m^{-2} leaf s^{-1}
V_j	rate of carboxylation limited by electron transport	µmol CO_2 m^{-2} leaf s^{-1}
a_2	quantum efficiency for electron transport of PS II based on absorbed light	mol mol^{-1}
Γ	CO_2 compensation point in the presence of dark respiration	µmol mol^{-1}
γ	psychrometric constant	kPa $°C^{-1}$
Γ_*	CO_2 compensation point in the absence of dark respiration	µmol mol^{-1}
Θ *	convexity factor for response of J_2 to PAR	-
λ	latent heat of water vaporization	J kg^{-1}
ρc_p	volumetric heat capacity	J m^{-3} $°C^{-1}$
χ_{jn} *	proportion factor for the relation of J_{max} to leaf N	µmol electron g^{-1} N s^{-1}
χ_{vcn} *	proportion factor for the relation of V_{cmax} to leaf N	µmol CO_2 g^{-1} N s^{-1}

To calculate C_i (intercellular CO_2 concentration) dynamically, the following assumption is used (adapted equation given by LEUNING 1995):

$$C_i / C_a = 1 - \left(1 - \Gamma / C_a \right) \left(c_0 + c_1 D_{al} \right) \qquad (2.2.2\text{–}9)$$

which expresses the ratio of C_i to atmospheric CO_2 concentration (C_a) as a function of the air-to-leaf vapour pressure deficit (D_{al}). The parameters c_0 and c_1 are empirically derived coefficients (using data from MORISON & GIFFORD 1983, cited by YIN & VAN LAAR 2005). The difference between the saturated vapour pressure of leaf temperature $e_{s(Tl)}$ and vapour pressure V (derived from the meteorological input parameter absolute humidity) yields $D_{al.}$

Temperature dependencies

Precise estimates of the temperature dependencies of Rubisco kinetic parameters are crucial for predicting the impact of global change on photosynthesis. An Arrhenius function is used to describe temperature dependencies of the kinetic constants on leaf temperature (T_l) with respect to a reference temperature (25 °C):

$$R_k(T) = R_k(25) \exp\left[\left(T_l - 25 \right) E_{Rub,k} / \left(298 R \left(T_l + 273 \right) \right) \right] \qquad (2.2.2\text{–}10)$$

where $R_k(T)$ and $R_k(25)$ represent one of the kinetic parameters at temperature T, and at 25 °C, respectively. Activation energy $E_{Rub,k}$ quantifies the corresponding kinetic energy of each substrate needed for the reaction to proceed, and R is the universal gas constant (VON CAEMMERER 2000). Equation (2.2.2–10) is applied to the parameters $V_{cmax,}$ K_{mC}, K_{mO} and R_d (leaf dark respiration). For J_{max}, the temperature dependency is expressed by a modified Arrhenius function (MEDLYN *et al.* 2002):

$$J_{max} = J_{max}(25) \exp\left(\frac{\left(T_l - 25 \right) E_{Jmax}}{298 R \left(T_l + 273 \right)} \right) \left(\frac{1 + \exp\left(298 S_J - D_J \right) / \left(298 R \right)}{1 + \exp\left[\left(T_l + 273 \right) S_J - D_J \right] / \left[R \left(T_l + 273 \right) \right]} \right) \qquad (2.2.2\text{–}11)$$

where J_{max25} refers to J_{max} at 25 °C, S_J is an entropy factor, E_{Jmax} is the activation energy, whereas D_J is the deactivation energy. E_{Jmax} describes the rate of decrease of the function below the optimum (analogous to $E_{Rub,k}$), and D_J depicts the rate of decrease of the function above the optimum temperature. Table 3 shows values of constants used in GECROS for modelling photosynthesis.

Table 3: Constants used for modelling photosynthesis and transpiration.
Sources for general constants (e.g. R) are not listed.

Symbol	Definition	Value	Source
D_J	energy of deactivation for J_{max}	200000 J mol^{-1}	MEDLYN *et al.* (2002)
E_{KmC}	activation energy for K_{mC}	79430 J mol^{-1}	BERNACCHI *et al.* (2001)
E_{KmO}	activation energy for K_{mO}	36380 J mol^{-1}	BERNACCHI *et al.* (2001)
E_{Rd25}	activation energy for R_d at 25°C	65330 J mol^{-1}	BERNACCHI *et al.* (2001)
E_{Vcmax}	activation energy for V_{cmax}	65330 J mol^{-1}	BERNACCHI *et al.* (2001)
f_{pseudo}	fraction of pseudocyclic electron transport	0	YIN & VAN LAAR (2005)
f_Q	fraction of electron transport that follows the Q-cycle	0 (for C_3) f_{cyc} (for C_4)	YIN & VAN LAAR (2005)
h	number of protons required to produce 1 mol ATP	3 mol mol^{-1}	FARQUHAR *et al.* (1980)
K_{mC25}	Michaelis-Menten constant for CO_2 at 25°C	404.9 µmol mol^{-1} (for C_3) 650.0 µmol mol^{-1} (for C_4)	BERNACCHI *et al.* (2001) VON CAEMMERER (2000)
K_{mO25}	Michaelis-Menten constant for O_2 at 25°C	278.4 mmol mol^{-1} for (C_3) 450.0 mmol mol^{-1} (for C_4)	BERNACCHI *et al.* (2001) VON CAEMMERER (2000)
O_i	intercellular oxygen concentration	210 mmol mol^{-1}	
R	universal gas constant	8.314 J K^{-1} mol^{-1}	
S_J	entropy term	650 J K^{-1} mol^{-1}	HARLEY *et al.* (1992)
γ	psychrometric constant	0.067 kPa °C-1	
ρc_p	volumetric heat capacity	1200 J m-3 °C-1	
ς	leakage of CO_2 back to the mesophyll as a fraction of the PEP carboxylation	0.2 (relevant for C_4)	YIN & VAN LAAR (2005)
Φ_{2m}	maximum electron transport efficiency of PS II	0.85 mol mol^{-1}	BERNACCHI *et al.* (2003)

C_4 photosynthesis

The presented concept of modelling photosynthesis was developed for C_3 plants. For modelling C_4 photosynthesis in a simplified way, only a few modifications are implemented according to the model GECROS.

C_4 plants like maize show different photosynthetic features compared with C_3 plants (Fig. 13). A special leaf anatomy characterized by a concentric layer of bundle sheath cells surrounded by mesophyll cells enables a CO_2 concentration mechanism. CO_2 is initially fixed into C_4 acids by the enzyme PEP (phosphoenolpyruvate) carboxylase in the mesophyll. The C_4 acids are then decarboxylated in the bundle sheath to provide CO_2 for the reactions equal to C_3 photosynthesis (VON CAEMMERER 2000). Because of the increased CO_2 concentration, the carboxylase activity of Rubisco dominates over the oxygenase activity. Thus photorespiration rates are reduced (NOBEL 2005).

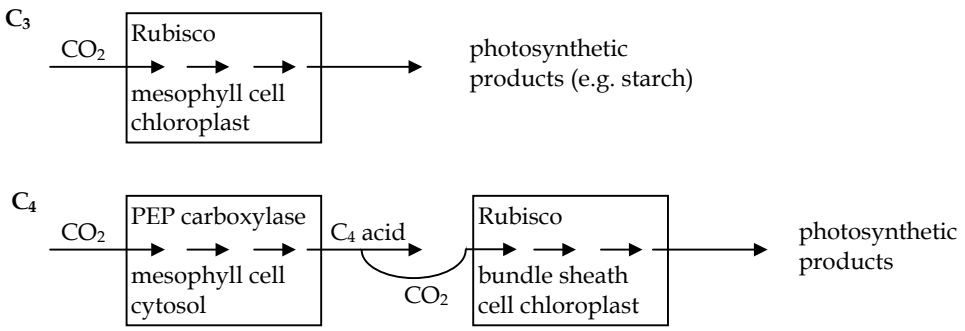

Fig. 13: Locations for the three photosynthetic pathways for C_3 and C_4 plants (redrawn from NOBEL (2005)).

In case of C_3 plants, an infinite mesophyll conductance is assumed. Consequently, chloroplastic equals intercellular CO_2 concentration ($C_c = C_i$). Regarding C_4 plants, C_c is set to 10 C_i to account for the higher CO_2 concentration in the bundle sheath cells. To include the additional ATP requirement due to the PEP carboxylation, the stoichiometry in equations (2.2.2–3) and (2.2.2–4) is modified:

$$V_j = J_2 \frac{\left(2 + f_Q - f_{cyc}\right) C_C}{h\left[2\left(C_C - \Gamma_*\right)/\left(1-\varsigma\right) + \left(3C_C + 7\Gamma_*\right)\right]\left(1 - f_{cyc}\right)} \quad (2.2.2\text{–}12)$$

with, f_{cyc}, f_{pseudo}, and f_Q, satisfying:

$$1 - f_{cyc} - f_{pseudo} = \frac{\left(4C_C + 8\Gamma_*\right)\left(2 + f_Q - f_{cyc}\right)}{h\left[2\left(C_C - \Gamma_*\right)/\left(1-\varsigma\right) + \left(3C_C + 7\Gamma_*\right)\right]} \quad (2.2.2\text{–}13)$$

where ς expresses leakage (i.e. CO_2 released by C_4 acid decarboxylation leaks back to the mesophyll) as a fraction of the PEP carboxylation rate. The first summand in the square brackets in eq. (2.2.2–13) describes the requirement for 2 mol ATP per mol CO_2 fixed during the PEP carboxylation. For C_4 photosynthesis, the CO_2 compensation point (eq. (2.2.2–8)) is divided by 10. The Rubisco kinetic constants K_{mC} and K_{mO} are higher for C_4 plants than for C_3 plants (Table 3). In GECROS, the empirically derived coefficient c_1 has a higher value for C_4 crops than for C_3 plants.

Leaf temperature

The difference ΔT between air (T_a) and leaf temperature (T_l) is determined via the leaf energy balance. Energy absorbed by a leaf is represented by net absorbed radiation R_n while energy dissipation occurs in form of latent (transpiration) and sensible heat:

$$\Delta T = T_l - T_a = \left(r_{bh} + r_t\right)\left(R_n - \lambda E_p\right) / \rho c_p \qquad (2.2.2\text{–}14)$$

where E_p is potential transpiration, ρc_p is the volumetric heat capacity (Table 3) and λ is latent heat of water vaporization. In GECROS, a constant value of λ is assumed. In the DANUBIA crop growth model λ is calculated dynamically as a function of air temperature (calibrated from data by NOBEL, 2005):

$$\lambda = \left(2502.3 - 2.4289\, T_a\right) \times 10^3 \qquad (2.2.2\text{–}15)$$

Potential rates of leaf transpiration and photosynthesis

The driving force for transpiration is the water vapour pressure difference between leaf and air. The analogy of electrical resistances and conductances is used to quantify the diffusion of water vapour and CO_2. The resistance for the diffusion of water vapour from leaves to the atmosphere is composed of stomatal ($r_{sw,p}$), boundary layer (r_{bw}) and turbulence resistance (r_t) in series. A thin laminar air layer at the leaf surface causes leaf boundary layer resistance. The resistance for the movement of water vapour and heat from the air within the canopy to the air above is described by turbulence resistance (PENNING DE VRIES *et al.* 1989).

Potential leaf transpiration (assuming no water stress) is calculated based on the *Penman-Monteith* equation (MONTEITH 1973, cited by YIN & VAN LAAR 2005):

$$E_p = \frac{s\, R_n + \rho c_p\, D_a / \left(r_{bh} + r_t\right)}{\lambda\left\{s + \gamma\left[\left(r_{bw} + r_t + r_{sw,p}\right) / \left(r_{bh} + r_t\right)\right]\right\}} \qquad (2.2.2\text{–}16)$$

where D_a is the water vapour pressure saturation deficit of air, s is the slope of the curve relating saturation vapour pressure to temperature, and γ represents the psychrometric constant. Calculation of the resistances r_{bh}, r_{bw}, and r_t as well as net absorbed radiation R_n are given in Appendix A.

Stomatal resistance to water transfer (assuming no water stress) $r_{sw,p}$ is:

$$r_{sw,p} = \left(1 / g_{c,p} - 1.3\, r_{bw} - r_t\right) / 1.6 \qquad (2.2.2\text{–}17)$$

where $g_{c,p}$ denotes the potential conductance for CO_2. The factors 1.3 and 1.6 consider the more rapid diffusion of water vapour compared with CO_2 in crossing boundary layers and stomata, respectively. $g_{c,p}$ is a function of potential leaf photosynthesis:

$$g_{c,p} = \left(P_p - R_d \right) \left[\left(273 + T_l \right) / 0.53717 \right] / \left(C_a - C_i \right) \quad (2.2.2\text{–}18)$$

where (C_a - C_i) quantifies the diffusion of CO_2 from air into the leaf and (P_p - R_d) gives the net assimilation rate (A). The term in square brackets converts CO_2 concentration from g m^{-3} into vpm (volumetric parts per million) depending on leaf temperature T_l (GOUDRIAAN & VAN LAAR 1994).

The slope of the curve relating saturation vapour pressure to temperature (s) is:

$$s = \left[e_{s(T_l)} - e_{s(T_a)} \right] / \left(T_l - T_a \right) \quad (2.2.2\text{–}19)$$

where the term in square brackets is the difference in saturated vapour pressure between the air inside and outside the leaf. Saturated vapour pressure is a function of air temperature (GOUDRIAAN & VAN LAAR 1994):

$$e_{s(T_a)} = 0.611 \exp\left(17.4\, T_a / \left(239 + T_a \right) \right) \quad (2.2.2\text{–}20)$$

The complex pattern of feedbacks between the controlling parameters complicates the modelling of gas exchange fluxes. For calculating potential transpiration E_p, the value of s is required. However, s is influenced by T_l which in turn depends on E_p. This calculation loop is avoided by substituting s in eq. (2.2.2–16) by the derivative of $e_{s(Ta)}$ with respect to T_a (s*) based on eq. (2.2.2–20):

$$s^* = 4158.6\ e_{s(T_a)} / \left(T_a + 239 \right)^2 \quad (2.2.2\text{–}21)$$

To minimize the error due to the use of s*, two iterations of the equations are performed (Fig. 14). In the first round, T_a and s* are used for T_l and s, respectively. Subsequently, T_l and s (eq. (2.2.2–14) and (2.2.2–19)) are calculated to be then used in the second round.

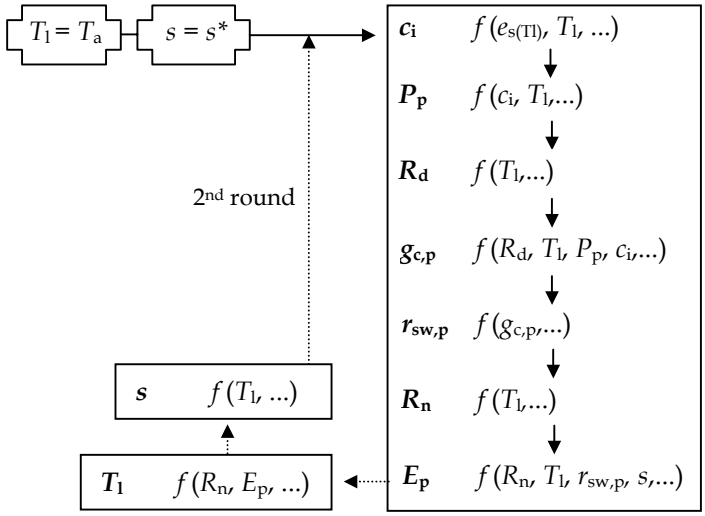

Fig. 14: Computation sequence for calculating photosynthesis and transpiration.

Actual rates of transpiration and photosynthesis

If the demand of potential leaf transpiration rate E_p cannot be satisfied by root water uptake, transpiration is reduced to actual transpiration E_a according to the available water supply (see chapter 2.2.6: *Water uptake*). Consequently, the rate of assimilation too is throttled because of the increased actual stomatal resistance $r_{sw,a}$ which is calculated as:

$$r_{sw,a} = \left(E_p - E_a \right) \left[s \left(r_{bh} + r_t \right) + \gamma \left(r_{bw} + r_t \right) \right] / \left(\gamma E_a \right) + r_{sw,p} E_p / E_a \qquad (2.2.2\text{–}22)$$

Derivation of eq. (2.2.2–22) is given in Appendix A. Leaf temperature T_l is recalculated using E_a instead of E_p in eq. (2.2.2–14). Using the new value of T_l, the following parameters are recalculated: c_i, P_p, and R_d. Actual leaf photosynthesis rate P_a is then given by:

$$P_a = \frac{1.6\, r_{sw,p} + 1.3\, r_{bw} + r_t}{1.6\, r_{sw,a} + 1.3\, r_{bw} + r_t} \left(P_p - R_d \right) + R_d \qquad (2.2.2\text{–}23)$$

Parameterization

Some parameters for the photosynthesis submodel can be derived from leaf-level gas exchange measurements. In order to minimize the parameterization procedure, fixed values for some of the parameters which are supposed to be invariant among crop species are used in GECROS (see Table 3). The value for Θ may vary, but in case of

missing data can be set to 0.7 (VON CAEMMERER 2000) as proposed in GECROS. Many different values of the crop-specific parameters V_{cmax25} and J_{max25} are published but MEDLYN *et al.* (2002) point to the fact that the assumed values of K_{mC} and K_{mO} in gas exchange measurements strongly influence the value of V_{cmax25}. Thus, published data are difficult to adopt.

Photosynthetic capacity is closely linked to the amount of nitrogen in the plant tissue because of the enzyme Rubisco being a nitrogen-rich compound. According to GECROS, both parameters V_{cmax25} and J_{max25} are a function of photosynthetically active leaf nitrogen (being the difference between leaf nitrogen content (n) and the crop-specific minimum leaf nitrogen for photosynthesis (n_b)).

$$V_{cmax25} = \chi_{vcn} \left(n - n_b \right) \tag{2.2.2–24}$$

$$J_{max25} = \chi_{jn} \left(n - n_b \right) \tag{2.2.2–25}$$

The proportion factors χ_{vcn} and χ_{jn} are crop-specific. WULLSCHLEGER (1993) examined numerous gas exchange measurement data and found a strong correlation between J_{max} and V_{cmax}. LEUNING (2002) scaled the results to a common temperature of 25 °C. His analysis of the ratio J_{max}/V_{cmax} resulted in a mean value of 2. In case of missing data, χ_{vcn} can be set to 60 µmol CO_2 g^{-1} N s^{-1} and χ_{jn} can be assumed to equal 2 χ_{vcn}.

In GECROS, R_{d25} is assumed to be proportional to V_{cmax25} (WATANABE *et al.* 1994):

$$R_{d25} = 0.0089 \times 44 \times 10^{-6} \, V_{cmax25} \tag{2.2.2–26}$$

Thus, according to GECROS, the only crop-specific values in the photosynthesis submodel are n_b, χ_{jn}, χ_{vcn}, Θ, and E_{Jmax}. These can be determined in leaf-level gas exchange measurements (see chapter 2.4.2).

2.2.3 Scaling of canopy parameters

Fluxes of photosynthesis and transpiration are calculated at the leaf level and have to be adapted to the canopy scale. Assuming a simple linear relationship between the calculated fluxes and leaf area index would lead to incorrect results because of the attenuation of radiation in canopies and the convex non-linear light response of photosynthesis (SPITTERS 1986).

To overcome the problem of scaling, the multi-layer approach divides the canopy into a number of horizontal units (assumed to be homogeneous with respect to

microclimate) and integrates the layer fluxes to provide the total flux (LEUNING *et al.* 1995). An alternative to multi-layer models is the sun-shade approach presented by DE PURY & FARQUHAR (1997) and WANG & LEUNING (1998), which is adopted in GECROS. Without distinguishing between different layers only the sunlit and shaded sections of the canopy are calculated separately. Compared with a multi-layer model far fewer calculations are needed and the results with respect to canopy photosynthesis are as accurate (DE PURY & FARQUHAR 1997). For the DANUBIA crop growth model, the concept and equations for scaling canopy parameters from the model GECROS (YIN & VAN LAAR 2005) are adopted. The following paragraphs of this sub-chapter describe the theory and list the equations.

Absorption of radiation in plant canopies

Sunlit and shaded foliage experience very dissimilar levels of irradiance. While sunlit leaves collect direct as well as diffuse radiation, shaded leaves only receive the diffuse component of radiation. Light intensity decreases within a canopy and depends on the amount of light at the top of the canopy and the attenuation of the various radiation components: direct and diffuse PAR as well as NIR. During the day the ratio between sunlit and shaded fractions changes with solar elevation. The sunlit fraction of a canopy decreases exponentially with the cumulative leaf area index from the canopy top. In the following, the distinction between sunlit and shaded is expressed by the subscripts "sun" and "shade".

At canopy depth with a known leaf area index (L_i), the sunlit fraction ($f_{sun,i}$), is calculated as (SPITTERS 1986):

$$f_{sun,i} = \exp\left(- k_b \, L_i \right) \qquad (2.2.3\text{–}1)$$

where L_i is the leaf area index between top of the canopy and considered depth and k_b is the direct beam extinction coefficient of the canopy. This coefficient characterizes the exponential attenuation of direct radiation within the canopy and according to GOUDRIAAN (1988) is calculated as:

$$k_b = O_{av} / \sin \beta \qquad (2.2.3\text{–}2)$$

with O_{av} being the average projection of leaves in the direction of a solar beam. For a uniform azimuthal orientation of the leaves in a canopy, O_{av} is in case of $\beta \geq \beta_L$:

$$O_{av} = \sin\beta \ \ \sin\beta_L \tag{2.2.3–3}$$

and in case of $\beta < \beta_L$:

$$O_{av} = 2\,(\sin\beta\cos\beta_L \arcsin(\tan\beta/\tan\beta_L) + \sqrt{\sin^2\beta_L - \sin^2\beta}) \ / \ \pi \tag{2.2.3–4}$$

where β_L is the leaf angle inclination. Details for derivation of eq. (2.2.3–4) are given by GOUDRIAAN (1988).

Table 4: Symbols, definitions and units used for modelling absorbed radiation. Crop-specific input parameters are marked with an asterisk.

Symbol	Definition	Unit
f_{shade}	fraction of shaded leaves in a canopy	-
f_{sun}	fraction of sunlit leaves in a canopy	-
$f_{sun,i}$	sunlit fraction of leaves at canopy depth with L_i	-
$I_{b,top}$	incident direct-beam radiation above the canopy	W m^{-2}
I_{beam}	absorbed direct-beam radation	W m^{-2}
I_c	absorbed radiation by canopy	W m^{-2}
$I_{c,shade}$	absorbed radiation by shaded leaves of canopy	W m^{-2}
$I_{c,sun}$	absorbed radiation by sunlit leaves of canopy	W m^{-2}
$I_{d,top}$	incident diffuse radiation above the canopy	W m^{-2}
$I_{diffuse}$	absorbed diffuse radiation	W m^{-2}
$I_{scat\ beam}$	absorbed scattered beam radiation	W m^{-2}
k_b	direct beam extinction coefficient	m^2 ground m^{-2} leaf
L	green leaf area index of canopy	m^2 leaf m^{-2} ground
L_i	L counted from top to the i-th layer of canopy	m^2 leaf m^{-2} ground
L_T	total leaf area index	m^2 leaf m^{-2} ground
O_{av}	average projection of leaves in the direction of a solar beam	m^2 ground m^{-2} leaf
β	solar elevation	degrees
β_L *	leaf angle inclination in canopy	degrees

The sunlit foliage of the whole canopy, f_{sun}, is given as (DE PURY & FARQUHAR 1997):

$$f_{sun} = \frac{1}{L}\int_0^L \exp(-k_b L_i)\ \mathrm{d}\ L_i = \left(1 - \exp(-k_b L_i)\right) / (k_b L) \tag{2.2.3–5}$$

Consequently, the shaded fraction is:

$$f_{shade} = 1 - f_{sun} \tag{2.2.3–6}$$

Not the incident radiation itself is a key variable for crop growth modelling but the amount of absorbed radiation which results from extinction and reflection processes within the canopy (Fig. 15). Different light extinction coefficients for direct and diffuse radiation as well as scattered radiation have to be accounted for when modelling the interaction of light with crop canopies. The sum of the absorbed radiation in the sunlit ($I_{c,sun}$) and shaded fraction ($I_{c,shade}$) constitutes the total absorbed irradiance (I_c).

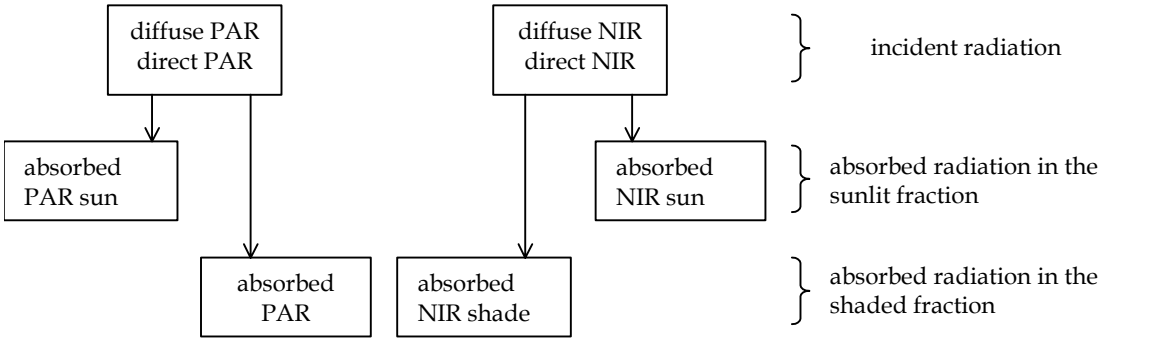

Fig. 15: Components of absorbed radiation in a canopy.

Radiation absorbed by a canopy, per unit ground area, consists of direct and diffuse components which are differently attenuated within the canopy (DE PURY & FARQUHAR 1997):

$$I_c = \left(1-\rho_{cb}\right) I_{b,top} \left(1-\exp\left(-k'_b L\right)\right) + \left(1-\rho_{cd}\right) I_{d,top} \left(1-\exp\left(-k'_d L\right)\right) \qquad (2.2.3\text{–}7)$$

Table 5: Coefficients for modelling absorbed radiation.

Symbol	Calculation		Unit
σ	leaf scattering coefficient (0.2 for PAR, 0.8 for NIR) (GOUDRIAAN & VAN LAAR 1994)		-
ρ_h	canopy reflection coefficient for horizontal leaves $\rho_h = \left(1-\sqrt{1-\sigma}\right) / \left(1+\sqrt{1-\sigma}\right)$ (GOUDRIAAN & VAN LAAR 1994)	(2.2.3–8)	-
ρ_{cb}	canopy reflection coefficient for direct-beam radiation $\rho_{cb} = 1 - \exp\left(-2\,\rho_h\, k_b / \left(1+k_b\right)\right)$ (GOUDRIAAN 1977, cited by YIN & VAN LAAR 2005)	(2.2.3–9)	-
ρ_{cd}	canopy reflection coefficient for diffuse radiation (0.057 for PAR, 0.389 for NIR) (GOUDRIAAN & VAN LAAR 1994)		-
k'_b	extinction coefficient for beam and scattered-beam radiation (GOUDRIAAN & VAN LAAR 1994) $k'_b = k_b \sqrt{1-\sigma}$	(2.2.3–10)	m^2 ground m^{-2} leaf
k'_d	extinction coefficient for diffuse and scattered-diffuse radiation (for standard overcast sky conditions) (GOUDRIAAN 1988) $k'_d = -\left(1/L_T\right) \ln \begin{pmatrix} 0.178\,\exp\left(-k_{b15}\sqrt{1-\sigma}\,L_T\right) \\ +0.514\,\exp\left(-k_{b45}\sqrt{1-\sigma}\,L_T\right) \\ +0.308\,\exp\left(-k_{b75}\sqrt{1-\sigma}\,L_T\right) \end{pmatrix}$	(2.2.3–11)	m^2 ground m^{-2} leaf

Table 5 shows values and calculations, respectively, of several coefficients used in equations (2.2.3–5) and (2.2.3–7).

The leaf scattering coefficient is the sum of leaf reflection and transmission coefficients and influences the value of the reflection and extinction coefficients. A high scatter coefficient will result in a high canopy reflection (GOUDRIAAN & VAN LAAR 1994). For direct-beam radiation, the canopy reflection coefficient (ρ_{cb}) depends on leaf angle inclination and solar elevation and is associated with the canopy reflection coefficient for horizontal leaves (GOUDRIAAN 1977, cited by YIN & VAN LAAR 2005).

For estimating the profile of diffuse sky radiation in the canopy, GOUDRIAAN (1988) presented a method to calculate the extinction coefficient for diffuse and scattered-diffuse radiation (k'_d). Diffuse radiation originates from different "ring zones" of the sky. Consequently, the correspondent extinction coefficients can be estimated by substituting solar height in equations (2.2.3–2), (2.2.3–3) and (2.2.3–4) for zone elevation. Three zone classes with centres at 15°, 45° and 75° are sufficient for an accurate description of the light profile. Subscripts of k_b in eq. (2.2.3–11) refer to these elevations of incoming radiation. Each summand is weighted according to the contribution from the three zones of a standard overcast sky with equal radiance all over. Details are given by GOUDRIAAN (1988).

DE PURY & FARQUHAR (1997) present an approach for deriving the canopy reflection coefficient for diffuse radiation (ρ_{cd}), but like in the model GECROS, standard values for spherical leaf angle distribution (where all orientations are equally represented) and uniform pattern of diffuse radiation across the sky are used (GOUDRIAAN & VAN LAAR 1994).

Scattering of direct-beam rays which produces further diffuse radiation is taken into account, so radiation absorbed by sunlit leaves is given as the sum of direct-beam (I_{beam}), diffuse ($I_{diffuse}$) as well as scattered direct-beam ($I_{scat\ beam}$) radiation (DE PURY & FARQUHAR 1997):

$$I_{beam} = I_{b,top}\left(1-\sigma\right)\left(1-\exp\left(-k_b L\right)\right) \qquad (2.2.3\text{–}12)$$

$$I_{diffuse} = I_{d,top}\left(1-\rho_{cd}\right)\frac{k'_d\left(1-\exp\left(-\left(k'_d+k_b\right)L\right)\right)}{k'_d+k_b} \qquad (2.2.3\text{–}13)$$

$$I_{\text{scat beam}} = I_{\text{b,top}} \left(\begin{array}{l} (1-\rho_{\text{cb}}) \; \dfrac{k'_{\text{b}} \left(1-\exp-\left(k'_{\text{b}}+k_{\text{b}} \right) L \right)}{k'_{\text{b}}+k_{\text{b}}} \\ -\left(1-\sigma \right) \dfrac{1-\exp\left(-2\,k_{\text{b}}\,L \right)}{2} \end{array} \right) \qquad (2.2.3\text{–}14)$$

$$I_{\text{c,sun}} = I_{\text{beam}} + I_{\text{diffuse}} + I_{\text{scat beam}} \qquad (2.2.3\text{–}15)$$

Absorbed radiation of the shaded leaves can be expressed as the sum of components of diffuse and scattered direct-beam radiation, but can more simply be calculated as:

$$I_{\text{c,shade}} = I_{\text{c}} - I_{\text{sun}} \qquad (2.2.3\text{–}16)$$

Because of the different scattering features (see coefficients listed in Table 5) the above equations (2.2.3–7) to (2.2.3–14) have to be calculated separately for PAR and NIR radiation (GOUDRIAAN & VAN LAAR 1994). The sum of absorbed PAR and absorbed NIR gives the total absorbed short-wave radiation.

Boundary layer conductances

Since the boundary layer conductances for heat as well as for water vapour are dependent on wind speed, they vary with depth in the canopy. Scaling up has to be done separately for the entire canopy, the sunlit and the shaded fraction.

Table 6: Symbols, definitions and units used for scaling conductances.
Crop-specific input parameters are marked with an asterisk.

Symbol		Definition	Unit
k_{w}		wind speed extinction coefficient	m² ground m^{-2} leaf
w	*	leaf blade width	m
u		wind speed	m s^{-1}
g_{bc}		total boundary layer conductance in canopy	m s^{-1}
$g_{\text{bc, sun}}$		boundary layer conductance for sunlit fraction of canopy	m s^{-1}
$g_{\text{bc, shade}}$		boundary layer conductance for shaded fraction of canopy	m s^{-1}

The attenuation of wind speed u in the canopy follows an exponential profile (LEUNING *et al.* 1995). Consequently, the boundary layer conductance (for heat) for the complete canopy (g_{bc}) can be expressed as:

$$g_{\text{bc}} = 0.01 \sqrt{u / w} \left(1 - \exp\left(-0.5\,k_{\text{w}}\,L \right) \right) / \left(0.5\,k_{\text{w}} \right) \qquad (2.2.3\text{–}17)$$

where w refers to crop-specific leaf width and k_{w} is the extinction coefficient of wind speed in the canopy. Boundary layer conductance (for heat) for the sunlit ($g_{\text{bc,sun}}$) fraction of the canopy is:

$$g_{\mathrm{bc,\,sun}} = 0.01\ \sqrt{u / w}\ \left[1 - \exp\left(-\left(0.5\,k_{\mathrm{w}} + k_{\mathrm{b}}\right)L\right)\right] / \left(0.5\,k_{\mathrm{w}} + k_{\mathrm{b}}\right) \qquad (2.2.3\text{–}18)$$

The difference between g_{bc} and $g_{\mathrm{bc,sun}}$ gives the boundary layer conductance (for heat) for the shaded fraction ($g_{\mathrm{bc,shade}}$):

$$g_{\mathrm{bc,\,shade}} = g_{\mathrm{bc}} - g_{\mathrm{bc,\,sun}} \qquad (2.2.3\text{–}19)$$

Derivation of equations (2.2.3–17) and (2.2.3–18) is given in Appendix A.

For water vapour, corresponding boundary layer conductances are derived by multiplying g_{bc}, $g_{\mathrm{bc,sun}}$, and $g_{\mathrm{bc,shade}}$ by the factor 1.075. This value considers the dissimilar velocity of boundary layer transport regarding heat and water vapour (GOUDRIAAN & VAN LAAR 1994). Reciprocal values of the conductances give boundary layer resistances. The total value of the turbulence resistance r_{t} is split into sunlit and shaded canopy fractions in linear proportion to f_{sun} and f_{shade}.

The reduction of potential transpiration to actual transpiration in case of water shortage is carried out according to sun and shade fractions. Subsequently, rates of actual photosynthesis are calculated separately for sunlit and shaded leaves.

Leaf nitrogen profile

The parameters V_{cmax25} and J_{max25} used for simulating photosynthesis are dependent on leaf nitrogen content n. The difference between n and the crop-specific minimum leaf nitrogen content required to support photosynthesis, n_{b}, yields the photosynthetically active leaf nitrogen content. Because n is supposed to decrease exponentially with depth in a canopy (YIN *et al.* 2000), photosynthetically active leaf nitrogen has to be scaled up separately for the entire canopy (N_{c}), for its sunlit fraction ($N_{\mathrm{c,sun}}$) and for its shaded fraction ($N_{\mathrm{c,shade}}$):

$$N_{\mathrm{c}} = n_0\ \left(1 - \exp\left(-k_{\mathrm{n}}\,L\right)\right)\ /\ k_{\mathrm{n}} - n_{\mathrm{b}}\,L \qquad (2.2.3\text{–}20)$$

$$N_{\mathrm{c,sun}} = n_0\ \left[1 - \exp\left(-\left(k_{\mathrm{n}} + k_{\mathrm{b}}\right)L\right)\right]\ /\ \left(k_{\mathrm{n}} + k_{\mathrm{b}}\right) - n_{\mathrm{b}}\ \left(1 - \exp\left(-k_{\mathrm{b}}\,L\right)\right)\ /\ k_{\mathrm{b}} \qquad (2.2.3\text{–}21)$$

$$N_{\mathrm{c,shade}} = N_{\mathrm{c}} - N_{\mathrm{c,sun}} \qquad (2.2.3\text{–}22)$$

Derivation of equations (2.2.3–20) and (2.2.3–21) is given in Appendix A. Calculations of n_0 and k_{n} are specified in the chapter 2.2.10 (*Leaf area and senescence*).

Table 7: Symbols, definitions and units used for scaling leaf nitrogen content. Crop-specific input parameters are marked with an asterisk.

Symbol		Definition	Unit
n_b	*	minimum leaf N for photosynthesis	g N m^{-2} leaf
n_0		canopy top-leaf N	g N m^{-2} leaf
k_n		N extinction coefficient	m^2 ground m^{-2} leaf
N_c		total photosynthetically active N in canopy	g N m^{-2}
$N_{c,sun}$		photosynthetically active N in sunlit leaves of canopy	g N m^{-2}
$N_{c,shade}$		photosynthetically active N in shaded leaves of canopy	g N m^{-2}

The concepts of scaling described in this subchapter allow for the dynamic modelling of sun- and shade-specific values of absorbed radiation, conductances, resistances, and photosynthetically active leaf nitrogen contents. These data are implemented for modelling photosynthesis and transpiration rates separately for sunlit and shaded fractions of the canopy (see chapter 2.2.2: *Photosynthesis and transpiration*). Results for sun and for shade leaves are summed to give total fluxes.

2.2.4 Respiration

A fraction of the daily carbon fixed by photosynthesis is dissipated due to respiration (oxidation of carbohydrate to CO_2 and water). Respiration includes release of CO_2 due to various biochemical processes and in contrast to photosynthetic carbon fixation is poorly represented in ecosystem models (CANNELL & THORNLEY 2000).

Plants respire substrates to produce carbon-skeleton intermediates, usable energy, and reducing power to support biosynthesis of new biomass and interrelated processes such as active transport of compounds. In addition, respiration is required to maintain existing biomass in a functional state. To simulate crop growth and its responses to environmental factors, relationships between respiration, growth and maintenance have to be quantified (AMTHOR 2000).

When considered over a 24-hour period, respiration can be 20 % of gross photosynthesis for a fast-growing plant community and can even exceed 50 % as the community matures. For a crop, respiration averaged over a growing season lies typically in the range of 30 to 50 % of gross photosynthesis (NOBEL 2005).

This rather large respiratory flux is tightly interrelated to processes of e.g. growth, allocation and nitrogen uptake. Resulting seasonal variation regarding the magnitude

and composition of total plant respiration during crop growth should be accounted for in models (CANNELL & THORNLEY 2000).

The algorithms used in the model GECROS (YIN & VAN LAAR 2005) for modelling respiration are adopted in the DANUBIA crop growth model. GECROS implements the theoretical framework presented by AMTHOR (2000) and CANNELL & THORNLEY (2000). Respiratory fluxes are grouped into two categories depending on energy requirement for biosynthesis of new structural biomass (growth respiration) and for maintenance of existing biomass (maintenance respiration). The second category integrates respiration due to various energy-requiring processes (as listed in Fig. 16). The respiratory cost associated with each process can be explicitly defined considering the metabolic costs and stoichiometries of CO_2 release. Multiplying the specific respiratory cost with the corresponding rate of the process (e.g. nitrate uptake rate) gives the respiratory flux for each component of maintenance respiration.

Thus respiration is related (semi-)mechanistically to underlying physiology and biochemistry (AMTHOR 2000).

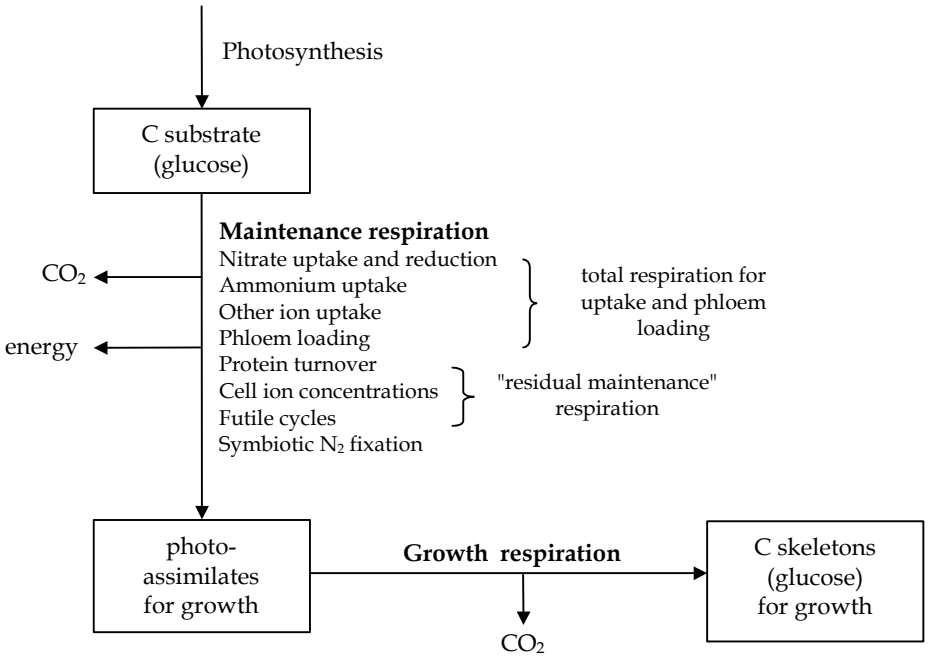

Fig. 16: Simplified scheme of the component respiration processes (following CANNELL & THORNLEY 2000). Arrows indicate fluxes.

Growth respiration

According to CANNELL & THORNLEY (2000), growth respiration is defined in terms of "growth yield", i.e. the units of carbon materialized in new biomass per unit of glucose carbon utilized for growth. This so-called growth efficiency depends on the chemical composition of the newly synthesized plant tissue. Its compounds are categorized into 5 distinct classes: carbohydrates, proteins, lipid, lignin and organic acids. Considering the diverse glucose requirements of these classes, growth efficiency for storage organs $Y_{G,S}$ is calculated as:

$$Y_{G,S} = \frac{30\left(0.444\, f_{car} + 0.531\, f_{pro} + 0.774\, f_{lip} + 0.667\, f_{lig} + 0.368\, f_{oac}\right)}{12\left(1.275\, f_{car} + 1.887\, f_{pro} + 3.189\, f_{lip} + 2.231\, f_{lig} + 0.954\, f_{oac}\right)} \qquad (2.2.4\text{–}1)$$

where f_{car}, f_{pro}, f_{lip}, f_{lig}, and f_{oac} are crop-specific fractions of the above-mentioned classes in newly constructed biomass of storage organs. The molar masses of glucose (CH_2O) and carbon are 30 and 12 g mol^{-1}, respectively. The coefficients in the numerator of eq. (2.2.4–1) represent the fractions of carbon in each class, whereas the coefficients in the denominator show the corresponding glucose requirements per unit weight (PENNING DE VRIES *et al.* 1989). Lipid and lignin are constructed at relatively high costs in comparison with the other classes.

Growth efficiency for vegetative organs $Y_{G,V}$ is a crop-specific input parameter, ignoring differences in chemical composition.

The "construction cost" or "glucose requirement" (carbon of a glucose substrate required per unit carbon of new biomass) is given by the reciprocal of growth efficiency. The "growth coefficient" (carbon respired per carbon unit of new biomass synthesized from a glucose substrate) is ((1 – growth efficiency) / growth efficiency) (CANNELL & THORNLEY 2000).

For calculating daily growth respiration R_G, daily increases in biomass are multiplied by the growth coefficient. Because of different values for $Y_{G,V}$ and $Y_{G,S}$, growth respiration is calculated separately for vegetative and storage organs. The sum of both, converted to units of g CO_2 m^{-2} d^{-1}, results in R_G.

Respiration for nitrate uptake and reduction

Respiratory cost for nitrate uptake is estimated as 0.34 g C (g NO_3-N)$^{-1}$. To be disposable for plant metabolism, absorbed nitrate is reduced to the ammonium level. The cost of nitrate reduction is about 1.71 g C (g reduced NO_3-N)$^{-1}$ (THORNLEY & CANNELL 2000). Total cost related to nitrate uptake results in 2.05 g C (g NO_3-N)$^{-1}$. Thus respiration for nitrate uptake and reduction ($R_{M,NO3}$) is:

$$R_{M,NO3} = 2.05\ U_{NO3}\ (\ 44 / 12\ ) \qquad (2.2.4\text{–}2)$$

where U_{NO3} is daily nitrate uptake and the molar masses of CO_2 (44 g mol^{-1}) and carbon (12 g mol^{-1}) convert units of carbon to units of CO_2.

Respiration for ammonium uptake

In analogy, respiration for ammonium uptake ($R_{M,NH4}$) is:

$$R_{M,NH4} = 0.17\ U_{NH4}\ (\ 44 / 12\ ) \qquad (2.2.4\text{–}3)$$

assuming a respiratory cost 0.17 g C (g NH_4-N)$^{-1}$ which is half the value for nitrate uptake (details are given in CANNELL & THORNLEY 2000). U_{NH4} denotes daily ammonium uptake.

Respiration for uptake of other ions

Uptake of minerals other than nitrogen is likewise associated with respiration. These minerals (phosphorus, potassium, calcium, magnesium etc.) constitute approximately 5 % of plant dry matter. To quantify the mineral uptake rate, it is related to daily production of dry matter. Mineral uptake and within-plant transport are assumed to cause respiratory costs of 0.06 g C g^{-1} (THORNLEY & CANNELL 2000). Consequently, respiratory cost of mineral uptake $R_{M,min}$ is expressed as:

$$R_{M,min} = 0.06\ 0.05\ /\ 0.454\ Y_{G,V}\ P_{Cnet} \qquad (2.2.4\text{–}4)$$

where 0.454 represents an average carbon fraction in crop biomass, $Y_{G,V}$ is the growth efficiency for vegetative organs, and P_{Cnet} is daily net photosynthesis.

Respiration for phloem loading

Sugars, amides, and other compounds are transported via the phloem within the plant. In this context, the respiratory cost for transport of carbon from the shoot into the root

system is considered and amounts to 0.06 g C g^{-1}. Details are given by AMTHOR (2000) and THORNLEY & CANNELL (2000). Respiration for phloem loading $R_{M,phl}$ is estimated as:

$$R_{M,phl} = 0.06 \ \lambda_{C,R} \ P_{net} \qquad (2.2.4–5)$$

where $\lambda_{C,R}$ is the fraction of newly assimilated C partitioned to root.

Respiratory cost for remobilization of carbon reserves (also assumed to be 0.06 g C g^{-1}) is directly subtracted when calculating remobilized carbon.

The sum of $R_{M,NO3}$, $R_{M,NH4}$, $R_{M,min}$ and $R_{M,phl}$ gives the total respiration for uptake and phloem loading ($R_{M,UP}$).

"Residual maintenance" respiration

Processes of protein turnover, maintenance of cell ion concentration, and all forms of wastage respiration are energy-requiring processes. Because the related respiratory costs concerning these processes are not as clearly defined as the above-mentioned costs, they are grouped together as "residual maintenance" respiration $R_{M,res}$ (CANNELL & THORNLEY 2000). $R_{M,res}$ is scaled with total nitrogen content in plant tissue (N_T):

$$R_{M,res} = 0.218 \left(N_T - n_{Lmin} \ W_S - n_{Rmin} \ W_R \right) \left(44 / 12 \right) \qquad (2.2.4–6)$$

W_S and W_R denote shoot and root weight, and n_{Lmin} and n_{Rmin} are the minimum nitrogen concentration in leaf and root, respectively. The daily specific rate of maintenance respiration is assumed to be 0.218 g C g^{-1} N d^{-1}.

The sum of $R_{M,UP}$ and $R_{M,res}$ gives the non-growth components of respiration R_M (excluding the cost of nitrogen fixation).

Respiration for symbiotic di-nitrogen fixation

In case of leguminous crops, respiratory cost of di-nitrogen fixation (R_{Nfix}) is estimated as:

$$R_{Nfix} = c_{Nfix} \ N_{fix} \left(44 / 12 \right) \qquad (2.2.4–7)$$

where N_{fix} denotes the flux of fixed nitrogen and c_{Nfix} is the proportion of substrate carbon respired and fixed nitrogen (THORNLEY & CANNELL 2000). R_{Nfix} includes respiratory costs of growth of nodule symbiotic structures and maintenance. In GECROS, c_{Nfix} is set to 6 g C g^{-1} N.

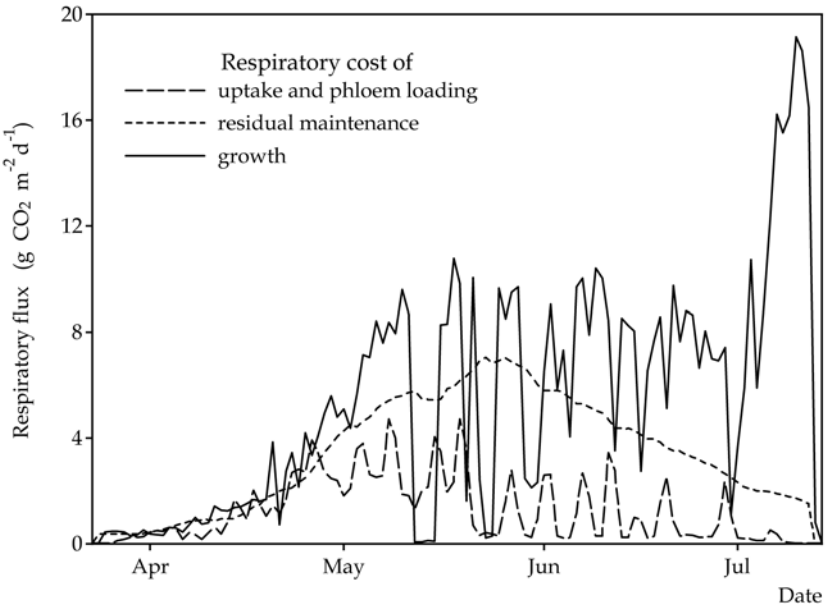

Fig. 17: Exemplary illustration of modelled respiratory fluxes during a crop growth season (data generated by the DANUBIA crop growth model, after YIN & VAN LAAR 2005).

Fig. 17 exemplarily shows the courses and dimensions of the different respiratory fluxes during crop growth. The proportions of the various respiration components change depending on crop growth and environmental conditions.

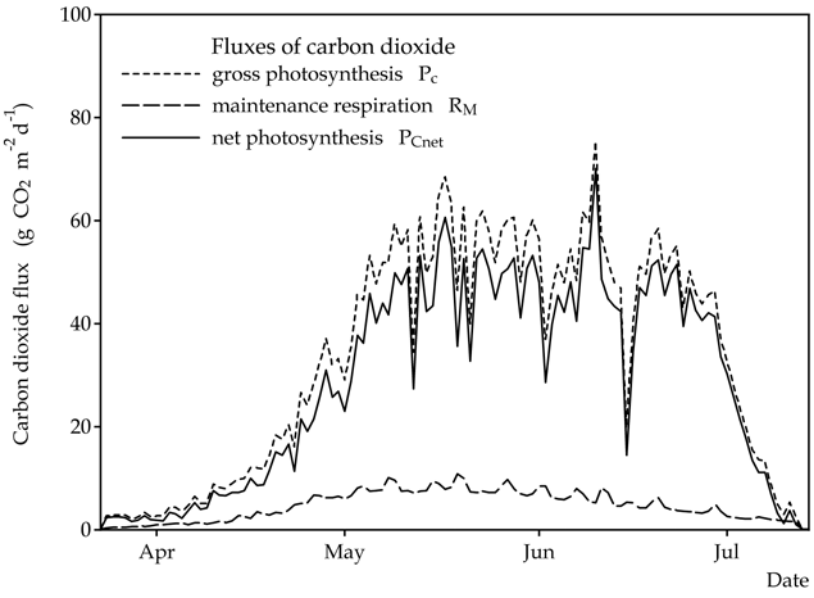

Fig. 18: Exemplary illustration of modelled carbon dioxide fluxes during a crop growth season (data generated by the DANUBIA crop growth model).

Taking account of the respiratory losses, daily net canopy photosynthesis P_{Cnet} results from:

$$P_{Cnet} = P_C - R_M - R_{Nfix} \quad (2.2.4\text{–}8)$$

P_{Cnet} (expressed in units of CO_2) quantifies the amount of photo-assimilates available for investing into structural material (see Fig. 18). Growth respiration is accounted for when modelling carbon production rate (see chapter 2.2.9: *Allocation of carbon and nitrogen*).

Table 8: Symbols, definitions and units for modelling respiration.
Crop-specific input parameters are marked with an asterisk.

Symbol	Definition	Unit
c_{Nfix}	carbon cost of symbiotic N fixation	g C g^{-1} N
f_{car}	fraction of carbohydrates in biomass of organs	g carbohydrate g^{-1}
f_{lig} *	fraction of lignin in biomass of organs	g lignin g^{-1}
f_{lip} *	fraction of lipid in biomass of organs	g lipid g^{-1}
f_{oac} *	fraction of organic acids in in biomass of organs	g organic acid g^{-1}
f_{pro}	fraction of proteins in biomass of organs	g protein g^{-1}
N_{fix}	symbiotically fixed N	g N m^{-2} d^{-1}
N_T	total N in living shoot and root	g N m^{-2}
P_C	daily gross canopy photosynthesis	g CO_2 m^{-2} d^{-1}
P_{Cnet}	daily net canopy photosynthesis	g CO_2 m^{-2} d^{-1}
R_G	growth respiration	g CO_2 m^{-2} d^{-1}
R_M	non-growth components of respiration (excluding the cost of N-fixation)	g CO_2 m^{-2} d^{-1}
$R_{M,min}$	respiratory cost of minerals uptake	g CO_2 m^{-2} d^{-1}
$R_{M,NH4}$	respiratory cost of ammonium-N uptake	g CO_2 m^{-2} d^{-1}
$R_{M,NO3}$	respiratory cost of nitrate-N uptake and reduction	g CO_2 m^{-2} d^{-1}
$R_{M,phl}$	respiratory cost due to phloem loading of C assimilates to roots	g CO_2 m^{-2} d^{-1}
$R_{M,res}$	residual maintenance respiration	g CO_2 m^{-2} d^{-1}
$R_{M,UP}$	total respiration for uptake and phloem loading	g CO_2 m^{-2} d^{-1}
R_{Nfix}	respiratory cost of N_2 fixation	g CO_2 m^{-2} d^{-1}
$Y_{G,S}$	storage organ (seed) growth efficiency	g C g^{-1} C
$Y_{G,V}$ *	vegetative-organ (leaf, stem, root) growth efficiency	g C g^{-1} C

2.2.5 Root growth

Root growth and above-ground plant growth are interacting processes. The root system provides plants with water and nutrients to maintain transpiration and assimilation which in turn determines root growth. Root distribution and soil conditions control uptake rates of water and nitrogen. Both soil water and nitrogen resources are decreased by root absorption.

In DANUBIA, the soil compartment is considered to be composed of horizontal layers, assuming homogeneous soil characteristics and uniform root distribution in every layer. Each soil layer has a set of constant characteristics (e.g. thickness, soil texture) and dynamic attributes like water content, temperature and nitrogen concentration. In the following, the subscript *i* refers to soil layer-specificity.

The DANUBIA soil model needs information on root length density in each soil layer. To meet this requirement the simulation of root distribution is adapted from the CERES-models (JONES & KINIRY, eds, 1986, RITCHIE & GODWIN 2000). In the model GECROS (YIN & VAN LAAR 2005), root length density for every soil layer is not explicitly simulated. For calculating rooting depth, a hybrid approach combining CERES and GECROS is chosen.

To determine potential uptake of water and nitrogen, root length density in each soil layer (R_{LDi}) is simulated based on soil conditions and the quantity of assimilates partitioned to roots.

First, the newly created root biomass (ΔW_{RT}, g m^{-2} d^{-1}) is transformed into daily root length increase (ΔR_L, cm root cm^{-2} ground) via a plant-specific conversion factor (R_{LM}, cm g^{-1}):

$$\Delta R_L = \Delta W_{RT} \; R_{LM} \tag{2.2.5–1}$$

A uniform distribution of roots all over the soil area is assumed. To distribute the new root biomass throughout the soil layers, current rooting depth is required.

Rooting depth (D) is initialized at sowing depth. During the phenological phase of germination, rooting depth increases daily as a linear function of daily thermal time for emergence (TT_{em}) (calculation see chapter 2.2.1: *Phenological development*, eq. (2.2.1–5))

$$D = D + F_{\Delta D,em} \; TT_{em} \tag{2.2.5–2}$$

where $F_{\Delta D,em}$ is a plant-specific coefficient.

According to GECROS, the daily rate of change in root depth (ΔD) after emergence is calculated as:

$$\Delta D = \min \left[\left(D_{max} - D \right) / \Delta t, \; \Delta W_{RT} / \left(w_{Rb} + k_R \, W_{RT} \right) \right] \tag{2.2.5–3}$$

where "min" specifies the minimum value of the two terms in square brackets. Rooting depth is restricted to a crop- or genotype-specific maximum value, D_{max}. The time-step of dynamic simulation is represented by Δt and the rate of change in total (living and dead) root weight is defined as $\Delta W_{RT.}$ The critical root weight density w_{Rb} restricts effective water or nutrient uptake (assumed value: 0.25 g m^{-2} cm^{-1}). The decline in root weight density with soil depth k_R is calculated as:

$$k_R = -\ln 0.05 \; / \; D_{max} \tag{2.2.5–4}$$

Details for the derivation of k_R and eq. (2.2.5–3) are given in Appendix A.

If the soil at the deepest root level is dry or if the plant itself suffers from water stress, the root depth is adjusted following the CERES-approach:

$$D = D + \Delta D \min\left(2 F_{PW}, F_{SW,i}\right) \quad (2.2.5\text{–}5)$$

where F_{PW} (plant water stress factor) indicates plant stress, based on the ratio of potential root water absorption and potential transpiration (see chapter 2.2.6: *Water uptake*). The soil water deficit factor F_{SW} quantifies soil water shortage in the deepest layer where roots grow (eq. (2.2.5–7)). In this way, root growth is restricted to soil depths with sufficient water content.

To estimate root distribution along the penetrated depth, a zero-to-one weighting factor for root length density (F_{RLD}) is calculated for each rooted soil layer:

$$F_{RLDi} = \min\left(F_{SW}, F_{SNi}\right) F_{RH} \quad z_i \quad (2.2.5\text{–}6)$$

where z indicates the soil layer thickness. Soil water deficit as well as nitrogen scarcity and soil compaction are assumed to limit root growth. The soil water deficit factor (F_{SW}), the layer-specific mineral nitrogen deficit factor (F_{SN}), and the "root hospitality factor" (F_{RH}) are defined as limiting factors. Each factor ranges from 0 for strong limitation to 1 for no limitation.

The soil water deficit factor F_{SW} equals 1 unless the volumetric soil water content θ in the deepest rooted layer declines below 25 % of the total plant-extractable soil water. In that case:

$$F_{SW} = \left(\theta_i - \theta_{WP_i}\right) / \left(0.25 \left(\theta_{FC_i} - \theta_{WP_i}\right)\right) \quad (2.2.5\text{–}7)$$

where all values of the soil hydrological parameters refer to the deepest layer reached by roots. The difference between the drained upper limit soil water content θ_{FCi} (equal to field capacity), and the lower limit of plant-extractable soil water θ_{WPi} (equal to wilting point) gives the total plant-extractable soil water.

Nitrogen shortage is expressed using an exponential factor F_{SN}:

$$F_{SNi} = 1 - 1.17 \exp\left(-0.15 N_{totali}\right) \quad (2.2.5\text{–}8)$$

where N_{totali} is the sum of ammonium and nitrate in the respective layer. F_{SN} is limited by a minimum plant-specific value (F_{SNmin}).

An user-defined "root hospitality factor" (F_{RH}) can be included optionally to mimic the mechanical impedance for root expansion. In this version of the DANUBIA crop growth model, F_{RH} is set to 1 (non-limiting).

The root length density factor of the deepest layer with roots is adjusted according to root depth. The sum of the root length density factors over the layers gives the total root length density factor (F_{RLDP}). The new root length density (R_{LD}) in cm cm^{-3} for each layer is added:

$$R_{LD_i} = R_{LD_i} + \left(F_{RLD_i} / F_{RLDP} \right) \left(\Delta R_L / z_i \right) - F_{RS} \; R_{LD_i} \qquad (2.2.5\text{–}9)$$

where the quotient of F_{RLD} and F_{RLDP} is the fraction of new root growth at each soil depth. The subtrahend accounts for root senescence. In the CERES-models, F_{RS} represents a constant, plant-specific root senescence factor. In the DANUBIA crop growth model, F_{RS} is a dynamically calculated factor, taking into account the simulated daily senesced root mass.

Table 9: Symbols, definitions and units for modelling root distribution.
Crop-specific input parameters are marked with an asterisk.

Symbol		Definition	Unit
D		rooting depth	cm
D_{max}	*	maximum rooting depth	cm
F_{PW}		plant water stress factor	-
F_{RH}		root hospitality factor	-
F_{RLDi}		factor for root length density in layer i	-
F_{RLDP}		factor for root length density in the soil profile	-
F_{RS}		root senescence factor	-
F_{SNi}		factor describing mineral N availability in layer i	-
F_{SNmin}	*	minimum value of F_{SN} (crop-specific)	-
F_{SW}		factor describing soil water deficit	-
$F_{\Delta D,em}$	*	factor for root depth increase before emergence	-
k_R		extinction coefficient of root weight density over soil depth	cm^{-1}
N_{totali}		sum of ammonium and nitrate in layer i	mg elemental N kg^{-1} soil
R_{LDi}		root length density of soil layer i	cm root cm^{-3} soil
R_{LM}	*	root length to mass ratio	cm root length g^{-1} root
TT_{em}		daily thermal time for emergence	°C day
w_{Rb}		critical root weight density	g m^{-2} cm^{-1}
z_i		thickness of soil layer i	cm
ΔD		rate of change in rooting depth	cm d^{-1}
ΔR_L		root length increase	cm root cm^{-2} ground
Δt		time step of dynamic simulation	d
ΔW_{RT}		rate of change in total root weight	g m^{-2} d^{-1}
θ_{FCi}		θ in layer i at field capacity	cm^3 water cm^{-3} soil
θ_i		volumetric soil water content in layer i	cm^3 water cm^{-3} soil
θ_{WPi}		θ in layer i at wilting point	cm^3 water cm^{-3} soil

Root length increase and rooting depth are simulated in a daily time-step. Root length density is updated in an hourly timestep to account for short-term conditions of water

stress. Soil layer-specific root length densities are exported to the DANUBIA soil model as input parameters for simulating nitrogen transformation processes.

2.2.6 Water uptake

Water uptake by roots is a central process in plant growth. Soil water is absorbed by roots, transported to the shoots of plants and partially released to the air by transpiration. Hence, plants connect water fluxes in soil and atmosphere.

According to the CERES-models (JONES & KINIRY, eds, 1986, RITCHIE & GODWIN 2000), root water absorption is determined by the soil water supply, root distribution and atmospheric demand.

First, soil-limited water uptake per unit of root length U_{Wr} is calculated as a function of root length density R_{LD} and available soil water in each soil layer i:

$$U_{\mathrm{Wr}i} = \frac{0.00267 \exp\left(62\left(\theta_i - \theta_{\mathrm{WP}i}\right)\right)}{6.68 - \ln\left(R_{\mathrm{LD}i}\right)} \qquad (2.2.6\text{–}1)$$

This equation is derived from the theory of radial flow to single roots and is based on simplified assumptions: a constant root radius and a stable water potential gradient between root and soil (RITCHIE 1998). Details for the derivation of eq. (2.2.6–1) are given in WANG & SMITH (2004). If the soil water content θ is below the wilting point θ_{WP}, no water uptake takes place. U_{Wr} is limited to a maximum flow rate of 0.03 $\mathrm{cm^3\,cm^{-1}\,d^{-1}}$.

Considering soil layer thickness z and root length density, U_{Wr} is converted to potential water uptake in each soil layer (U_{Wp}):

$$U_{\mathrm{Wp}i} = U_{\mathrm{Wr}i}\ R_{\mathrm{LD}}\ z_i \qquad (2.2.6\text{–}2)$$

Water uptake and transpiration are interrelated processes. Potential transpiration rate is governed by atmospheric conditions, whereas actual transpiration rate relies on water supply from the soil. The minimum value of the total potential water uptake from the rooted soil profile U_{WpP} (sum of values of $U_{\mathrm{Wp}i}$ in all layers) and the potential transpiration rate (E_{p}, converted to cm $\mathrm{h^{-1}}$), gives the actual total water uptake (U_{WaP}).

If the potential transpiration rate is less than U_{WpP}, actual water uptake in each layer ($U_{\mathrm{Wa}i}$) is reduced proportionally:

$$U_{\mathrm{Wa}i} = U_{\mathrm{Wp}i}\ \left(E_{\mathrm{p}} \,/\, U_{\mathrm{WpP}}\right) \qquad (2.2.6\text{–}3)$$

In the reverse case, when potential transpiration exceeds potential total water uptake, plants suffer from water stress because the transpiration demand cannot be met by root absorption. In this case, actual transpiration (E_a) is set equal to potential total water uptake. Under limiting soil water conditions plants curtail transpiration by partial stomata closure. According to the reduced transpiration rate, gas exchange processes have to be recalculated in the model (see chapter 2.2.2: *Photosynthesis and transpiration*). The ratio of potential water uptake and potential transpiration is defined as the zero-to-unity plant water stress factor (F_{PW}).

Table 10: Symbols, definitions and units for modelling water uptake.

Symbol	Definition	Unit
U_{Wai}	actual water uptake from soil layer *i*	cm h^{-1}
U_{Wpi}	potential water uptake from soil layer *i*	cm h^{-1}
U_{WpP}	potential water uptake from soil profile	cm h^{-1}
U_{Wri}	water uptake per unit of root length	cm^3 cm^{-1} d^{-1}
U_{WaP}	actual water uptake from soil profile	cm h^{-1}
z	soil layer thickness	cm

In spite of the simplification, the CERES water uptake algorithm performed well in comparative studies (e.g. JARA & STOCKLE 1999; LI *et al.* 2001). Many other root-water uptake models have been published (e.g. WU *et al.* 1999; LAI & KATUL 2000) but the CERES description is considered to have an adequate level of process detail for the DANUBIA crop growth model.

Hourly water uptake rates for each soil layer are exported to the DANUBIA soil model for simulating soil water balance.

2.2.7 Nitrogen uptake

Roots assimilate mineral nitrogen in form of either nitrate (NO_3^-) or ammonium (NH_4^+) ions. Like other mineral nutrients, nitrogen is absorbed from the soil solution. Consequently, insufficient soil water content in the rooting zone limits nitrogen uptake. Nitrogen and water uptake are highly correlated processes and both depend on the plants´ demand and accessibility in the soil environment.

Nitrogen uptake is modelled according to the model CERES (JONES & KINIRY, eds, 1986, GODWIN & SINGH 1998). Nitrate as well as ammonium uptake from each soil

layer are simulated as function of root length density, soil water content, soil mineral nitrogen reservoirs and nitrogen demand of the plants.

First, the potential nitrate and ammonium uptake rates (U_{NO3} and U_{NH4}) for each rooted soil layer are determined. Limiting factors (which range from 0 for strong limitation to 1 for no limitation) concerning nitrogen concentration and soil water content are accounted for.

Potential availability factors for nitrate (F_{NO3}) and ammonium (F_{NH4}) are:

$$F_{NO3i} = 1 - \exp\left(- X_{NO3} \; N_{NO3i} \right) \tag{2.2.7–1}$$

$$F_{NH4i} = 1 - \exp\left(- X_{NH4} \; N_{NH4i} \right) \tag{2.2.7–2}$$

where X_{NO3} and X_{NH4} are crop-specific supply coefficients and N_{NO3} and N_{NH4} are the concentrations of nitrate and ammonium, respectively, in the specific soil layer. To obtain these concentrations (mg elemental N kg^{-1} soil), the mass nitrogen input data (kg m^{-2}) provided by the soil model are multiplied with soil bulk density ρ_b (g soil cm^{-3} soil) and soil layer thickness z. The potential nitrogen availability factors are limited to a maximum value of 1 and are set to 0 if falling below a crop-specific minimum value (F_{Nmin}).

To include the effect of current soil water limitations on nitrogen uptake, the zero-to-unity soil water factor $F_{H2O,N}$ is determined layer-specifically:

$$F_{H2O,Ni} = \frac{\theta_i - \theta_{WPi}}{\theta_{FCi} - \theta_{WPi}} \tag{2.2.7–3}$$

where θ is the volumetric soil water content. The difference between the two soil water contents at field capacity θ_{FC} and at wilting point θ_{WP} gives the total plant-extractable soil water. Potential nitrogen uptake is not only assumed to decline under soil water-limiting conditions but also at soil water contents higher than field capacity θ_{FC} because of decreased root function and increased anaerobiosis. In this case, $F_{H20,N}$ is reduced proportionally to the level of soil water saturation:

$$F_{H2O,Ni} = 1 - \frac{\theta_i - \theta_{FCi}}{\theta_{SATi} - \theta_{FCi}} \tag{2.2.7–4}$$

where θ_{SAT} is the soil water content at saturation.

The above described factors together with root length density R_{LD}, soil layer thickness z, and a crop-specific maximum nitrogen uptake rate per unit length of root (U_{NRmax})

give the potential uptake rate of nitrate (U_{NO3p}) and ammonium (U_{NH4p}) respectively in each soil layer:

$$U_{NO3pi} = R_{LDi} \; F_{H2O,Ni}{}^{2} \; z_i \; 100 \; F_{NO3i} \; U_{NRmax} \qquad (2.2.7\text{–}5)$$

$$U_{NH4pi} = R_{LDi} \; F_{H2O,Ni}{}^{2} \; z_i \; 100 \; F_{NH4i} \; U_{NRmax} \qquad (2.2.7\text{–}6)$$

The coefficient 100 allows for conversion of units. Summed values of U_{NO3p} and U_{NH4p} over all soil layers give the potential nitrogen uptake rate from the whole soil profile (U_{Np}).

The actual nitrogen uptake rate U_N is obtained through comparison of U_{Np} with the current crop nitrogen demand N_{dem}, which is simulated according to the model GECROS (see chapter 2.2.8: *Nitrogen demand*). In correspondence to the concept used for defining actual water uptake, the interrelation of nitrogen demand and uptake is considered.

If the crop demand N_{dem} exceeds the potential nitrogen supply U_{Np}, actual uptake U_N is equal to potential uptake. However, if the demand is less than the potential uptake, the latter is reduced to actual uptake ($U_{NO3\,i}$ and $U_{NH4\,i}$) in each layer:

$$U_{NO3i} = U_{NO3pi} \left(N_{dem} / U_{Np} \right) \qquad (2.2.7\text{–}7)$$

$$U_{NH4i} = U_{NH4pi} \left(N_{dem} / U_{Np} \right) \qquad (2.2.7\text{–}8)$$

Values of U_{NO3i} and U_{NH4i} are not allowed to cause soil nitrogen concentrations of less than 0.25 mg kg^{-1} (for nitrate) and 0.5 mg kg^{-1} (for ammonium). Actual nitrogen uptake from the soil profile (U_N) is the sum of U_{NO3i} and U_{NH4i} over all soil layers.

If the nitrogen concentration in the living shoot (n_{act}) is greater than the critical shoot nitrogen concentration (n_{cri}), exudation of organic nitrogen from the roots occur (following the CERES modelling approach). Both nitrogen concentrations of the shoot are modelled according to GECROS (see chapter 2.2.9: *Allocation of carbon and nitrogen*). The daily exuded nitrogen N_{ex} is assumed to be 5 % of the nitrogen contained in roots. This value as well as the uptake rates of nitrate and ammonium are used by the DANUBIA soil model to update the different nitrogen pools for simulating nitrogen transformation processes.

Table 11: Symbols, definitions and units for modelling nitrogen uptake.
Crop-specific input parameters are marked with an asterisk.

Symbol		Definition	Unit
$F_{H2O,Ni}$		soil water factor affecting N uptake	-
F_{NH4i}		soil ammonium supply factor in soil layer *i*	-
F_{Nmin}	*	critical value of N supply factors	-
F_{NO3i}		soil nitrate supply factor in soil layer *i*	-
n_{act}		actual N concentration in living shoot	g N g^{-1}
n_{cri}		critical shoot N concentration	g N g^{-1}
N_{dem}		crop N demand	g N m^{-2} d^{-1}
N_{ex}		exuded N from roots	g N m^{-2} d^{-1}
N_{NH4i}		ammonium N in layer *i*	mg N kg^{-1}
N_{NO3i}		nitrate N in soil layer *i*	mg N kg^{-1}
U_N		actual N uptake rate from the soil profile	kg N ha^{-1} d^{-1}
U_{NH4i}		actual ammonium uptake in soil layer *i*	kg N ha^{-1} d^{-1}
U_{NO3i}		actual nitrate uptake in soil layer *i*	kg N ha^{-1} d^{-1}
U_{NRmax}	*	maximum N uptake rate per unit length of root	kg N ha^{-1} cm^{-1} root
U_{Np}		potential N uptake rate from the soil profile	kg N ha^{-1} d^{-1}
U_{NH4pi}		potential uptake rate of ammonium in soil layer *i*	kg N ha^{-1} d^{-1}
U_{NO3pi}		potential uptake rate of nitrate in soil layer *i*	kg N ha^{-1} d^{-1}
X_{NH4}	*	supply coefficient for ammonium	-
X_{NO3}	*	supply coefficient for nitrate	-
θ_{SATi}		volumetric soil water content at saturation in layer *i*	cm^3 water cm^{-3} soil
ρ_b		soil bulk density	g soil cm^{-3} soil

2.2.8 Nitrogen demand

Plants have a high demand on nitrogen which is an essential element of organic compounds. Nitrogen is indispensable for the utilization of carbohydrates and needed for the synthesis of proteins, chlorophyll and enzymes (GODWIN & SINGH 1998). GASTAL & LEMAIRE (2002) give an overview of the dependence of crop growth processes on nitrogen.

In agro-ecosystems, nitrogen reservoirs in the soil are replenished by fertilizer applications. Nitrogen uptake and crop growth are interacting processes. During their life cycle, crops have variable needs for nitrogen depending on biomass increase and growth of different organs.

Crop nitrogen content does not increase linearly with crop mass. Additional nitrogen uptake per unit of additional biomass declines as crops grow bigger (GASTAL & LEMAIRE 2002).

The dynamic simulation of crop nitrogen demand in relation to plant growth is adapted from the model GECROS (YIN & VAN LAAR 2005). The modelling concept differentiates between deficiency-driven and growth activity-driven demand.

The deficiency-driven demand (N_{demD}) guarantees the maintenance of the actual plant nitrogen concentration (n_{act}) above a critical concentration (n_{cri}). Critical nitrogen concentration is defined as the minimum concentration which allows maximum growth rate. Comparison of n_{cri} and n_{act} quantifies the nitrogen nutrition status of a crop. Concentrations below this critical concentration reduce growth whereas higher concentrations cause no increased growth. During growth of annual crops, the fraction of newly produced plant tissue with high nitrogen concentration declines in relation to existing biomass. Consequently, the critical above-ground nitrogen concentration (n_{cri0}) gradually decreases (GODWIN & SINGH 1998). GASTAL & LEMAIRE (2002) show critical nitrogen concentration curves in relation to above-ground biomass available in literature for different crops.

The model GECROS assumes a crop- or genotype-specific value of initial critical above-ground nitrogen concentration (n_{cri0}) at the beginning of the life cycle. The seasonal course of n_{cri} is estimated as a function of development stage (φ):

$$n_{cri} = n_{cri0} \exp\left(-0.4\ \varphi\right) \tag{2.2.8–1}$$

N_{demD} is calculated using the critical and actual nitrogen concentration in biomass:

$$N_{demD} = W_S \left(n_{cri} - n_{act}\right) \left(1 + N_R / N_S\right) / \Delta t \tag{2.2.8–2}$$

where n_{cri} is corrected for the difference between root (N_R) and shoot nitrogen content (N_S). To account for the temporal component, the time step of dynamic simulation Δt (here one day) is included in the equation.

Growth activity-driven demand (N_{demA}) is modelled based on the functional-balance theory (see chapter 2.2.9: *Allocation of carbon and nitrogen*). According to this concept, plants maximize their relative carbon gain through optimum nitrogen concentration (HILBERT 1990). In order to realize the optimum nitrogen-carbon ratio, relative root activity σ_N and relative shoot activity σ_C have to be balanced as:

$$\sigma_N = \sigma_C^{\,2} / \left(\mathrm{d}\sigma_C / \mathrm{d}\kappa\right) \tag{2.2.8–3}$$

with $\mathrm{d}\sigma_C/\mathrm{d}\kappa$ being the first-order derivative of σ_C regarding the plants´ nitrogen-carbon ratio κ.

Relative root activity σ_N puts nitrogen gain ΔN in relation to root carbon content C_R. In analogy, relative shoot activity σ_C relates carbon gain ΔC to shoot carbon content C_S:

$$\sigma_N = \left(\Delta N / \Delta t\right) / C_R \tag{2.2.8–4}$$

$$\sigma_C = (\Delta C / \Delta t) / C_S \quad (2.2.8\text{–}5)$$

Nitrogen gain ΔN is equivalent to nitrogen uptake U_N while carbon gain ΔC corresponds to net primary production. The derivation of eq. (2.2.8–3) is given in Appendix A. Growth activity-driven demand N_{demA} is calculated as:

$$N_{demA} = C_R \sigma_N = C_R \sigma_C^2 / (d\sigma_C / d\kappa) \quad (2.2.8\text{–}6)$$

The derivative $d\sigma_C / d\kappa$ is determined numerically:

$$d\sigma_C / d\kappa = \left[\sigma_{C(\kappa+\Delta\kappa)} - \sigma_{C(\kappa)} \right] / \Delta\kappa \quad (2.2.8\text{–}7)$$

where $\Delta\kappa$ is an increment in plant nitrogen-carbon ratio (value of κ multiplied by 0.001) and $\sigma_{C(\kappa+\Delta\kappa)}$ and $\sigma_{C(\kappa)}$ are the relative shoot activities with incremented κ, and with unchanged κ, respectively.

The maximum value of N_{demD} and N_{demA} determines the crop nitrogen demand (N_{dem}). A crop-specific maximum daily uptake rate N_{maxup} restricts N_{dem}.

$$N_{dem} = \min \left[N_{maxup}, \max (N_{demD}, N_{demA}) \right] \quad (2.2.8\text{–}8)$$

Table 12: Symbols, definitions and units for modelling nitrogen demand. Crop-specific input parameters are marked with an asterisk.

Symbol		Definition	Unit
C_R		C in living root	g C m^{-2}
C_S		C in living shoot	g C m^{-2}
N_{dem}		crop N demand	g N m^{-2} d^{-1}
N_{demA}		activity-driven crop N demand	g N m^{-2} d^{-1}
N_{demD}		deficiency-driven crop N demand	g N m^{-2} d^{-1}
N_{maxup}	*	maximum crop N uptake rate	g N m^{-2} d^{-1}
N_R		N in living root	g N m^{-2}
N_S		N in living shoot	g N m^{-2}
W_S		weight of living shoot	g m^{-2}
σ_C		relative shoot activity	g C g^{-1} C d^{-1}
σ_N		relative root activity	g N g^{-1} C d^{-1}
κ		nitrogen-carbon ratio in crop	g N g^{-1} C
n_{act}		actual N concentration in living shoot	g N g^{-1}
n_{cri}		critical shoot N concentration	g N g^{-1}
n_{cri0}	*	initial critical shoot N concentration	g N g^{-1}
$\Delta C/\Delta t$		net rate of shoot C fixation	g C m^{-2} d^{-1}
$\Delta N/\Delta t$		rate of root N uptake	g N m^{-2} d^{-1}
$\Delta\kappa$		increment in κ	g N g^{-1} C

For modelling growth of leguminous crops like peas or beans, their ability to fix atmospheric nitrogen needs to be considered. The model GECROS provides algorithms to account for the symbiotic nitrogen fixation. As in this study no legumes are modelled, the calculations are not quoted here.

2.2.9 Allocation of carbon and nitrogen

During crop growth, acquired carbon (by photosynthesis) and nitrogen (by root absorption) are incorporated into the tissues of different plant organs. The distribution of the two elements within the plant depends on phenological development and environmental conditions.

Because of feedback mechanisms, allocation plays a critical role in plant growth. For example, distributed carbon to the root system augments root length density and thus enables increased potential nutrient and water uptake rates.

Especially in crop growth modelling, the processes of carbon and nitrogen allocation are of key importance. Economic yield is determined by the carbon and nitrogen content of the harvested products. In the past, many models made use of fixed distribution keys relating the allocation of biomass to development stage. Examples are the models CERES (e.g. JONES & KINIRY, eds, 1986), LINTUL (e.g. GOUDRIAAN & VAN LAAR 1994) and SUCROS (VAN KEULEN *et al.* 1997). However, to depict the influence of altered environmental conditions, the flexibility of allocation has to be accounted for.

In the model GECROS (YIN & VAN LAAR 2005), allocation is simulated dynamically and includes the response to water and nitrogen shortages. Therefore, the GECROS concept of modelling allocation is adopted in the DANUBIA crop growth model.

The model plant consists of root and shoot compartments. The shoot is further subdivided into leaf, stem and storage organ sections. Without differentiating between seed, grain, or tuber, in the following the corresponding storage organ of the crop is designated "seed". Plant organs are classified according to their function rather than morphology. The seed is regarded as part of the shoot, also in cases of sugar beet and potato where the storage organs are below-ground. The section "leaf" represents photosynthetic function and therefore comprises green surface area of ears or stems.

Fig. 19 shows the different plant organ sections used in modelling carbon allocation. Structural and non-structural (metabolic) components of plant carbon are considered. Non-structural components form two reserve pools, one related to the shoot compartment, the other to the root section. If the carbon supply exceeds the demand, reserve pools are filled. Later, the reserve carbon can be remobilized to form structural components.

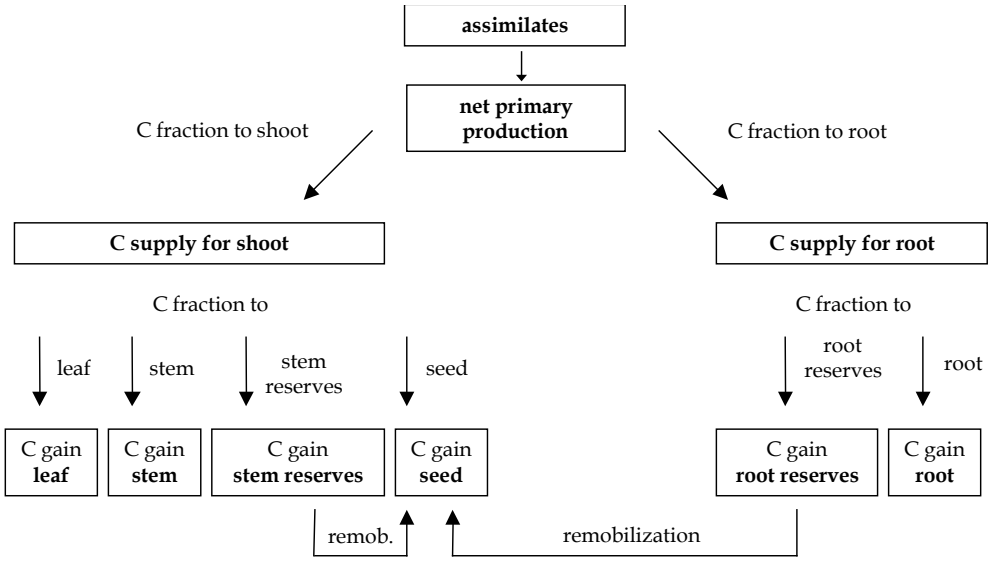

Fig. 19: Scheme for modelling carbon allocation.

The model GECROS simulates the partitioning of carbon and nitrogen between root and shoot according to the concept of functional balance. The theory of a "functional balance" was formulated by BROUWER (1962) (cited by POORTER & NAGEL 2000). Activity of the shoot (which supplies carbon) and activity of the roots (which provide nitrogen) are balanced. The central part of this theory is that a plant changes its allocation pattern towards the shoot under conditions of reduced above-ground resources (e.g. CO_2 and light) which lessen carbon gain. In correspondence, allocation to the root system is increased in case of limited soil resources (nutrients or water). Consequently, the regulation of shoot-root allocation is adjusted to the given environmental conditions in order to maximize resource capture and relative growth rate (POORTER & NAGEL 2000). Changes in shoot and root biomass are tightly linked by this functional equilibrium. Other models (e.g. *ecosys*, GRANT 2001) too simulate allocation according to this concept.

Partition between root and shoot

The following equations are taken from the model GECROS, where algorithms from YIN & SCHAPENDONK (2004) are adapted for root-shoot partitioning.

In this context, the plants´ nitrogen-carbon ratio κ is represented by the current growth activity-driven nitrogen demand N_{demA} set in relation to the current carbon gain:

$$\kappa = \min \left(N_{maxup}, N_{demA} \right) / \left[P_{Cnet} \left(12 / 44 \right) Y_{G,V} \right] \qquad (2.2.9\text{–}1)$$

Carbon gain (net primary production) results from P_{Cnet} (daily net canopy photosynthesis). Units of (g CO_2 m^{-2} d^{-1}) are converted to (g C m^{-2} d^{-1}) by means of the molar masses of carbon (12 g mol^{-1}) and carbon dioxide (44 g mol^{-1}). Finally, the term is multiplied by the growth efficiency of vegetative organs $Y_{G,V}$. Because plants absorb the majority of nitrogen before the start of seed fill, $Y_{G,V}$ is used.

The newly distributed carbon and nitrogen amounts to each plant compartment are expressed as fractions of total available carbon and nitrogen, respectively. The fraction of newly assimilated carbon partitioned to shoot $\lambda_{C,S}$ is given by:

$$\lambda_{C,S} = \frac{1}{1 + \left(\kappa / \sigma_C \right) \, d\sigma_C / d\kappa} \tag{2.2.9–2}$$

with $d\sigma_C/d\kappa$ being the first-order derivative of relative shoot activity σ_C regarding κ, already introduced in the chapter 2.2.8 (*Nitrogen demand*).

The fraction of newly absorbed nitrogen invested in shoot $\lambda_{N,S}$ is computed as:

$$\lambda_{N,S} = \frac{1}{1 + \left[\kappa \, N_R \, C_S / \left(\sigma_C \, N_S \, C_R \right) \right] \, d\sigma_C / d\kappa} \tag{2.2.9–3}$$

using the following parameters: living root content of carbon (C_R), and nitrogen (N_R), and living shoot content of carbon (C_S), and nitrogen (N_S). The carbon fraction partitioned to root ($\lambda_{C,R}$) is given by (1 - $\lambda_{C,S}$), and the nitrogen fraction partitioned to root ($\lambda_{N,R}$) equals (1 - $\lambda_{N,S}$).

Daily carbon supply from current photosynthesis for root (Cs_R) and for shoot growth (Cs_S) is calculated as:

$$Cs_R = \left(12 / 44 \right) \, \lambda_{C,R} \, P_{Cnet} \tag{2.2.9–4}$$

$$Cs_S = \left(12 / 44 \right) \, \lambda_{C,S} \, P_{Cnet} \tag{2.2.9–5}$$

where P_{Cnet} is daily net canopy photosynthesis. Correspondingly, with U_N being the daily nitrogen uptake, daily nitrogen supply for shoot Ns_S, and for root Ns_R, respectively, is given by:

$$Ns_S = \lambda_{N,S} \, U_N \tag{2.2.9–6}$$

$$Ns_R = \lambda_{N,R} \, U_N \tag{2.2.9–7}$$

Allocation of carbon within the shoot

Carbon supply for shoot and root from current assimilates is further subdivided (see Fig. 19). GECROS implements the theory that allocation of carbon responds to the demand of growing plant organs which serve as sinks.

Expected relative growth rates of either seed or stem ($RG_{\varphi i}$) at phenological stage φ_i are modelled based on the differential form of a beta sigmoid function for asymmetric determinate growth (YIN *et al.* 2003a).

$$RG_{\varphi i} = \frac{\left(2\varphi_e - \varphi_m\right)\left(\varphi_e - \varphi_i\right)}{\varphi_e\left(\varphi_e - \varphi_m\right)^2}\left(\frac{\varphi_i}{\varphi_e}\right)^{\varphi_m/(\varphi_e - \varphi_m)} \qquad (2.2.9\text{–}8)$$

Growth is assumed to start at the stage of zero, to reach maximum growth rate at stage φ_m, and to end at stage φ_e. Details are described by YIN *et al.* (2003a). Fig. 20 shows the schematic course of expected relative growth rates both for stem and seed, assuming a constant development rate.

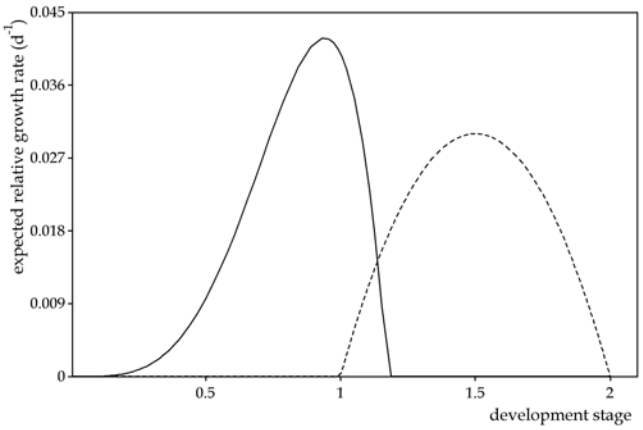

Fig. 20: Expected relative growth rates (d^{-1}) of stem (solid line) and of seed (dashed line) for an indeterminate crop during crop development (data from the DANUBIA crop growth model).

Daily demand of carbon for either seed or stem growth ($C_{\varphi i}$) at stage φ_i is calculated as:

$$C_{\varphi i} = \omega_i \; C_{max} \; RG_{\varphi i} \qquad (2.2.9\text{–}9)$$

with ω_i representing the development rate at stage φ_i. Total demand of carbon at the end of growth is given by C_{max}. Depending on the use of equations (2.2.9–8) and (2.2.9–9) either for seed or for stem growth, the influencing parameters differ (as shown in Table 13).

Table 13: Symbols, definitions, calculations and units for modelling expected growth rates. Crop-specific input parameters are marked with an asterisk.

Symbol		Definition and calculation	Unit
$C_{\varphi i}$		C demand for growth of seed or stem	g C m^{-2} d^{-1}
$RG_{\varphi i}$		expected relative growth rate of seed or stem	d^{-1}
ω_i		daily development rate	d^{-1}
φ_i		development stage during the growth of stem or seed	-
t_e	*	development stage for the end of seed-number determining period	-
		Equations (2.2.9–8) and (2.2.9–9) used for calculating expected seed growth	
φ_e		development stage at the end of growth of seed $\varphi_e = 1$	-
φ_m		development stage at the time of maximal growth rate of seed $\varphi_m = I_{m,seed}$	-
$I_{m,seed}$	*	crop-specific fraction of sigmoid curve inflexion in entire seed growth period	-
C_{max}		maximum C content of seed at the end of its growth $C_{max} = S_f \; S_w \; f_{c,S} \; / \; Y_{G,S}$ (2.2.9–10)	g C m^{-2}
S_f		number of seeds $S_f = N_{res} \; / \; f_{Npre} \; / \; n_{SO} \; / \; S_w$ (2.2.9–11)	seeds m^{-2}
N_{res}		estimated vegetative-organ N remobilizable for seed growth	g N m^{-2}
n_{SO}	*	crop-specific standard N concentration in seed	g N g^{-1}
f_{Npre}	*	crop-specific fraction of seed N that comes from remobilizable vegetative-organ N accumulated before t_e	-
S_w	*	crop-specific seed weight	g seed^{-1}
$f_{c,S}$		fraction of C in seed biomass calculation: see chapter 2.2.4: *Respiration*, eq. 1: part in parentheses in the numerator	g C g^{-1}
$Y_{G,S}$		storage organ (seed) growth efficiency calculation: see chapter 2.2.4: *Respiration*, eq. 1	g C g^{-1} C
		Equations (2.2.9–8) and (2.2.9–9) used for calculating expected stem growth	
φ_e		development stage at the end of growth of stem $\varphi_e = (1 + t_e) \; / \; 2$ (2.2.9–12)	-
φ_m		development stage at the time of maximal growth rate of stem $\varphi_m = I_{m,stem} \; (1 + t_e) \; / \; 2$ (2.2.9–13)	-
$I_{m,stem}$	*	crop-specific fraction of sigmoid curve inflexion in entire plant height growth period	-
C_{max}		maximum C content of stem at the end of its growth $C_{max} = (\rho \; H_{max} \; f_{c,V} \; / \; Y_{G,V}) \; f_h$ (2.2.9–14)	g C m^{-2}
ρ	*	crop-specific proportion factor between stem biomass and plant height	g m^{-2} m^{-1}
H_{max}	*	crop-specific maximum plant height	m
$f_{c,V}$	*	fraction of C in vegetative-organ biomass	g C g^{-1}
$Y_{G,V}$		vegetative-organ (leaf, stem, root) growth efficiency	g C g^{-1} C
f_{ht}		integral factor of stresses on plant height growth	-

One of the influencing parameters is the development stage for the end of seed-number determining period (t_e). It corresponds to the start of seed fill in case of determinate crops or to a later stage in case of indeterminate crops. In contrast to indeterminate crops (e.g. barley, potato, sugar beet) the vegetative growth of determinate crops (e.g. maize and wheat) stops when seed-filling starts.

The number of seeds S_f is calculated using the accumulated difference between nitrogen uptake and nitrogen incorporated in structural biomass of vegetative organs (N_{res}) and standard seed nitrogen concentration (n_{SO}). When t_e is reached, N_{res} by remobilization is available for seed growth. A crop-specific fraction of seed nitrogen (f_{Npre}) is supposed to originate from N_{res}.

Available carbon firstly is allocated to the seed, next to structural stem, then to the leaf compartment, and finally to the shoot reserve pool. If the daily demand of carbon for either stem or seed growth ($C_{\varphi i}$) is not met by the corresponding flow of allocated carbon, the missing quantity is added to the demand of the following time-step.

Fractions of new shoot carbon partitioned to seed ($\lambda_{C,seed}$) and stem ($\lambda_{C,stem}$) are given by the ratio of the demand for seed and stem growth ($C_{\varphi i}$), respectively, and carbon supply for shoot (Cs_S). The demand for stem growth might be reduced by the zero-to-unity factor f_{ht}, being the ratio between the current carbon supply and the demand for stem growth in the previous time-step. Taking the value of the preceding time-step avoids the need for a calculation loop.

The fraction of shoot carbon allocated to leaf ($\lambda_{C,leaf}$) is:

$$\lambda_{C,leaf} = 1 - \lambda_{C,seed} - \lambda_{C,stem} \qquad (2.2.9\text{–}10)$$

if canopy growth is limited by carbon ($L_C < L_N$). In case of nitrogen-limited growth ($L_C \geqq L_N$), $\lambda_{C,leaf}$ is set to zero. The concept of leaf area index modelling is explained in chapter 2.2.10 (*Leaf area and senescence*). After the end of the seed-determining development period (t_e), $\lambda_{C,stem}$ as well as $\lambda_{C,leaf}$ are set to zero.

Carbon reserves

Subsequent to allocation to seed, stem and leaf, the remaining fraction of shoot carbon is assigned to the shoot reserve pool ($\lambda_{C,Sres}$):

$$\lambda_{C,Sres} = 1 - \lambda_{C,seed} - \lambda_{C,stem} - \lambda_{C,leaf} \qquad (2.2.9\text{–}11)$$

If carbon limits root growth, carbon supply for root is apportioned completely to the root. If on the other hand nitrogen limits root growth (see chapter 2.2.10: *Leaf area and senescence*), carbon supply for root is entirely allocated to the root reserve pool.

In case of deficient carbon supply with regard to demand for seed fill, shoot and root reserves are remobilized impartially to form structural seed biomass. Carbon losses

during remobilization due to energy consumption and growth respiration (see chapter 2.2.4: *Respiration*) are taken into account.

Plant height

Plant height (assumed to equal stem length) is needed to determine turbulence resistance (see Appendix A). The value of maximum plant height (genotype- or crop-specific input parameter, H_{max}) divided by 1000 initializes plant height. In the model, for determinate crops H_{max} appears at the start of seed-fill. For indeterminate crops, H_{max} is reached in the middle between the start of seed fill and t_e.

The rate of change in plant height (R_{HT}) is calculated as:

$$R_{HT} = RG_{\varphi i} \; H_{max} \; f_{ht} \tag{2.2.9–12}$$

where $RG_{\varphi i}$ refers to the expected relative growth rate of stem (see eq. (2.2.9–8) and Table 13).

Allocation of nitrogen within the shoot

For the distribution of Ns_s to the different plant organs, some crop-specific input parameters are used: the standard nitrogen seed concentration n_{SO} (as target value), the minimum nitrogen concentration in stem (including shoot reserve pool, n_{Smin}) as well as in root (n_{Rmin}). The minimum leaf nitrogen concentration (n_{Lmin}) is calculated from the specific leaf area constant s_{la} and the minimum specific leaf nitrogen content n_b, both crop-specific input parameters.

Regarding the user-defined target seed nitrogen concentration n_{SO}, sensitivity-analysis options are provided in GECROS. Three user-defined parameters are introduced to enable modification of the expected nitrogen dynamics during seed fill (see Table 14).

The factor for dynamics of seed nitrogen concentration during seed fill $f_{N,S}$ is:

$$f_{N,S} = f_{N,S,ini} + \frac{\left(f_{N,S,fin} - f_{N,S,ini} \right) \left(4 - \varphi_{tr} - \varphi \right)}{\left(2 - \varphi_{tr} \right) \left(\varphi - 1 \right)^{1/(2-\varphi_{tr})}} \tag{2.2.9–13}$$

The expected seed nitrogen concentration dynamics during seed fill ($n_{SO,ex}$) is calculated as:

$$n_{SO,ex} = f_{N,S} \; n_{SO} \tag{2.2.9–14}$$

where $f_{N,S}$ is restricted to the range between $f_{N,S,ini}$ and $f_{N,S,fin}$.

Table 14: Symbols, definitions and units for modelling expected seed nitrogen concentration. Crop-specific input parameters are marked with an asterisk.

Symbol		Definition	Unit
$f_{N,S}$		factor for dynamics of seed N concentration during seed fill	-
$f_{N,S,ini}$	*	factor for initial N concentration of seed fill	-
$f_{N,S,fin}$	*	factor for final N concentration of seed fill	-
$n_{SO,ex}$		expected seed-N concentration dynamics during seed fill	g N g^{-1} N
φ_{tr}	*	development stage when transition from $f_{N,S,ini}$ to $f_{N,S,fin}$ is fastest	-

If the value of minimum leaf nitrogen concentration n_{Lmin} is exceeded, the remobilizable nitrogen in leaves (N_{LVres}) is calculated as:

$$N_{LVres} = \left(N_{LV} - W_{LV} \; n_{Lmin} \right) / \Delta t \qquad (2.2.9\text{–}15)$$

In analogy, if the value of minimum root nitrogen concentration n_{Rmin}, is surpassed, the remobilizable nitrogen in roots (N_{RTres}) is calculated as:

$$N_{RTres} = \left(N_{R} - W_{R} \; n_{Rmin} \right) / \Delta t \qquad (2.2.9\text{–}16)$$

The sum of N_{LVres} and N_{RTres} defines the total amount of nitrogen available for remobilization.

Table 15: Symbols, definitions and units for modelling allocation. Crop-specific input parameters are marked with an asterisk.

Symbol		Definition	Unit
Cs_R		daily C supply from photosynthesis for root growth	g C m^{-2} d^{-1}
Cs_S		daily C supply from photosynthesis for shoot growth	g C m^{-2} d^{-1}
L_C		carbon-determined LAI	m^{-2} leaf m^{-2}
L_N		nitrogen-determined LAI	m^{-2} leaf m^{-2}
n_b	*	minimum leaf N for photosynthesis	g N m^{-2} leaf
n_{Lmin}		minimum N concentration in leaf	g N g^{-1}
N_{LV}		N in living leaves	g N m^{-2}
N_{LVres}		amount of N in leaves available for remobilization	g N m^{-2} d^{-1}
N_R		N in living root	g N m^{-2}
n_{Rmin}	*	minimum N concentration in root	g N g^{-1}
N_{RTres}		amount of N in roots available for remobilization	g N m^{-2} d^{-1}
n_{Smin}	*	minimum N concentration in stem	g N g^{-1}
Ns_R		daily N supply for root growth	g N m^{-2} d^{-1}
Ns_S		daily N supply for shoot growth	g N m^{-2} d^{-1}
P_{Cnet}		daily net canopy photosynthesis	g CO_2 m^{-2} d^{-1}
R_{HT}		rate of change in plant height	m d^{-1}
W_{LV}		dry weight of living leaves	g m^{-2}
W_R		dry weight of living roots	g m^{-2}
$\lambda_{C,leaf}$		fraction of newly assimilated shoot C partitioned to leaf	g C g^{-1} C
$\lambda_{C,R}$		fraction of newly assimilated C partitioned to root	g C g^{-1} C
$\lambda_{C,S}$		fraction of newly assimilated C partitioned to shoot	g C g^{-1} C
$\lambda_{C,seed}$		fraction of newly assimilated shoot C partitioned to seed	g C g^{-1} C
$\lambda_{C,Sres}$		fraction of newly assimilated shoot C partitioned to stem reserve pool	g C g^{-1} C
$\lambda_{C,stem}$		fraction of newly assimilated shoot C partitioned to structural stem	g C g^{-1} C
$\lambda_{N,R}$		fraction of newly absorbed N partitioned to root	g N g^{-1} N
$\lambda_{N,S}$		fraction of newly absorbed N partitioned to shoot	g N g^{-1} N

The requirement for nitrogen by stem is given by n_{Smin}. If the demand for nitrogen by stem or by seed is satisfied, residual shoot nitrogen is allocated to leaves. If the demand cannot be met, the reserves in leaf (N_{LVres}) and root (N_{RTres}) are used impartially. This remobilization of leaf and root nitrogen induces senescence (see chapter 2.2.10: *Leaf area and senescence*). Loss of leaf and root nitrogen due to senescence is accounted for in calculating nitrogen allocation.

The simulated seed nitrogen concentration multiplied by the dry weight of seed and the conversion factor 6.25 gives the amount of seed protein.

Root nitrogen accumulation results from root nitrogen supply Ns_R less remobilized nitrogen as well as nitrogen lost due to senescence.

Biomass formation

In the model, the plant organ compartments (seed, leaf, stem, root) are subdivided into various components (Fig. 21). Each attribute of these sub-groups is treated as a state variable (e.g. amount of carbon). Starting from net photosynthesis rate and using the framework of allocation described above, carbon production rates (rate variables) are calculated for each time-step and biomass sub-group. The calculation of these carbon production rates integrate various aspects: carbon gain due to photosynthesis, the fraction partitioned to the specific plant organ, growth efficiency, remobilization of carbon reserves and carbon loss due to senescence (see chapter 2.2.10: *Leaf area and senescence*).

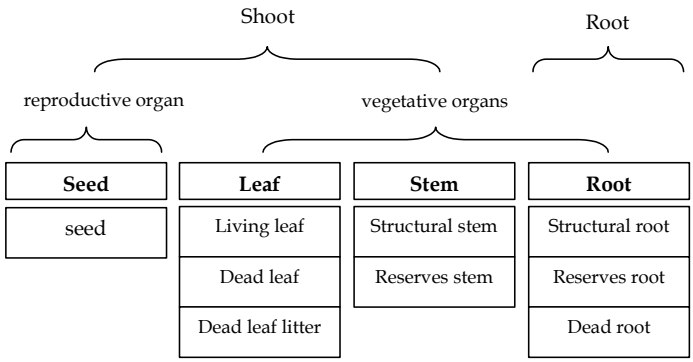

Fig. 21: Subdivision of biomass compartments for modelling carbon allocation.

The resulting rates of change in carbon amount per time-step (g C m^{-2} d^{-1}) are added to the already existing carbon quantities in each biomass sub-group (g C m^{-2}). As long as

carbon loss does not exceed carbon increase, the carbon amount of the specific sub-group gradually will gradually rise.

Dividing the rates of changes in carbon amount by the crop-specific carbon fractions in biomass ($f_{c,V}$ for vegetative organs and $f_{c,S}$ for seed) gives rates of change in dry weight (g m^{-2} d^{-1}). Dry weight of each plant-organ is updated.

In analogy, rates of change in amount of nitrogen (g N m^{-2} d^{-1}) are used for updating the amount of nitrogen in plant organs (g N m^{-2}). Division by the corresponding dry weight results in nitrogen concentrations (g N g^{-1}).

Carbon and nitrogen recirculation from crop to soil

The biomass sections "dead root" and "dead leaf" (Fig. 21) represent senescent plant material (see chapter 2.2.10: *Leaf area and senescence*). Carbon and nitrogen incorporated in senescent matter enter the soil during crop growth. These amounts of litter carbon and litter nitrogen are modelled dynamically and are exported to the DANUBIA soil model in each time-step.

Modelled rates of carbon loss for roots and leaves give the rates of dry weight loss. These are used to derive the rates of nitrogen loss, assuming that only a minimum nitrogen concentration (n_{Rmin} for roots, n_{Lmin} for leaves) in senescent material is left.

Regarding dead roots, total quantities of carbon and nitrogen constitute soil litter amounts. Whereas from dead leaves, the carbon amount entering the soil is calculated as a function of surface temperature and the crop-specific base and optimum temperatures (defined for modelling phenology, see chapter 2.2.1: *Phenological development*). According to GECROS, a user-defined fraction of dead leaf nitrogen is supposed to be incorporated into soil litter nitrogen. In the DANUBIA crop growth model, this fraction is set to the constant value of 1 and surface temperature is substituted by the mean of air temperature and upper soil layer temperature.

2.2.10 Leaf area and senescence

Leaf area is a key variable in crop growth modelling because it governs the fluxes of transpiration and photosynthesis. These fluxes are modelled at the leaf scale and via the leaf area index (LAI) are integrated to the canopy scale. The concept of modelling LAI as well as senescence of leaves and roots is adopted from the model GECROS (YIN

& VAN LAAR 2005). LAI development is modelled based on the theory of carbon-nitrogen interaction. The underlying principle is described in detail by YIN *et al.* (2000, 2003b).

Leaf area index

Since dead leaves do not contribute to transpiration and photosynthesis but influence the absorption of radiation, LAI is differentiated in green LAI (L), including only green leaf area, and total LAI (L_T) which comprises green and senescent leaf area.

While the leaf mass of a crop grows, LAI increases accordingly. Later, development of green LAI directly is influenced by senescence of leaves. Senescence is supposed to occur when the nitrogen content of leaves falls below the base content required for photosynthesis. During the regenerative phase of development, remobilization of nitrogen from leaves to seed causes a decrease in green LAI (YIN *et al.* 2000). Leaf senescence and therefore decrease of green LAI are computed as a function of nitrogen reduction in the canopy. Green LAI L is modelled as the minimum value of carbon-limited (L_C) and nitrogen-limited LAI (L_N).

Leaf nitrogen content per unit leaf area declines exponentially from top to bottom within the canopy. In the course of the crop´s life cycle leaves near the bottom of the canopy die. The nitrogen-determined LAI (L_N) is expressed as a function of nitrogen in living leaves in the canopy (N_{LV}):

$$L_N = \left(1 / k_N \right) \ln\left(1 + k_N \, N_{LV} / n_b \right) \qquad (2.2.10\text{–}1)$$

where k_N denotes the nitrogen extinction coefficient (eq. (2.2.10–7)). The crop-specific input parameter n_b represents the base leaf nitrogen content needed for photosynthesis. This logarithmic relationship of L_N to leaf nitrogen is valid for a completely developed canopy with senescent leaves near the bottom (YIN *et al.* 2003b).

The rate of change of L_C (ΔL_C) quantifies the LAI development without nitrogen limitation and is modelled depending on the current value of L_C. Following YIN *et al.* (2003b), bottom leaves in a young canopy ($L_C \leqq 1$), are still photosynthetically active. Thus, in eq. (2.2.10–1) n_b has to be replaced by n_{bot}, the leaf nitrogen at canopy bottom. A differential form of this modified equation gives:

$$L_C \leq 1 \qquad \Delta L_C = \left(n_{bot} \, \Delta N_{LV} - N_{LV} - \Delta n_{bot} \right) / \left[n_{bot} \left(n_{bot} + k_n \, N_{LV} \right) \right] \qquad (2.2.10\text{–}2)$$

where ΔN_{LV} is the rate of change in N_{LV} whereas Δn_{bot} describes the rate of change in n_{bot}. As eq. (2.2.10–2) shows, L_C is determined by nitrogen during the early growth phase. Due to the interrelated processes of nitrogen demand and uptake, nitrogen and carbon allocation, as well as photosynthesis, effects of nitrogen supply, radiation and atmospheric CO_2 concentration are implicitly considered (YIN *et al.* 2003b).

If L_C has reached a value above 1, ΔL_C is simply modelled as a function of the crop-specific input parameter s_{la} (specific leaf area constant) and the rate of change in living leaf carbon ΔC_{LV}:

$$L_C > 1 \qquad \Delta L_C = s_{la}\ \Delta C_{LV} / f_{c,V} \tag{2.2.10–3}$$

Equation (2.2.10–2) includes the state variable n_{bot} and its rate of change Δn_{bot}. The latter is given by:

$$\Delta n_{bot} = \left(n_{botE} - n_{bot} \right) / \Delta t \tag{2.2.10–4}$$

where $n_{bot\,E}$ represents the value of n_{bot} derived from the exponential profile of leaf nitrogen in the canopy. Details are given by YIN *et al.* (2003b).

On the basis of this exponential profile, $n_{bot\,E}$ is calculated as:

$$n_{botE} = k_n\, N_{LV} \exp\left(-k_n\, L \right) / \left(1 - \exp\left(-k_n\, L \right) \right) \tag{2.2.10–5}$$

The nitrogen content of the top leaves in the canopy n_0 (introduced in eq. (2.2.3–20) in the chapter 2.2.3 *Scaling of canopy parameters)* is:

$$n_0 = k_n\, N_{LV} / \left(1 - \exp\left(-k_n\, L \right) \right) \tag{2.2.10–6}$$

The nitrogen extinction coefficient k_n dynamically can be computed as (YIN *et al.* 2003b):

$$k_n = \frac{1}{L_T} \ln \left[\frac{k_r \left(N_{LV} - n_b\, L_T \right) + n_b \left(1 - \exp\left(-k_r\, L_T \right) \right)}{k_r \left(N_{LV} - n_b\, L_T \right) \exp\left(-k_r\, L_T \right) + n_b \left(1 - \exp\left(-k_r\, L_T \right) \right)} \right] \tag{2.2.10–7}$$

where k_r is the extinction coefficient for PAR. The diffuse fraction of PAR is believed to predominantly govern the distribution of nitrogen in a canopy (ANTEN 1997, cited in YIN & VAN LAAR 2005). In GECROS, k_r is assumed to equal the extinction coefficient for diffuse radiation (k'_d) related to PAR (introduced in the chapter 2.2.3: *Scaling of canopy parameters*).

Fig. 22 schematically shows the modelled time course of L_C and L_N during a crop growth phase. The minimum value of both defines L. Senescence starts as soon as the value of L_N falls below L_C for the first time.

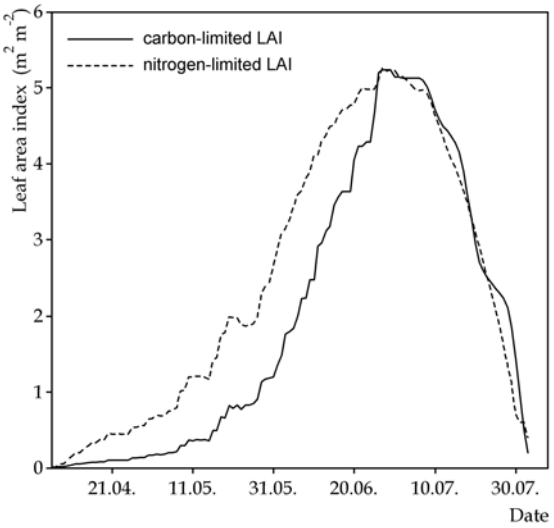

Fig. 22: Exemplary illustration of modelled LAI development (carbon-limited and nitrogen-limited, data from the DANUBIA crop growth model).

Leaf senescence

Simulation of leaf senescence is tightly coupled to modelling LAI development. Leaf death is quantified by the difference between L_C and L_N. Formulated as loss of leaf weight (ΔW_{LV}^-), leaf senescence is given by:

$$\Delta W_{LV}^- = \left[L_C - \min\left(L_C, L_N\right)\right] / \left(s_{la}\, \Delta t \right) \qquad (2.2.10\text{–}8)$$

During early canopy development, L_N has a higher value than L_C. Thus according to eq. (2.2.10–8), ΔW_{LV}^- is zero. Assuming only a minimum nitrogen concentration (n_{Lmin}) in dead leaves, the loss rate of leaf nitrogen ΔN_{LV}^- is:

$$\Delta N_{LV}^- = \Delta W_{LV}^- \; n_{Lmin} \qquad (2.2.10\text{–}9)$$

If nitrogen remobilization from leaves to seed is restricted because the demand for seed fill is none or low due to e.g. water scarcity, eq. (2.2.10–8) will predict little or no senescence. In this case, after the end of seed-number determining period (t_e), ΔW_{LV}^- is simulated as 3 % of W_{LV}. Accordingly, n_{Lmin} in eq. (2.2.10–9) is replaced by the nitrogen concentration in living leaves (n_L) to account for the higher nitrogen concentration as

well as increased nitrogen volatilization in senescent leaves under stress conditions (WEILAND *et al.* 1982, cited by YIN & VAN LAAR 2005).

Table 16: Symbols, definitions and units for modelling leaf area and senescence. Crop-specific input parameters are marked with an asterisk.

Symbol		Definition	Unit
k_n		N extinction coefficient	m² ground m^{-2} leaf
k_r		diffuse PAR extinction coefficient	m² ground m^{-2} leaf
k_{Rn}		extinction coefficient of root N concentration	m² g^{-1}
L		green leaf area index of canopy	m² leaf m^{-2} ground
L_C		carbon-determined L	m² leaf m^{-2} ground
L_N		nitrogen-determined L	m² leaf m^{-2} ground
L_T		total (green and senescent) leaf area index	m² leaf m^{-2} ground
n_0		canopy top-leaf N	g N m^{-2} leaf
n_b	*	minimum leaf N for photosynthesis	g N m^{-2} leaf
n_{bot}		canopy bottom-leaf N	g N m^{-2} leaf
n_{botE}		n_{bot} calculated from exponential N profile	g N m^{-2} leaf
n_L		N concentration in living leaf	g N g^{-1}
N_{LV}		N in living leaf	g N m^{-2}
N_R		N in living root	g N m^{-2}
n_{Rmin}	*	minimum N concentration in root	g N g^{-1}
N_{SR}		N in living structural root	g N m^{-2}
s_{la}	*	specific leaf area constant	m² leaf g^{-1} leaf
W_{LV}		weight of living leaf	g m^{-2}
W_{SR}		weight of living structural root	g m^{-2}
$W_{SR,N}$		nitrogen-determined W_{SR}	g m^{-2}
ΔC_{LV}		rate of change in living-leaf C	g C m^{-2} d^{-1}
ΔL_C		rate of change of L_C	m² leaf m^{-2} d^{-1}
ΔN_{LV}^-		loss rate of leaf N because of senescence	g N m^{-2} d^{-1}
ΔN_R^-		loss rate of root N because of senescence	g N m^{-2} d^{-1}
Δn_{bot}		rate of change of n_{bot}	g N m^{-2} leaf d^{-1}
ΔN_{LV}		rate of change of N_{LV}	g N m^{-2} d^{-1}
ΔW_{LV}^-		loss rate of leaf weight because of senescence	g m^{-2} d^{-1}
ΔW_R^-		loss rate of root weight because of senescence	g m^{-2} d^{-1}

Root senescence

During crop development, senescence of roots too occurs. Loss rate of structural root biomass ΔW_R^- is modelled equivalent to leaf senescence:

$$\Delta W_R^- = \left[W_{SR} - \min\left(W_{SR}, W_{SR,N}\right)\right] / \Delta t \qquad (2.2.10\text{–}10)$$

where W_{SR} denotes the weight of living structural roots. $W_{SR,N}$ is the nitrogen-determined W_{SR} which is determined as:

$$W_{SR,N} = \left(1 / k_{Rn}\right) \ln\left(1 + k_{Rn}\, N_{SR} / n_{Rmin}\right) \qquad (2.2.10\text{–}11)$$

where k_{Rn} is the extinction coefficient for root nitrogen concentration, already introduced in the chapter 2.2.5 (*Root growth*). N_{SR} represents the amount of structural

root nitrogen which results from the difference between total root nitrogen (N_R) and nitrogen in the root reserve pool. The latter is derived from multiplying the amount of carbon in root reserves (see chapter 2.2.9: *Allocation of carbon and nitrogen*) by n_{Rmin}, the crop-specific input parameter for minimum nitrogen concentration. In analogy to eq. (2.2.10–9), the loss rate of root nitrogen due to senescence ΔN_R^- is obtained by multiplying ΔW_R^- by n_{Rmin}.

Crop carbon and nitrogen balance check

According to GECROS (YIN & VAN LAAR 2005), a check on the carbon as well as nitrogen balance is performed at the end of crop growth. The amount of carbon fixed by photosynthesis minus the amount lost by respiration must equal the quantity of carbon incorporated in living and senescent plant material. In analogy, the amount of nitrogen which is absorbed by the root system must equal the sum of nitrogen contained in living biomass and in senescent plant material.

2.3 Required input data

Several sets of external input data are needed to run the DANUBIA crop growth model: meteorological drivers, site-specific information, soil features and farming practices. Within the modelling platform DANUBIA, these data are imported via the defined interfaces (see chapter 2.1.1: *Modelling framework).*

However, for the purpose of evaluating the crop growth model, not all models implemented in DANUBIA are needed. Thus, simulations with chosen sets of input data can be performed efficiently without superfluous calculations. For the present study, the DANUBIA crop growth model is principally coupled to the DANUBIA soil model (author Prof. Dr. Ralf Ludwig) and the DANUBIA surface model (author Dr. Stefan Niemayer) for simulations. For this study, the functionalities of the model *Radiation balance* (author Dr. Stefan Niemayer) being important for simulating crop growth have been implemented in the crop growth model.

Consequently, the feedback processes between the plant, the soil and surface environment are exactly the same as in the complete DANUBIA simulation system. All results presented in this study are derived from coupled simulations of these three models.

Input data assume homogeneity in terms of soil, climate and management of the considered area which they represent. The model´s internal spatial unit for computing is 1 m². Input data and corresponding model results have no spatial reference *per se*. They may refer to an area of 1 km² (as it is realized in DANUBIA), or for instance to a single field of smaller size.

Table 17: Dynamic and static input data of the DANUBIA crop growth model (for coupled simulations with the DANUBIA soil and surface models).

Dynamic input data (hourly time-step)	**Unit**
Meteorological drivers	
air pressure	Pa
global incident radiation	W m^{-2}
air temperature	K
air humidity	kg m^{-3} or fraction
wind speed	m s^{-1}
atmospheric carbon dioxide concentration	kg m^{-3} or µmol mol^{-1}
Soil data	
soil moisture (layer-specific)	kg m^{-3}
soil ammonium content (layer-specific)	kg m^{-2}
soil nitrate content (layer-specific)	kg m^{-2}
soil temperature of the top soil layer	K
Static input data	**Unit**
Soil data	
number of soil layers	**-**
thickness of soil layers	cm
field capacity (layer-specific)	cm water cm^{-1} soil
saturation (layer-specific)	cm water cm^{-1} soil
wilting point (layer-specific)	cm water cm^{-1} soil
bulk density (layer-specific)	g soil cm^{-3} soil
Site-specific information	
latitude	degree
Farming practices	
crop type	-
sowing date	Julian day
harvest date	Julian day

Dynamic input data are provided with a time-step of 1 h during the whole simulation. In contrast, static input data do not change their value and therefore are only needed once during the simulation.

Climate

Required meteorological drivers are hourly data of air pressure, global incident radiation, air temperature, air humidity, wind speed and atmospheric carbon dioxide

concentration (see Table 17). According to meteorological conventions, air temperature and humidity as well as wind speed refer to measurements at a height of 2 m.

If no data of air pressure are available, the value can be derived from standard air pressure and elevation of the test site. The partitioning of global incident radiation in its direct and diffuse components is described in Appendix C. For carbon dioxide concentration, a standard value is assumed. For studies of Global Change effects, the value can be set accordingly. Global incident radiation, air temperature, air humidity and wind speed are standard values provided by many weather stations of the *German Meteorological Service* as well as of agro-climatological networks.

Soil

Data needed with respect to the soil compartment include soil moisture, ammonium as well as nitrate reservoirs and soil temperature. These data are simulated by the coupled process-based soil model in an hourly time-step. The soil profile is divided in different layers and layer-specific soil data are provided. The crop growth model simulates processes of root growth, water and nitrogen uptake layer-specifically. Obviously, number and thickness of the soil layers have to be known. Soil temperature of only the top soil layer is needed (for modelling germination and recirculation of carbon and nitrogen from crop to soil).

Soil hydrological parameters (field capacity, saturation and wilting point) as well as bulk density are dependent on soil texture. The crop growth model needs these static parameters for modelling root growth, water and nitrogen uptake.

Site-specific data

Latitude of the site is needed for calculating day-length (required for modelling phenology) and partitioning of global radiation into its direct and diffuse components.

Farming practices

Agricultural management information includes crop type as well as dates of sowing and harvesting. Fertilizer treatments (date, amount and composition of fertilizer) serve as input data for the process-based soil model. Date and quantity of irrigation, too, are considered by the soil model for the dynamic simulation of soil moisture.

2.4 Crop-specific parameters

This chapter addresses the crop-specific parameters, implemented in the DANUBIA crop growth model. First, an overview of these parameters is given. The selection and derivation of values for the crop-specific parameters is presented in chapters 2.4.1 and 2.4.2. The specific values for sugar beet, spring barley, maize, winter wheat and potato are tabulated in Appendix D. Chapter 2.4.3 describes the definition of initial values in the model using crop-specific parameters. The crop-specific parameters which describe the various crops are shown in Table 18. Parameters of low certainty are marked with "~", genotype-specific parameters with "+" and parameters that are probably related to genotypic differences with "(+)". In the case of the parameters of low certainty, their default value as well as their likely range of values are given (according to YIN & VAN LAAR, 2005).

In GECROS, genotype-specific characteristics within a crop species are represented by parameters related to phenology, morphology, and seed features. In the current version of the DANUBIA crop growth model, no explicit genotypes are modelled. However, for the model validation by comparison with measurements on the field scale, genotype-specific parameters related to phenological development are adjusted. In GECROS, the initial shoot carbon ($f_{C,ini}$) and nitrogen ratio ($f_{N,ini}$) are assumed to be crop-independent. In the DANUBIA crop growth model, these two parameters are implemented as crop-specific parameters to allow flexibility. However, in this version of the model, the default values of 0.5 for $f_{C,ini}$ and 0.62 for $f_{N,ini}$ from GECROS (YIN & VAN LAAR 2005) are used for all crops.

Table 18: Crop-specific input parameters.
For parameters of low certainty, the default value and likely range of values are given.

Symbol	Definition	Unit
	Parameters related to biomass composition	
$f_{C,ini}$	initial fraction of C allocated to shoot	-
$f_{c,V}$	fraction of C in vegetative-organ biomass	g C g^{-1}
f_{lig}	fraction of lignin in biomass of organs	g lignin g^{-1}
f_{lip}	fraction of fat in in biomass of organs	g fat g^{-1}
$f_{N,ini}$	initial fraction of N allocated to shoot	-
f_{oac}	fraction of organic acids in biomass of organs	g organic acid g^{-1}
$Y_{G,V}$	growth efficiency for vegetative organs	g C g^{-1} C
ε_g	efficiency of germination	g g^{-1}
	Parameters related to leaf photosynthesis	
E_{Jmax}	activation energy for J_{max}	J mol^{-1}
n_b	minimum leaf N for photosynthesis	g N m^{-2} leaf
Θ	convexity factor for response of J_2 to PAR	-
χ_{jn}	proportion factor for the relation of J_{max} to leaf N	µmol electron g^{-1} N s^{-1}
χ_{vcn}	proportion factor for the relation of V_{cmax} to leaf N	µmol CO_2 g^{-1} N s^{-1}

Symbol			Definition		Unit
			Parameters related to root growth and nitrogen uptake		
F_{Nmin}			critical value of N supply factors		-
F_{SNmin}			minimum value of factor describing mineral N availability		-
$F_{\Delta D,em}$			factor for root depth increase before emergence		-
N_{maxup}	(+)	~	maximum crop N uptake rate	0.5 (0.4~0.8)	g N m^{-2} d^{-1}
R_{LM}			root length to mass ratio		cm length g^{-1}
U_{NRmax}			maximum N uptake rate per unit length of root		kg N ha^{-1} cm^{-1} root
X_{NH4}			supply coefficient for ammonium		-
X_{NO3}			supply coefficient for nitrate		-
			Parameters related to morphology		
D_{max}	(+)		maximum rooting depth		cm
f_{Npre}		~	fraction of seed N that comes from remobilizable vegetative-organ N accumulated before t_e	0.8 (0.6~0.95)	-
H_{max}	+		maximum plant height		m
$I_{m,seed}$		~	fraction of sigmoid curve inflexion in entire seed growth period	0.5 (0.4~0.7)	-
$I_{m,stem}$		~	fraction of sigmoid curve inflexion in entire plant height growth period	0.8 (0.6~0.9)	-
s_{la}			specific leaf area constant		m^2 leaf g^{-1} leaf
w			leaf blade width		m
β_L	+		leaf angle inclination in canopy		degrees
ρ			proportion factor between stem biomass and plant height		g m^{-2} m^{-1}
			Parameters related to phenology		
c_t	+	~	curvature factor for temperature response	1.0 (0.5~3.0)	-
$E_{m,a}$			coefficient for determining threshold for emergence		-
$E_{m,b}$			factor for determining threshold for emergence		-
p_{sen}	+		photoperiod sensitivity		h-1
$R_{max,r}$	+		maximum daily development rate in the reproductive (seed fill) phase		d-1
$R_{max,v}$	+		maximum daily development rate in the vegetative phase		d-1
T_b			base temperature		°C
$T_{b,em}$			base temperature for emergence		°C
T_c			ceiling temperature		°C
t_e	(+)	~	development stage for the end of seed-number determining period	(1.10~1.45) determinate crops: 1	-
T_o			optimum temperature		°C
φ_1	+	~	development stage at which photoperiod sensitivity starts	0.2 (0.0~0.5)	-
φ_2	+	~	development stage at which photoperiod sensitivity ends	0.7 (0.5~0.8)	-
			Parameters related to biomass nitrogen content		
$f_{N,S,fin}$			factor for final N concentration of seed fill		-
$f_{N,S,ini}$			factor for initial N concentration of seed fill		-
n_{cri0}			initial critical shoot N concentration		g N g^{-1}
n_{Rmin}			minimum N concentration in root		g N g^{-1}
n_{Smin}			minimum N concentration in stem		g N g^{-1}
φ_{tr}			development stage when transition from $f_{N,S,ini}$ to $f_{N,S,fin}$ is fastest		-
			Parameters related to seed characteristics		
n_{SO}	+		standard N concentration in seed		g N g^{-1}
S_w	+		seed weight		g $seed^{-1}$
			Parameters related to management		
D_s			sowing depth		cm
d_p			plant density		plants m^{-2}

Many values of crop-specific parameters needed for the DANUBIA crop growth model are already provided by the models CERES and GECROS. Others have to be derived either from literature data, sensitivity analysis or experiments.

The derivation of values of leaf photosynthesis parameters from gas exchange measurements, carried out by the author, is described in chapter 2.4.2.

For the parameters $f_{N,S,ini}$, $f_{N,S,fin}$ and φ_{tr} the values listed in the GECROS-source code are used (as proposed in a personal communication by Dr. Xinyou Yin, *Wageningen University and Research Centre*, 2006). These values may be checked by sensitivity analysis in further studies. The parameters f_{Npre}, $I_{m,seed}$, $I_{m,stem}$ and t_e were determined for each crop with the help of sensitivity analyses. For determinate crops, t_e corresponds to the start of seed fill and is therefore set to 1. Only in the case of indeterminate crops may genotypic variation influence t_e.

Despite the difficulties mentioned in chapter 2.2.1, related to the interpretation of growing degree-days, maximum development rates ($R_{max,v}$ and $R_{max,r}$) can be derived from growing degree-days by dividing the latter by the optimum temperature (T_o). The reciprocal value then gives the maximum development rate. The parameters p_{sen} and φ_2, both related to photoperiodic response, can be derived from the CERES crop growth models.

In this version of the DANUBIA crop growth model, sowing depth (D_s) as well as plant density (d_p) are supposed to be crop-specific parameters rather than variable management input parameters. Standard values of the parameters sowing depth (D_s), plant density (d_p), seed weight (S_w) and standard nitrogen concentration in seed (n_{SO}) are taken from the literature for all crops (KTBL, ed., 2005). The mean value and the given intervals of these data are presented in Appendix D.

In GECROS, default values and likely range of the empirical coefficients (c_0 and c_1) for calculating intercellular CO_2 concentration (c_i) are given (Table 19). c_1 has different values for C_3 and C_4 crops and may be related to genotypic variations. In the DANUBIA crop growth model, the default values are implemented.

Table 19: Values of empirical coefficients c_0 and c_1.

Symbol	Description	Default value	Likely range
c_0	empirical coefficient for calculating c_i	0.14	0.10~0.20
c_1	empirical coefficient for calculating c_i	0.116 kPa^{-1} (for C_3) 0.195 kPa^{-1} (for C_4)	0.10~0.15 kPa^{-1} 0.15~0.25 kPa^{-1}

2.4.1 Selection of crop-specific parameters

In the following paragraphs, the selection of crop-specific parameters for sugar beet, spring barley, maize, winter wheat and potato is presented. The values and corresponding sources are listed in Appendix D.

Crop-specific parameters for sugar beet

Because the CERES crop growth models do not include sugar beet, LEVIEL *et al.* (2003) developed a CERES-type model for this crop. All crop-specific parameters related to root growth and nitrogen uptake are taken from this model (CERES-BEET). Details of the model are given by LEVIEL (2000). Its source code is available from the homepage of the *French National Institute for Agricultural Research*[*].

For N_{maxup} (maximum crop nitrogen uptake), the maximum value (0.8 g N m^{-2} d^{-1}) of the interval given by YIN & VAN LAAR (2005) is chosen.

The three crop-specific phenological parameters for simulating emergence ($E_{m,a}$, $E_{m,b}$ and $T_{b,em}$) are also adopted from CERES-BEET. A specific feature is the use of the sowing date (in Julian days) for the phenological parameter $E_{m,a}$ (coefficient for determining threshold for emergence) instead of a constant value. This feature is derived from the source code of CERES-BEET and was personally affirmed by Mr. Benoît Gabrielle, *French National Institute for Agricultural Research,* (2006). Thus, according to eq. 2.2.1-6 in chapter 2.2.1 (*Phenological development*) the value of the threshold for emergence ($E_{m,th}$) is smaller for early sown sugar beet crops.

Standard values of the maximum development rates ($R_{max,v}$ and $R_{max,r}$) are derived from the literature. In CERES-BEET, 900 °C d growing degree-days are assumed until taproot development starts. According to DLG (ed., 1987), 700 °C d growing degree-days are needed. KENTER *et al.* (2006) observed that the dry matter of taproot increases exponentially after reaching 700 °C d growing degree-days. Based on these data, a value of 750 °C d is assumed. As a result $R_{max,v}$ is defined as 0.033 d^{-1}.

For the model evaluation through comparison with field data, the start of taproot growth can be estimated from the taproot measurements. The reciprocal value of the cumulative temperature response (*f(T)*) upto this date results in the specific value of

[*] http://www-egc.grignon.inra.fr/ecobilan/cerca/cerca.html

$R_{max,v}$ (e.g. a cumulative value of 40 for *f(T)* results in a value of 0.025 d^{-1} for $R_{max,v}$). Because $R_{max,v}$ is a genotype-specific parameter, this adaptation is justified.

The maximum development rate after the start of taproot development ($R_{max,r}$) is derived from the value of 2900 °C d (DLG, ed., 1987) required from sowing until harvesting. Considering a value of 750 °C d until taproot development starts, roughly, the value of 2150 °C d is assumed to be needed from the start of taproot development until harvesting. Thus $R_{max,v}$ is set to 0.012 d^{-1}. Sugar beet remains in the reproductive stage until the harvesting date. According to the BBCH-scale, the phenological stage of maturity is described as "beet root has reached harvestable size". Consequently, the value of $R_{max,v}$ is less important than for other crops and is assumed to be constant for all sugar beet varieties.

Leaf photosynthesis parameters E_{Jmax}, χ_{jn} and Θ are derived from leaf-level gas exchange measurements carried out by the author (see chapter 2.4.2).

For sugar beet, the initialization of the parameters C_{LV} (carbon in living leaves), (C_R) (carbon in living roots) and N_R (nitrogen in living roots) is modified (see chapter 2.4.3: *Definition of initial values*). In the model, the reservoir of carbon and nitrogen in the light-weight seeds of sugar beet is not sufficient to produce enough initial biomass. Therefore, the factor 10 for the initial calculation of all three parameters is introduced. Without this factor, modelled leaf area index and consequently biomass increases far too slowly. Because the pragmatic assumption of a factor 10 yielded very good results, this modification is adopted in the current version of the DANUBIA crop growth model.

Another modification for modelling sugar beet is adopted. Initial model test runs showed that after the start of taproot development, total assimilated carbon was allocated to the taproot. However, measurements demonstrate clearly that aboveground biomass continues to increase. To overcome this discrepancy, the parameter $C_{\varphi i}$ (carbon demand for growth of storage organ) is divided by 10. The calculation of $C_{\varphi i}$ is given in chapter 2.2.9 (*Allocation of carbon and nitrogen)*. Because this second pragmatic assumption showed very good results, it is implemented in the current version of the DANUBIA crop growth model.

Crop-specific parameters for spring barley

All crop-specific parameters related to root growth and nitrogen uptake are adopted from the CERES model for barley. Phenological parameters for simulating emergence ($E_{m,a}$, $E_{m,b}$ and $T_{b,em}$) are also taken from CERES. The values are obtained either from the documentation (RITCHIE & GODWIN 2000) or from the model´s source code. Spring barley is a typical long-day plant. The parameters p_{sen} (photoperiod sensitivity) and φ_2 (development stage at which photoperiod sensitivity ends) are both derived from the CERES model for barley. The calculation of the photoperiod effect *f(P)* in GECROS (chapter 2.2.1: *Phenological development*, eq. 2.2.1-3) and the equivalent calculation of photoperiod sensitivity implemented in CERES are opposed in order to fit the value of p_{sen} using the least squares method (quasi-Newton method provided by *Solver* in *Microsoft Excel*®).

The phenological stage of flowering in CERES corresponds to the development stage $\varphi = 1$ in the DANUBIA crop growth model. Consequently, φ_2 is given by the ratio of growing degree-days needed until the end of photoperiod sensitivity (= 605 °C d) and the growing degree-days required until flowering (= 755 °C d). Maximum development rates $R_{max,v}$ and $R_{max,r}$ are also derived from growing degree-days.

The values of the growing degree-days are adopted from the model PROMET-V (SCHNEIDER 1999), being representative for Bavaria.

The parameter φ_1 (development stage at which photoperiod sensitivity starts) is taken from a study by YIN *et al.* (2005), representing the mean value of the spring barley varieties *Apex* and *Prisma*.

Crop-specific parameters for maize

All crop-specific parameters related to root growth and nitrogen uptake as well as simulation of emergence ($E_{m,a}$, $E_{m,b}$ and $T_{b,em}$) are taken from the model CERES-Maize. Values for these parameters were obtained from its documentation (JONES & KINIRY, eds, 1986) or from the CERES source code.

Standard values of the maximum development rates ($R_{max,v}$ and $R_{max,r}$) are derived from the values of the growing degree-days employed in the model PROMET-V (SCHNEIDER 1999), being representative for Bavaria.

The leaf photosynthesis parameter χ_{jn} (proportion factor for the relation of J_{max} to leaf nitrogen) is derived from leaf-level gas exchange measurements carried out by the author (see chapter 2.4.2).

Crop-specific parameters for wheat

All crop-specific parameters related to root growth and nitrogen uptake as well as simulation of emergence ($E_{m,a}$, $E_{m,b}$ and $T_{b,em}$) are taken from the model CERES. Values for these parameters were obtained from its documentation (JONES & KINIRY, eds, 1986, RITCHIE & GODWIN 2000) or from the CERES source code.

Standard values of the maximum daily development rates ($R_{max,v}$ and $R_{max,r}$) are derived from the values of the growing degree-days employed in the model PROMET-V (SCHNEIDER 1999), being representative for Bavaria. According to STRECK *et al.* (2003b), the maximum development rate in the vegetative phase ($R_{max,v}$) for winter wheat is further subdivided, based on the key phenological stage of terminal spikelet initiation (see chapter 2.2.1: *Phenological development*). $R_{max,v}$ is multiplied by 0.7 to give the value of R_{max} in the emergence till terminal spikelet initiation phase ($R_{max,v1}$), whereas multiplying $R_{max,v}$ by 1.4 results in the value of R_{max} for the subsequent phase until start of seed fill ($R_{max,v2}$) (STRECK *et al.* 2003b).

Critical temperatures in terms of phenology are assumed to increase with advancing development. Values for each sub-phase (listed in Appendix D) are taken from PORTER & GAWITH (1999), as proposed by STRECK *et al.* (2003b).

As described in the case of spring barley, the value of photoperiod sensitivity (p_{sen}) as well as the development stage at which photoperiod sensitivity ends (φ_2) are derived from the CERES model for wheat.

Crop-specific parameters for potato

Appendix D lists the values of the crop-specific parameters for potato together with the corresponding sources. Crop-specific parameters related to nitrogen uptake are taken from the model SIMPOTATO (HODGES *et al.* 1992), which uses the same concept for modelling nitrogen uptake as the CERES models. Values for these parameters were obtained from its documentation (HODGES 1997). The value of root length to mass ratio (R_{LM}) used in SIMPOTATO was found in RENWICK (1999). Missing values for root

growth and nitrogen uptake parameters are adopted from the CERES-BEET model (LEVIEL 2000).

Leaf photosynthesis parameters χ_{jn} (proportion factor for the relation of J_{max} to leaf nitrogen), E_{Jmax} (activation energy for J_{max}) and Θ (convexity factor for response of J_2 to PAR) are derived from leaf-level gas exchange measurements carried out by the author (see chapter 2.4.2: *Derivation of leaf photosynthesis parameters*).

Since data was missing, crop-specific phenology parameters were adopted from the model CERES-BEET or were estimated, representing only a tentative approach. According to MACKERRON (2004), no photoperiod sensitivity is assumed.

2.4.2 Derivation of leaf photosynthesis parameters

In this subchapter, the experimental design and data analysis for the derivation of values for the crop-specific leaf photosynthesis parameters are presented.

GECROS provides crop-specific values of n_b (the minimum leaf nitrogen content for photosynthesis) for all considered crops. Values of the activation energy for J_{max} (E_{Jmax}) listed by YIN & VAN LAAR (2005) are estimated from curve-fitting with gas exchange data, assuming a constant ratio between χ_{jn} and χ_{vcn} (the proportion factors for the relationship between J_{max} and V_{cmax}, respectively). χ_{jn} is assumed to equal 2 χ_{vcn}. For sugar beet and potato, no values of E_{Jmax} are given in GECROS. These values have been derived from leaf-level gas exchange measurements carried out by the author for use in the DANUBIA crop growth model. In GECROS, the parameter Θ (convexity factor for response of J_2 to photosynthetic active radiation) is implemented as a constant value for reasons of simplicity (YIN & VAN LAAR 2005). In the DANUBIA crop growth model, this parameter is considered to be crop-specific and values for sugar beet and potato have been derived from measurements. Values of χ_{vcn} were determined for sugar beet, potato and maize.

Experimental design

The measurements were performed using the portable infra-read gas analyzer system CIRAS-1 together with the Automatic Universal Leaf Cuvette PLC6 (U) (*PP Systems*, Hitchin, Hertfordshire, UK). The leaf cuvette enclosed a leaf area of 4.5 cm².

The response of photosynthesis to varying CO_2 concentration was measured. Since the rate of net assimilation (A) in response to external CO_2 concentration (C_a) is affected by boundary layer as well as stomatal and mesophyll processes, the response of A to intercellular CO_2 concentration (C_i) is measured (LONG & BERNACCHI 2003). The value of C_i is calculated by CIRAS-1 using the CO_2 concentration of the air inside the leaf cuvette (C_a), as well as the transpiration and photosynthesis rate, and the total conductance of CO_2 transfer (PP SYSTEMS 2003).

The so-called A/C_i – curves were measured in summer 2005 on fully developed young leaves of different crops (sugar beet, potato, maize) in the field. During the construction of one A/C_i – curve, the same leaf remained in the leaf cuvette. To modify C_i, the CO_2 concentration in the leaf cuvette (C_a) was varied stepwise. According to PARSONS *et al.* (1997) the measurements were simultaneously conducted at ambient temperature, at saturated photosynthetic photon flux density (1500 µmol m^{-2} s^{-1}, generated by a LED light source) and finally at high ambient humidity to ensure open stomata. The series of measurements required for each A/C_i – curve proceeded from the value of ambient C_a (~ 370 µmol mol^{-1}). To avoid the effect of stomatal closure at high C_a, values of C_a were first decreased (in steps of 50 µmol mol^{-1}), and then - after returning to ambient concentration - increased (in steps of 100 to 200 µmol mol^{-1}). Measurements were recorded after A stabilized. When the first measurement of A at ambient C_a shows no systematic variation over a period of five minutes, steady-state activation of rubisco is assured (LONG & BERNACCHI 2003).

Fig. 23: Measurement of A/C_i – curves with the leaf cuvette.

Data analysis

The measured A/C_i - curves provide data of photosynthetic photon flux density, leaf temperature and C_i which served as input data for modelling photosynthesis rate according to the model GECROS. The corresponding model equations are given in chapter 2.2.2 (*Photosynthesis and transpiration).* Additionally, the photosynthetically active nitrogen content of leaves (g N m^{-2}) is needed for each A/C_i - curve. This value is either derived from the mean leaf nitrogen content (n) measured in the field (see chapter 3.1.1) or estimated in case of missing data. Table 20 lists the corresponding photosynthetically active nitrogen content, leaf temperature as well as date and number of measurements for each A/C_i - curve.

Table 20: Characteristics of measured A/C_i – curves.
Standard errors of the mean leaf temperature are shown.

crop and denotation	**date and number of measurements**	**leaf temperature (°C)**	**photosynthetically active leaf N content (g N m^{-2})**	
sugar beet a	22.06.2005 (16)	31.3 ± 0.49	2.38	(measured on same day)
sugar beet b	29.06.2005 (14)	28.1 ± 0.89	2.07	(interpolated from measurements taken on 22.06. and 8.07.)
sugar beet c	18.08.2005 (13)	25.7 ± 0.70	2.04	(interpolated from measurements taken on 10.08. and 31.08.)
potato a	20.07.2005 (16)	23.1 ± 0.31	1.56	(measured on same day)
potato b	03.08.2005 (15)	24.0 ± 0.28	1.19	(interpolated from measurements taken on 20.07. and 10.08.)
maize a	13.07.2005 (16)	35.0 ± 0.33	1.25	(estimated)
maize b	18.08.2005 (15)	30.8 ± 0.18	1.25	(estimated)

By comparing measured and modelled data, selected parameters were fitted using the least squares method (quasi-Newton method provided by *Solver* in *Microsoft Excel*®).

Only a small number of measured A/C_i – curves of sugar beet, potato and maize provided consistent values and therefore proved suitable for further analysis.

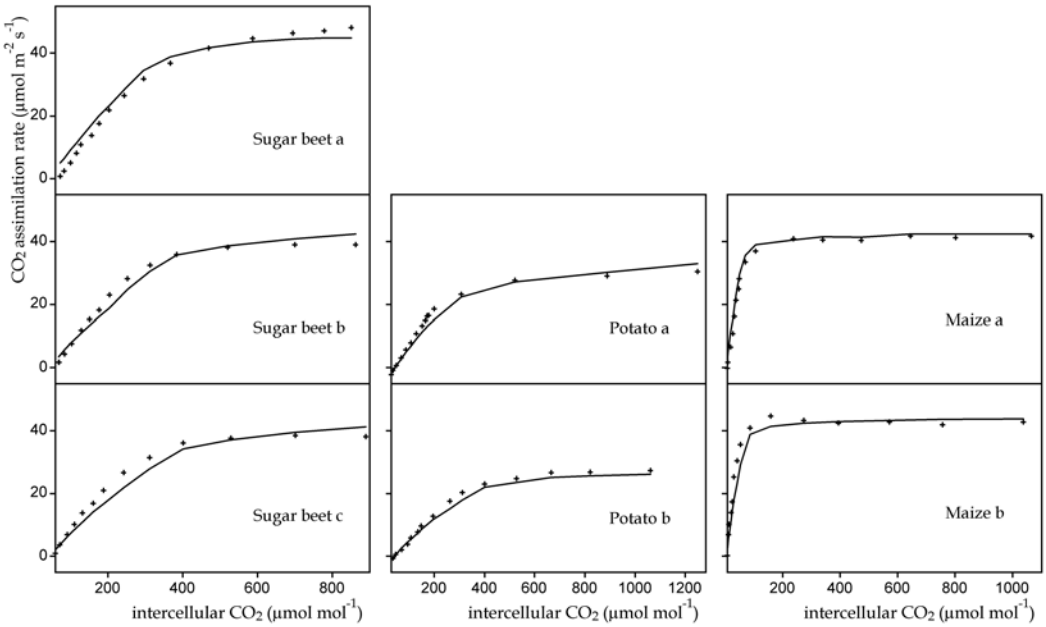

Fig. 24: Measured and modelled A/C_i – curves.

For analysis of all A/C_i – curves χ_{jn} is assumed to equal 2 χ_{vcn}. For potato and sugar beet, values of χ_{vcn}, Θ and E_{Jmax} were determined. Data of the different A/C_i – curves were pooled together for each crop to optimize the selected parameters (see Table 21).

Table 21: Optimized parameters derived from analysis of A/C_i – curves.

	χ_{vcn} (µmol CO_2 g^{-1} N s^{-1})	Θ (-)	E_{Jmax} (J mol^{-1})
sugar beet	50.31	0.67	39 600
potato	58.86	0.72	84 180
maize	62.00	-	-

Fig. 24 shows the measured and modelled A/C_i – curves with optimized parameters for sugar beet, potato and maize. Statistical criteria of measured versus modelled data for the A/C_i – curves, singly and in combination, are presented in Table 22. The modelling efficiency index (MEF) shows very close agreement. For the calculation of the statistical criteria, see Appendix F.

In case of maize, only the value of χ_{jn} was derived. The default value of Θ and the given value of E_{Jmax} according to the model GECROS were left unchanged. The results of the analysis (shown in Table 21 and Table 22) can be considered as a random sample for the affirmation of the C_4-photosynthesis model. The fitted value of χ_{vcn} only differs slightly from the default value of 60 µmol CO_2 g^{-1} N s^{-1}.

Table 22: Statistical characteristics of the fitted A/C_i – curves.
Values of root mean squared error (RMSE) and modelling efficiency statistic (MEF) are listed.

	RMSE	**MEF**
sugar beet a	9.49	0.973
sugar beet b	6.74	0.975
sugar beet c	9.95	0.961
sugar beet a-c combined	8.84	0.971
potato a	5.34	0.967
potato b	2.36	0.985
potato a-b combined	4.18	0.976
maize a	9.07	0.973
maize b	22.52	0.942
maize a-b combined	16.97	0.959

Although there were only few measurements to work upon, the presented analysis demonstrates the validity of the photosynthesis model and of the simplifying assumptions regarding the parameterization.

2.4.3 Definition of initial values

When a plant is sown in the model, several crop parameters are initialized using crop-specific data. Table 23 shows the calculation of initial values in the DANUBIA crop growth model. Initialization is performed according to the model GECROS (YIN & VAN LAAR 2005).

Calculation of storage organ growth efficiency ($Y_{G,S}$) is explained in the sub-chapter 2.2.4 (*Respiration*). The initial carbon amount in leaves (C_{LV}) and roots (C_R), respectively, is derived from plant density (d_p), seed weight (S_w), fraction of carbon in seed biomass ($f_{c,S}$), efficiency of germination (ε_g) and an initial fraction of carbon allocated to the shoot ($f_{C,ini}$). Calculation of the initial nitrogen amount in leaves (N_{LV}) and roots (N_R), respectively, is based on the initial critical shoot nitrogen concentration n_{cri0}. An initial fraction of nitrogen allocated to the shoot ($f_{N,ini}$) is introduced for calculating N_R. Rooting depth D is initialized with crop-specific sowing depth.

Table 23: Initialization of crop parameters.

Calculation of initial value	Unit	
fraction of proteins in biomass of organs $f_{pro} = 6.25\ n_{SO}$	-	(2.4.3–1)
fraction of carbohydrates in biomass of organs $f_{car} = 1 - f_{pro} - f_{lip} - f_{lig} - f_{oac} - f_{min}$	-	(2.4.3–2)
fraction of carbon in seed biomass $f_{c,S} = 0.444\ f_{car} + 0.531\ f_{pro} + 0.774\ f_{lip} + 0.667\ f_{lig} + 0.368\ f_{oac}$	g C g^{-1}	(2.4.3–3)
storage organ growth efficiency $Y_{G,S} = \frac{f_{c,S}}{1.275\ f_{car} + 1.887\ f_{pro} + 3.189\ f_{lip} + 2.231\ f_{lig} + 0.954\ f_{oac}} \frac{30}{12}$	g C g^{-1} C	(2.4.3–4)
carbon in living leaf $C_{LV} = d_p\ S_w\ f_{c,S}\ \varepsilon_g\ f_{C,ini}$	g C m^{-2}	(2.4.3–5)
carbon in living root (including root reserves) $C_R = d_p\ S_w\ f_{c,S}\ \varepsilon_g \left(1 - f_{c,ini}\right)$	g C m^{-2}	(2.4.3–6)
nitrogen in living leaf $N_{LV} = n_{cri0}\ C_{LV} / f_{c,V}$	g N m^{-2}	(2.4.3–7)
nitrogen in living root $N_R = p_d\ S_W\ \varepsilon_g\ n_{cri0}\ f_{C,ini} / f_{N,ini} - N_{LV}$	g N m^{-2}	(2.4.3–8)
minimum N concentration in leaf $n_{Lmin} = s_{la}\ n_b$	g N g^{-1}	(2.4.3–9)
green leaf area index of canopy $L = C_{LV} / f_{c,V}\ S_{la}$	m^2 leaf m^{-2}	(2.4.3–10)
specific leaf N content in bottom leaves of canopy $n_{bot} = N_{LV} / L$	g N m^{-2} leaf	(2.4.3–11)
plant height $H = H_{max} / 1000$	m	(2.4.3–12)

3 Model validation and application

First, the validation analysis of the DANUBIA crop growth model for the various crops considered is presented in this chapter. Secondly, the application of the model to simulate yield is demonstrated on the regional scale. Additionally, the application to Global Change effects is included to evaluate the responsiveness of the model.

All model results presented in this study are derived from coupled simulations of the DANUBIA crop growth model, the DANUBIA soil model and the DANUBIA surface model.

3.1 Validation

For the validation of the DANUBIA crop growth model, measurements on the field scale are compared with model results. The various experimental data sets used for the validation analysis are described in chapter 3.1.1. The results of the comparison between simulated and measured data for the different crops (sugar beet, spring barley, maize, winter wheat, potato) are presented in chapter 3.1.2.

3.1.1 Experimental data sets

For the validation analysis, several data sets of field measurements are employed including the author´s own measurements taken in the years 2004 and 2005 as well as data from the literature. Fig. 25 shows the location of the test sites and Table 24 gives an overview of the data sets considered for each crop.

Related input data (meteorological drivers, soil data, latitude of the site and farming practices) for each experimental data set are used for coupled model test runs of the DANUBIA crop growth model, DANUBIA soil model and DANUBIA surface model (see chapter 2.3).

Table 24: Experimental data sets used for validation.

Crop, denotation and year	Location	Source
sugar beet		
Feienberg 2004 and 2005	50°52′ N, 7°13′ E	author´s measurements
Nienwohlde 1990	52°50′ N, 10°35′ E	MCVOY *et al.* (1995)
Euerhausen 2000	49°36′ N, 9°56′ E	KENTER (2003)
Friemar 2000	50°58′ N, 10°44′ E	KENTER (2003)
Plattling 2000 and 2001	48°48′ N, 12°50′ E	KENTER (2003)
spring barley		
Nienwohlde 1991	52°50′ N, 10°35′ E	MCVOY *et al.* (1995)
Wilzhofen 1997	47°52′ N, 11°09′ E	University of Munich
maize		
Feienberg 2004 and 2005	50°52′ N, 7°13′ E	author´s measurements
Wilzhofen 1997	47°52′ N, 11°09′ E	University of Munich
winter wheat		
Feienberg 2003/04	50°52′ N, 7°13′ E	author´s measurements
Bockschlag 1990/91	52°01′ N, 10°27′ E	MCVOY *et al.* (1995)
Neuenkirchen 1990/91	52°01′ N, 10°27′ E	MCVOY *et al.* (1995)
potato		
Hofferhof 2004 and 2005	50°55′ N, 7°13′ E	author´s measurements

Table 25 lists the experimental test sites along with the corresponding specifications for climate and topography. All measurements were conducted on commercial farming fields. In the following, these data sets are described classified by their origin. Information on management practices is given in chapter 3.1.2.

Table 25: Description of experimental test sites.

Experimental site	Soil type and texture	Precipitation (mm a^{-1})	Mean annual air temperature (°C)	Altitude (m)
Feienberg	Luvisol, silt loam	803 *	9.6 *	165
Hofferhof	Luvisol, silt loam	803 *	9.6 *	170
Bockschlag	Loess; silt loam	590	8.6	151
Neuenkirchen	Loess; silt loam	590	8.6	145
Nienwohlde	Luvisol; sand	650	9.0	103
Wilzhofen	Histosol; silt	1110#	7.5#	550
Euerhausen	Luvisol; silty loam	625	9.1	310
Friemar	Chernozem; silty loam	519	7.5	285
Plattling	Luvisol; silty loam	800	7.6	325

* data from the meteorological station Köln-Wahn (92 m), average values for 1961-1990 (DWD 2007)
# data from the meteorological station Attenkam (672 m), average values for 1961-1990 (DWD 2007)

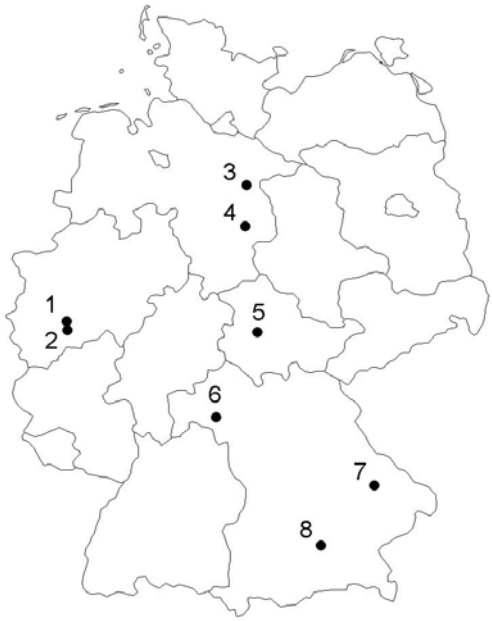

Fig. 25: Location of the experimental sites (1: Hofferhof, 2: Feienberg, 3: Nienwohlde, 4: Bockschlag and Neuenkirchen, 5: Friemar, 6: Euerhausen, 7: Plattling, 8: Wilzhofen).

Author´s field measurements

During the growing seasons 2004 and 2005 the author conducted extensive field measurement campaigns. The two test sites Feienberg and Hofferhof are located south-east of Cologne within the catchment area of the river Sieg (approx. 2 850 km², 50°47′ N, 7°18′ E). Fig. 26 shows its orographical structure including areas of low mountain ranges, hill country and lowland with altitudes ranging from 40 m to 677 m. The Sieg catchment area constitutes part of the Rhenish Slate Mountains. As is to be expected from the heterogeneous relief structure, annual precipitation ranges from 700 to 1400 mm (FEDERAL MINISTRY FOR ENVIRONMENT, NATURE CONSERVATION AND NUCLEAR SAFETY, ed., 2000). The test sites are situated on plateaus characterized by thick loess covers providing fertile soils (luvisols). The soil texture is silt loam (8 % sand, 22 % clay and 70 % silt). The test sites were explicitly chosen for the homogeneous soils. Fig. 26 shows the location of the test sites.

Because no meteorological data were recorded in the vicinity of the test sites, data from weather stations of the *German National Weather Service* were used. To generate hourly data for the two study sites, the **Pr**ocess **O**riented **M**odular **E**nvironmen**t** and **V**egetation model (PROMET-V) (SCHNEIDER 1999, 2003) was utilized to interpolate measured data from the six nearest stations. First, measured data (three records per day) are interpolated using a spline interpolation scheme to provide hourly data.

Global radiation is derived from cloud cover data according to MÖSER & RASCHKE (1983). Spatial interpolation is performed using a digital elevation model (50 m * 50 m) of the Sieg catchment area.

Based on the known elevations at the meteorological stations a linear regression between elevation and meteorological parameter is calculated. Furthermore, the residue of the measured value to the regression line is computed. The regression equation is then used together with the digital elevation model to account for the variance of the meteorological parameter explained by the topography. The spatial pattern of the residues is modelled using an inverse distance weighting technique. Summing up the result derived from the regression equation and from the inverse distance weighting method reproduces the measured values at the meteorological stations exactly and provides realistic spatial patterns of the meteorological parameters. Further details of the temporal and spatial interpolation are given by SCHNEIDER (1999) and STRASSER (1998).

In both years, crops of winter wheat, maize, sugar beet and potato were monitored (one field per crop). Field measurements were carried out at intervals of one to four weeks. Fresh and dry matter of biomass, its nitrogen content, leaf area index, canopy height, phenological stage and plant density were determined. For the monitored winter wheat, maize and sugar beet fields in 2005, measurements of soil moisture as well as nitrate and ammonium content in three soil layers (each 30 cm deep) are available (measurements by Christian W. Klar, *Department of Geography, University of Cologne*).

Crop measurements were carried out at three sampling locations per field. Phenological stage was documented according to the BBCH-scale (MEIER, ed., 2001). In the case of row crops, at least three representative plants per sampling point were taken. Wheat plants were harvested from a 60 cm long row. To determine fresh weight, the plants were divided into their constituents of living and dead leaves, stem (including leaf sheath) and storage organ (including grain, glume and rest of the ear in the case of maize and wheat). The fresh weight of the plant organs was determined for each single sampled plant of maize, potato and sugar beet.

For the determination of dry matter, sub-samples of each portion were dried at 105 °C until constant weight was reached. Further sub-samples of the dried plant material were homogenized in a mortar and subsequently ground in a planetary mill for the

determination of total nitrogen content by means of an elemental analyser (CNS Elemental Analyser Vario EL, *Elementar Analysensysteme GmbH*, Hanau, Germany).

Leaf area index was measured using a destructive (direct) method (LI-3000A Area Meter, *LI-COR Biosciences*, Lincoln, NE, USA). The leaf area is measured by a scanning head combined with a transparent belt conveyer. As the leaves have already been collected to be weighed for dry matter determination, this procedure requires only little extra effort.

In 2004, LAI of sugar beet and winter wheat was additionally recorded using the non-destructive, indirect SunScan Canopy Analysis System (*Delta T-Devices*, Cambridge, UK). Six measurements were taken at each sampling point. The SunScan system allows rapid measurements of LAI based on simultaneous radiation measurements above and within the canopy. In contrast to the direct method it is not possible to make a distinction between leaves and stems or between brown (non-photosynthetic) and green leaves. Another disadvantage is that LAI of crops at an early growth stage cannot be determined. In addition, the indirect system cannot be utilized in potato fields because of the hilled rows. A review of LAI measurement methods is given by BRÉDA (2003). For the validation analysis, the direct LAI measurements are used.

Measured crop data are listed in Appendix G. All fields were cultivated according to standard farming practices. Detailed information on plant density, planting and harvesting dates as well as on use of fertilizers (dose, formulation, dates) was provided by the farmers.

The combination of soil and crop measurements as well as accurate management information for the year 2005 presents an ideal validation data set for agro-ecosystem models.

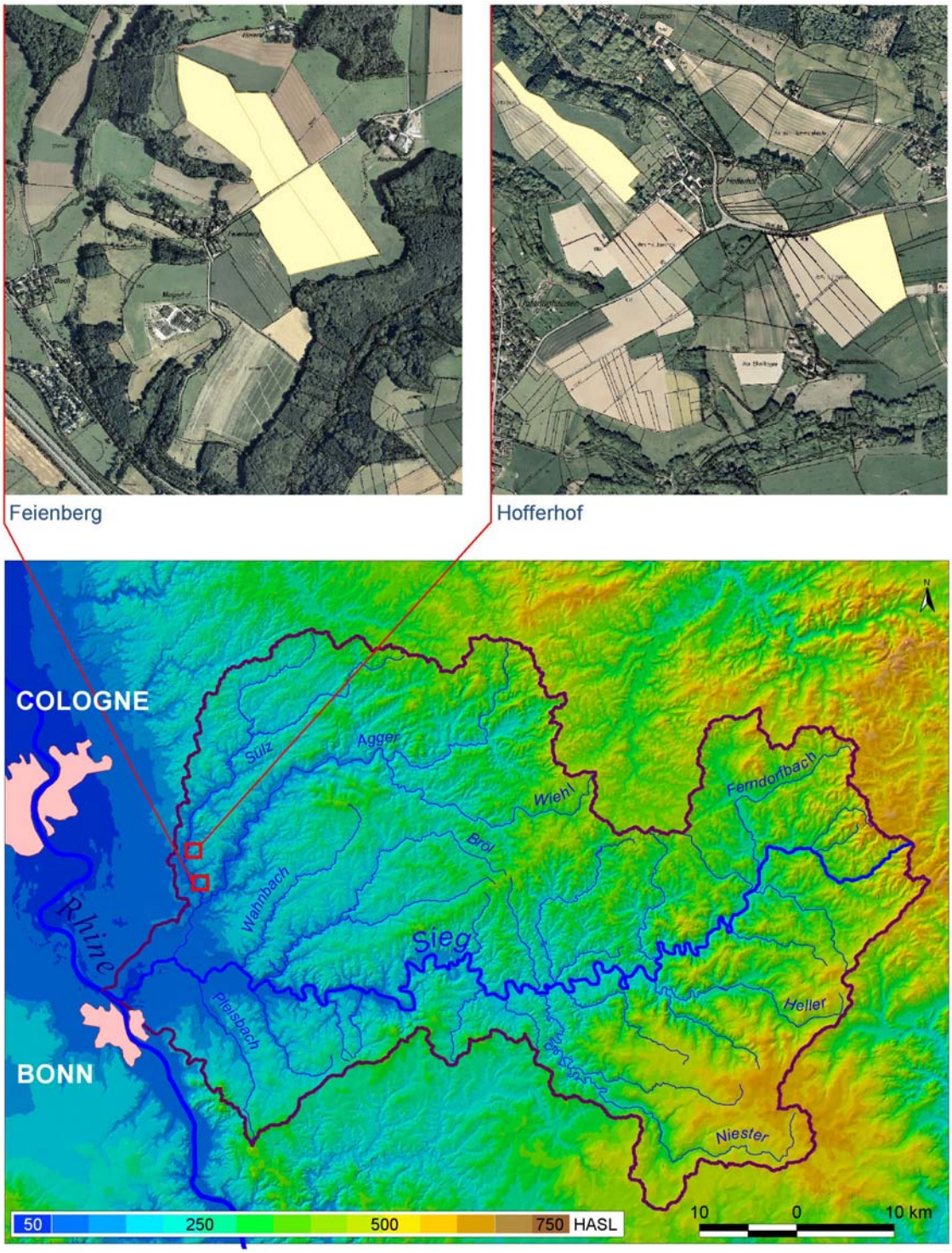

Fig. 26: Location of the test sites Feienberg and Hofferhof in the Sieg catchment area. The test fields of the years 2004 and 2005 are marked with yellow. Maps are based on data from the *Land Survey Office of North Rhine-Westphalia.*

McVoy - data set

A multi-year data set for various fields at three locations in Northern Germany is documented by MCVOY *et al.* (1995). These data have been specially published for the evaluation of agro-ecosystem models. For the validation of the DANUBIA crop growth model, field measurements of summer barley, sugar beet and winter wheat from the years 1990 and 1991 are used. Hourly meteorological data, recorded at the test sites, were provided by the *Institute of Geography and Geoecology, Technical University of Braunschweig*.

Measurements of dry weight and nitrogen concentration of biomass as well as determination of canopy height, LAI and development stage are provided for six dates between planting and harvesting of the crops (measurements partly incomplete). Development stages were documented according to the Zadoks-scale (ZADOKS *et al.* 1974). In the case of cereals, an area of approx. 0.4 m² from three rows was harvested at each of the four sampling points in a field. The biomass was divided into leaf, stem (including leaf sheath) and ear (including grain, glume and rest of the ear). Sugar beet plants were collected from an area of ca. 7 m² at each of the six sampling points. For further analysis, the plants were separated into beets and leaves (including petioles). The nitrogen content of biomass was determined by Kjeldahl extraction. It is assumed that LAI was measured using a direct system and that only green leaves were considered.

In addition to the crop data, measurements of soil water and nitrogen (nitrate and ammonium) content in three soil layers are presented. Management information for each field (crop variety, planting and harvesting dates, fertilizer dose, its formulation and dates when applied) are listed in detail. Unfortunately, the significant parameter plant density is not mentioned at all. In some of the fields, different fertilizer treatments were carried out to monitor the response of the agro-ecosystem. The farmer´s standard fertilizing procedure is denoted by "N4", whereas "N0" and "N6" signify "no fertilizer used" and "reduced fertilizer dose" respectively.

Because of the ample measurement data at disposal, numerous publications (e.g. GRANT 1995, KERSEBAUM 1995, WANG & ENGEL 1998, WANG & ENGEL 2002) deal with the validation of ecosystem models using the MCVOY-data set. More details about the presented data set are reported by MCVOY *et al.* (1995).

University of Munich – data set

Many field data sets for the validation of ecosystem models have been collected in recent years by researchers from the *Department of Geography, University of Munich.* The fields are located in the Ammer catchment area south-west of Munich. For the validation of the DANUBIA crop growth model, field measurements of maize and spring barley at the test site Wilzhofen in the year 1997 are used.

Hourly meteorological data were provided by the DANUBIA component *Atmostations* which interpolates measured station data utilizing a digital elevation model. The procedure is the same as described above for the model PROMET-V (see "Author´s field measurements" in this chapter). Measurements of leaf area index and dry matter were taken eleven times during the vegetation period. At each of three sampling points, three maize plants were harvested. Barley plants were harvested from a 25 cm long row. Direct measurements of LAI were carried out with an automatic area meter (AAM-8, *Hayashi Denko Co. Ltd.*, Tokyo, Japan).

The field was cultivated according to standard farming practices. Detailed management information is not available.

Kenter – data set

Measurements of leaf area index and biomass for sugar beet at different test sites during 2000 and 2001 are published by KENTER (2003). Hourly meteorological input data were obtained from nearby weather stations provided by the *Agro-Meteorological Network Bavaria* (stations Euerhausen and Uttenkofen) and the *Thuringian Regional Office for Agriculture* (station Friemar).

Biomass and leaf area index measurements were taken six times during the growing season. Each time an area of 10 m² in a random grid pattern across the field was harvested and four replications taken. For the determination of dry weight, the plants were separated into beets and leaves (including petioles). Leaf area index was determined using an indirect measurement system, the LAI-2000 Plant Canopy Analyzer (*LI-COR Biosciences*, Lincoln, NE, USA). In each of the four sample areas, four LAI measurements were taken to derive a representative value for the field.

The sugar beet crops were cultivated according to standard farm practices. Information on variety, plant density and sowing date has been published (KENTER 2003). For the purpose of the model validation analysis, the large sample size of 80 – 100 single plants

per date and field is very advantageous, whereas the missing dates and the lack of fertilizer dose specification are a drawback.

Detailed information on the described data sets is given by KENTER (2003) and KENTER *et al.* (2006).

None of the available data sets includes measurements of root biomass or root length density. These data would add to a comprehensive validation of biomass allocation, root growth as well as water and nitrogen uptake.

Ideally, validation data sets for process-based crop growth models should include measurements, for instance, of sap flow and transpiration, too, which offer the possibility of directly validating the modelled processes.

3.1.2 Comparison of model results with measurements

The ability of the model to simulate plant growth is assessed by comparing model predictions with observed data on the field scale. The results of this analysis are presented in a number of graphs as well as through a set of model performance statistics for each crop. Graphs of modelled and measured data versus time give a first impression of the extent of agreement between both sets of values and illustrate where the model results differ from measurements.

Model performance statistics

WILLMOTT (1982) underlines the fact that the frequently used coefficient of correlation r and the coefficient of determination r^2 may prove misleading because both neglect to consider systematic errors. The magnitudes of r and r^2 are not consistently related to the accuracy of model simulations.

For the validation of the DANUBIA crop growth model, several model performance statistics are applied. The root mean squared error (RMSE), the relative root mean squared error (RRMSE) and the mean absolute error (MAE) are chosen to describe the average discrepancy between simulated and observed data. Agreement between model and measurements is quantified by two normalized measures: the index of agreement (IA, proposed by WILLMOTT 1981) and the modelling efficiency statistic (MEF).

The formulas of the model performance statistics are listed in Appendix F according to WALLACH (2006).

Assessment of the adequacy of a model needs to be undertaken in terms of its objectives. Taking the function of the crop growth model within the decision support system DANUBIA into account, special emphasis is laid on the prediction of yield, transpiration, nitrogen uptake and leaf area index as the determinant of transpiration.

3.1.2.1 Sugar beet

In 2005, sugar beet was cultivated on 419 000 hectares in Germany, representing 3.5 % of the entire arable land (WIRTSCHAFTLICHE VEREINIGUNG ZUCKER, ed., 2007). Among root crops, the area under sugar beet cultivation constitutes more than half (Fig. 27).

71 000 ha of the sugar beet cultivation area lie in Bavaria, with an average yield of 655 quintals ha^{-1} (1 quintal = 100 kg) between 1999 to 2004 (BAVARIAN MINISTRY OF AGRICULTURE AND FORESTRY, ed., 2006).

In Germany, sugar beet grows predominantly on very fertile loess or chernozem soils. Other locations of sugar beet crops are on fertile alluvial soils, on glacial lowlands or on sandy soils in river valleys. In the latter case, a certain amount of irrigation may be necessary. From the soils listed it may be seen that sugar beet crops are found primarily in the lowlands, but are also raised in loess-covered hill regions. (MÄRLÄNDER *et al.* 2003)

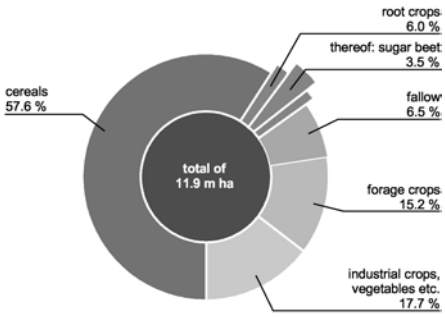

Fig. 27: Area under sugar beet cultivation in Germany in 2005
(redrawn from WIRTSCHAFTLICHE VEREINIGUNG ZUCKER, ed., 2007).

Sugar beet typically evidences a nitrogen requirement of 200-250 kg ha^{-1}. Because 100-150 kg ha^{-1} are mineralized from the soil during the growth period, only about 100 kg ha^{-1} of fertilizer is needed on fertile loess soils. Increased nitrogen uptake does not imply a higher yield as in the case of most other crops, because the produced sucrose should be free of nitrogen. (MÄRLÄNDER *et al.* 2003)

Seven field data sets are used for the validation of the DANUBIA crop growth model for sugar beet. Table 26 lists the cultivation data and Table 28 summarizes model performance statistics for each data set.

Since plant organs in the model are classified according to their functional rather than their morphological features, the petioles of the sugar beet leaves are considered as stems. For comparison with measurement data, modelled stem and leaf are combined.

Table 26: Cultivation data of sugar beet fields (figures in italics are estimated).

	plant density (plants m^{-2})	**sowing date**	**harvesting date**	**fertilizer date**	**amount (kg N ha^{-1})** NH_4	NO_3	Urea
Feienberg 2004	10.6	21.04.	15.09.	20.04.	-	80	-
Feienberg 2005	10.4	18.04.	05.10.	01.04.	-	-	30
				14.04.	-	50	50
Nienwohlde 1990	*10*	31.03.	29.09.	24.02.	-	-	57
				30.04.	-	-	60
				08.06.	-	-	73
Euerhausen 2000	8.5	21.03.	09.10. *	*15.03.*	*21*	*21*	*42*
				04.05.	*9*	*9*	*18*
Friemar 2000	8.1	07.04.	18.10. *	*05.04.*	*21*	*21*	*42*
				29.04.	*9*	*9*	*18*
Plattling 2000	7.8	10.04.	10.10. *	*09.04.*	*21*	*21*	*42*
				19.05.	*9*	*9*	*18*
Plattling 2001	9.2	25.04.	22.10. *	*24.04.*	*21*	*21*	*42*
				29.05.	*9*	*9*	*18*

* last measurement date

Feienberg 2004

Based on the measurements, the phenological parameter $R_{max,v}$ (maximum development rate in the period before taproot development) was set to 0.0345 d^{-1}.

In contrast to the two preceding years, in 2004 the agro-meteorological situation was not aberrant in any way.

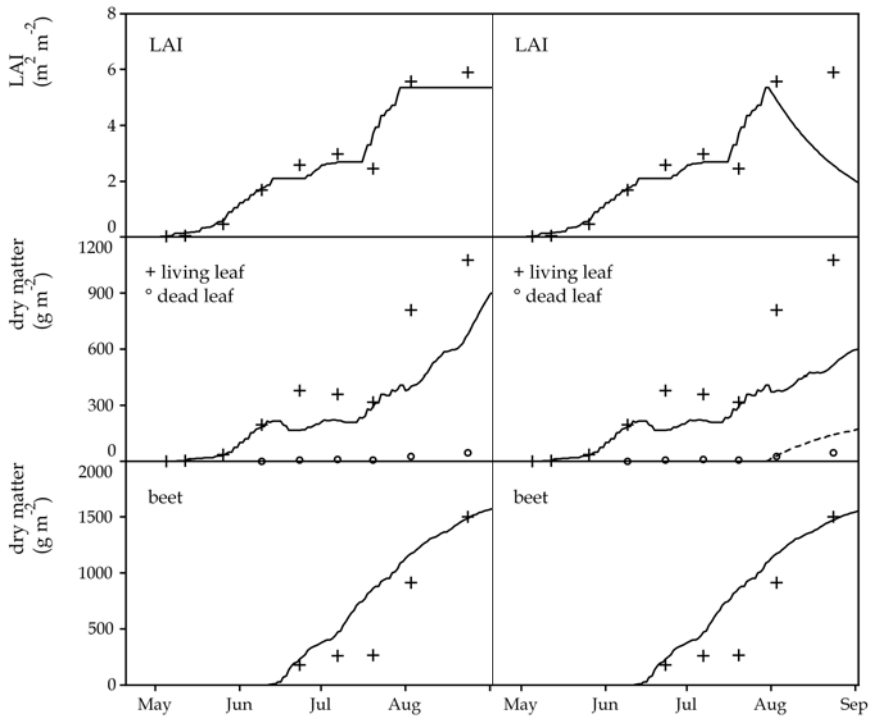

Fig. 28: Modelled (lines) and measured (symbols) LAI (leaf area index) and biomass data of sugar beet, Feienberg 2004 (left: not assuming standard senescence, right: assuming standard senescence).

Fig. 28 compares measured and modelled data. The model results illustrated by the graphs on the left do not assume standard senescence, those on the right do. The field measurements show the presence of dead leaves, which are entirely absent in the first case and are overestimated in the second. In the following, all statements refer to the modelled results assuming no standard senescence.

The simulated LAI development shows close agreement with the measured values, particularly at the onset of growth. The steep increase of LAI in the first half of August is well captured by the model. The measured data show no decrease of green LAI towards harvest date. In the model results, the nitrogen-determined LAI does not fall below the carbon-determined LAI, consequently no senescence is induced. Ignoring the assumption of a standard senescence (3 % loss of leaf weight per day) after the end of the seed-number determining period (see chapter 2.2.10: *Leaf area and senescence*) results in a constant LAI at the end of the growing period.

The modelled biomass of living leaves tallies well only with the first measurement data. At the time when beet growth starts, the model allocates the assimilated carbon to the beet, with leaf weight even decreasing at the beginning. Compared with the field data, beet biomass in the following weeks increases too rapidly at the expense of leaf biomass. While the simulated beet biomass almost exactly matches the field value at

the final measurement date, the leaf biomass is substantially underestimated. This inaccuracy is acceptable, since the prediction of yield and LAI as the determinant of transpiration is most important within the context of this study.

Concerning the water budget of the crop, total precipitation sum from sowing to harvesting is 417 mm, distributed rather evenly without long periods of no rainfall. No water stress was modelled and the transpiration sum amounted to 312 mm.

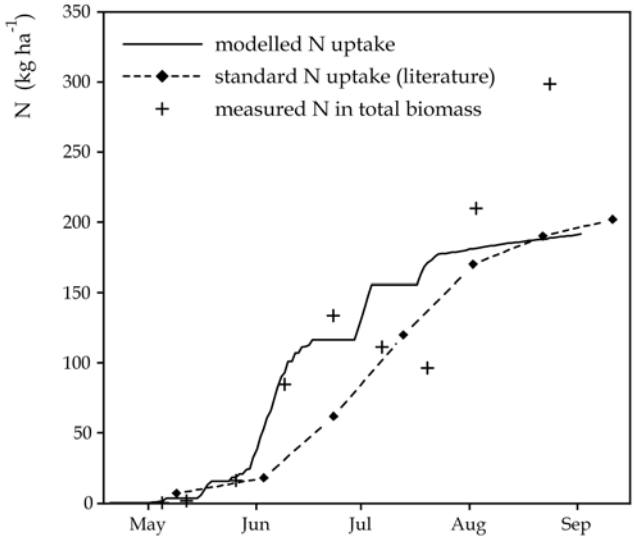

Fig. 29: Cumulative nitrogen uptake of sugar beet, Feienberg 2004.
Data of measured nitrogen in total biomass refer to living and dead biomass, excluding roots.

Fig. 29 shows the modelled nitrogen uptake as well as the measured nitrogen content in total biomass (excluding roots). Also given here is a commonly observed course of nitrogen uptake for sugar beet as found in data from the literature (HEGE 1998).

The modelled cumulative nitrogen uptake gives 191 kg N ha^{-1}, an amount that corresponds well to the total nitrogen generally needed by sugar beet, taking into account the early harvesting date.

As Fig. 29 shows, the modelled data match the measured data very well at the outset. However, they subsequently diverge from the trend found in the relevant literature. The measured nitrogen value at the seventh sampling date (August 3rd) is open to conjecture, as it shows a decline. The last measured value gives an unlikely, very high value of nearly 350 kg N ha^{-1}. The magnitude of the analyzed nitrogen concentration in biomass shows realistic values. These analyzed data are extrapolated via the measured dry matter of biomass to give the nitrogen content in mass per area. This fact indicates that the measured dry matter values are probably not representative for the whole

field. The rather small sample size may be the reason. An analysis of the total fresh weight per plant – as well as relative allocated fractions of carbon to the different plant organs – revealed large variances. At the beginning of growth, the individual plants are quite homogeneous but grow more and more disparate as they develop.

Feienberg 2005

Based on the measurements, the phenological parameter $R_{max,v}$ was set to 0.0286 d^{-1}. Fig. 30 shows the modelled and observed data for the sugar beet crop in Feienberg 2005. Compared with the data set for 2004, results match better. At the beginning, LAI increase is only slightly overestimated by the model. However, the last measured values are substantially exceeded. Thus the mean absolute error averaged over the growing season for green LAI is 0.54. Senescence is induced because of nitrogen remobilization from the leaves to the storage organ. The predicted amount of dead leaves fits the measured value at the last sampling date. Living leaf mass is accurately predicted by the model at the start, but later shows significant deviations. Beet biomass is slightly overestimated. The statistical analysis in terms of beet mass shows very good results (see Table 28).

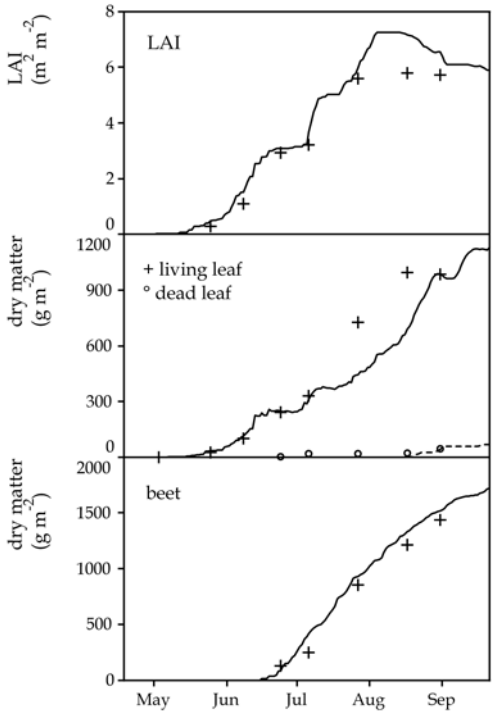

Fig. 30: Modelled (lines) and measured (symbols) LAI and biomass data of sugar beet, Feienberg 2005.

From sowing until harvesting the total precipitation is 528 mm, with no prolonged periods without rainfall. More than one-tenth (57 mm) accumulated within only five hours on June 30th. The modelled total transpiration results in 351 mm. Moderate water stress is modelled on many days in September. The total rainfall in September 2005 is only half (47 mm) what it was in September of the preceding year.

Fig. 31 presents the modelled transpiration and water uptake rates from the three soil layers. At the end of the growing season, potential transpiration is reduced due to soil water shortage. Comparison of measured water content in three soil layers (simulated by the DANUBIA soil model) shows close agreement except for a too pronounced decline of soil moisture towards harvesting. Probably, the rather high modelled LAI causes an overestimation of transpiration.

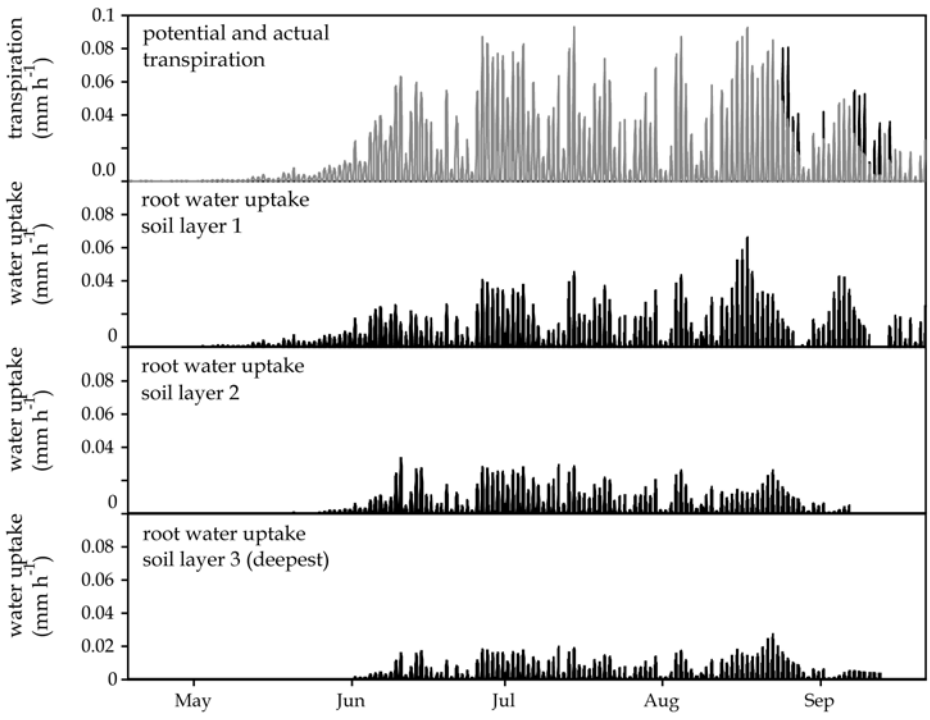

Fig. 31: Modelled hourly transpiration and water uptake rates of sugar beet, Feienberg 2005. Actual transpiration is depicted in grey.

Fig. 32 compares measured with modelled mineral nitrogen content (calculated by the DANUBIA soil model) at a depth of 0-90 cm. The increase caused by mineralization as well as the following decrease in soil mineral nitrogen content caused by crop nitrogen uptake is very well depicted.

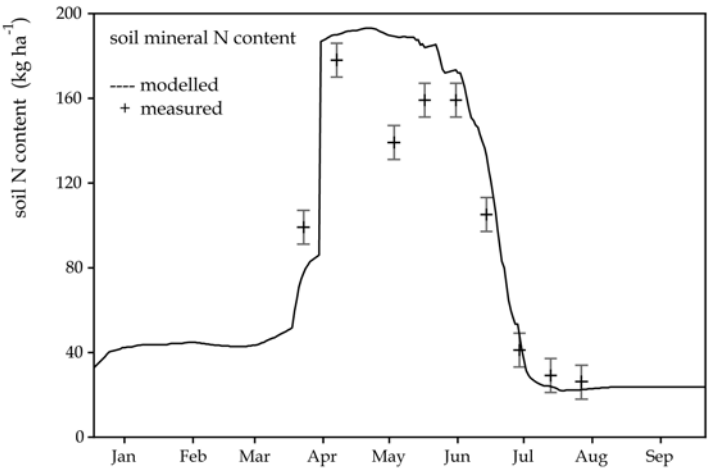

Fig. 32: Measured and modelled soil mineral nitrogen content (0-90 cm) for sugar beet, Feienberg 2005. Error bars depict measurement accuracy (± 8 kg N ha^{-1}). Measurements provided by C. W. Klar.

As described for the validation of sugar beet in Feienberg 2004, Fig. 33 compares the modelled, standard and measured nitrogen uptake. The modelled cumulative nitrogen uptake is 190 kg N ha^{-1}. In analogy to Fig. 29, at first the modelled and measured data agree closely and show a different trend compared with the literature data. The last three measured values of nitrogen content in biomass are unrealistically high. Because of the causal relationship between measured biomass and nitrogen content per area, the hypothesis gains weight that the sampled plants at late measurement dates are not representative of the whole field.

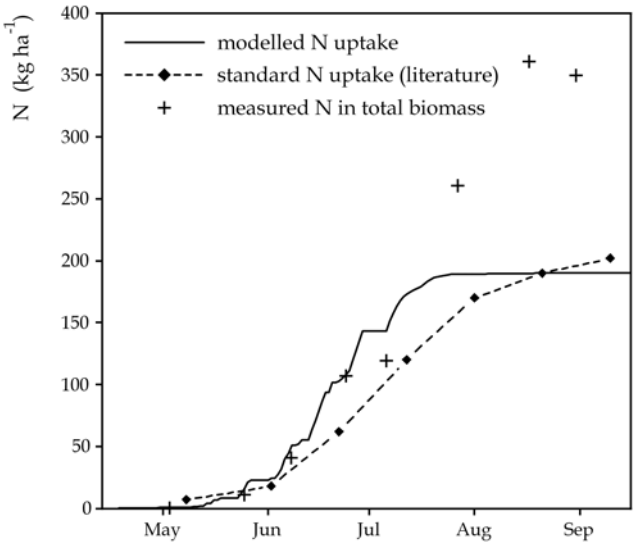

Fig. 33: Cumulative nitrogen uptake of sugar beet, Feienberg 2005.
Data of measured nitrogen in total biomass refer to living and dead biomass, excluding roots.

Nienwohlde 1990

Based on the measurements, the phenological parameter $R_{max,v}$ is set to 0.0357 d^{-1}. Plant density, being unknown, is set to 10 plants m^{-2}. Fig. 34 shows the modelled and observed LAI and biomass data for the sugar beet crop at Nienwohlde in 1990.

The modelled LAI curve deviates strongly from two of the only four measured values. Leaf as well as beet biomass are simulated fairly well. Standard senescence leads to the LAI declining after the end of the seed-determining period. No measurements for dead leaves are available. Seasonal coverage of the sampling is too sparse to allow a thorough validation. Because of the sandy soil, the field was irrigated on the 13th and 27th July (28 mm and 29 mm) and on the 2nd and 16th August (45 mm and 38 mm). According to the model, no water stress occurs. The modelled transpiration sum gives 383 mm.

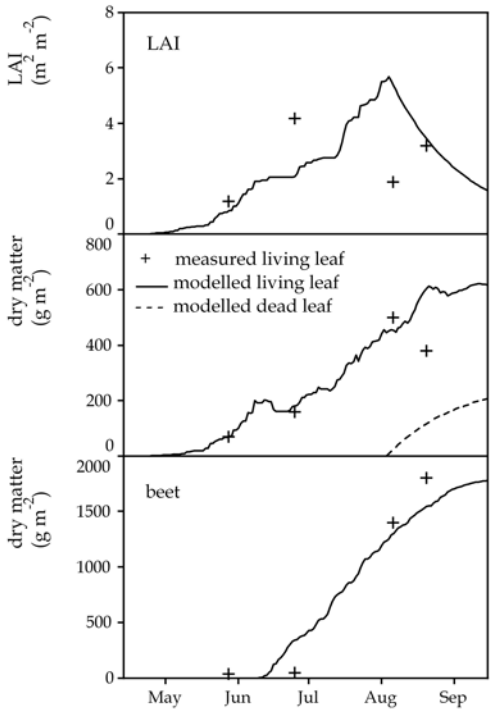

Fig. 34: Modelled (lines) and measured (symbols) LAI and biomass data of sugar beet, Nienwohlde 1990.

Fig. 35 compares the modelled, standard and measured nitrogen uptake. The modelled nitrogen uptake over the growing season reaches 198 kg N ha^{-1}. When compared with the literature data, modelled and measured data show a stronger nitrogen uptake at the beginning. This finding coincides with the two former validation data sets (Feienberg 2004 and 2005). Towards harvesting date, values of all three nitrogen uptake sums displayed in the graph show a very close agreement.

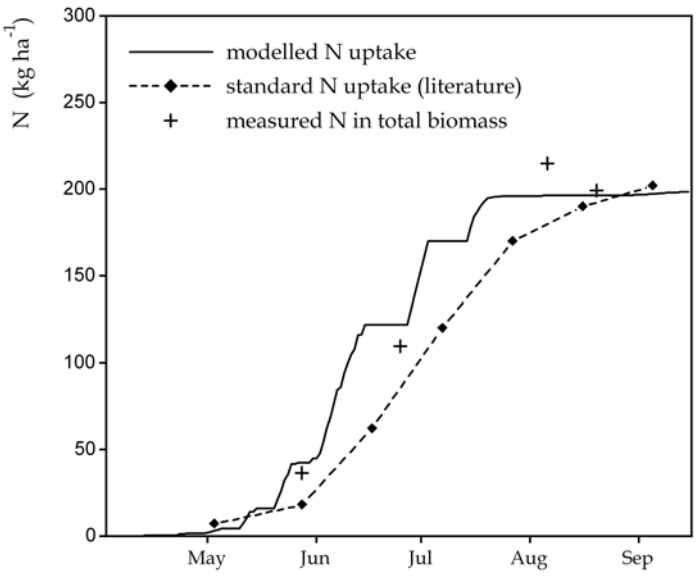

Fig. 35: Cumulative nitrogen uptake of sugar beet, Nienwohlde 1990.
Data of measured nitrogen in total biomass refer to living and dead biomass, excluding roots.

For an additional validation of the modelled nitrogen uptake, measurements of soil mineral nitrogen content are employed. Fig. 36 compares these measurements with data at a depth of 0-90 cm, as modelled by the DANUBIA soil model. The effect of the three fertilizer applications is clearly reflected in steep increases. Since the measured maximum value fits the modelled one, the overestimation seen in the subsequent measurements indicates that the depletion of the soil nitrogen pool probably is underestimated by the soil model. A likely reason is the underestimation of nitrate leaching in the sand soil.

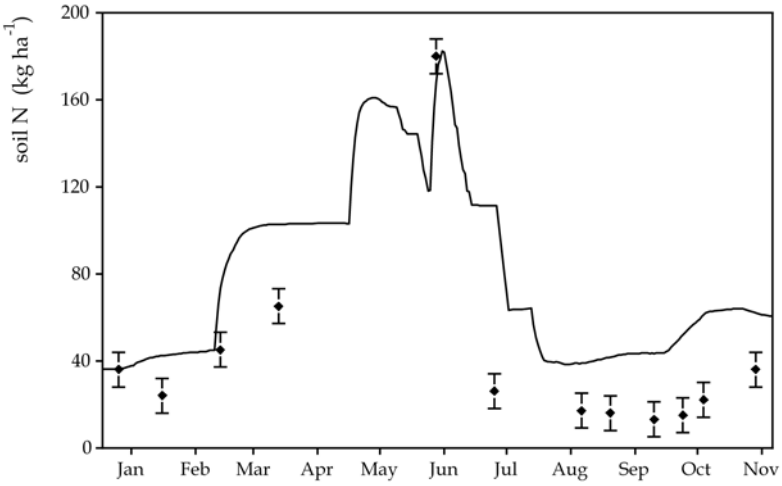

Fig. 36: Measured and modelled soil mineral nitrogen content (0-90 cm) for sugar beet, Nienwohlde 1990.
Error bars depict measurement accuracy (± 8 kg N ha^{-1}).

This assumption is affirmed by the good agreement between measured and modelled nitrogen data shown in Fig. 35. Two of the first four measured values of soil nitrogen before the sowing date are already substantially overestimated by the model (Fig. 36). These discrepancies are possibly also due to nitrate leaching being underestimated. Additional measurement data, especially when gathered in the first weeks after sowing, would allow a more detailed analysis.

Euerhausen 2000, Friemar 2000, Plattling 2000, Plattling 2001

For comparison with the field measurements published by KENTER (2003), the phenological parameter $R_{max,v}$ was set to the standard value of 0.0333 d^{-1}.

Because of lack of information about timing and quantity of fertilizer applied, a standard fertilization (120 kg N ha^{-1}) was assumed. MÄRLÄNDER *et al.* (2003) state that a fertilizer dose of ~ 100 kg N ha^{-1} is typical on fertile loess soils and that on more than 75 % of the sugar beet fields less than 120 kg N ha^{-1} are being applied. Without knowing the preceding crop, assumptions about use of fertilizer are uncertain. To avoid nitrogen deficiency, the value of 120 kg N ha^{-1} was presumed. Fertilizer is assumed to have been applied for the first time shortly before sowing, making up 66 % of the total amount, according to OEHMICHEN (1986). The second application is supposed to take place roughly one month after sowing. It should be applied before canopy closure (MÄRLÄNDER *et al.* 2003). Both times, a formulation of 25 % ammonium, 25 % nitrate and 50 % urea is assumed.

Fig. 37 and Fig. 38 compare modelled and measured values. Because the LAI measurements do not differentiate between dead and living leaves, the modelled total LAI is depicted in the graphs and is used for calculating model performance statistics.

In former model test runs, LAI with advancing development was overestimated for all four fields and consequently biomass accumulation, too (results not shown here). Thus for reducing the LAI, once taproot development started, the specific leaf area constant (s_{la}) was set to half of its original value of 0.02 m^2 leaf g^{-1}. This adaptation resulted in a very good agreement of LAI values for two of the fields (Euerhausen 2000 and Plattling 2001). In the case of the other two fields, modelled LAI development improved but some discrepancies remained.

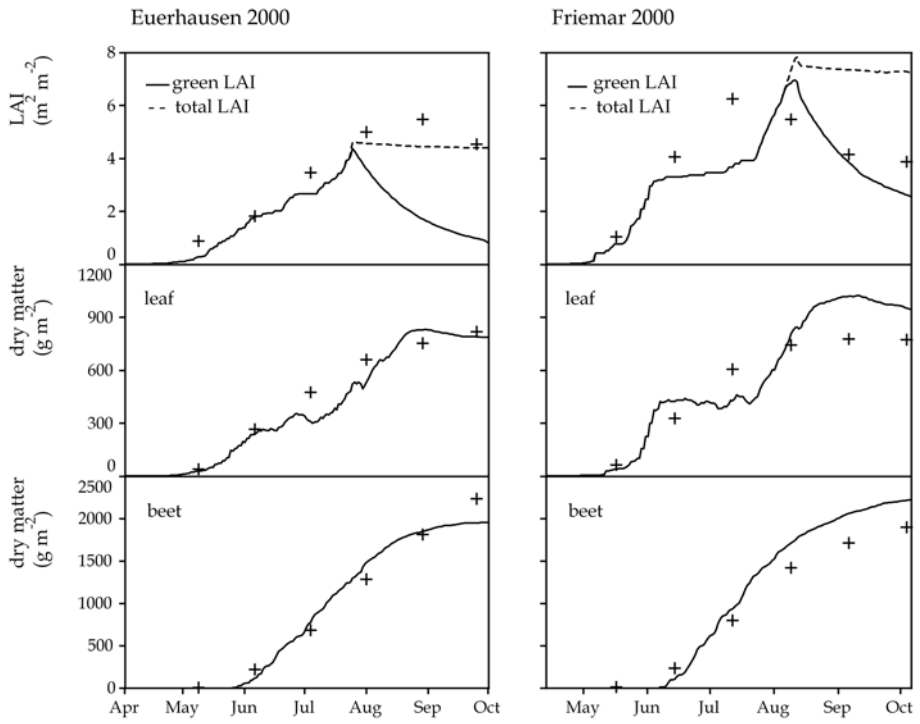

Fig. 37: Modelled (lines) and measured (symbols) LAI and biomass data of sugar beet in Euerhausen 2000 and Friemar 2000.

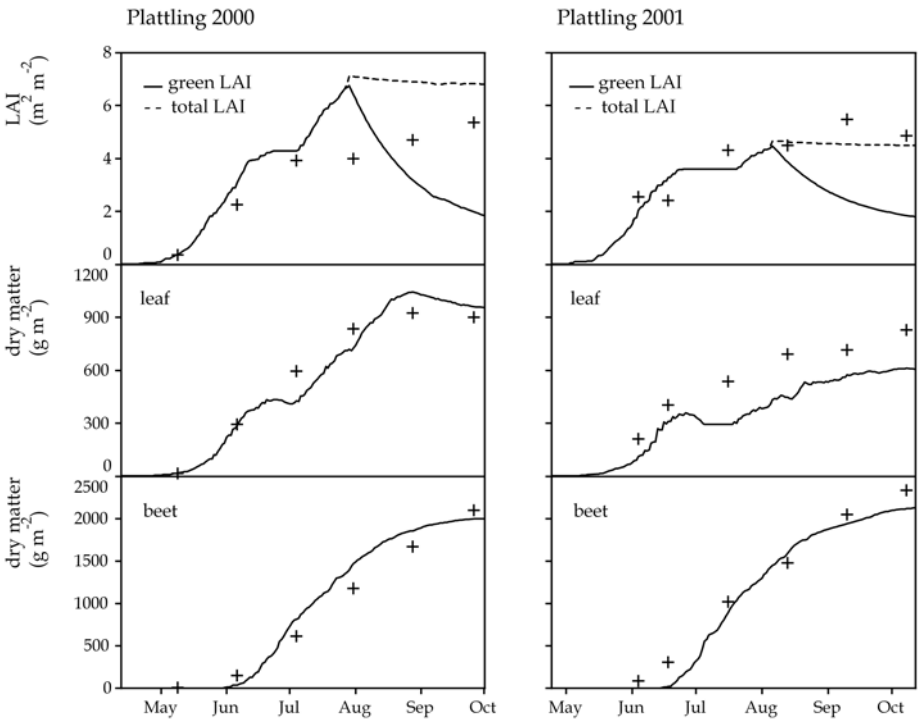

Fig. 38: Modelled (lines) and measured (symbols) LAI and biomass data of sugar beet in Plattling 2000 and 2001.

However, leaf as well as beet mass are precisely simulated for all four monitored sugar beet crops. At the beginning of growth, LAI development is not coupled to the specific leaf area constant. It is conceivable that a standard value of s_{la} is not suitable for the long growing season of sugar beet, though it produced good results for the validation data sets described above.

Table 27 lists the modelled transpiration and nitrogen uptake sums for each of the four fields. Nitrogen uptake over the growing season fits the standard values well. The high transpiration sum of the crop in Friemar 2000 can be explained by the high LAI. Therefore water stress is simulated here for a brief period. For the other three fields, no water stress is modelled.

Table 27: Modelled transpiration and nitrogen uptake sums for sugar beet.

	transpiration sum (mm)	**total nitrogen uptake (kg ha^{-1})**
Euerhausen 2000	353	203
Friemar 2000	458	214
Plattling 2000	383	221
Plattling 2001	267	228

The model results for sugar beet are summarized in Table 28. The incongruent LAI field data from Nienwohlde 1990 result in a negative value of MEF. In general, simulated beet biomass shows a very good agreement with measured data (value of IA > 0.92 for each data set). For the discussion of the results, see chapter 4.1.1.

Table 28: Model performance statistics for sugar beet
(root mean squared error RMSE, relative RMSE (RRMSE), mean absolute error MAE, index of agreement IA, modelling efficiency statistic MEF).

	RMSE	RRMSE	MAE	IA	MEF
Feienberg 2004					
green leaf area index	0.51	0.21	0.35	0.984	0.939
living leaf	207.01	0.59	131.69	0.869	0.825
beet	230.70	0.66	132.54	0.929	0.852
Feienberg 2005					
green leaf area index	0.67	0.19	0.54	0.978	0.898
living leaf	147.04	0.35	79.35	0.956	0.934
beet	85.96	0.18	66.34	0.992	0.986
Nienwohlde 1990					
green leaf area index	2.03	0.78	1.54	0.419	-2.108
living lea	114.97	0.41	73.37	0.906	0.874
beet	202.68	0.25	171.69	0.980	0.968
Euerhausen 2000					
total leaf area index	0.61	0.17	0.50	0.966	0.868
leaf	91.90	0.18	71.97	0.973	0.974
beet	152.09	0.15	119.82	0.991	0.987
Friemar 2000					
total leaf area index	2.33	0.56	2.01	0.645	-1.043
leaf	151.06	0.28	130.37	0.938	0.938
beet	238.73	0.24	205.19	0.978	0.963
Plattling 2000					
total leaf area index	1.70	0.50	1.33	0.842	-0.040
leaves	98.40	0.17	77.89	0.980	0.979
beet	175.78	0.19	149.08	0.988	0.979
Plattling 2001					
total leaf area index	0.65	0.16	0.16	0.897	0.967
leaf	184.91	0.33	173.44	0.813	0.904
beet	171.40	0.14	155.75	0.990	0.986
mean values of all data sets					
leaf area index	1.22	0.37	0.92	0.819	0.069
leaf	142.18	0.33	105.44	0.919	0.918
beet	179.62	0.26	142.92	0.978	0.960

3.1.2.2 Spring barley

In Bavaria, spring barley covers 162 800 ha (approx. 8 % of the total arable land) with an average yield of 46.7 quintals ha^{-1} (data comprise the years 1999 - 2004). This most important spring grain crop in Bavaria is mainly used as malting barley, 30 % of the total malting barley produced in Germany coming from this region. Time series of the area under cultivation and the average yield from 1950-2005 show that whereas the area has decreased by half, the yield has almost doubled. (BAVARIAN MINISTRY OF AGRICULTURE AND FORESTRY, ed., 2006)

Barley for malting needs to produce a high grain yield within a restricted period of only 110-130 days. For this reason, unfavourable weather conditions such as prolonged spells of drought, wetness or cold can scarcely be compensated for. For quality and yield, spring barley is more dependent on even growth conditions than other grains. (BAUMER 1998)

Spring grain typically requires 120 kg of nitrogen ha^{-1} (KTBL, ed., 2005). Nitrogen depletion from the preceding crop, generally cereals, typically leaves 40-50 kg N ha^{-1} obtainable from the soil. A supplement of 40-50 kg N ha^{-1} is therefore usually applied shortly before or after sowing. A second fertilizer dose of 20-30 kg N ha^{-1} is only needed on light and permeable soils and is carried out before tillering is completed. (BAUMER 1998)

For the validation of the DANUBIA crop growth model, two field data sets are used: one for Nienwohlde published by MCVOY *et al.* (1995) and the other for Wilzhofen provided by the *University of Munich.* The first includes measurements for two different fertilizer treatments and allows an analysis of the model´s capacity to predict the crop´s response to reduced nitrogen supply.

Table 29: Cultivation data of spring barley fields (figures in italics are estimates).

	plant density (plants m^{-2})	**sowing date**	**harvesting date**	**fertilizer date**	**amount (kg N ha^{-1})** NH_4	NO_3	Urea
Nienwohlde 1991	*250*	20.03.	08.08.	21.03.	49	-	-
				06.04.	-	-	50
				26.05.	4	4	8
				30.05.	4	4	7
Wilzhofen 1997	*400*	*21.03*	*13.08.*	*10.04.*	*30*	*30*	-

The two fertilizer treatments applied in Nienwohlde 1991 are a standard fertilizing procedure (N4) and a reduced one (N6). Table 29 shows the dates and formulation of N4. In the case of N6, the fertilizer application on April 6th was omitted. To avoid water stress on the sandy soil, the field was irrigated several times: on May 30th (25 mm), on June 11th (25 mm) and on July 19th and 30th (25 mm and 31 mm).

Model performance statistics for each data set are summarized in Table 30 at the end of this sub-chapter.

Nienwohlde 1991

Based on the phenological field observations, the maximum development rates $R_{max,v}$ and $R_{max,r}$ are set to 0.0431 d^{-1} and 0.0376 d^{-1}, respectively. Plant density, being unknown, was optimized by sensitivity analysis, taking into account the standard values for spring barley.

Since the measurements of the storage organ refer to the ear (including glume, grain and the remaining part of the ear), a direct comparison with modelled seed biomass is rendered difficult. In the model, seed biomass (grains) only forms after flowering. The first measurement of the ear (June 19th) cannot include grains because the phenological stage of flowering has not yet been reached (BBCH-stage 49/50). Consequently, this measured value of ear biomass (N4-treatment: 120 g m^{-2}, N6-treatment: 73 g m^{-2}) is added to the measured stem mass. The subsequent biomass measurements are not modified because the proportion of grains to other parts of the ear increases with advancing development. Thus it is thought acceptable to compare measured ear with modelled seed biomass.

Concerning the water budget of the crop, total precipitation from sowing until harvesting amounts to 310 mm and is supplemented by 106 mm irrigation. No water stress is modelled.

Fig. 39 compares modelled and measured values of LAI and biomass for both fertilizer treatments.

First, the results for the N4 fertilizer treatment are described.

The model captures the increase of LAI very well but overestimates the measured values after start of senescence (RMSE 1.09). This may be caused either by an underestimation of the senescence rate, or by an overestimation of the maximum LAI, or else by a delayed start of senescence. In terms of leaf biomass, the model underestimates the measured values after the start of senescence.

These contrary results are attributable to some ambiguity in the measurements: The decline of LAI is not reflected by the leaf biomass. Although not explicitly noted by McVoy *et al.* (1995), it is assumed that the measured leaf biomass relies only on living leaves, since the published values for cereals generally show a pronounced decline towards harvesting. It is the last measured values particularly that do not match: 120 g m^{-2} leaf biomass and a corresponding LAI value of 0.76, resulting in an extremely low specific leaf area of 0.00633 m^2 leaf g^{-1} leaf, which appears to be questionable.

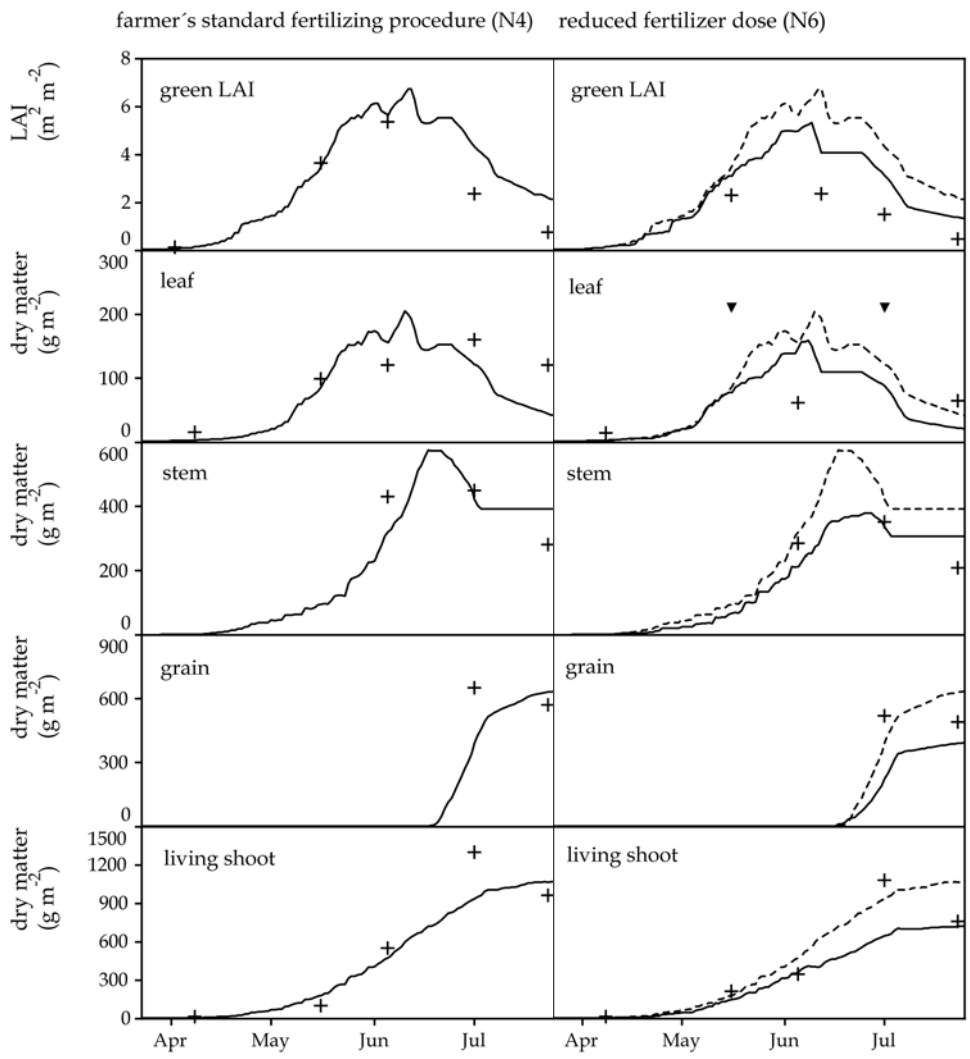

Fig. 39: Modelled (lines) and measured (symbols) LAI and biomass data of spring barley, Nienwohlde 1991
(left: fertilization N4; right: fertilization N6, with modelled results for N4 shown in broken lines).
Measured data marked by a triangle are omitted from the statistical analysis.

The computed stem and grain biomass curves illustrate the remobilization of carbon reserves from the stem to the grain. Although the last measured stem biomass value indicates a further decrease in stem weight which is not depicted by the model, the modelled yield conforms closely to the observed one (difference +61 g m^{-2}).

Modelled total transpiration and nitrogen uptake amount to 177 mm and 157 kg N ha^{-1} respectively. The latter reflects the rather high total fertilizer dose (130 kg N ha^{-1}).

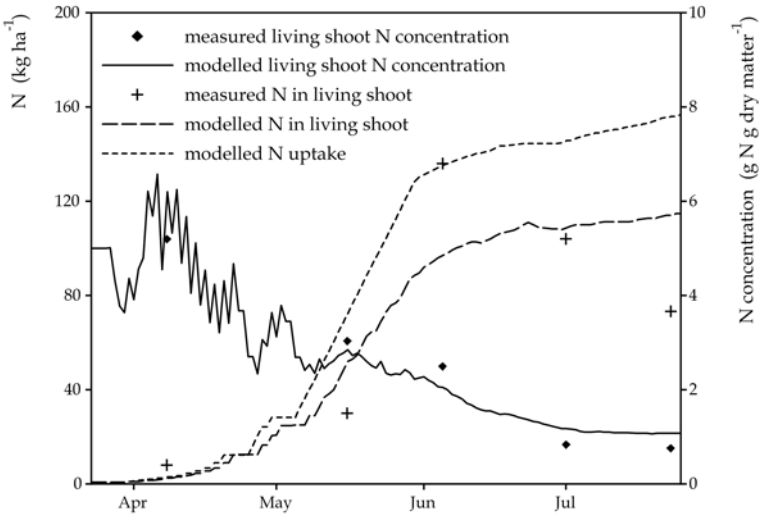

Fig. 40: Modelled (lines) and measured (symbols) of living shoot nitrogen content, nitrogen concentration and nitrogen uptake of spring barley, Nienwohlde 1991, N4 fertilizing procedure.

Fig. 40 shows the comparison between modelled and measured nitrogen concentration and nitrogen content of living shoot biomass. Additionally, modelled nitrogen uptake is depicted. The model faithfully predicts the decline of nitrogen concentration in the shoot during the growing season.

Because of only five available measurements of biomass nitrogen content, it is difficult to identify outliers. Computed biomass nitrogen content increases too sharply as compared with the measured value at the end of May. Its maximum value in mid-June fits the modelled uptake in the graph, but because of roots being excluded, it is actually overestimated. Modelled nitrogen content tallies very well with the measured value in mid-July. Its sharp decline towards harvest date is not reproduced by the model.

Fig. 40 proves the capacity of the model to predict nitrogen uptake and its allocation to the shoot with an adequate degree of accuracy.

In the following, the model results for the N6 fertilizer treatment are described.

The observed phenological stages in the field are almost identical for both fertilizing procedures, but measurements of LAI and biomass clearly differ (see Fig. 39).

The model consistently overestimates LAI development (RMSE = 1.32). The maximum measured LAI has a value of 2.4 whereas the modelled maximum reaches 5.3. A comparison is difficult because it is likely that the LAI reached its maximum between the dates of the first two measured values and is therefore not documented. Once again, measurements of leaf biomass and LAI are not consistent. The two maximum

values (both 210 g m^{-2}) of leaf biomass are very unlikely and are therefore not considered in the calculation of the model performance statistics. Modelled stem biomass again shows the remobilization of carbon reserves to the grain and agrees sufficiently well with the measurements (MAE = 60 g m^{-2}). The model underestimates final grain biomass by 97 g m^{-2}, reaching only approx. 80 % of the observed value.

Modelled total transpiration results in 132 mm and total nitrogen uptake in 109 kg ha^{-1}. The maximum of the measured values of nitrogen content in biomass (excluding roots) is measured on July 15th and totals 93 kg ha^{-1}. This value tallies well with the modelled sum for this date, amounting to 102 kg ha^{-1}.

Wilzhofen 1997

For the spring barley crop in Wilzhofen, management information is not documented. Plant density and sowing date were estimated by sensitivity analysis, whereas information on fertilizer application is adopted from the model PROMET-V, as described by SCHNEIDER (1999).

Maximum development rates $R_{max,v}$ and $R_{max,r}$ are set to general values for Bavaria: 0.0331 d^{-1} and 0.0431 d^{-1}, respectively.

Fig. 1 compares modelled and measured LAI and biomass data. The measurements marked with a triangle are supposed to be outliers and are not considered in the calculation of the model performance statistics. As described above, a comparison between measured ear biomass and modelled seed biomass is difficult. For the spring barley crop in Wilzhofen 1991, phenological stages were not documented. According to the modelled phenology, the stage of flowering is reached on June 22nd. Consequently, the two first measurements of ear (June 11th: 52 g m^{-2} and June 25th: 181 g m^{-2}) are added to the measured stem biomass. One half (119 g m^{-2}) of the value for July 2nd is also added to the stem biomass.

The increase of LAI and stem biomass is very well reproduced by the model, whereas leaf biomass is underestimated. Senescence of LAI is underestimated, too. Once again, measured data of LAI and leaf biomass are mutually exclusive with advancing development.

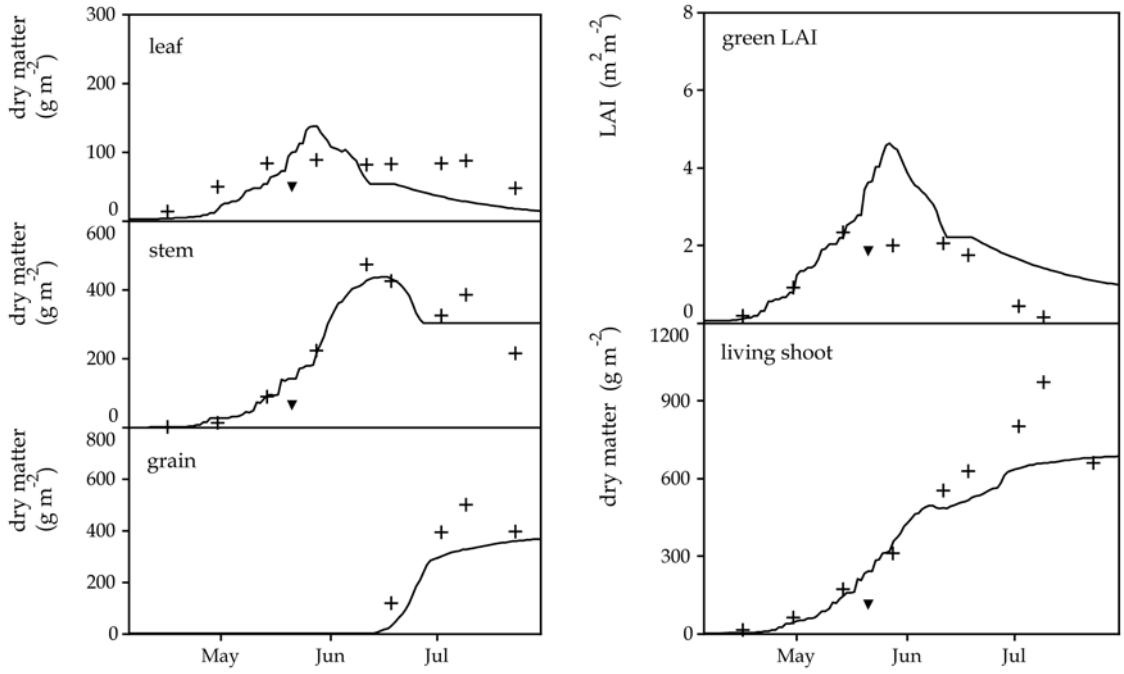

Fig. 41: Modelled (lines) and measured (symbols) LAI and biomass data of spring barley, Wilzhofen 1997. Measured data marked with a triangle are omitted from the statistical analysis.

According to model results of PROMET-V, nitrogen stress occurs after mid-June. This is also simulated by the DANUBIA crop growth model: The nitrogen reservoirs in the upper soil layers are nearly depleted at the beginning of June. Modelled root depth reaches the deepest soil layer on May 19th. In the first days of June, root length density is as yet unable to draw up all the nitrogen it needs from the deepest soil layer. Senescence of LAI is induced on June 11th.

Sums of nitrogen uptake modelled by PROMET-V (SCHNEIDER 1999) and by the DANUBIA crop growth model approach each other closely: 99.7 kg ha^{-1} and 92.2 kg ha^{-1}, respectively. Modelled total transpiration amounts to 133 mm, being almost identical with the value of the crop in Nienwohlde 1991 (reduced fertilizer dose).

Table 30 summarizes the model results for spring barley. Performance statistics based on fewer than four measurements are marked with a cross.

For the N6 fertilizer treatment in Nienwohlde, low values of IA and negative values of MEF (in terms of LAI and biomass components) indicate a poor performance of the model. However, the sparseness and incongruity of the field data complicate a quantification of the model´s accuracy in predicting spring barley growth in Nienwohlde 1991 (both the fertilizer procedures).

Incongruity of the LAI and leaf biomass measurements in Wilzhofen 1997 results in poor values of IA and MEF. However, results for stem (IA = 0.93) and grain (IA = 0.86) show a good agreement with the field data.

Table 30: Model performance statistics for spring barley
(root mean squared error RMSE, relative RMSE (RRMSE), mean absolute error MAE, index of agreement IA, modelling efficiency statistic MEF). Where fewer than four measurements were available, the value is marked with a cross.

	RMSE	RRMSE	MAE	IA	MEF
Nienwohlde 1991 N4					
green leaf area index	1.09	0.44	0.77	0.918	0.673
living leaf	41.90	0.41	34.76	0.831	0.242
stem	91.83+	0.24+	83.29+	0.258+	-0.465+
grain	154.82+	0.26+	118.48+	0+	-21.013+
living shoot	177.47	0.30	128.03	0.961	0.870
Nienwohlde 1991 N6					
green leaf area index	1.32	0.79	1.25	0.630	-1.959
living leaf	55.89+	1.18+	46.71+	0.509+	-4.720+
stem	69.05+	0.25+	60.29+	0.509+	-0.459+
grain	195.33+	0.38+	174.71+	0.077+	-189.77+
living shoot	204.17+	0.53+	145.53+	0.914+	0.403+
Wilzhofen 1997					
green leaf area index	1.11	0.90	0.77	0.723	-0.707
living leaf	37.29	0.54	34.46	0.693	-1.323
stem	75.68	0.38	57.92	0.927	0.673
grain	108.55	0.31	97.39	0.864	0.406
living shoot	127.30	0.27	87.05	0.950	0.841
mean values of all data					
green leaf area index	1.17	0.71	0.93	0.757	-0.664
living leaf	45.03	0.71	38.64	0.678	-1.934
stem	78.85	0.29	67.17	0.565	-0.084
grain	152.90	0.32	130.19	0.314	-70.126
living shoot	169.65	0.37	120.20	0.942	0.705

3.1.2.3 Maize

In 2005, maize was cultivated on 416 000 hectares in Bavaria, comprising 20 % of the arable land. A quarter of this area is devoted to growing grain maize, the remainder to silage maize. Average yields between 1999 to 2004 amounted to 88.6 quintals ha^{-1} (grain maize) and 491.5 quintals ha^{-1} (silage maize). (BAVARIAN MINISTRY OF AGRICULTURE AND FORESTRY, ed., 2006)

Both maize crops are mainly grown for providing forage. It is likely that in the future the production of bioenergy will further boost the importance of maize in agriculture. For quantifying water, carbon and nitrogen fluxes as well as agricultural yield in the

Upper Danube Basin both now and in the future, crop growth modelling of maize is of fundamental significance.

Maize as a tropical plant is susceptible to cold, requiring warm temperatures and plenty of sunshine. It is not particular as to rainfall, as long as it receives about 150 mm of rain in the short interval just before and after flowering. Maize will tolerate poor soils. Ideally, the soil should be able to offset unfavourable weather conditions. (EDER 1998)

Maize typically requires 230 kg of nitrogen per hectare (BAUMGÄRTEL & SCHARPF 2002). The nitrogen made available from the soil through mineralization during the growth period may range from 30 kg on light sandy soils to 150 kg on fertile soils.The amount of nitrogen lacking can be administered through fertilizer in good time before sowing. Where the soil tends to be leachy, it is advisable to apply the dose in instalments. (EDER 1998)

Table 31 lists the cultivation data of the three field data sets used for the validation of the DANUBIA crop growth model. Model performance statistics for maize are summarized in Table 32 at the end of the sub-chapter.

Table 31: Cultivation data of maize fields (figures in italics are estimates).

	plant density (plants m^{-2})	**sowing date**	**harvesting date**	**fertilizer date**	**amount (kg N ha^{-1})** NH_4	NO_3	Urea
Feienberg 2004	10	30.04.	01.10.	23.04.	15	-	15
				30.04.	89	41	-
Feienberg 2005	9	01.05.	12.10.	18.04.	-	-	50
				25.06.	15	15	30
				07.09.	-	-	50
Wilzhofen 1997	*10*	*10.05.*	*20.09.*	*05.05.*	*15*	*15*	-
				14.06.	*35*	*35*	-
				29.06.	*50*	*50*	-

Feienberg 2004 and 2005

According to the monitored phenological stages, maximum development rates $R_{max,v}$ and $R_{max,r}$ are adjusted to 0.0345 d^{-1} and 0.0265 d^{-1}, respectively (for both Feienberg 2004 and 2005). Fig. 42 compares model results with LAI and biomass measurements.

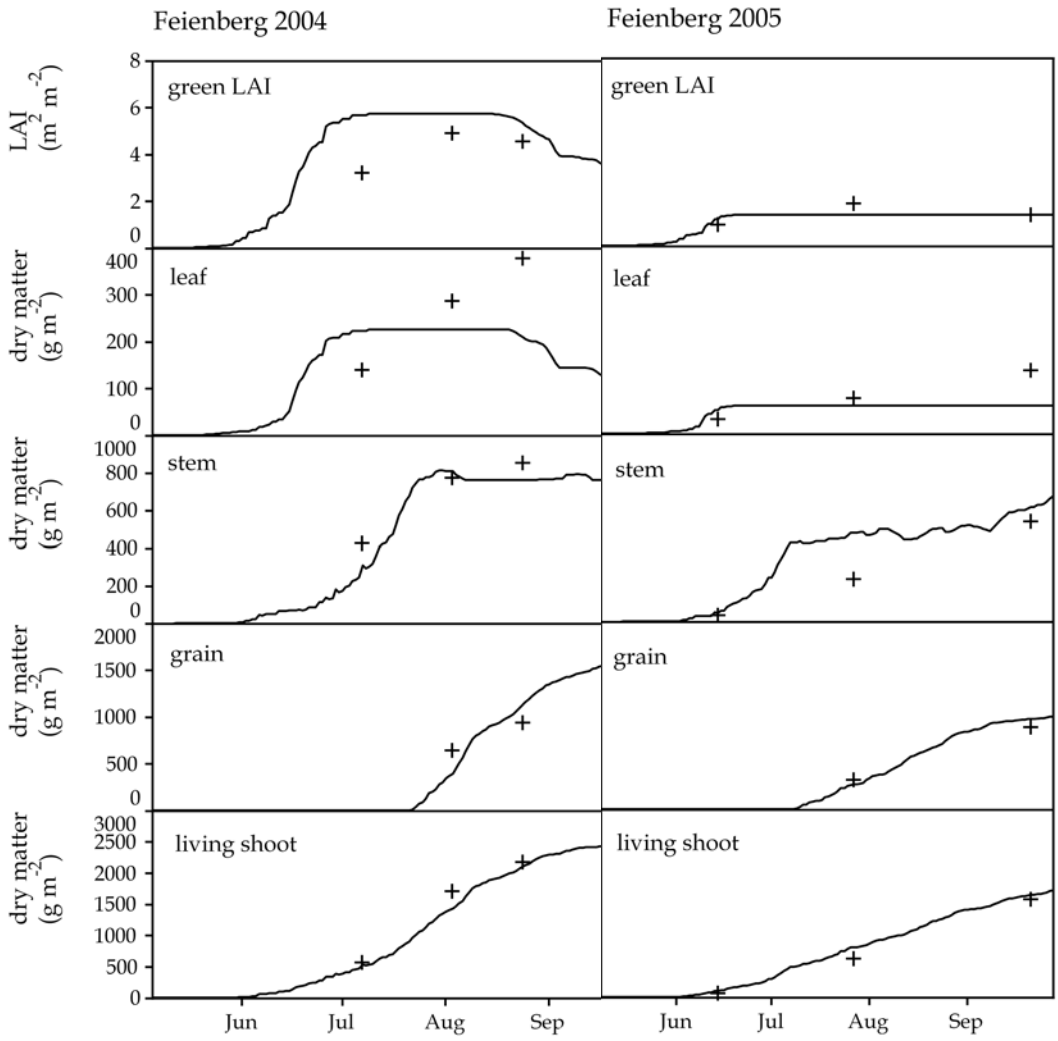

Fig. 42: Modelled (lines) and measured (symbols) LAI and biomass data of maize, Feienberg 2004 and 2005.

In Feienberg 2004, the increase of LAI and leaf biomass at the onset of growth is overestimated by the model. The following leaf biomass measurements for August and September are underestimated. In both years, the last leaf biomass measurements reveal an increase towards harvesting date. However, because of maize being a determinate plant, leaf biomass does not as a rule increase after flowering. This fact is taken account of in the model, where the fraction of new shoot carbon partitioned to leaves is set to zero after flowering (according to GECROS, YIN & VAN LAAR 2005). For both data sets, the assumption of a standard senescence in the model (3 % loss of leaf weight per day, see chapter 2.2.10: *Leaf area and senescence*) is ignored. Stem as well as grain biomass are well predicted for 2004.

In 2005, an unusually cold period in May and in the first days of June led to a reduced LAI development and leaf biomass production. Subsequent warming resulted in an

earlier onset of flowering as compared with 2004. Therefore LAI and leaf biomass growth did not catch up, which is very well depicted by the model. The small LAI causes 29 % less biomass production and 31 % less transpiration (200 mm) compared with 2004 (290 mm). In both years, water supply was sufficient and no water stress was modelled. Total computed nitrogen uptake gives and 249 kg ha^{-1} (2004) and 228 kg ha^{-1} (2005).

These few crop measurements alone do not allow a comprehensive validation analysis. However, the dynamic interaction between the DANUBIA crop growth model and the DANUBIA soil model permits an assessment of how efficiently nitrogen and water uptake can be simulated. Fig. 43 compares measured and modelled data of soil moisture and soil mineral nitrogen content (calculated by the DANUBIA soil model) for 2005.

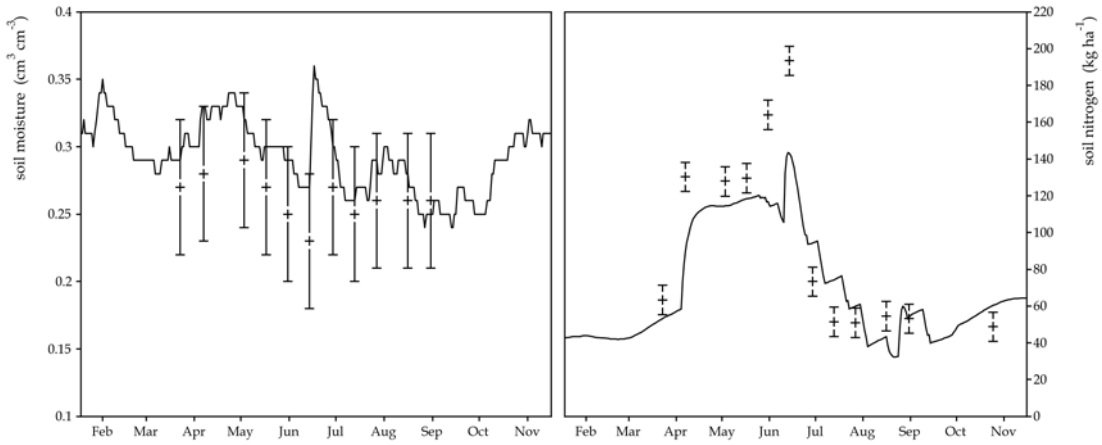

Fig. 43: Modelled (lines) and measured (symbols) soil moisture and nitrogen (0-90 cm) for maize, Feienberg 2005. Error bars depict measurement accuracy (± 3 cm^3 cm^{-3} and ± 8 kg ha^{-1}). Measurements provided by C. W. Klar.

Each soil moisture measurement matches the modelled curve (taking into account the measurement accuracy). Modelled soil nitrogen is underpredicted by the model before the sowing date. Despite the nonconcordance of measured and modelled soil nitrogen reservoirs, the same trend is seen to be followed. Minimal growth until mid-June necessitating hardly any nitrogen uptake is reflected by both modelled and measured data.

The comparison reveals a remarkable degree of conformity between the two soil parameters, thereby proving the capability of the model to predict water and nitrogen uptake by the crop.

Wilzhofen 1997

The estimated cultivation data for the maize crop in Wilzhofen 1997 are listed in Table 31. Fertilizer applications are chosen according to the standard cultivation practice as implemented in the model PROMET-V (SCHNEIDER 1999) and are representative for the test-site region. These standard fertilizer doses were slightly increased to forestall any deficiency of soil nitrogen supply.

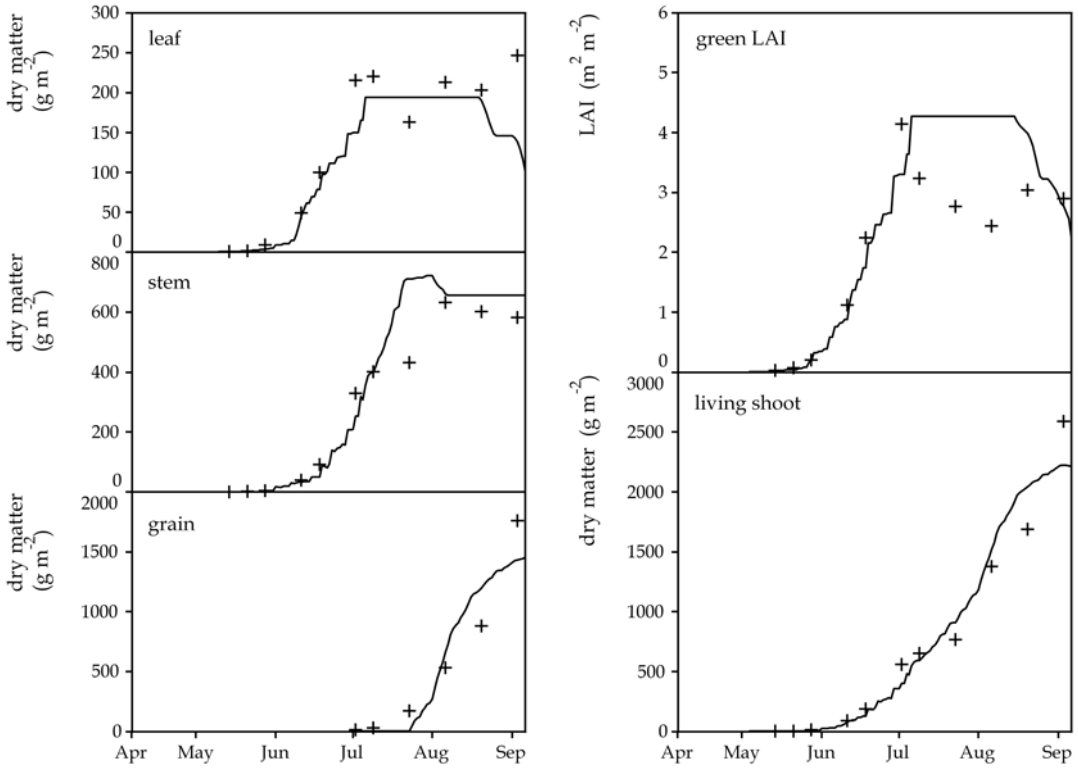

Fig. 44: Modelled (lines) and measured (symbols) LAI and biomass data of maize, Wilzhofen 1997.

Model results are compared with LAI and biomass measurements in Fig. 44. To prevent a too early decline of LAI, the model´s assumption of a standard senescence is ignored. Until mid-July, a striking conformity to the measurements may be seen. In the subsequent second half of the growth period, some discrepancies occur. These might be due to the rather small sample size. As in the case of sugar beet, young individual plants are quite homogeneous but grow more and more disparate as they develop.

The last measured value of grain biomass is conspicuously underestimated by the model (difference of 330 g m^{-2}). Modelled stem biomass illustrates the remobilization of stored assimilates. During the maturing process, these assimilates in the form of glucose are transferred to the ear and transformed into starch.

Total transpiration according to the model is 284 mm, with no water stress occuring. Cumulative nitrogen uptake amounts to 239 kg ha^{-1}. For all compared parameters in Wilzhofen 1997, the IA yields values greater than 0.91, demonstrating a close agreement.

Table 32: Model performance statistics for maize
(root mean squared error RMSE, relative RMSE (RRMSE), mean absolute error MAE, index of agreement IA, modelling efficiency statistic MEF). Where fewer than four measurements were available, the value is marked with a cross.

	RMSE	RRMSE	MAE	IA	MEF
Feienberg 2004					
green leaf area index	1.57+	0.37+	1.37+	0.433+	-3.593+
living leaf	113.49+	0.42+	103.72+	0.370+	-0.343+
stem	88.48+	0.13+	81.42+	0.954+	0.773+
grain	222.29+	0.28+	220.44+	0.813+	-1.310+
living shoot	164.59+	0.11+	125.42+	0.985+	0.940+
Feienberg 2005					
green leaf area index	0.30+	0.22+	0.23+	0.591+	0.303+
living leaf	46.02+	0.57+	37.08+	0.504+	-0.183+
stem	149.61+	0.56+	111.51+	0.895+	0.468+
grain	72.69+	0.12+	70.79+	0.987+	0.933+
living shoot	114.92+	0.15+	97.88+	0.991+	0.965+
Wilzhofen 1997					
green leaf area index	0.89	0.44	0.65	0.914	0.576
living leaf	41.24	0.32	26.65	0.942	0.808
stem	92.39	0.33	51.30	0.971	0.863
grain	206.24	0.37	164.78	0.970	0.888
living shoot	173.03	0.24	117.55	0.988	0.954
mean values of all data					
green leaf area index	0.92	0.35	0.75	0.646	-0.905
living leaf	66.92	0.44	55.81	0.606	0.094
stem	110.16	0.34	81.41	0.940	0.701
grain	167.07	0.26	152.00	0.923	0.170
living shoot	150.85	0.17	113.62	0.988	0.953

Table 32 summarizes the model results for maize. Field data from Feienberg in 2004 and 2005 being sparse, negative values of MEF result. On the whole, stem and grain biomass are more accurately predicted (IA > 0.92) than LAI development and leaf biomass.

3.1.2.4 Winter wheat

In 2005, winter wheat was cultivated on 470 300 ha in Bavaria (22.6 % of the arable land). Yield between 1999 to 2004 averages 69 quintals ha^{-1} (BAVARIAN MINISTRY OF AGRICULTURE AND FORESTRY, ed., 2006).

Of all Federal provinces in Germany, Bavaria leads in wheat production. About 3 million t are being harvested annually. The cultivation of winter wheat has been expanded over the last decades, supplanting other grain crops, mainly winter rye and oats. (ZIMMERMANN 1998)

In view of the vast area under cultivation for winter wheat, a growth model for this prime crop in the Upper Danube Basin is of special relevance.

Winter wheat is more dependent on suitable climatic conditions than other grain crops, particularly in respect of warmth and moisture. The late harvest makes it imperative for sufficient soil moisture to be present until well into July. All wheat soils must ensure that nutrients and moisture are available in adequate amounts at all times. Very light soils with frequent dry spells in early summer are not suitable for wheat. (ZIMMERMANN 1998)

As a rule, the nitrogen demand of winter wheat amounts to 190-250 kg ha^{-1} (BAUMGÄRTEL & SCHARPF 2002). The required nitrogen fertilizer should be administered in at least 3 doses.

Table 33: Cultivation data of winter wheat fields (figures in italics are estimates).

	plant density (plants m^{-2})	**sowing date**	**harvesting date**	**fertilizer date**	**amount (kg N ha^{-1})** NH_4	NO_3	Urea
Feienberg 2003/04	280	18.10.	08.08.	23.03.	45	45	-
				25.04.	22	23	-
				26.05.	22	23	-
Bockschlag 1990/91	*250*	16.11.	26.08.	14.03.	13	14	27
				12.04.	9	9	18
				03.05.	9	9	18
				05.06.	15	14	29
				15.06.	8	7	14
Neuenkirchen 1990/91	*250*	10.11.	22.08.	13.03.	9	9	18
				16.04.	10	11	22
				06.05.	10	11	22
				02.06.	11	11	22
				17.06.	33	16	17

Three field data sets are drawn upon for testing the predictive ability of the DANUBIA crop growth model. Table 33 lists the corresponding cultivation data.

Feienberg 2003/04

Following the monitored phenological stages, maximum development rates $R_{max,v}$ and $R_{max,r}$ are adjusted to 0.0217 d^{-1} and 0.0239 d^{-1}, respectively.

The first measurement of the ear (June 9th) could not include grains because the phenological stage of flowering (BBCH-stage 61) had not yet passed. Consequently, this measured value of ear biomass (214 g m^{-2}) is added to the stem biomass.

The increase of green LAI is exactly reproduced by the model and the modelled senescence rate tallies very well with the measurements until mid-July. Towards harvest date, green LAI is overpredicted (Fig. 45).

Despite the remarkable degree of conformity between measured and modelled LAI development (IA = 0.976), aboveground biomass is conspicuously underestimated (440 g m^{-2}). The reduced grain biomass is caused by underpredicted stem biomass, the reason being the lack of carbon for remobilization from stem to grain. The model simulates the course of living leaf biomass development very well, although absolute values are considerably underestimated throughout the season. This difference leads to discrepancies between simulated and measured leaf biomass (RMSE = 67 g m^{-2}).

The amount of assimilates does not suffice to produce the observed shoot biomass. Modelled root biomass lies within a size range that excludes its overestimation at the expense of shoot biomass.

Modelled sums of nitrogen uptake (249 kg ha^{-1}) and transpiration (241 mm) are well within the expected size range. The model registers water stress only for a few hours on June 7th, 8th and 9th.

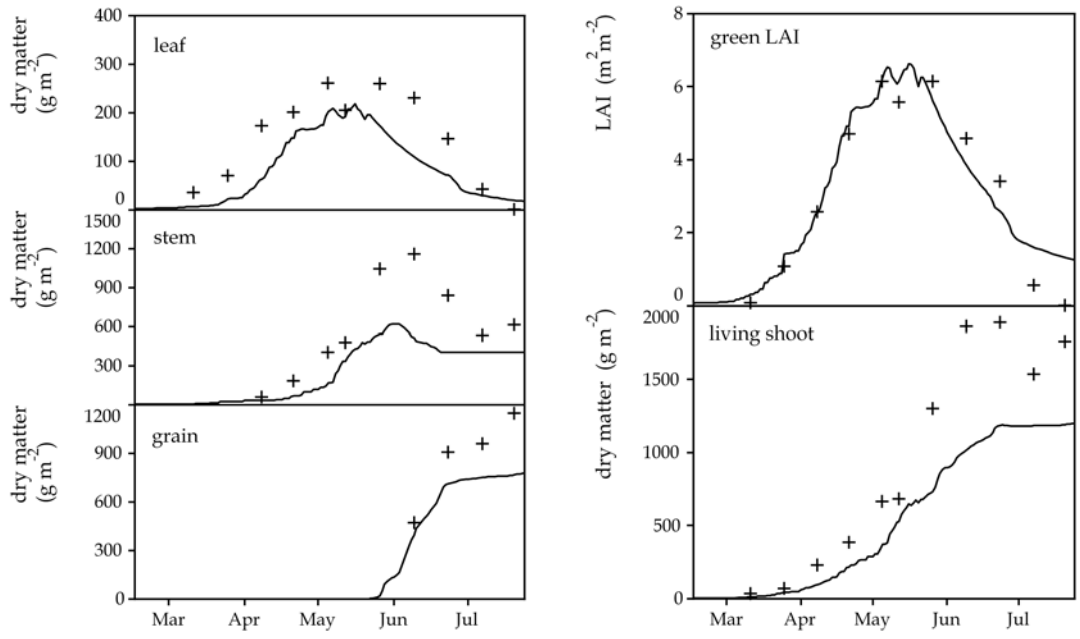

Fig. 45: Modelled (lines) and measured (symbols) LAI and biomass data of winter wheat, Feienberg 2004.

The decline of nitrogen concentration in living shoot biomass during the growing season is followed very closely by the model (see Fig. 46). The measured nitrogen concentration in mid-May can be regarded as an outlier. Simulated living shoot nitrogen content on the whole is underestimated, reflecting the difference between modelled and observed biomass.

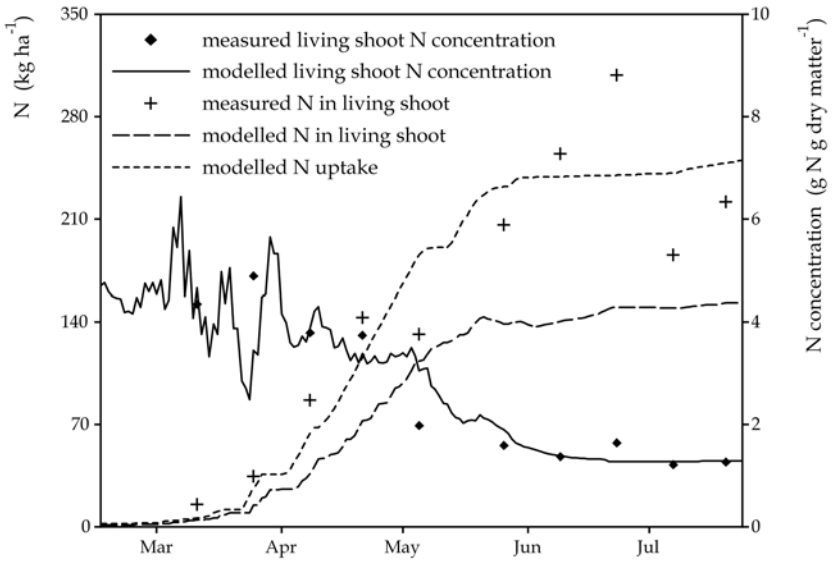

Fig. 46: Modelled (lines) and measured (symbols) of living shoot nitrogen content, nitrogen concentration and nitrogen uptake of winter wheat, Feienberg 2004.

Bockschlag 1990/91

The value of the maximum development rate $R_{max,v}$ (0.0286 d^{-1}) is adopted from the model PROMET-V (SCHNEIDER 1999). $R_{max,r}$ is adjusted to 0.025 d^{-1} according to the observed phenological stages in the field. Plant density, being unknown, was optimized by sensitivity analysis (Table 33), taking into account the standard values for winter wheat.

Since the phenological stage of flowering had just been reached (BBCH-stage 60/61), the measured value of ear biomass on June 27th (120 g m^{-2}) could not include grains. Its value therefore is added to the measured stem biomass.

The comparison of modelled and measured LAI and biomass data (Fig. 47) shows a close agreement for stem biomass. Grain biomass towards harvesting date is nearly exactly reproduced (difference +6 g m^{-2}). LAI development is generally overestimated. In terms of leaf biomass, obvious discrepancies occur. However, total living shoot biomass reveals a more than satisfactory degree of conformity between modelled and measured data (IA = 0.973).

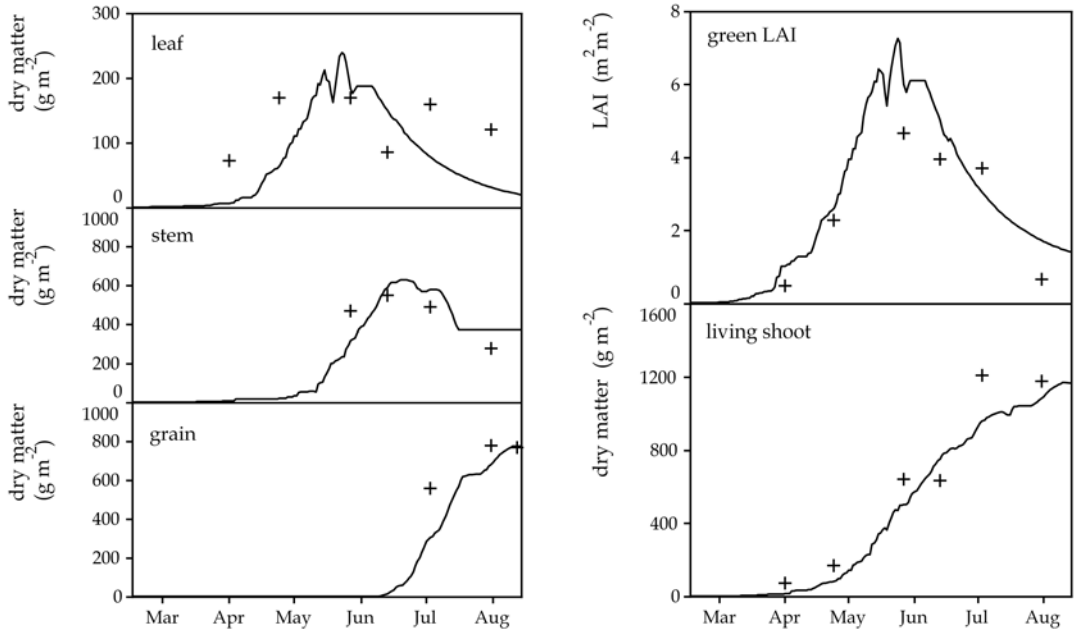

Fig. 47: Modelled (lines) and measured (symbols) LAI and biomass data of winter wheat, Bockschlag 1991.

The last measured nitrogen content in living shoot (165 kg ha^{-1}) is nearly identical with the modelled value (159 kg ha^{-1}). Simulated total nitrogen uptake results in 245 kg ha^{-1}

and total transpiration in 265 mm. Moderate water stress is modelled at the end of July when soil moisture in the upper two layers (0-30 cm and 30-60 cm; simulated by the DANUBIA soil model) falls below 15 cm^3 cm^{-3}.

Neuenkirchen 1990/91

For the maximum development rates as well as plant density, the same values as in the case of Bockschlag 1991 are used.

Fig. 48 compares modelled and measured LAI and biomass data. Firstly, the results depicted in solid lines are described. The model predicts the increase of LAI very well, but underestimates senescence rate. The maximum value of stem biomass is underpredicted, resulting in a too low value of grain biomass as well. Total living shoot biomass initially tallies well with the measurements but later deviates strongly in consequence of the underestimated values of of leaf, stem and grain biomass.

The model computes water stress for two periods (June 13th until 23rd and July 9th until 12th). Model results without taking into account the effect of water stress are shown in broken lines (Fig. 48). These results are not depicted for leaf biomass and LAI, since water stress in the model does not occur until shortly before flowering, having almost no effect on these two parameters.

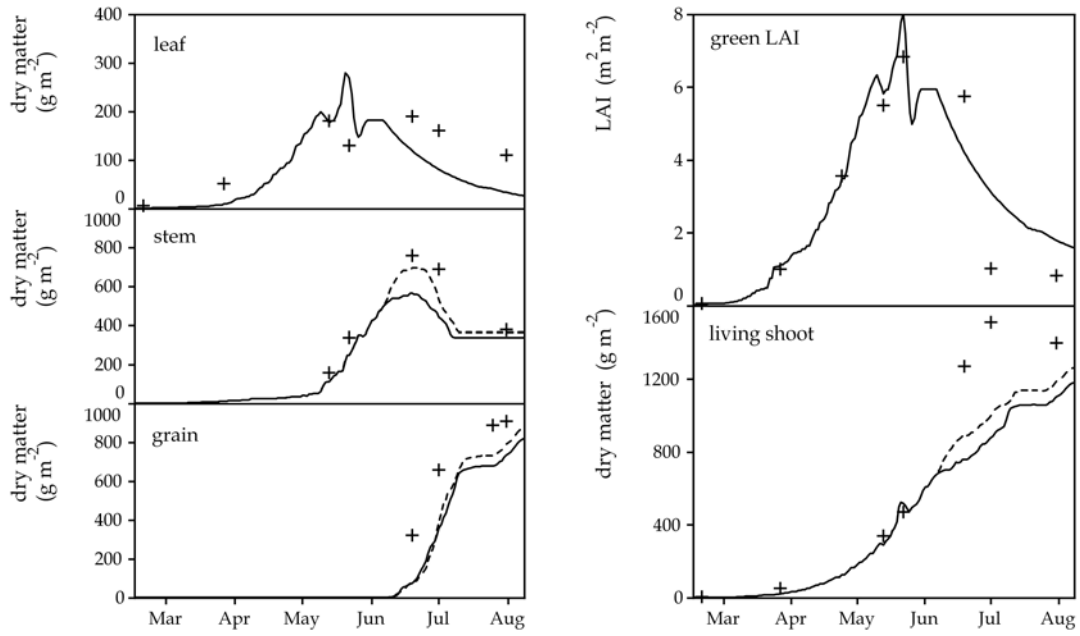

Fig. 48: Modelled (lines) and measured (symbols) LAI and biomass data of winter wheat, Neuenkirchen 1991. Broken lines show results when no water stress is considered.

Data show that water stress in the second half of June reduces the increase of stem biomass conspicuously (the maximum difference is 157 g m^{-2}, representing almost 25 % less biomass).

Water scarcity curtails total transpiration from 285 mm to 272 mm and total nitrogen uptake only slightly from 272 kg ha^{-1} to 269 kg ha^{-1}.

The following model results include the simulation of water stress effects.

Fig. 49 compares measured and modelled data of soil moisture and soil mineral nitrogen content (calculated by the DANUBIA soil model). Simulated and measured soil moisture follow the same trend. A slight systematic underestimation by the model points at too low values of soil moisture at model initialization. In mid-June, modelled soil moisture decreases, resulting in water stress. Since measured data, however, show higher values, the simulated water scarcity could be unrealistic. Therefore model performance statistics (Table 34) refer to modelled LAI and biomass without the impact of water stress.

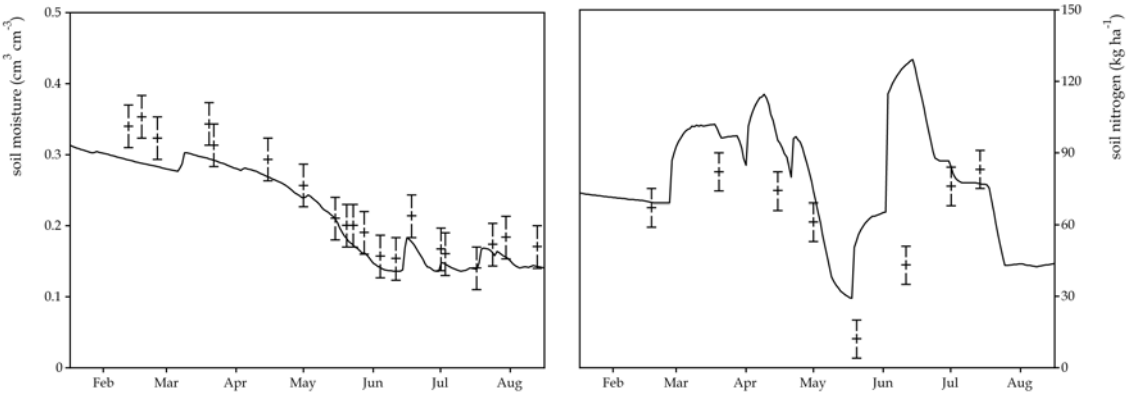

Fig. 49: Modelled (lines) and measured (symbols) soil moisture and nitrogen (0-90 cm) for winter wheat, Neuenkirchen 1991. Error bars depict measurement accuracy (± 3 cm^3 cm^{-3} and ± 8 kg ha^{-1}).

A comparison between measured and modelled soil mineral nitrogen content reveals some discrepancies. To some extent, these differences can be explained by an offset due to underestimation of crop nitrogen uptake in spring.

Table 34 summarizes model performance statistics for winter wheat. The high values of IA for green LAI are striking. In all data sets, it is the leaf biomass values that deviate most. However, when considering total living shoot biomass (average IA = 0.929), these discrepancies carry little weight. The model´s ability to predict grain biomass is acceptable (average MAE = 164 g m^{-2}).

Table 34: Model performance statistics for winter wheat
(root mean squared error RMSE, relative RMSE (RRMSE), mean absolute error MAE, index of agreement IA, modelling efficiency statistic MEF). Where fewer than four measurements were available, the value is marked with a cross.

	RMSE	RRMSE	MAE	IA	MEF
Feienberg 2004					
green leaf area index	0.67	0.21	0.54	0.976	0.918
living leaf	67.35	0.46	56.98	0.846	0.447
stem	333.13	0.57	270.36	0.715	0.082
grain	215.68	0.31	175.95	0.910	0.726
living shoot	440.29	0.47	349.40	0.870	0.607
Bockschlag 1991					
green leaf area index	0.90	0.34	0.84	0.928	0.687
living leaf	75.94	0.59	70.22	0.541	-2.609
stem	100.81	0.23	92.55	0.761	0.005
grain	157.29+	0.22+	119.35+	0.769+	-1.405+
living shoot	137.96	0.21	123.44	0.973	0.901
Neuenkirchen 1991					
green leaf area index	1.08	0.35	0.80	0.951	0.814
living leaf	73.98	0.63	58.76	0.739	-0.309
stem	90.04	0.19	75.80	0.957	0.840
grain	205.51	0.30	196.40	0.864	0.253
living shoot	253.64	0.35	175.04	0.942	0.824
mean values of all data					
green leaf area index	0.88	0.30	0.72	0.952	0.806
living leaf	72.42	0.56	61.99	0.709	-0.823
stem	174.66	0.33	146.24	0.811	0.309
grain	192.83	0.28	163.90	0.848	-0.142
living shoot	277.30	0.34	215.96	0.929	0.778

3.1.2.5 Potato

Over the past decades the potato, once one of the principal crops grown in Germany as a staple food and for feeding livestock, has declined in importance (HEPTING 1998).

Time series of the area under cultivation in Bavaria reveal a steady decrease since 1950. 2005 saw the area under potato cultivation drop for the first time below 50 000 ha (48 000 ha, approx. 2.3 % of the total arable land). The average yield amounts to 372.2 quintals ha^{-1} (data cover the years 1999 - 2004). (BAVARIAN MINISTRY OF AGRICULTURE AND FORESTRY, ed., 2006)

The potato adapts easily to both climate and soil. At the onset of tuberization and in the first stages of tuber growth, the crop requires water in adequate and evenly distributed amounts. A total of 250 mm of rain is needed between June and August. The potato thrives best when grown in not too heavy soils and in humous, sand soils with some loam or light loamy soils. (HEPTING 1998)

Potato crops typically require 150-250 kg of nitrogen ha^{-1}. Nitrogen made available from the soil through mineralization during the growth period can be well utilized. (BAUMGÄRTEL & SCHARPF 2002)

Depending on crop variety and on how much nitrogen can be mobilized from the soil, 80-160 kg N ha^{-1} of fertilizer is required. Where nitrogen exceeds 100 kg ha^{-1} , one-third of the nitrogen should be administered in a second dose. (HEPTING 1998)

For the validation of the DANUBIA crop growth model, two field data sets of potato crops in consecutive years are used. Because of lack of fertilizer application data, standard doses (total amount 140 kg N ha^{-1}) for 2005 are assumed. Table 35 lists the cultivation data and Table 36 summarizes the model performance statistics at the end of the sub-chapter.

Table 35: Cultivation data of potato fields (figures in italics are estimates).

	plant density (plants m^{-2})	**planting date**	**harvesting date**	**fertilizer date**	**amount (kg N ha^{-1})**		
					NH_4	NO_3	Urea
Hofferhof 2004	4.5	12.04.	21.09.	12.04.	100	100	200
Hofferhof 2005	4	*10.05.*	*17.09.*	*10.05.*	*25*	*25*	*50*
				14.06.	*10*	*10*	*20*

Hofferhof 2004 and 2005

Modelled and measured values of LAI and biomass for both data sets are compared in Fig. 50, showing stem and leaf biomass summarized as shoot biomass.

LAI and shoot biomass are overestimated at the beginning of growth in 2004. For 2005 the planting date, being unknown, was optimized by sensitivity analysis. Here, the steep increase of green LAI as well as of shoot biomass until tuberization is very well depicted by the model. However, after the onset of tuber growth, the model in both years allocates total assimilated carbon to the tuber. Thus the following measured increase of shoot biomass and green LAI is not captured. After remobilization of assimilates to the tuber, shoot biomass remains constant until senescence starts. Simulated potato tuber growth is overestimated in 2004 (MAE = 151 g m^{-2}, IA = 0.916) but tallies well with the observed values in 2005 (MAE = 66 g m^{-2}, IA = 0.974).

In neither year was water stress modelled. Simulated total transpiration amounts to 193 mm in 2004 and to 164 mm in 2005. Despite the very high fertilizer dose in 2004

and an overestimation of tuber growth by the model, simulated total nitrogen uptake results in only 141 kg ha^{-1}. Almost the same value, 144 kg ha^{-1}, is modelled for 2005.

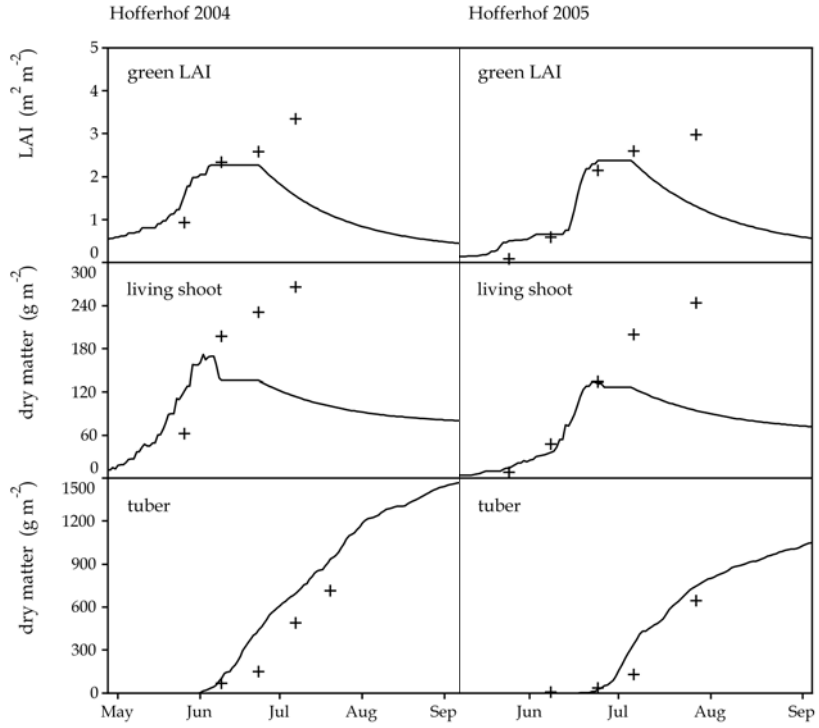

Fig. 50: Modelled (lines) and measured (symbols) LAI and biomass data of potato, Hofferhof 2004 and 2005.

On the whole, the validation analysis shows satisfying results for LAI and biomass (IA > 0.6). In the case of both data sets, simulation of tuber growth is more accurately predicted (mean IA = 0.945) than LAI development and shoot biomass.

Table 36: Model performance statistics for potato
(root mean squared error RMSE, relative RMSE (RRMSE), mean absolute error MAE, index of agreement IA, modelling efficiency statistic MEF).

	RMSE	RRMSE	MAE	IA	MEF
Hofferhof 2004					
green leaf area index	0.97	0.42	0.71	0.514	-0.231
living shoot	99.40	0.53	92.08	0.462	-0.660
potato tuber	15.51	0.05	150.97	0.916	0.519
Hofferhof 2005					
green leaf area index	0.79	0.47	0.53	0.833	0.518
living shoot	75.70	0.59	49.53	0.745	0.282
potato tuber	1.87	0.89	66.18	0.974	0.869
mean values of all data					
green leaf area index	0.88	0.45	0.62	0.673	0.143
living shoot	87.55	0.56	70.80	0.603	-0.189
potato tuber	8.69	75.93	108.58	0.945	0.694

3.2 Simulation of yield on the regional scale

In the context of the present study, the simulation of agricultural yield is of key relevance. Yield is a determinant for future land use changes which affect the water, carbon and nitrogen fluxes on large scales. To illustrate the application of the DANUBIA crop growth model on the regional scale, the simulation of yield in the administrative district Passau (1 530 km²) in Bavaria is presented.

First, the base and input data sets are described. The region was selected because a detailed soil map is available, offering a spatial resolution of 200 m * 200 m (*Bodenübersichtskarte* (BÜK) 200, sheet CC 7942 Passau). The year 1995 was chosen for the reason that a detailed land use classification exists, provided by the GLOWA-Danube project group *Hydrology / Remote Sensing (Department of Earth and Environmental Sciences, University of Munich).* This land use classification is derived from LANDSAT-TM satellite data utilizing the method described by STOLZ (1997). The spatial resolution of the land use map is 30 m * 30 m. For the simulation, both the land use and soil maps are scaled to a grid size of 100 m * 100 m.

Hourly meteorological input data were obtained from the weather station Kringell (48°40'52'' N, 13°29'35'' E, altitude 450 m) provided by the *Agro-Meteorological Network Bavaria.* The sowing and harvesting dates are chosen within the typical ranges for this region, based on the information given in KTBL (ed., 2002). In the case of cereals, harvesting is simulated within the given ranges after the phenological stage of maturity is reached. Standard fertilizer applications are assumed.

The distribution of the considered crops winter wheat, grain maize, spring barley, potato and sugar beet is shown in Fig. 51. The discrepancy between the northern and southern regions is due to the topography. In the mountainous landscape in the north, land use is dominated by meadows and forests. The five considered crops are only sparsely distributed. In contrast, land use in the southern basin is dominated by the cultivation of field crops. Among these, grain maize and winter wheat are the most prevalent.

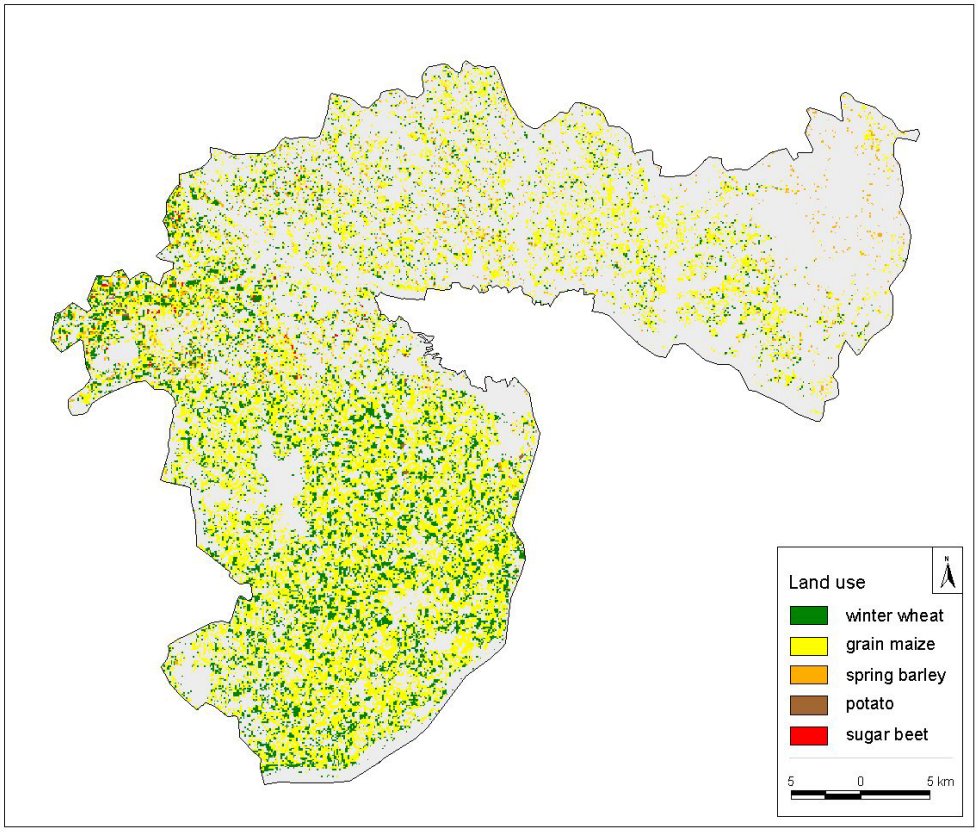

Fig. 51: Distribution of winter wheat, grain maize, spring barley, potato and sugar beet in the administrative district Passau in 1995.

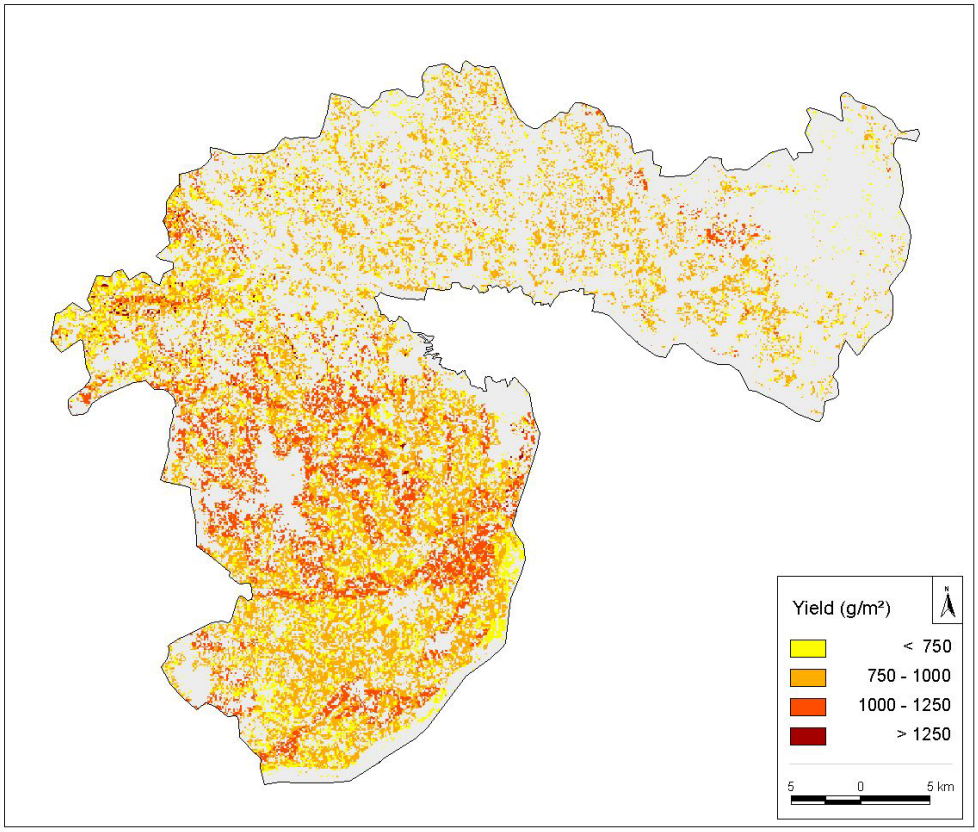

Fig. 52: Simulated yield of winter wheat, grain maize, spring barley, potato and sugar beet in the administrative district Passau in 1995.

The distribution of simulated yield shown in Fig. 52 reveals patterns that are not explained by land use distribution alone but are caused by differences in soil characteristics. The simulated yields of crops cultivated on clay soil are higher than those of crops grown for instance on soils characterized by a reduced capacity to store water. Since only one data set of meteorological drivers and the same cultivation practices are employed for the whole area, the model results clearly show the differences in yield caused by edaphic conditions.

Meteorological data with a higher spatial resolution considering topography, as well as dynamically simulated cultivation practices (dates of sowing and harvesting, dates and amounts of fertilizer applications dependent on phenology and nitrogen status of the crops) would allow for a more detailed simulation of crop development and growth. These results would offer the possibility to validate the crop growth model on the regional scale by comparing modelled yields with agricultural yield statistics at administrative district level.

3.3 Application to Global Change effects

In the following chapter it will be shown how the DANUBIA crop growth model can be used to assess the effects of Global Change on biomass production and water demand. In what ways are crops affected by mounting carbon dioxide concentrations in the atmosphere (denoted here as CO_2) and rising air temperatures? Also evaluated here is the influence exercised by agro-ecosystem management through nitrogen input to the soil.

First of all, the response of crop growth to Global Change effects is illustrated by examining data on the field scale. This is followed up by a numerical rating of the Global Change impact on the regional scale.

The word scenario as used here is defined as an assumption of changes in environmental factors (air temperature, CO_2) related to Global Change and of changes in agro-ecosystem management (nitrogen availability). These scenarios are used only for the purpose of examining the response of the crop growth model. A Global Change scenario, when defined as an consistent set of Global Change conditions, can only be analyzed by using an integrated simulation system like DANUBIA, which considers manifold interactions between the models. However, in an integrated Global Change

simulation, the suitability of each single participating model needs to be assured. Thus the presented analysis investigates the responsiveness of the DANUBIA crop growth model to Global Change effects.

3.3.1 Simulation on the field scale

Various scenarios have been chosen to demonstrate the model´s response to Global Change effects and to investigate the impact on biomass production, water and nitrogen demand on the field scale.

Measured meteorological data, present-day CO_2 (365 ppm) and standard nitrogen fertilizer doses serve as baseline scenarios. To represent Global Change effects, the input parameters CO_2 and air temperature are modified. Increased CO_2 (500 ppm and 750 ppm) and temperature rise (+ 1 °C) are assumed both singly and in combination as well as coupled with nitrogen in both standard doses and assuming unrestricted availability. Although CO_2 increase invariably entails rising temperatures, the scenarios considering only modified CO_2 are included to illustrate what CO_2 enrichment in itself brings about.

The modelled impacts on water, carbon and nitrogen fluxes are assessed by quantifying sums of transpiration, gross photosynthesis, nitrogen uptake and carbon incorporated in biomass from sowing to harvesting. The effect on biomass partitioning and yield formation is measured by the root/shoot ratio (including living and senescent material) and yield biomass at harvesting. The simulated results of the mentioned crop characteristics are compared with the results of a baseline scenario.

For analyzing the response of the crops to Global Change, the assumed increase of temperature in the scenarios is ignored for modelling phenological development: The unchanged air temperature is used as input parameter for calculating the progress in phenological development. Consequently, phenological development is assumed to be the same as in the baseline scenarios. Temperature increase prolongs the vegetation period but also accelerates phenological development and can adversely affect crops requiring vernalization. Whereas a longer growth phase can result in a higher yield in the case of e.g. sugar beet, cereals like wheat or barley, which are characterized by defined phenological stages, show a reduced yield due to the shorter grain-filling period (WEIGEL 2005).

Therefore, manipulating the growth period by shifting sowing and harvesting dates is one of the foremost strategies for adapting to Global Change. Additionally, the choice of cultivar is of cardinal importance since phenology is decisively controlled by cultivar-specific physiological parameters. By ignoring the increase of temperature for modelling phenological development, acclimated cultivars are taken into account and the same phenology for each of the applied scenarios is assumed.

In the following, case studies for spring barley and maize are presented. Spring barley serves to illustrate the response of C_3 plants and maize that of C_4 plants.

Response of spring barley

As a baseline scenario for spring barley, the dataset "Nienwohlde 1991, standard fertilizer treatment (N4)" is employed, which has already been used for the validation analysis (see chapter 3.1). To what extent scenario results diverge from the baseline scenario is expressed in absolute as well as relative differences in Table 37.

Table 37: Changes in modelled spring barley crop characteristics for specified scenarios with modified atmospheric CO_2 concentration, air temperature and N availability.
Definition and coding of the scenarios are listed, with ↑ N designating unrestricted N availability. The first line of values gives the modelled results for the baseline scenario. All other scenario results are expressed as changes (absolute and relative) from the baseline scenario.

Scenarios	**total transpiration**	**total gross photosynthesis**	**total N uptake**	**total C in biomass**	**yield**	**root/shoot ratio**
	mm	g CO_2 m^{-2}	kg ha^{-1}	g C m^{-2}	g m^{-2}	-
Baseline (Nienwohlde 1991)	**177**	**3300**	**157**	**673**	**636**	**0.15**
C500 500 ppm CO_2	-44 -25 %	+252 +7.6 %	+2 +1.4 %	+106 +15.8 %	-5 -0.8 %	+0.05 +31.2 %
$C500_{N+}$ 500 ppm CO_2, ↑ N	+18 +10.2 %	+1601 +48.5 %	+83 +53.2 %	+330 +49.1 %	+560 +88.0 %	+0.06 +41.4 %
C750 750 ppm CO_2	-83 -53.4 %	+133 +4.0 %	+3 +2.1 %	+111 +16.5 %	+60 +9.5 %	+0.04 +26.2 %
$C750_{N+}$ 750 ppm CO_2, ↑ N	-21 -11.9 %	+2559 +77.5 %	+93 +59.1 %	+504 +74.9 %	+678 +106.7 %	+0.02 +13.0 %
T1 + 1 °C	+18 +10.2 %	+114 +3.5 %	+4 +2.3 %	+45 +6.6 %	+49 7.7 %	+0.06 +37.6 %
T1 C500 + 1 °C, 500 ppm CO_2	-37 -20.7 %	+199 +6.0 %	+2 +1.3 %	+111 +16.5 %	-26 -4.1 %	+0.07 +47.4 %
T1 $C500_{N+}$ + 1 °C, 500 ppm CO_2, ↑ N	+48 +27.1 %	+1975 +59.8 %	+88 +56.1 %	+384 +57.0 %	+580 +91.2 %	+0.06 +38.8 %

At first an increase of CO_2 to 500 ppm (scenario C500) results in a higher amount of gross photosynthesis and accumulated carbon in biomass, a higher root/shoot ratio, but less transpiration compared with the baseline scenario. Values of yield and total nitrogen uptake remain almost the same due to nitrogen deficiency, which is diagnosed by the model. At the onset of growth, leaf area expansion is enhanced but senescence sets in earlier, affecting transpiration and photosynthesis. Therefore scenario $C500_{N+}$ assumes an unrestricted nitrogen availability, leading to greatly augmented photosynthesis, nitrogen uptake, biomass (all three increase by about 50 %) and yield formation (almost double the value) when compared with the baseline scenario. Transpiration increases by 10 %.

The same effect is observed assuming 750 ppm CO_2 with and without nitrogen limitation (scenarios C750 and $C750_{N+}$). Ample CO_2 supply stimulates photosynthesis and at the same time reduces the water loss through transpiration since stomatal conductivity is decreased. This leads to a comparatively slight rise in transpiration rate in scenario $C500_{N+}$ and even to a decline in scenario $C750_{N+}$, although leaf area increased in both cases.

Raising air temperature by 1 °C (scenario T1) at ambient CO_2 results in positive changes of all considered crop characteristics, although on a modest scale. Photosynthesis rate is favourably influenced by temperature increase as long as the optimum leaf temperature (assumed as 25 °C in the model) is not exceeded. Transpiration rate is also enhanced through stomatal control as well as through the direct effect of warming.

Assuming 1 °C temperature increase as well as 500 ppm CO_2 in scenario C500 T1 results in nitrogen-limited growth, characterized by premature senescence as described above. Results of the scenario T1 $C500_{N+}$ with unrestricted nitrogen availability show significant increases for all quantified crop characteristics. Transpiration sum changes by + 27 %, total nitrogen uptake by + 56 % and yield almost doubles.

Each scenario reveals a higher ratio of root to shoot carbon in comparison with the baseline scenario.

Response of maize

To serve as a baseline scenario for maize the data set "Wilzhofen 1997" is chosen, which has already been used for the validation analysis (see chapter 3.1). The absolute and relative differences of the scenario results as juxtaposed to the baseline scenario are listed in Table 38.

As described for spring barley, the growth effect of CO_2 enrichment alone (scenarios C500 and C750) is inhibited by lack of nitrogen availability. Therefore only moderate changes in the examined crop characteristics occur when compared with the baseline scenario, except for an obvious decrease in total transpiration. The reasons for this lie in the reduced stomatal conductance due to higher CO_2 as well as the decreased leaf area through premature senescence following nitrogen deficiency.

Table 38: Changes in modelled maize crop characteristics for specified scenarios with modified atmospheric CO_2 concentration, air temperature and N availability.
Definition and coding of the scenarios are listed, with ↑ N designating unrestricted N availability. The first line of values gives the modelled results for the baseline scenario. All other scenario results are expressed as changes (absolute and relative) from the baseline scenario.

Scenarios	**total transpiration**	**total gross photosynthesis**	**total N uptake**	**total C in biomass**	**yield**	**root/shoot ratio**
	mm	g CO_2 m^{-2}	kg ha^{-1}	g C m^{-2}	g m^{-2}	-
Baseline (Wilzhofen 1997)	**284**	**6723**	**239**	**1321**	**1455**	**0.17**
C500 500 ppm CO_2	-46 -16.2 %	+50 +0.7 %	+7 +2.8 %	+144 +10.9 %	+16 +1.1 %	+0.04 +25.8 %
$C500_{N+}$ 500 ppm CO_2, ↑ N	-11 -3.8 %	+1183 +17.6 %	+34 +14.4 %	+266 +20.4 %	+141 +9.7 %	+0.06 +34.4 %
C750 750 ppm CO_2	-100 -35.1 %	+185 +2.7 %	+7 +2.8 %	+166 +12.5 %	-29 -2.0 %	+0.12 +68.6 %
$C750_{N+}$ 750 ppm CO_2, ↑ N	-74 -26.1 %	+1300 +19.3 %	+49 +20.3 %	+315 +23.8 %	+315 +21.6 %	+0.06 +33.5 %
T1 + 1 °C	-0.4 -0.1 %	-246 -3.7 %	-0.4 -0.2 %	+28 +2.1 %	+2.8 +0.2 %	+0.04 +22.7 %
T1 C500 + 1 °C, 500 ppm CO_2	-23 -8.0 %	+426 6.3 %	+11 +4.4 %	+146 +11.1 %	+43 +3 %	+0.08 +45.2 %
T1 $C500_{N+}$ + 1 °C, 500 ppm CO_2, ↑ N	+4 +1.5 %	+1276 19.0 %	+38 +15.9 %	+274 +20.7 %	+168 +11.5 %	+0.07 +42.9 %

The assumption of a CO_2 enrichment in combination with unrestricted nitrogen supply (scenarios $C500_{N+}$ and $C750_{N+}$) results in apparent positive changes in all considered crop characteristics, excluding the decrease in transpiration sums (-4 % and -26 %

respectively). The positive changes in scenario $C750_{N+}$ compared with scenario $C500_{N+}$ are enhanced only to a minor degree.

The warming effect by 1 °C alone (scenario T1) produces a slight drop in total gross photosynthesis instead of a rise. The reason lies in the increased allocation to the root at the expense of leaf biomass and consequently leaf area, right from the onset of growth. However, when accompanied by an increased CO_2 to 500 ppm (scenario T1 C500), total gross photosynthesis is favourably influenced. Furthermore, assuming no nitrogen limitation (scenario T1 $C500_{N+}$), greatly heightens the impact on all examined crop characteristics. Compared with the baseline scenario, total gross photosynthesis changes by +19 %, total nitrogen uptake by +16 %, yield by +12 %, with total transpiration amounting to almost the same value.

As in the case of spring barley, each of the Global Change scenarios shows a higher ratio of root to shoot carbon compared with the baseline scenario.

3.3.2 Simulation on the regional scale

One of the Global Change scenarios applied on the field scale in the preceding chapter is now employed on the regional scale. This scenario, denoted T1 $C500_{N+}$, assumes a rise in air temperature by 1 °C, an increased atmospheric carbon dioxide concentration (500 ppm) as well as unrestricted nitrogen availability. The area examined is the administrative district Passau. The base and input data sets for the application of the model in this region have already been described in chapter 3.2. As pointed out there, only one data set of meteorological drivers and the same cultivation practices are utilized for the whole area. The meteorological data measured by the weather station Kringell serve as baseline scenario. For the scenario T1 $C500_{N+}$, the measured air temperatures were increased by 1 °C.

The application of this scenario on the regional scale is solely for the purpose of demonstrating how the response of crops to Global Change effects is influenced by small-scale variability in a landscape. In this simplified example, spatial variability is caused only by the different soil properties. In the following, the transpiration sums from sowing up to harvesting are chosen to illustrate the crop reaction.

First, the distribution of simulated transpiration sums of the crops considered in this study in 1995 is shown (Fig. 53). The areas under sugar beet and potato cultivation show the highest transpiration sums. However, as in the case of yield (see chapter 3.2),

the map reveals patterns that are not explained by land use alone but originate from differences in soil properties. Transpiration sums on soils with a reduced capacity to store water are smaller than those on soils promoting crop water availability.

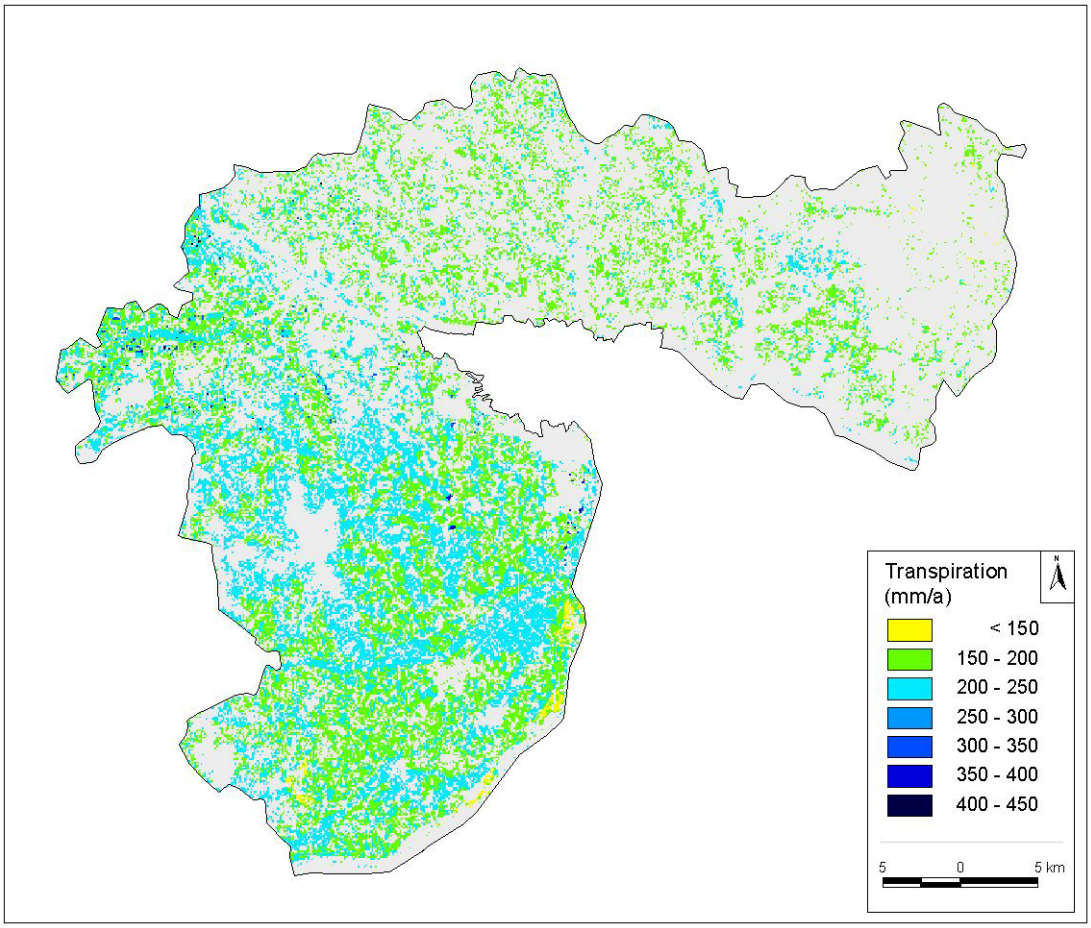

Fig. 53: Simulated transpiration of winter wheat, grain maize, spring barley, potato and sugar beet in the administrative district Passau. Transpiration sums from 01.11.1994 to 31.10.1995 are shown.

Fig. 54 maps the changes in simulated transpiration sums from the baseline scenario for the scenario T1 $C500_{N+}$. The changes range from -19 % (maize) to +53 % (winter wheat). All negative values refer to maize, which represents the only C_4 crop. The diverse soil properties in the investigated area are responsible for variegated patterns of response even within one crop. For maize, values range from -19 % to -5 %, whereas values for sugar beet range from +1 % to +49 %. The other ranges of values are: +13 % to +32 % (spring barley), +19 % to +53 % (winter wheat) and +1 % to +18 % (potato).

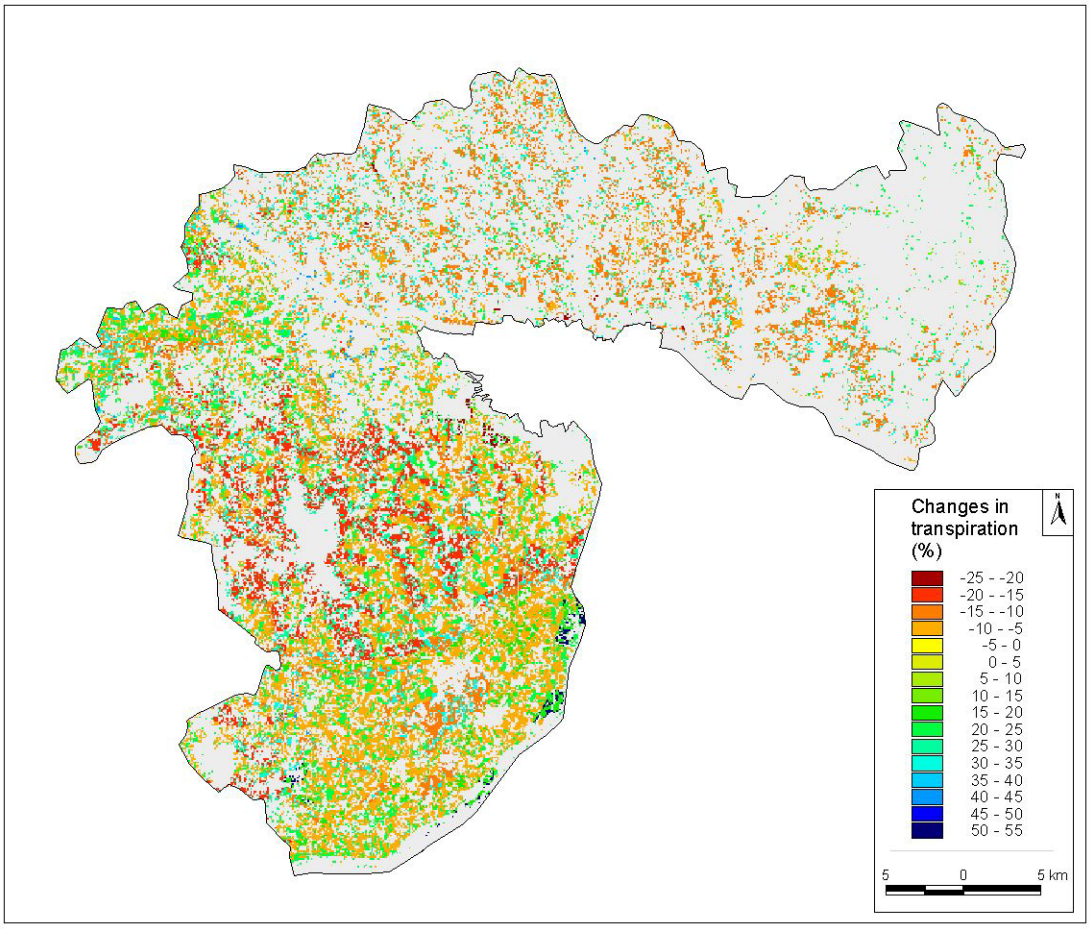

Fig. 54: Changes in simulated transpiration of winter wheat, grain maize, spring barley, potato and sugar beet for the scenario T1 C500N+ in the administrative district Passau. Data are expressed as changes (in percent) in the transpiration sums (01.11.1994 to 31.10.1995) as opposed to the baseline scenario.

The results demonstrate the importance of examining Global Change effects at the landscape level. Areas that are particularly sensitive to Global Change need to be pinpointed to successfully direct management decisions.

4 Results and discussion

In this chapter, the efficiency of the DANUBIA crop growth model in simulating the relevant processes of crop development and growth under varying environmental conditions with different farming practices will be discussed. Its ability to adequately quantify water and nitrogen demand as well as biomass production of various crops will be assessed. First, the accuracy of the model in predicting crop growth is evaluated by discussing the results of the validation analysis. Secondly, the responsiveness of the model to defined changes in environmental conditions and farming practices is illustrated and discussed. Additionally, uncertainties influencing the model results are addressed.

So far no results of the model GECROS are published, except for a sample data set (without corresponding field measurements) simulating pea growth (YIN & VAN LAAR 2005). Therefore the two models are not compared here for accuracy and sensitivity in simulating crop growth.

4.1 Accuracy of the model

In this chapter, the results of the validation analysis are discussed separately for each considered crop, followed by general statements.

4.1.1 Sugar beet

The seven employed field data sets for sugar beet cover a wide range of sowing dates. At the onset of growth, modelled LAI and leaf biomass tally very well with the measurements. This indicates that the earliest phenological stages of germination and emergence are accurately simulated.

With advancing development, some disparities between measured and modelled LAI appear, leading to an overall MAE of 0.92 $m^2\ m^{-2}$ for the whole growing period. These are demonstrated by negative values of MEF for three data sets (Nienwohlde 1990, Friemar 2000 and Plattling 2000). For the field data of Feienberg 2004, the assumption of a standard senescence in the model seems to be incorrect. However, this does not apply to the other data sets.

To avoid an obvious overestimation of LAI, the specific leaf area was reduced in the case of four of the data sets (after the onset of taproot growth). It is supposed that specific leaf area decreases with age and size of the leaves. Large old leaves are tougher than the young leaves produced later in the growing season. In these four data sets the fertilizer applications are merely estimated and this in ignorance of the preceding crop. This gap in information makes a thorough analysis of LAI development difficult. Moreover, the measured data would need to distinguish between living and dead leaves. Focussing on specific leaf area and the process of senescence will improve LAI modelling.

Despite these difficulties relating to LAI development, the model simulates aboveground biomass fairly accurately (overall IA 0.919). In terms of the output parameter agricultural yield, the precise simulation of taproot biomass (overall IA 0.978) is particularly important. An analysis of the differences between modelled and measured taproot biomass at the last sampling date shows no consistent trend (Fig. 55). The modelled results are well in conformance with the last measured taproot biomass values (mean value of absolute model error 9.1 %). The highest absolute model error of all presented validation data sets is 16.5 % (317 g m^{-2}) for the crop in Friemar 2000.

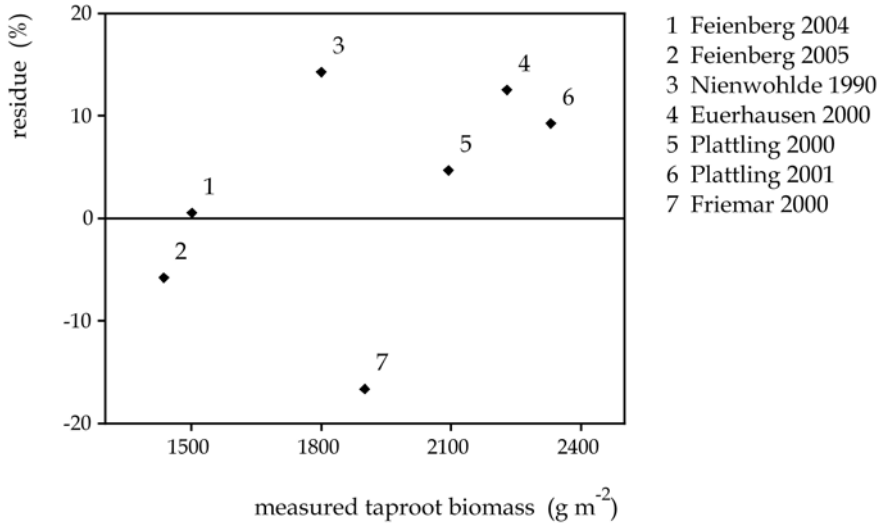

Fig. 55: Model error (%) versus final measured taproot mass for all sugar beet validation data sets.

Within DANUBIA, the simulated yield data are exported by the crop growth model to serve to determine future land use changes. Here, some peculiarities for sugar beet need to be considered. Official data of sugar beet yields are determined by the sugar industry and are generally given in fresh instead of dry matter. Secondly, the upper

parts of the taproots are chopped off during harvesting and are not included in the official yield data.

Consequently, for the purpose of export the simulated sugar beet yield data have to be adapted to match the official data used in agro-economics. For the transformation of dry matter into fresh matter, the standard value of 77 % water content (KTBL, ed., 2005) in harvested taproots can be used. Since the taproots are of various sizes, the chopped off biomass expressed as percentage of the whole taproot cannot be precisely defined by using a standard value. Here a transfer function needs to be developed. This must also be borne in mind when comparing modelled taproot biomass with yield statistics data for validating the model.

In respect of total modelled nitrogen uptake as well as total transpiration over the growing season, all seven data sets yielded values that were well within the expected size range. In general, the simulated course of nitrogen uptake compares well with measured data both of soil and biomass nitrogen content.

For the two data sets Feienberg 2005 and Euerhausen 2000, values of IA for LAI, leaf as well as taproot biomass are higher than 0.95, testifying to a very good performance of the model.

On the whole, the DANUBIA crop growth model proved its ability to accurately simulate carbon, nitrogen and water fluxes as well as agricultural yield for sugar beet crops.

4.1.2 Spring barley

An assessment of the model´s accuracy in predicting spring barley growth is hampered by the incongruities associated with the field data. Taking together all three validation data sets, the MAEs are 0.93 for LAI, 38.6 g m^{-2} for living leaf, 67.2 g m^{-2} for stem, 130.2 g m^{-2} for grain and 120.2 g m^{-2} for living shoot biomass, respectively. For the crop in Wilzhofen 1997, the values of IA for each considered parameter are greater than 0.69. These are good results, bearing in mind the lack of management information.

Field data sets providing reliable measurements at short intervals as well as precise management information would allow a more detailed validation analysis. Although definite conclusions cannot be reached from the analyzed data, the results do suggest

that the DANUBIA crop growth model simulates agricultural yield, water and nitrogen uptake of spring barley accurately.

4.1.3 Maize

The model´s capacity to predict maize growth under varying environmental conditions is proved through the validation analysis. The response of the maize crop to the unfavourable agrometeorological conditions in Feienberg 2005 is very well simulated by the model. Here crop field data for the validation analysis were supplemented by soil water and soil nitrogen measurements.

The three validation data sets showed that the model´s assumption of a standard senescence is not realistic. This finding calls for further analysis. Taking all data sets together, the MAEs are 0.75 for LAI, 55.8 g m^{-2} for living leaf, 81.4 g m^{-2} for stem and 152 g m^{-2} for grain, respectively. A quantification of the model´s accuracy expressed by the two normalized measures IA and MEF is impeded in the case of Feienberg 2004 and 2005 by the insufficient quantity of crop data.

However, for Wilzhofen 1997, each value of IA for LAI, leaf, stem as well as grain is higher than 0.91, demonstrating an efficient performance of the model.

On average, grain biomass is simulated with a RRMSE of 26 %, corresponding to a RMSE of 167 g m^{-2}. In the case of silage maize, agricultural yield comprises the total aboveground biomass. Here leaves contribute only a small fraction compared with stems and grains. Thus the model´s capacity to predict the yield of silage maize benefits from the generally favourable results for stem and grain biomass. The mean values of RMSE and IA for living shoot biomass are 151 g m^{-2} and 0.988, respectively.

Total modelled nitrogen uptake as well as total transpiration over the growing season yielded values well within the expected size range for all data sets.

4.1.4 Winter wheat

On the whole, the DANUBIA crop growth model results for winter wheat are highly satisfactory. The very close agreement between modelled and measured LAI increase at the onset of regrowth in early spring demonstrates the exactitude of simulating phenology. The interaction between vernalization, photoperiod sensitivity and temperature effect is clearly depicted.

The reason for the underestimation of shoot biomass in Feienberg 2003/04 cannot be clearly determined. The observed grain and total shoot biomass is markedly higher than average. A standard value for winter wheat grain mass is 720 g m^{-2}, the rest of the shoot biomass amounting to 700 g m^{-2} (KTBL, ed., 2005). On the last sampling date, measured grain biomass yields an extraordinarily high value (1145 g m^{-2}). Stem and dead leaf biomass together result in 790 g m^{-2}. Since total shoot biomass is systematically underestimated, it appears not a matter of allocation but of too little biomass production. The very accurately modelled LAI development is at variance with the simulated biomass production. A higher value of modelled leaf biomass at the onset of regrowth in March to match the measurements would inevitably result in a higher LAI with advancing development. The same would happen if e.g. leaf photosynthesis parameters were modified in order to increase carbon fixation. Because of the higher LAI, more assimilates and biomass would be simulated. However, the modelled LAI would be overestimated. This finding calls for further analysis through investigating the effects of specific leaf area and cultivar-specific characteristics.

One more aspect to be considered is that the use of plant growth regulators to curb stem growth and enhance lodging resistance of cereals frequently promotes grain growth (RAJALA & PELTONEN-SAINIO 2001). Therefore, this intervention altering allocation is important for simulating growth of cereals, but is not taken into account by the model.

Model results for Bockschlag 1990/91 conform very closely to the measurements. On the last measurement day, grain and living shoot biomass deviate by only +6 g m^{-2} and -93 g m^{-2}, respectively. WANG & ENGEL (2002) publish results of the model SPASS (**S**oil-**P**lant-**A**tmosphere **S**ystems **S**imulation) using the same validation data set. Here, biomass production was greatly overestimated: +190 g m^{-2} for grain and +1330 g m^{-2} for shoot biomass (resulting in more than double the measured value). Their results for Neuenkirchen 1990/91 also show a pronounced overestimation of shoot biomass (+950 g m^{-2}), although LAI development is well simulated. Working with the same data set, the DANUBIA crop growth model also reproduced LAI and biomass production with great precision: values of IA for LAI and total living shoot biomass are 0.951 and 0.942, respectively.

Taking all three validation data sets collectively, the model verifies its ability to accurately predict LAI development (IA = 0.952). The less convincing figures

associated with leaf biomass (IA = 0.709) are not significant for quantifying transpiration and agricultural yield. The latter is predicted acceptably well (IA = 0.848).

Modelled sums of nitrogen uptake and transpiration for all data sets remain well within the expected size range.

In summary, an efficient performance of the DANUBIA crop growth model in simulating development and growth of winter wheat crops is demonstrated.

4.1.5 Potato

In the main, the validation results for potato are satisfactory. For the two crops in Hofferhof 2004 and 2005, the values of IA for each considered parameter (green LAI, living shoot biomass and tuber biomass) show rather low values, but are greater than 0.5. The model underestimates shoot biomass after tuberization in both data sets. Some further analysis using more field data sets is needed to overcome this discrepancy. However, despite a trend towards overestimation, growth of potato tubers is very well depicted in both years (mean IA = 0.945). These results do suggest that the DANUBIA crop growth model simulates agricultural yield of potato crops acceptably well. Measurements of soil moisture and soil nitrogen would be needed to allow a sound statement on the model`s capacity to predict transpiration and nitrogen uptake of potato crops.

The simulation of phenology needs to be improved. In contrast to the seeds of cereals and sugar beet, the seed potato with its high moisture content relies less on soil moisture for germination. All parameters used for simulating phenology need to be further elaborated.

A specific feature of potato crop management is the destruction of the haulm towards harvesting date. By this practice, maturity of the tubers is forced in order to manipulate the quality of yield and the harvesting date. This intervention causes transpiration and assimilation to rapidly cease and thus has an impact on water, carbon and nitrogen fluxes. Where this management method is common practice, it should be taken into consideration when applying the model on the regional scale.

4.1.6 General discussion of results

To summarize, the validation analysis testifies to the ability of the DANUBIA crop growth model to accurately simulate development and growth of various crops belonging to the categories of C_3 and C_4 plants, winter and spring grains, root crops, as well as long-day, short-day and photoperiod-insensitive crops. Fluxes of water, nitrogen and carbon as well as agricultural yield are adequately quantified, as the comparisons with measurements show.

For validation on the field scale, 18 data sets covering a wide range of meteorological and pedological conditions as well as farming practices are employed. No site-specific calibration is used in the validation analysis, although in some cases plant density and the genotype-specific phenological parameters $R_{max,v}$ and $R_{max,r}$ (maximum daily development rates) were adjusted to the given situation. However, general values of these parameters for the application on the regional scale in the Upper Danube Basin are given in Appendix D. Spatial transferability, claimed by the process-based modelling approach, is proved by the DANUBIA crop growth model through the validation analysis.

In terms of total transpiration as well as total nitrogen uptake over the growing season, all analyzed data sets yielded values that are well within the expected size range. Comparisons of the simulated courses of water and nitrogen uptake with corresponding soil measurements proved the capacity of the DANUBIA crop growth model to accurately predict the uptake rates of water and nitrogen. This feature is of fundamental significance since complex feedback mechanisms arise from dynamic modelling of the interplay between soil and crops. The uptake rates being controlled by the water and nitrogen budgets in the soil at the same time influence these. The water and nitrogen budgets in turn affect processes of soil nitrogen fluxes and transformation.

Another feature of prime relevance is the simulation of agricultural yield. On the basis of these results, the economic optimization model within DANUBIA (KRIMLY *et al.* 2004) calculates the farmer´s land use plans for the next vegetation period. On the whole, the DANUBIA crop growth model is found to simulate the yields of the various examined crops with good precision.

Issues that need to be addressed in further analyses are set out in the subchapters above. Among these, the assumptions of a constant specific leaf area and a standard

senescence are of particular importance. Assessing the model´s accuracy is sometimes hampered by the incongruities presented by the field data. The use of supplementary validation data sets will help to better assess how accurate the simulation results are.

A better quality of the field data in terms of a greater number of samples per field and shorter intervals between the measurements would allow a more detailed validation analysis. Data on phenological stages, root biomass and where possible root length density, soil nitrogen and soil water measurements as well as precise management information for each data set would further contribute to a thorough judgement of the model´s performance.

Measurements of water and carbon dioxide fluxes in ecosystems using the eddy covariance method or e.g. sap flow data are becoming more readily available, thus offering the opportunity to directly validate the modelled processes.

4.2 Sensitivity of the model

To evaluate the performance of the DANUBIA crop growth model in numerically rating crop responses to altered environmental conditions and farming practices, the sensitivity of the model to clearly defined alterations in various influencing factors is discussed. In quantifying the changes caused by these modifications, the responses to nitrogen and water availability as well as to Global Change conditions are assessed.

4.2.1 Nitrogen availability

To illustrate the model´s sensitivity to nitrogen supply, the results of the validation analysis for the standard (N4) and reduced (N6) fertilizer treatments of the spring barley crop in Nienwohlde 1991 (chapter 3.1.2.2) are employed.

A comparison of the simulated data for both fertilizer procedures demonstrates the model´s response to the reduced fertilizer dose (see chapter 3.1.2.2). A few days after the omitted fertilizer dose on April 6th, LAI development is reduced in the N6 fertilizer treatment when compared with N4. Senescence is induced earlier in the case of N6, indicating the decrease in leaf nitrogen concentration.

Due to the reduced LAI development, less carbon dioxide is assimilated and consequently less biomass produced.

Modelled carbon dioxide assimilation and transpiration for both fertilizer treatments are opposed in Fig. 56. The course of the two fluxes is very similar because both share the same pathway via the stomata. An intercomparison of the fluxes for both fertilizer treatments reveals the same trend, ascribable to the identical meteorological conditions. The very limited incoming global radiation on June 28th is reflected by strongly reduced transpiration and assimilation in both cases. However, the magnitudes of both the fluxes for N6 are reduced due to decreased LAI expansion and lowered leaf nitrogen concentration.

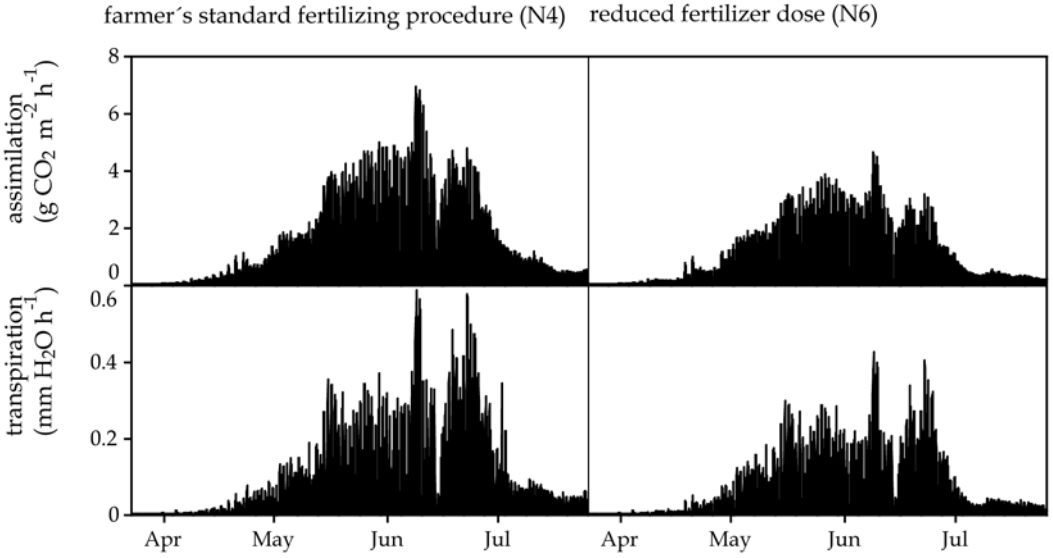

Fig. 56: Modelled carbon dioxide assimilation and transpiration of spring barley, Nienwohlde 1991 (N4 and N6 fertilizer treatment).

Table 39 lists some characteristic model results in which both fertilizer procedures N4 and N6 are compared. In the case of N6, total transpiration is reduced by 25 %. Values of transpiration ratio (mass of water transpired divided by mass of dry matter produced) are the same. In this study, transpiration ratio considers total produced dry matter, including roots. The ratio of assimilated carbon to absorbed nitrogen also shows similar values: 5.74 for N4 and 6.25 for N6. These results prove that in biomass production the water, nitrogen and carbon budgets are well in equilibrium.

Table 39: Comparison of modelled results for spring barley, Nienwohlde 1991, N4 and N6 fertilizer treatment.

fertilizer treatment	total assimilated C (g C m^{-2})	total transpiration (mm H_2O)	total N uptake (kg N ha^{-1})	total produced dry matter (g m^{-2})	transpiration ratio (kg H_2O kg^{-1} dry matter)
N4	901	177	157	1683	105
N6	681	132	109	1253	105

Fig. 57 demonstrates the impact of nitrogen supply on modelled biomass partitioning (left graph) and on biomass nitrogen concentrations (right graph). All data displayed refer to July 7th. In the case of N6, more root biomass is produced in order to increase the uptake of the limited resource nitrogen. The leaf nitrogen concentration is reduced compared with N4, resulting in a smaller photosynthesis rate.

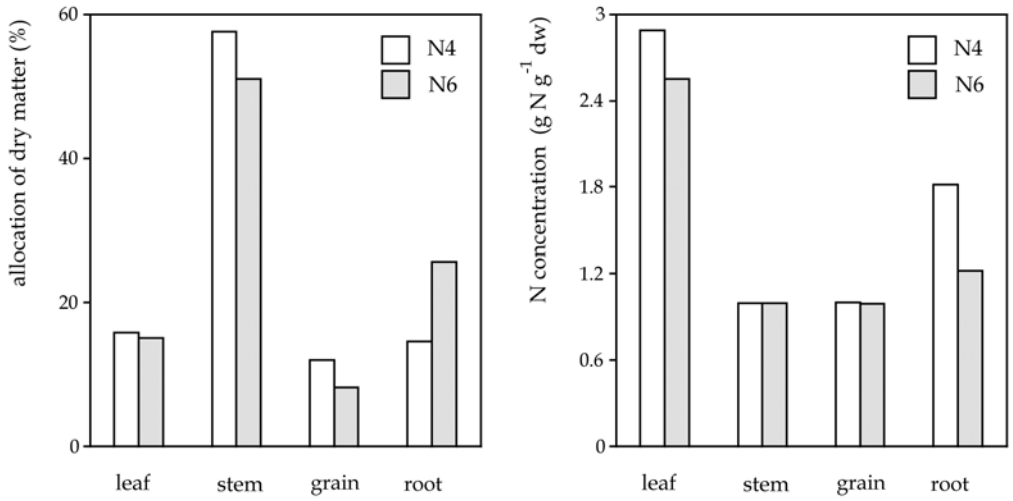

Fig. 57: Allocation of dry matter (left) and nitrogen concentration in biomass (right) of spring barley, Nienwohlde 1991 (July 7th). Data of the fertilizing procedures N4 and N6 are compared.

The DANUBIA crop growth model proved its sensitivity to different fertilizing procedures.

4.2.2 Water availability

The results of the validation analysis for the winter wheat crop in Neuenkirchen 1990/91 (chapter 3.1.2.4) illustrate the model´s sensitivity to soil water scarcity. Moderate water stress during a few days around anthesis reduces grain and total living shoot biomass at harvesting date by 6.3 % and 6.4 %, respectively. Total transpiration decreased by nearly 5 %, total nitrogen uptake by 1.5 %.

A far more pronounced impact on biomass production and transpiration would be simulated if water scarcity occurred during the phenological phases of LAI development (before flowering). The curtailed transpiration rate would reduce photosynthesis rate, resulting in lowered leaf biomass production and retarded LAI development. The smaller LAI would also curb the production of assimilates for the rest of the growth period.

4.2.3 Sensitivity to Global Change effects

The responsiveness of the DANUBIA crop growth model to various Global Change scenarios is demonstrated and quantified on the field scale in chapter 3.3.1. Here, the simulated results of one of the Global Change scenarios are discussed.

This Global Change scenario, denoted T1 $C500_{N+}$, assumes a rise in air temperature by 1 °C, an increased atmospheric carbon dioxide concentration (500 ppm) as well as unrestricted nitrogen availability. The modelled results for the growth of spring barley and maize are used to discuss the responsiveness of C_3 (spring barley) and C_4 plants (maize). The data sets Nienwohlde 1991 (spring barley) and Wilzhofen 1997 (maize) serve as baseline scenarios serve the, both already employed for the validation analysis (see chapter 3.1). The simulated relative changes in several crop characteristics are shown for spring barley and maize in Fig. 58.

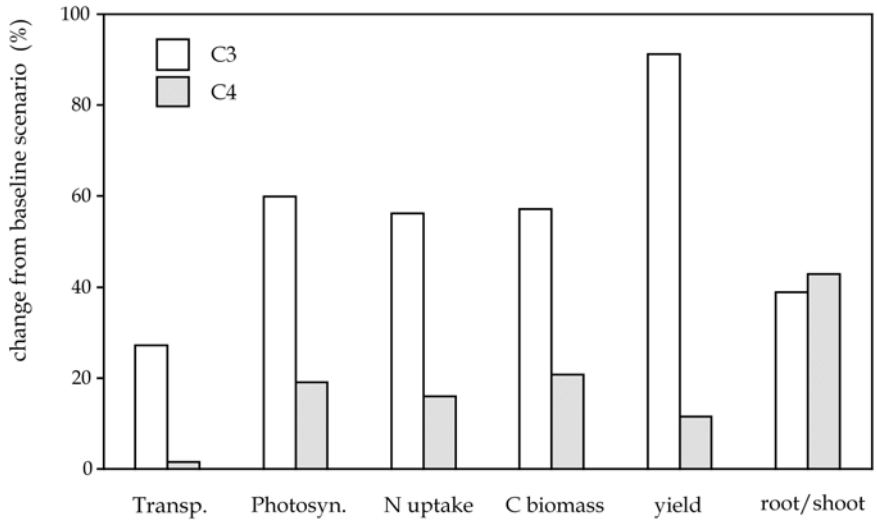

Fig. 58: Simulated relative changes in crop characteristics of a Global Change scenario (T1 $C500_{N+}$: 500 ppm CO_2, 1 °C air temperature rise, unrestricted N availability) from the corresponding baseline scenario. Responses of C_3 crops (spring barley) and C_4 crops (maize) are compared. Illustrated data are: total transpiration sum (mm), total gross photosynthesis (g CO_2 m^{-2}), total nitrogen uptake (kg ha^{-1}), total carbon in biomass (g C m^{-2}), yield (g dry matter m^{-2}) and root/shoot ratio.

Each considered characteristic of both crops exhibits a positive change. However, the magnitude of these changes differs strikingly between spring barley and maize. In the case of spring barley, significant increases are simulated: the transpiration sum changes by +27 %, total nitrogen uptake by +56 % and yield almost doubles. For maize, the transpiration sum is altered by +1.5 %, total nitrogen uptake by +16 % and yield by +12 %. On the whole, the impact on crop growth is less pronounced for maize than for

spring barley. This is caused by the dissimilarity of C_3 and C_4 photosynthesis, which the DANUBIA crop growth model takes into account.

C_3 photosynthesis is not CO_2-saturated at present-day atmospheric CO_2 concentrations. Because of specific physiological features, C_4 plants are able to exploit the CO_2 supply more efficiently and thus their response to a CO_2 increase is less pronounced. The more efficient use of CO_2 reduces water loss by transpiration due to decreased stomatal opening. C_4 crops are generally characterized by a higher amount of biomass produced per unit water transpired than C_3 crops.

Considering the leaf level for both C_3 and C_4 crops, CO_2 enrichment increases photosynthesis rate and decreases transpiration rate. The photosynthesis rate is positively influenced by the repression of photorespiration and enhanced CO_2 availability (POORTER & NAVAS 2003) whereas the transpiration rate is decreased due to the resulting partial stomatal closure (NOBEL 2005). These direct effects of increased CO_2 raise the amount of CO_2 fixed by photosynthesis per unit water transpired for both C_3 and C_4 plants (NOBEL 2005).

As is seen in Fig. 58, the change in gross photosynthesis is higher than in transpiration for both crops. This result emphasizes the key importance of coupled photosynthesis and transpiration modelling to capture the interaction of both gas exchange processes.

The above described consequences of increased CO_2 at the leaf level hold true only where there is no change in leaf area. In the simulation results, the benefits of the so-called CO_2 fertilizer effect on crop growth leads to expanded leaf area, counteracting the effect of reduced transpiration rates at the leaf level when considering the absolute transpiration rates of the crop. However, the simulation results clearly demonstrate the change in the ratio of transpiration to photosynthesis. The Global Change scenario reveals a transpiration ratio for spring barley of 85 kg H_2O kg^{-1} dry matter (- 20 % change from the baseline scenario) and for maize of 72 kg H_2O kg^{-1} dry matter (- 14 % change).

The yield-enhancing effect shown for both crops in the Global Change scenario results is accompanied by a higher nitrogen demand. An unadapted fertilizer supply would lead to nitrogen deficiency, thus accelerating leaf senescence and consequently biomass production. In the case of cereals, nitrogen deficiency decreases protein content in grains, reducing yield quality and therefore economic gain. The higher nitrogen demand simulated under Global Change conditions underscores the relevance of

considering the interaction between crop growth, environmental conditions and management strategies. It must also be born in mind that a higher supply of nitrogen fertilizer entails detrimental effects on the environment. Excessive nitrate in the soil given enough water leads to nitrate leaching, impairing both surface and groundwater quality.

Simulation results exhibit a distinct positive change in the root/shoot-ratio for both crops (each by approx. 40 %). This proves the responsiveness of the model to Global Change effects that it modifies the allocation of assimilates. As to be expected, this shift in allocation expressed as a ratio produces almost the same result for spring barley and for maize. The increased root/shoot ratio is one of the anticipated responses of plants under Global Change conditions (NOBEL 2005). According to the functional balance theory as incorporated in the DANUBIA crop growth model (see chapter 2.2.9), all those positive conditions of above-ground resources (in these scenarios CO_2 and temperature) that increase carbon gain result in an enhanced allocation of carbon to the root in order to balance activities of the shoot (carbon supply) and root (nitrogen supply).

The enhanced allocation to the root at the expense of the shoot as well as the augmented biomass production and the decreased transpiration ratio resulting from CO_2 enrichment have been numerously observed in experiments (WEIGEL 2005). Much research has been devoted to the study of how crops respond to Global Change conditions. Observed crop reactions span a wide range. POORTER & NAVAS (2003) point to the rather diffuse picture emerging from experiments at the whole plant level. Because of varying experimental settings, it is difficult to deduce general statements from the results. BLOOM (2006) lists the relative changes in grain yield at increased CO_2 as derived from several chamber experiments as well as free-air CO_2 enrichment (FACE) experiments. For maize, values range from - 35 % to + 93 %, representing the outcomes of 57 studies. The mean value for chamber experiments is given as + 29 %, whereas the mean value for FACE experiments is given as ~ 0 %. These values show the wide scatter in published results. The need for systematic experiments to improve the generalizations from the observed findings is emphasized by POORTER & NAVAS (2003).

The response of crops to Global Change effects has also been addressed by innumerable investigators using crop growth models (e.g. WESSOLEK & ASSENG 2006), WOLF & VAN OIJEN 2003). One of the few comprehensive studies comparing observed

experimental data with simulated results of a complex model is presented by GRANT *et al.* (2004). In their study, the observed response of sorghum is compared with results of the model *ecosys*. As mentioned before, this model incorporates the biochemical approach in modelling photosynthesis as well as the functional balance approach for modelling allocation.

The simulation results of the Global Change scenario discussed in the present study are merely case studies to demonstrate the sensitivity of the DANUBIA crop growth model. The employed Global Change scenario is no more than a combination of CO_2 and air temperature rise by a constant value; ignoring other factors such as changes in precipitation and the effect of Global Warming on the seasonal curve of temperature are disregarded for the present.

However, the DANUBIA crop growth model proved its sensitivity to Global Change effects. The fundamental significance of several modelling approaches are highlighted: biochemical photosynthesis, stomatal control of transpiration and photosynthesis, dynamic allocation, response to nitrogen availability, physiologically based senescence and the difference in C_3 and C_4 photosynthesis.

The simulation results suggest that the DANUBIA crop growth model is a suitable tool for numerically assessing the consequences of Global Change on biomass production and water demand, taking into account the manifold interactions and feedback mechanisms of water, carbon and nitrogen fluxes within agro-ecosystems.

4.3 Uncertainties influencing model results

Like every ecosystem model, the DANUBIA crop growth model in simplifying real-life conditions is prone to inaccuracies. For the most part, these stem from the model structure itself, the input data and the parameters applied (MONOD *et al.* 2006). A few examples of how uncertainties may arise here are now briefly discussed.

Model structure

Here the choice of modelling approach with the mathematical equations involved may produce misrepresentative values, for instance when one of the simulated processes is disregarded. In setting up a simulation model, selecting and implementing modelling approaches are necessarily dictated by the end in view. The DANUBIA crop growth model aims to simulate all important processes with the necessary degree of complexity. For the present purpose, no shortcomings regarding model structure and modelling approaches could be discerned, as proved by the successful validation. However, an error potential is always present.

Input data

It is beyond the scope of this study to evaluate in detail the error sources traceable to the vast body of input variables required by the DANUBIA crop growth model. However, a few instances are given of how imprecise values in input data can influence model results. The values of static input data such as soil hydrological parameters move within (sometimes extensive) ranges of values typical for the soil texture in question. For instance, the value of field capacity for sandy loam ranges between 0.13 and 0.29 cm^3 water cm^{-3} soil (RAWLS *et al.* 1993). Obviously, the value selected can at times be misrepresentative.

Dynamic input data such as meteorological drivers may either suffer from inexact measurements in the case of observed data, or are themselves subject to uncertainties where they represent model results.

Another category of dynamic input data are parameters which at the same time are affected by the simulated crop growth processes. These input data are results of models coupled to the crop growth model. One example is soil water content, which as a key input parameter is in a state of continuous change through root water absorption. This makes cause and effect relationships difficult to diagnose. The model initialization

of parameters such as soil water content is another point in question. Quantifying the influence of inaccuracies originating from these simulated input data requires a comprehensive analysis of error propagation. However, in general terms, the interplay of dynamic soil input data and crop growth processes is accurately depicted, as proved by comparing soil water and nitrogen measurements with modelled results (see chapter 3.1.2).

Input data represent meteorological and edaphic characteristics as well as farming practices of an agro-ecosystem within a defined spatial unit. Assuming this spatial unit to be homogeneous throughout often leads to erroneous conclusions. It was to minimize any misleading effects of these uncertainties that the validation analysis to assess the accuracy of the DANUBIA crop growth model was carried out on the field scale (see chapter 3.1.2).

For application on the regional scale, the input data related to farming practices will need to be modified in future: The sowing date will be simulated depending on meteorological conditions, and dates of fertilizer applications will be dynamically determined taking into account phenological development. Additionally, a major improvement would be to use a knowledge of the nitrogen status of the crop to derive both dates and amounts of fertilizer doses. The latter are input data used by the DANUBIA soil model, but with a direct bearing on simulated crop growth.

Model parameters

Third and last, deficiencies in the model parameters are addressed. The DANUBIA crop growth model utilizes a number of crop-specific parameters. These are tabulated in chapter 2.4. Parameters of low reliability, genotype-specific parameters as well as parameters that are probably related to genotype-specific differences are marked according to YIN & VAN LAAR (2005). Simulating the various cultivars of a crop individually would improve the model results. The object-oriented model structure can be easily expanded to include a variety of different cultivars. However, information on the cultivar planted and the corresponding values of the genotype-specific parameters are prerequisites for this elaboration. So far, genotype-specific parameters are not easily accessible.

Generally, uncertainties in model results due to imperfect parameterization can be reduced by conducting experiments in controlled environments (e.g. for assessing

photoperiod sensitivity as described by YIN *et al.*, 2005), by making use of advances in molecular biology and functional genomics (MCMASTER 2005) and by performing comprehensive sensitivity and uncertainty analyses. An overview of the various methods for sensitivity and uncertainty analyses is for example presented by MONOD *et al.* (2006).

For application on the regional scale, the parameters plant density and sowing depth should work not with average values but with such as are specific to the region. Since these parameters affect the model results in a non-linear way, values spanning the extremes of a range of data instead of mean values should be used to capture the spatial variability of cultivation practices. The ranges of values are given in Appendix D.

The author of this study applied crop-specific leaf photosynthesis parameters derived from gas exchange measurements. Here uncertainties may also arise. The procedure and results of deriving the parameters is presented in chapter 2.4.2. To obtain reliable results many more data-sets need to be acquired. To derive the activation energy for J_{max} (E_{Jmax}) with precision, gas exchange data measured at various temperatures are needed. In addition to too few measurements, another source of error affecting comparability of measured and modelled data is the value chosen to represent the photosynthetically active leaf nitrogen content. This parameter is essential in modelling the rate of photosynthesis. Ideally this value should be derived from the nitrogen content of the single leaf or even only of the small leaf area which was positioned inside the leaf cuvette of the gas analyzer system.

5 Conclusions

It was the goal of this study to present the DANUBIA crop growth model as a powerful instrument for investigating the response of agro-ecosystems to Global Change effects. The model efficiently simulates the development and growth of a range of crops under various environmental conditions and with different farming practices, as is proved in the validation analysis. The intricate responsiveness of the model to Global Change effects is confirmed by examining its reactions to rising air temperatures and atmospheric carbon dioxide concentrations.

Both the results of the validation analysis and the application to Global Change effects affirm the need for the ecohydrological modelling approach realized in the model. The interplay of water, carbon and nitrogen fluxes in the soil-plant-atmosphere system as well as feedback mechanisms between physiological processes are well captured by the model. This ability qualifies the model to adequately simulate the processes of transpiration, photosynthesis, respiration, root growth, water and nitrogen uptake as well as carbon and nitrogen allocation. Therefore, the model allows a numerical rating of water demand, carbon assimilation, nitrogen absorption and biomass production of crops from sowing up to harvesting.

In simulating water demand, the impact of crops on the water balance in a chosen region is quantified. Although transpiration constitutes a large share of the water fluxes at the landsurface, information on spatial patterns of transpiration is very sparse. In general, evaporation and transpiration are considered as one, although the ratio between the two is a highly fluctuating one in view of the complex interactions between the atmosphere, soil and plants. Through its ability to place numerical measures on transpiration alone, the crop growth model offers promising opportunities.

In the case of crops, not only the total amount but also the temporal distribution of transpiration is influenced by the choice of crop and cultivation practices. This opens the way to adaptive management strategies in order to mitigate the negative impacts of Global Change on agro-ecosystems. In a wider context, the employment of the crop growth model in an integrated simulation system like the Global Change decision support system DANUBIA is indispensable when investigating integrative strategies to secure a sustainable water use in the examined area. Here the simulation of agricultural yield is also of key relevance as a determinant for future land use changes

affecting water, carbon and nitrogen fluxes. Having proved its suitability to model yields of the various crops, the DANUBIA crop growth model is well able to exercise this function.

WEIGEL (2005) states that for Germany´s variegated agricultural regions so far hardly any systematic studies have been carried out which deal with the anticipated effects of planetary warming. Here is scope for the process-based crop growth model, being as it is not bound to any one particular region. Furthermore, it can be extended to include additional crops.

It may be repeated here that process-based modelling is the only method for comprehensively assessing the effects of global climate change on crop growth. LONG *et al.* (2006) point out that in most models so far used the magnitude of CO_2 fertilization factors is for the most part based on data from three literature reviews from the 1980s. The reviews in question refer to experimental data from enclosure studies (e.g. controlled environmental or open-top chambers). It is for this reason that LONG *et al.* (2006) criticize the use of these data and emphasize the advantages of FACE (free-air CO_2 enrichment) experiments. They conclude that "much lower CO_2 fertilization factors should be used in model projections" and state that interactive effects should be examined through more elaborate experiments.

Although there can be no doubt that experiments are essential for research, it is hard to imagine how "CO_2 fertilization factors" derived from experiments could possibly represent the impact of a changing environment with its multitude of interacting and interrelated processes. It is here that state-of-the-art models like the DANUBIA crop growth model provide solutions and answers to many problems confronting present-day research.

6 Future challenges

The challenges posed by Global Change are many in number. Before efforts in the direction of responsible stewardship for natural resources can be undertaken, it is necessary to gauge the potential impacts. This is where models like the DANUBIA crop growth model offer promising approaches. In the following, aspects considered in the present study will be broadened by giving a few examples of how the scope of the DANUBIA crop growth model can be appropriately expanded.

Considering that photosynthesis is the only natural process that sequesters a vast amount of carbon dioxide from the atmosphere (CENTRITTO & LORETO 2005), the significance of agro-ecosystems as carbon sinks is of special relevance today. Carbon fixed by crops enters the soil in form of plant residues, therefore potentially mitigating the rise in atmospheric carbon dioxide concentration (PRIOR *et al.* 2005). Carbon storage in the soil is favoured by certain cultivation practices like permanent cropping, reduced tillage and soil improvements (e.g. DESJARDINS *et al.* 2005, GRANT *et al.* 2001). Investigation of effective managerial options in order to maximize long-term soil carbon sequestration in agro-ecosystems is imperative. Here, the role of scientists as advisors to policy makers is highlighted, since this carbon sink can compensate for greenhouse gas emissions as set forth in the *Kyoto Protocol* (UNITED NATIONS 1998). By enabling a numerical rating of photosynthesis, the DANUBIA crop growth model can make a valuable contribution to efforts aimed at promoting soil carbon sequestration. In this context, the dynamic simulation of carbon allocation to shoot and root is of key importance, since carbon allocated to roots usually remains in the soil after harvesting, directly augmenting soil organic matter.

One aspect that in future may be added to the crop growth model is response to ozone. Global Change is characterized by rising concentrations of surface ozone. Like carbon dioxide, ozone is absorbed by the stomata. Ozone is toxic to plants at concentrations as low as 30 ppb. So far, the effects of the interaction of carbon dioxide and ozone on crops have not been adequately defined. (LONG *et al.* 2006, WEIGEL 2005)

However, upcoming results of studies will enable ozone and its impacts to be included in crop growth models.

Among the many factors influencing crop growth are also plant diseases and pests. The agents of these (insects, bacteria, fungi, etc.) are also affected by environmental changes and the complex interactions between these biotic factors and crops within

agro-ecosystems need to be considered when assessing the potential impacts of Global Change (WEIGEL 2005). The crop growth model can be dynamically coupled to a model simulating the biotic factors in agro-ecosystems. Based on the results of coupled simulations, adaptive management strategies can be developed to minimize the risk of crop failure and use of pesticides, thus contributing to the sustainable use of environmental resources.

Finally, the forthcoming challenge of interactively coupling crop growth models and climate models is pointed out.

Present-day studies of climate impacts on crops ignore the influence of growing crops on the atmosphere. For example, transpiration influences boundary layer humidity and the energy available for convection. So far, crops in climate models are typically represented by natural grasslands. Therefore, the seasonal development of crops as a key determinant for the temporal and spatial patterns of surface fluxes is disregarded. A coupled crop and climate model will offer the possibility to investigate mutual interactions between crops and climate change. (OSBORNE *et al.* 2007)

Here, the particular challenge that needs to be faced is how the different spatial scales of the crop and climate model can be made compatible with each other. In order to comprehensively capture Global Change effects, the crop model ideally operates on the regional scale, whereas climate models operate on larger spatial scales.

The mentioned examples underline the fact that a concerted effort of cross-boundary research is mandatory if the emerging challenges are to be efficiently tackled. With the world awakened to the threat of Global Change, advances in our understanding of the nature, magnitude and direction of future changes are more than ever required to mitigate and anticipate potential impacts.

7 References

ACOCK, B. & V.R. REDDY (1997): Designing an object-oriented structure for crop models. *Ecological Modelling* **94**, 33-44.

ADAMS, S.R., PEARSON, S. & P. HADLEY (2001): Improving quantitative flowering models through a better understanding of the phases of photoperiod sensitivity. *Journal of Experimental Botany* **52**, 655-662.

ALEXANDROV, V., EITZINGER, J., CAJIC, V. & M. OBERFORSTER (2002): Potential impact of climate change on selected agricultural crops in north-eastern Austria. *Global Change Biology* **8**, 372-389.

AMTHOR, J.S. (2000): The McCree - de Wit - Penning de Vries - Thornley respiration paradigms: 30 years later. *Annals of Botany* **86**, 1-20.

ANTEN, N.P.R. (1997): Modelling canopy photosynthesis using parameters determined from simple non-destructive measurements. *Ecological Research* **12**, 77-88.

BARTH, M., HENNICKER, R., KRAUS, A. & M. LUDWIG (2004): DANUBIA: An Integrative Simulation System for Global Change Research in the Upper Danube Basin. *Cybernetics and Systems* **35**, 639-666.

BAUMER, M. (1998): Getreidebau - Gerste. In: *Die Landwirtschaft. Band 1: Pflanzliche Erzeugung.* (Eds Munzert, M. & H. Hüffmeier), p. 286-308. BLV Verlagsgesellschaft München, Landwirtschaftsverlag Münster-Hiltrup, 11th edition, München.

BAUMGÄRTEL, G. & H.-C. SCHARPF (2002): Gute fachliche Praxis der Stickstoffdüngung, aid infodienst Verbraucherschutz, Ernährung, Landwirtschaft e.V., 9th edition, Bonn, 76 p.

BAUMGARTNER, A. & H.-J. LIEBSCHER (1996): Lehrbuch der Hydrologie, Band 1, Allgemeine Hydrologie - Quantitative Hydrologie. Gebrüder Borntraeger, 2nd edition, Berlin - Stuttgart, 694 p.

BAVARIAN MINISTRY OF AGRICULTURE AND FORESTRY (ed.) (2006): Bayerischer Agrarbericht 2006. München.

BERNACCHI, C.J., SINGSAAS, E.L., PIMENTEL, C., PORTIS JR, A.R. & S.P. LONG (2001): Improved temperature response functions for models of Rubisco-limited photosynthesis. *Plant, Cell and Environment* **24**, 253-259.

BERNACCHI, C.J., PIMENTEL, C. & S.P. LONG (2003): In vivo temperature response functions of parameters required to model RuBP-limited photosynthesis. *Plant, Cell and Environment* **26**, 1419-1430.

BLOOM, A.J. (2006): Rising carbon dioxide concentrations and the future of crop production. *Journal of the Science of Food and Agriculture* **86**, 1289-1291.

BOOCH, G., RUMBAUGH, J., & I. JACOBSON (1999): The Unified Modeling Language user guide. Addison-Wesley, Reading, MA, 482 p.

BRÉDA, N.J.J. (2003): Ground-based methods of leaf area index measurements: a review of methods, instruments and current controversies. *Journal of Experimental Botany* **54**, 2403-2417.

BRISSON, N., GARY, C., JUSTES, E., ROCHE, R., MARY, B., RIPOCHE, D., ZIMMER, D., SIERRA, J., BERTUZZI, P., BURGER, P., BUSSIERE, F., CABIDOCHE, Y.M., CELLIER, P., DEBAEKE, P., GAUDILLERE, J.P., HENAULT, C., MARAUX, F., SEGUIN, B. & H. SINOQUET (2003): An overview of the model STICS. *European Journal of Agronomy* **18**, 309-332.

BROOKING, I.R. (1996): Temperature response of vernalization in wheat: A developmental analysis. *Annals of Botany* **78**, 507-512.

BROUWER, R. (1962): Nutritive influences on the distribution of dry matter in the plant. *Netherlands Journal of Agricultural Sciences* **10**, 361-376.

CANNELL, M.G.R. & J.H.M. THORNLEY (2000): Modelling the components of plant respiration: Some guiding principles. *Annals of Botany* **85,** 45-54.

CENTRITTO, M. & F. LORETO (2005): Photosynthesis in a changing world: photosynthesis and abiotic stresses. *Agriculture, Ecosystems and Environment* **106**, 115-117.

DADHWAL, V.K. (2004): Crop growth and productivity monitoring and simulation using remote sensing and GIS. In: *Proceedings of the Training Workshop, July 7-11, 2003, Dehra Dun, India.* (Eds Sivakumar, M.V.K., Roy, P.S., Harmsen, K. & S.K. Saha), p. 263-289. World Meteorological Organization, Geneva.

DE PURY, D.G.G. & G.D. FARQUHAR (1997): Simple scaling of photosynthesis from leaves to canopy without the errors of big-leaf models. *Plant, Cell and Environment* **20**, 537-557.

DELTA-T DEVICES LTD (1999): Sunshine Sensor, Type BF2, User Manual Version 1.0b, Cambridge, United Kingdom.

DESJARDINS, R.L., SMITH, W., GRANT, B., CAMPBELL, C. & R. RIZNEK (2005): Management strategies to sequester carbon in agricultural soils and to mitigate greenhouse gas emissions. *Climatic change* **70**, 283-297.

DLG (DEUTSCHE-LANDWIRTSCHAFTS-GESELLSCHAFT) (ed.) (1987): Pflichtenheft für die Datenverarbeitung in der Pflanzenproduktion. Expertenwissen für Landwirte, Berater und Programmierer. DLG-Verlag, Frankfurt am Main, 307 p.

DWD (DEUTSCHER WETTERDIENST) (2007): Klimadaten ausgewählter deutscher Stationen. (14.03.2007) <http://www.dwd.de/de/FundE/Klima/KLIS/daten/online/>

EDER, J. (1998): Getreidebau - Mais. In: *Die Landwirtschaft. Band 1: Pflanzliche Erzeugung.* (Eds Munzert, M. & H. Hüffmeier), p. 322-348. BLV Verlagsgesellschaft München, Landwirtschaftsverlag Münster-Hiltrup, 11th edition, München.

FALGE, E.M. (1997): Die Modellierung der Kronendachtranspiration von Fichtenbeständen (Picea abies (L.) KARST.). *PhD thesis,* Bayreuther Forum Ökologie **48**, Bayreuth, 221 p.

FARQUHAR, G.D., VON CAEMMERER, S. & J.A. BERRY (1980): A biochemical model of photosynthetic CO_2 assimilation in leaves of C_3 species. *Planta* **149**, 78-90.

FEDERAL MINISTRY FOR ENVIRONMENT, NATURE CONSERVATION AND NUCLEAR SAFETY (2000) (ed.): Hydrologischer Atlas von Deutschland. Freiburger Verlagsdienste GmbH, Bonn - Berlin.

FLEISHER, D.H., SHILLITO, R.M., TIMLIN, D.J., KIM, S.-H. & V.R. REDDY (2006): Approaches to modeling potato leaf appearance rate. *Agronomy Journal* **98**, 522-528.

FORRESTER, J.W. (1961): *Industrial Dynamics*. MIT Press, Waltham, Massachusetts, 464 p.

FRIEND, A.D. (1995): PGEN: An integrated model of leaf photosynthesis, transpiration, and conductance. *Ecological Modelling* **77**, 233-255.

FRIEND, A.D., STEVENS, A.K., KNOX, R.G. & M.G.R. CANNELL (1997): A process-based, terrestrial biosphere model of ecosystem dynamics (Hybrid v3.0). *Ecological Modelling* **95**, 249-287.

GARCIA-QUIJANO, J.F. & A.P. BARROS (2005): Incorporating canopy physiology into a hydrological model: photosynthesis, dynamic respiration, and stomatal sensitivity. *Ecological Modelling* **185**, 29-49.

GASTAL, F. & G. LEMAIRE (2002): N uptake and distribution in crops: an agronomical and ecophysiological perspective. *Journal of Experimental Botany* **53**, 789-799.

GAYLER, S., WANG, E., PRIESACK, E., SCHAAF, T. & F.-X. MAIDL (2002): Modeling biomass growth, N-uptake and phenological development of potato crop. *Geoderma* **105**, 367-383.

GERWITZ, A. & E.R. PAGE (1974): An empirical mathematical model to describe plant root systems. *Journal of Applied Ecology* **11**, 773-781.

GODWIN, D.C. & U. SINGH (1998): Nitrogen balance and crop response to nitrogen in upland and lowland cropping systems. In: *Understanding Options for Agricultural Production* (Eds Tsuji, G.J., Hoogenboom, G. & P.K. Thornton), p. 55-77. Kluwer Academic Publishers, Dordrecht.

GOUDRIAAN, J. (1977): Crop micrometeorology: a simulation study. Simulation Monographs, Pudoc, Wageningen, 257 p.

GOUDRIAAN, J. (1988): The bare bones of leaf-angle distribution in radiation models for canopy photosynthesis and energy exchange. *Agricultural and Forest Meteorology* **43**, 155-169.

GOUDRIAAN, J. & H.H. VAN LAAR (1994): Modelling potential crop growth processes. Kluwer Academic Publishers, Dordrecht, 238 p.

GRANT, R.F. (1995): Dynamics of energy, water, carbon and nitrogen in agricultural ecosystems: simulation and experimental validation. *Ecological Modelling* **81**, 169-181.

GRANT, R.F. (2001): A review of the Canadian ecosystem model ecosys. In: *Modeling Carbon and Nitrogen Dynamics for Soil Management* (Ed. Shaffer, M.), p. 173-264. CRC Press, Boca Raton, Florida.

GRANT, R.F., JUMA, N.G., ROBERTSON, J.A., IZAURRALDE, R.C. & W.B. MCGILL (2001): Long-term changes in soil carbon under different fertilizer, manure, and rotation: Testing the mathematical model *ecosys* with data from the Breton Plots. *Soil Science Society of America Journal* **65**, 205-214.

GRANT, R.F., KIMBALL, B.A., WALL, G.W., TRIGGS, J.M., BROOKS, T.J., PINTER JR, P.J., CONLEY, M.M., OTTMAN, M.J., LAMORTE, R.L., LEAVITT, S.W., THOMPSON, T.L. & A.D. MATTHIAS (2004): Modeling elevated carbon dioxide effects on water relations, water use, and growth of irrigated sorghum. *Agronomy Journal* **69**, 1693-1705.

GUÉRIF, M. & C.L. DUKE (2000): Adjustment procedures of a crop model to the site specific characteristics of soil and crop using remote sensing data assimilation. *Agriculture, Ecosystems and Environment* **81**, 57-69.

HAN, T., WU, C., MENTREDDY, R.S., ZHAO, J., XU, X. & J. GAI (2005) : Post-flowering photoperiod effects on reproductive development and agronomic traits of long-day and short-day crops. *Journal of Agronomy & Crop Science* **191**, 255-262.

HARLEY, P.C., THOMAS, R.B., REYNOLDS, J.F. & B.R. STRAIN (1992): Modelling photosynthesis of cotton grown in elevated CO_2. *Plant, Cell and Environment* **15**, 271-282.

HEGE, U. (1998): Pflanzenernährung und Düngung. In: *Die Landwirtschaft. Band 1: Pflanzliche Erzeugung*. (Eds Munzert, M. & H. Hüffmeier), p. 107-186. BLV Verlagsgesellschaft München, Landwirtschaftsverlag Münster-Hiltrup, 11th edition, München.

HEPTING, L. (1998): Hackfruchtbau - Kartoffeln. In: *Die Landwirtschaft. Band 1: Pflanzliche Erzeugung*. (Eds Munzert, M. & H. Hüffmeier), p. 349-377. BLV Verlagsgesellschaft München, Landwirtschaftsverlag Münster-Hiltrup, 11th edition, München.

HILBERT, D.W. (1990): Optimization of plant root:shoot ratios and internal nitrogen concentration. *Annals of Botany* **66**, 91-99.

HODGES, T. (1997): The SIMPOTATO growth simulation model. Version 1.60. Programmer´s manual. USDA-ARS, Prosser, Washington.

HODGES, T. & J.T. RITCHIE (1991): The CERES-Wheat phenology model. In: *Predicting crop phenology* (Ed. Hodges, T.), p. 133-141. CRC Press, Boston.

HODGES, T., JOHNSON, S.L. & B.S. JOHNSON (1992): A modular structure for crop simulation models: implemented in the SIMPOTATO model. *Agronomy Journal* **84**, 911-915.

HOOGENBOOM, G. (2000): Contribution of agrometeorology to the simulation of crop production and its applications. *Agricultural and Forest Meteorology* **103**, 137-157.

HOOGENBOOM, G., JONES, J.W., PORTER, C.H., BOOTE, K.J., BATCHELOR, W.D., HUNT, L.A., GIJSMAN, A.J., WILKENS, P.W., SINGH, U. & W.T. BOWEN (2003): DSSAT v4, Cropping System Simulation Model. In: *Decision Support System for Agrotechnology Transfer Version 4.0. Volume 1: Overview.* (Eds Hoogenboom, G., Jones, J.W., Porter, C.H., Wilkens, P.W., Boote, K.J., Batchelor, W.D., Hunt, L.A. & G.Y. Tsuji), p. 9-60. University of Hawaii, Honolulu, Hawaii.

HUMPHRIES, S.W. & S.P. LONG (1995): WIMOVAC: a software package for modelling the dynamics of plant leaf and canopy photosynthesis. *Computer Applications in the Biosciences* **11**, 361-371.

IPCC (INTERGOVERNMENTAL PANEL ON CLIMATE CHANGE) (2007): Climate Change 2007: The Physical Science Basis. Summary for Policymakers. Contribution of Working Group I to the Fourth Assessment Report of the IPCC. (11.03.2007) <http://www.ipcc.ch>

JAME, Y.W. & H.W. CUTFORTH (1996): Crop growth models for decision support systems. *Canadian Journal of Plant Science* **76**, 9-19.

JAME, Y.W., CUTFORTH, H.W. & J.T. RITCHIE (1998): Interaction of temperature and daylength on leaf appearance rate in wheat and barley. *Agricultural and Forest Meteorology* **92**, 241-249.

JAME, Y.W. & H.W. CUTFORTH (2004): Simulating the effects of temperature and seeding depth on germination and emergence of spring wheat. *Agricultural and Forest Meteorology* **124**, 207-218.

JARA, J. & C.O. STOCKLE (1999): Simulation of water uptake in maize, using different levels of process detail. *Agronomy Journal* **91**, 256-265.

JONES, C.A. & J.R. KINIRY (eds) (1986): CERES-Maize. A simulation model of maize growth and development. Texas A&M University Press, College Station, Texas, 194 p.

JONES, J.W., HOOGENBOOM, G., PORTER, C.H., BOOTE, K.J., BATCHLOR, W.D., HUNT, L.A., WILKENS, P.W., SINGH, U., GIJSMAN, A.J. & J.T. RITCHIE (2003): The DSSAT cropping system model. *European Journal of Agronomy* **18**, 235-265.

JONES, J.W., MAKOWSKI, D. & D. WALLACH (2006): Introduction to Section II. In: *Working with dynamic crop models.* (Eds Wallach, D., Makowski, D. & J.W. Jones), p. 251-256. Elsevier, Amsterdam.

JONGSCHAAP, R. E. E. (2006): Run-time calibration of simulation models by integrating remote sensing estimates of leaf area index and canopy nitrogen. *European Journal of Agronomy* **24**, 316-324.

KEATING, B.A., CARBERRY, P.S., HAMMER. G.L., PROBERT, M.E., ROBERTSON, M.J., HOLZWORTH, D., HUTH, N.I., HARGREAVES, J.N.G., MEINKE, H., HOCHMAN, Z., MCLEAN, G., VERBURG, K., SNOW, V., DIMES, J.P., SILBURN, M., WANG, E., BROWN, S., BRISTOW, K.L., ASSENG, S., CHAPMAN, S., MCCOWN, R.L., FREEBAIRN, D.M. & C.J. SMITH (2003): An overview of APSIM, a model designed for farming systems simulation. *European Journal of Agronomy* **18**, 267-288.

KENTER, C. (2003): Ertragsbildung von Zuckerrüben in Abhängigkeit von der Witterung. *PhD thesis*, Georg-August-University Göttingen, Cuvillier, Göttingen, 98 p.

KENTER, C., HOFFMANN, C. M. & B. MÄRLÄNDER (2006): Effects of weather variables on sugar beet yield development (*Beta vulgaris* L.). *European Journal of Agronomy* **24**, 62-69.

KERSEBAUM, K.C. (1995): Application of a simple management model to simulate water and nitrogen dynamics. *Ecological Modelling* **81**, 145-156.

KIM, S.H., REDDY V.R. & D.J. TIMLIN (2004): Modeling maize phenology as a function of temperature and photoperiod using nonlinear rate equations [abstract]. In: *Biological Systems Simulation Conference, March 8-10, 2004, Gainesville, Florida,* p. 45.

KÖRBER-GROHNE, U. (1987): Nutzpflanzen in Deutschland. Kulturgeschichte und Biologie. Konrad Theis Verlag, Stuttgart, 490 p.

KRIMLY T., WINTER T. & S. DABBERT (2004): Agrarökonomische Modellierung der Landnutzung im Einzugsgebiet der Oberen Donau zur Integration in das interdisziplinäre Entscheidungsunterstützungssystem DANUBIA. In: *Perspektiven in der Landnutzung - Regionen, Landschaften, Betriebe - Entscheidungsträger und Instrumente.* (Eds Dabbert, S., Grosskopf, W., Heidhues, F. & J. Zeddies), Schriften der Gesellschaft für Wirtschafts- und Sozialwissenschaften des Landbaues e.V., Band **39**, p. 191-199. Landwirtschaftsverlag, Münster-Hiltrup.

KRYSANOVA, V., MÜLLER-WOHLFEIL, D.I. & A. BECKER (1998): Development and test of a spatially distributed hydrological/water quality model for mesoscale watersheds. *Ecological Modelling* **106**, 261-289.

KRYSANOVA, V., WECHSUNG, F., ARNOLD, J., SRINIVASAN, R. & J. WILLIAMS (2000): PIK Report Nr. 69 *SWIM (Soil and Water Integrated Model), User Manual*. Potsdam Institute for Climate Impact Research, Potsdam, 239 p.

KRYSANOVA, V., HATTERMANN, F. & F. WECHSUNG (2007): Implications of complexity and uncertainty for integrated modelling and impact assessment in river basins. *Environmental Modelling & Software* **22**, 701-709.

KTBL (KURATORIUM FÜR TECHNIK UND BAUWESEN IN DER LANDWIRTSCHAFT) (ed.) (2002): Taschenbuch Landwirtschaft. Daten für betriebliche Kalkulationen in der Landwirtschaft. Landwirtschaftsverlag GmbH, 21st edition, Münster, 280 p.

KTBL (KURATORIUM FÜR TECHNIK UND BAUWESEN IN DER LANDWIRTSCHAFT) (ed.) (2005): Faustzahlen für die Landwirtschaft. Deutscher Landwirtschaftsverlag, 13th edition, Darmstadt, 1095 p.

LAI, C.-T & G. KATUL (2000) : The dynamic role of root-water uptake in coupling potential to actual transpiration. *Advances in Water Resources* **23**, 427-439.

LAUNAY, M. & M. GUERIF (2005): Assimilating remote sensing data into a crop model to improve predictive performance for spatial applications. *Agriculture, Ecosystems & Environment* **111**, 321-339.

LEUNING, R. (1995): A critical appraisal of a combined stomatal-photosynthesis model for C_3 plants. *Plant, Cell and Environment* **18**, 339-355.

LEUNING, R. (2002): Temperature dependence of two parameters in a photosynthesis model. *Plant, Cell and Environment* **25**, 1205-1210.

LEUNING, R., KELLIHER, F.M., DE PURY, D.G.G. & E-D. SCHULZE (1995): Leaf nitrogen, photosynthesis, conductance and transpiration: scaling from leaves to canopies. *Plant, Cell and Environment* **18**, 1183-1200.

LEVIEL, B. (2000): Evaluation of risks and monitoring of nitrogen fluxes at the crop level on the Romanian and Bulgarian plain. Application to maize, wheat, rapeseed and sugar beet. *PhD thesis*, Institut National Polytechnique de Toulouse, Toulouse, France, 312 p.

LEVIEL, B., CRIVINEANU, C. & B. GABRIELLE (2003): CERES-BEET, a prediction model for sugar beet yield and environmental impact. In: *Sugar beet growth and growth modelling. Advances in sugar beet research, vol. 5,* p. 143-152. Institut International de Recherches Betteravières (IIRB), Brussels.

LI, K.Y., DE JONG, R. & J.B. BOISVERT (2001): Comparison of root-water-uptake models. In: *Sustaining the Global Farm - Selected papers from the 10th International Soil Conservation Meeting, May 24-29, 1999, West Lafayette.* (Eds Stott, D.E., Mohtar, R.H. & G.C. Steinhardt), p. 1112-1117. International Soil Conservation Organization in cooperation with the USDA and Purdue University, West Lafayette, Indiana.

LONG, S.P. & C.J. BERNACCHI (2003): Gas exchange measurements, what can they tell us about the underlying limitations to photosynthesis? Procedures and sources of error. *Journal of Experimental Botany* **54**, 2393-2401.

LONG, S.P., AINSWORTH, E.A., LEAKEY, A.D.B., NÖSBERGER, J. & D.R. ORT (2006): Food for thought: lower-than-expected crop yield stimulation with rising CO_2 concentrations. *Science* **312**, 1918-1921.

LUCHT, W., SCHAPHOFF, S., ERBRECHT, T., HEYDER, U. & CRAMER, W. (2006): Terrestrial vegetation redistribution and carbon balance under climate change. *Carbon Balance and Management* **1,** 6.

LUDWIG, M. (2007): Modellierung und Architektur eines integrativen Umwelt-simulationssystems. *PhD thesis*, Ludwig-Maximilians-University Munich (in preparation).

LUDWIG, R., MAUSER, W., NIEMEYER, S., COLGAN, A., STOLZ, R., ESCHER-VETTER, H., KUHN, M., REICHSTEIN, M., TENHUNEN, J., KRAUS, A., LUDWIG, M., BARTH, M., & R. HENNICKER (2003): Web-based modelling of energy, water and matter fluxes to support decision making in mesoscale catchments – the integrative perspective of GLOWA-Danube. *Physics and Chemistry of the Earth* **28**, 621–634.

MACKERRON, D.K.L. (2004): What is necessary and what is sufficient? Cases drawn from some of the DSS described in this book. In: *Decision support systems in potato production.* (Eds MacKerron, D.K.L. & A.J. Haverkort), p. 217-223. Wageningen Academic Publishers, Wageningen.

MÄRLÄNDER, B., HOFFMANN, C., KOCH, H.-J., LADEWIG, E., MERKES, R., PETERSEN, J. & N. STOCKFISCH (2003): Environmental situation and yield performance of the sugar beet crop in Germany: Heading for sustainable development. *Journal of Agronomy & Crop Science* **189**, 201-226.

MATTHEWS, R. & W. STEPHENS (2002): Concluding remarks. In: *Crop-soil simulation models. Applications in developing countries.* (Eds Matthews, R.B. & W. Stephens), p. 231-234. CABI Publishing, Wallingford, UK.

MAUSER, W. & LUDWIG, R. (2002): GLOWA-Danube: A research concept to develop integrative techniques, scenarios and strategies regarding global changes of the water cycle. In: *Climatic Change: Implications for the hydrological cycle and for water management. Advances in Global Change Research 10* (Ed. Beniston, M.), p. 171-188. Kluwer Academic Publishers, Dordrecht.

MCMASTER, G.S. & W.W. WILHELM (1997): Growing degree-days: one equation, two interpretations. *Agricultural and Forest Meteorology* **87**, 291-300.

MCMASTER, G.S. (2005): Phytomers, phyllochrons, phenology and temperate cereal development. *The Journal of Agricultural Science* **143**, 137-150.

MCMASTER, G.S., WILHELM, W.W. & A.B. FRANK (2005): Developmental sequences for simulating crop phenology for water-limiting conditions. *Australian Journal of Agricultural Research* **56**, 1277-1288.

MCVOY, C.W., KERSEBAUM, K.C., ARNING, M., KLEEBERG, P., OTHMER, H. & U. SCHRÖDER (1995): A data set from north Germany for the validation of agroecosystem models: documentation and evaluation. *Ecological Modelling* **81**, 265-300.

MEDLYN, B.E., DREYER, E., ELLSWORTH, D., FORSTREUTER, M., HARLEY, P.C., KIRSCHBAUM, M.U.F., LE ROUX, X., MONTPIED, P., STRASSEMEYER, J., WALCROFT, A., WANG, K. & D. LOUSTAU (2002): Temperature response of parameters of a biochemically based model of photosynthesis. II. A review of experimental data. *Plant, Cell and Environment* **25**, 1167-1179.

MEIER, U. (ed.) (2001): *Growth stages of mono- and dicotyledonous plants*. BBCH Monograph. German Federal Biological Research Centre for Agriculture and Forestry, 2nd edition, Braunschweig - Berlin, 158 p.

MIRSCHEL, W., WENKEL, K.-O., SCHULTZ, A., POMMERENING, J. & G. VERCH (2005): Dynamic phenological model for winter rye and winter barley. *European Journal of Agronomy* **23**, 123-135.

MONOD, H., NAUD, C. & D. MAKOWSKI (2006): Uncertainty and sensitivity analysis for crop models. In: *Working with dynamic crop models.* (Eds Wallach, D., Makowski, D. & J.W. Jones), p. 55-99. Elsevier, Amsterdam.

MONTEITH, J.L. (1973): Principles of environmental physics. Edward Arnold, London, 241 p.

MORISON, J.I.L. & R.M. GIFFORD (1983): Stomatal sensitivity to carbon dioxide and humidity. *Plant Physiology* **71**, 789-796.

MÖSER, W. & E. RASCHKE (1983): Mapping of global radiation and of cloudiness from METEOSAT image data. *Meteorologische Rundschau* **36**, 33-41.

NEWMAN, B.D., WILCOX, B.P., ARCHER, S.R., BRESHEARS, D.D., DAHM, C.N., DUFFY, C.J., MCDOWELL, N.G., PHILLIPS, F.M., SCANLON, B.R. & E.R. VIVONI (2006): Ecohydrology of water-limited environments: A scientific vision. *Water Resources Research* **42**, W06302.

NOBEL, P.S. (2005): Physiochemical and environmental plant physiology. Elsevier Academic Press, 3rd edition, Burlington, MA, 567 p.

OEHMICHEN, J. (1986): Pflanzenproduktion, Band 2: Produktionstechnik. Paul Parey, Berlin-Hamburg, 607 p.

OLESEN, J., JENSEN, T. & J. PETERSEN (2000): Sensitivity of field-scale winter wheat production in Denmark to climate variability and climate change. *Climate Research* **15**, 221-238.

OSBORNE, T.M., LAWRENCE, D.M., CHALLINOR, A.J., SLINGO, J.M. & T.R. WHEELER (2007): Development and assessment of a coupled crop-climate model. *Global Change Biology* **13**, 169-183.

PAPAJORGJI, P., BECK, H.W. & J.L. BRAGA (2004): An architecture for developing service-oriented and component-based environmental models. *Ecological Modelling* **179**, 61-76.

PARSONS, R., WEYERS, T. LAWSON, T. & I.M. GOBDER (1997): Rapid and straightforward estimates of photosynthetic characteristics using a portable gas exchange system. *Photosynthetica* **34**, 265-279.

PENNING DE VRIES, F.W.T., JANSEN, D.M., TEN BERGE H.F.M. & A. BAKEMA (1989): Simulation of ecophysiological processes of growth in several annual crops. International Rice Research Institute, Los Baños and Pudoc, Wageningen, 271 p.

POORTER, H. & O. NAGEL (2000): The role of biomass allocation in the growth response of plants to different levels of light, CO_2, nutrients and water: a quantitative review. *Australian Journal of Plant Physiology* **27**, 595-607.

POORTER, H. & M.-L. NAVAS (2003): Plant growth and competition at elevated CO_2: on winners, losers and functional groups. *New Phytologist* **157**, 175-198.

PORTER, J.R. & M. GAWITH (1999): Temperatures and the growth and development of wheat: a review. *European Journal of Agronomy* **10**, 23-36.

PP SYSTEMS (2003): CIRAS Photosynthesis Equations Manual, Version 1.21, *PP Systems*, Hitchin, Hertfordshire, UK.

PRIOR, S.A., RUNION, G.B., ROGERS, H.H., TORBERT, H.A. & D.W. REEVES (2005): Elevated atmospheric CO_2 effects on biomass production and soil carbon in conventional and conservation cropping systems. *Global Change Biology* **11**, 657-665.

QI, A., KENTER, C., HOFFMANN, C. & K.W. JAGGARD (2005): The Broom´s Barn sugar beet growth model and its adaptation to soils with varied available water content. *European Journal of Agronomy* **23**, 108-122.

RAJALA, A. & P. PELTONEN-SAINIO (2001): Plant growth regulator effects on spring cereal root and shoot growth. *Agronomy Journal* **93**, 936-943.

RAWLS, W.J., AHUJA, L.R., BRAKENSIEK, D.L. & A. SHIRMOHAMMADI (1993): Infiltration and soil water movement. In: *Handbook of hydrology*. (Ed. D.R. Maidment), 5.1-5.51, McGraw-Hill, Inc., New York.

RAWSON, H.M., ZAJAC, M. & L.D.J. PENROSE (1998): Effect of seedling temperature and its duration on development of wheat cultivars differing in vernalizing response. *Field Crops Research* **57**, 289-300.

REICHSTEIN, M. (2001): Drought effects on carbon and water exchange in three Mediterranean ecosytems. *PhD thesis,* Bayreuther Forum Ökologie **89**, Bayreuth, 150 p.

RENWICK, R.R. (1999): Evaluation of a crop simulation model for potatoes. *Master thesis,* University of Manitoba, Winnipeg, Canada, National Library of Canada, Ottawa, 125 p.

RIELAND, M. (2004): Das BMBF-Programm GLOWA: Instrumente für ein vorausschauendes Management großer Flusseinzugsgebiete. *Hydrologie und Wasserbewirtschaftung* **48**, 83-84.

RITCHIE, J.T. (1991): Wheat phasic development. In: *Modeling Plant and Soil Systems* (Eds R.J. Hanks & J.T. Ritchie), p. 31-54. ASA, CSSA, SSSA, Madison, Wisconsin.

RITCHIE, J.T. (1998): Soil water balance and plant water stress. In: *Understanding Options for Agricultural Production* (Eds Tsuji, G.J., Hoogenboom, G. & P.K. Thornton), p. 41-54. Kluwer Academic Publishers, Dordrecht.

RITCHIE, J.T. & D. GODWIN (2000): CERES Wheat 2.0. Documentation. (02.10.2006) <http://nowlin.css.msu.edu/wheat_book/>

SCHNEIDER, K. (1999): Gekoppelte, flächenverteilte Modellierung von Pflanzenwachstum und Verdunstung im Ammereinzugsgebiet mit dem prozeßorientierten Evapotranspirations- und Vegetationsmodell PROMET-V. *Habilitation thesis,* Department of Geography, Ludwig-Maximilians-University Munich, 263 p.

SCHNEIDER, K. (2003): Assimilating remote sensing data into a land-surface process model. *International Journal of Remote Sensing* **24**, 2959-2980.

SINCLAIR, T.R. & N.G. SELIGMAN (1996): Crop modeling: from infancy to maturity. *Agronomy Journal* **88**, 698-704.

SPITTERS, C.J.T. (1986): Separating the diffuse and direct component of global radiation and its implications for modeling canopy photosynthesis. Part II. Calculation of canopy photosynthesis. *Agricultural and Forest Meteorology* **38**, 231-242.

SPITTERS, C.J.T., TOUSSAINT, H.A.J.M. & J. GOUDRIAAN (1986): Separating the diffuse and direct component of global radiation and its implications for modeling canopy photosynthesis Part I. Components of incoming radiation. *Agricultural and Forest Meteorology* **38**, 217-229.

STEPHENS, W. & T. MIDDLETON (2002): Why has the uptake of decision support systems been so poor? In: *Crop-soil simulation models. Applications in developing countries.* (Eds Matthews, R.B. & W. Stephens), p. 129-147. CABI Publishing, Wallingford, UK.

STEWART, D.W., DWYER, L.M. & L.L. CARRIGAN (1998): Phenological temperature response of maize. *Agronomy Journal* **90**, 73-79.

STÖCKLE, C., DONATELLI, M. & R. NELSON (2003): CropSyst, a cropping systems simulation model. *European Journal of Agronomy* **18**, 289-307.

STOLZ, R. (1997): Die Verwendung der Fuzzy Logic Theorie zur wissensbasierten Klassifikation von Fernerkundungsdaten. *PhD thesis*, Münchener Geographische Abhandlungen, **B 26**, Munich, 177 p.

STRASSER, U. (1998): Regionalisierung des Wasserhaushalts mit einem SVAT-Modell am Beispiel des Weser-Einzugsgebiets. *PhD thesis*, Münchener Geographische Abhandlungen, **B 28**, Munich, 146 p.

STRECK, N.A., WEISS, A. & P. S. BAENZIGER (2003a): A generalized vernalization function for winter wheat. *Agronomy Journal* **95**, 155-159.

STRECK, N.A., WEISS, A., XUE, Q. & P. S. BAENZIGER (2003b): Improving predictions of developmental stages in winter wheat: a modified Wang and Engel model. *Agricultural and Forest Meteorology* **115**, 139-150.

THORNLEY, J.H.M. & M.G.R. CANNELL (2000): Modelling the components of plant respiration: representation and realism. *Annals of Botany* **85**, 55-67.

UNITED NATIONS (1998): Kyoto Protocol to the United Nations Framework Convention on Climate Change. United Nations Framework Convention on Climate Change: Kyoto Protocol. (03.04.2007) <http://unfccc.int/resource/docs/convkp/kpeng.pdf>

VAN ITTERSUM, M.K., LEFFELAAR, P.A., VAN KEULEN, H., KROPFF, M.J., BASTIAANS, L. & J. GOUDRIAAN (2003): On approaches and applications of the Wageningen crop models. *European Journal of Agronomy* **18**, 201-234.

VAN KEULEN, H., GOUDRIAAN, J., STROOSNIJDER, L., LANTINGA, E.A. & H.H. VAN LAAR (1997): Crop growth model for water-limited conditions (SUCROS2). In: *SUCROS97: Simulation of crop growth for potential and water-limited production situations - as applied to spring wheat.* Quantitative Approaches in Systems Analysis No. 14. (Eds van Laar, H.H., Goudriaan, J. & H. van Keulen), p. 21-53. C.T. de Wit Graduate School for Production Ecology, Wageningen.

VAN KRAALINGEN, D.W.G., RAPPOLDT, C. & H.H. VAN LAAR (2003): The FORTRAN simulation translator, a simulation language. *European Journal of Agronomy* **18**, 359-361.

VON CAEMMERER, S. (2000): Biochemical models of leaf photosynthesis. Techniques in Plant Sciences No. 2. CSIRO Publishing, Collingwood, Victoria, Australia, 165 p.

WALLACH, D. (2006): Evaluating crop models. In: *Working with dynamic crop models.* (Eds Wallach, D., Makowski, D. & J.W. Jones), p. 11-54. Elsevier, Amsterdam.

WANG, E. & T. ENGEL (1998): Simulation of phenological development of wheat crops. *Agricultural Systems* **58**, 1-24.

WANG, E. & T. ENGEL (2002): Simulation of growth, water and nitrogen uptake of a wheat crop using the SPASS model. *Environmental Modelling & Software* **17**, 387-402.

WANG, E. & C.J. SMITH (2004): Modelling the growth and water uptake function of plant root systems: a review. *Australian Journal of Agricultural Research* **55**, 501-523.

WANG, Q., MASATAKA, W. & OUYANG, Z. (2005): Simulation of water and carbon fluxes using BIOME-BGC model over crops in China. *Agricultural and Forest Meteorology* ***131*****,** 209-224.

WANG, Y.P. & R. LEUNING (1998): A two-leaf model for canopy conductance, photosynthesis and partitioning of available energy. I. Model description and comparison with a multi-layered model. *Agricultural and Forest Meteorology* **91**, 89-111.

WATANABE, F.D., EVANS, J.R. & W.S. CHOW (1994): Changes in the photosynthetic properties of Australian wheat cultivars over the last century. *Australian Journal of Plant Physiology* **21**, 169-183.

WEIGEL, H.J. (2005): Gesunde Pflanzen unter zukünftigem Klima. *Gesunde Pflanzen* **57**, 6-17.

WEILAND, R.T., STUTTE, C.A. & P.R.F. SILVA (1982): Nitrogen volatilization from plant foliage. Report series, No. 226, Agricultural Experiment Station, University of Arkansas, Fayetteville, Arkansas, 40 p.

WEIR, A.H., BRAGG, P.L., PORTER, J.R. & J.H. RAYNER (1984): A winter wheat crop simulation model without water or nutrient limitations. *Journal of Agricultural Science* **102**, 371-382.

WENKEL, K.-O. & W. MIRSCHEL (Eds) (1995): Agroökosystemmodellierung, Grundlage für die Abschätzung von Auswirkungen möglicher Landnutzungs- und Klimaänderungen. ZALF-Bericht 24. ZALF, Müncheberg, Germany.

WESSOLEK, G. & S. ASSENG (2006): Trade-off between wheat yield and drainage under current and climate change conditions in northeast Germany. *European Journal of Agronomy* **24**, 333-342.

WHITE, A., CANNELL, M.G.R. & A.D. FRIEND (1999): Climate change impacts on ecosystems and the terrestrial carbon sink: a new assessment - challenges for the future. *Global Environmental Change* **9**, 21-30.

WHITE, M.A., THORNTON, P.E., RUNNING, S.W. & R.R. NEMANI (2000): Parameterization and Sensitivity Analysis of the BIOME–BGC Terrestrial Ecosystem Model: Net Primary Production Controls. *Earth Interactions* **4**, 1-85.

WILKENS, P. & U. SINGH (2003): A code-level analysis for temperature effects in the CERES models. In: *Modeling Temperature Response in Wheat and Maize: Proceedings of a Workshop, CIMMYT, El Batán, Mexico, 23-25 April 2001* (Ed. J.W. White), p. 1-7. NRG-GIS Series 03-01. CIMMYT (International Maize and Wheat Improvement Center), Mexico.

WILLMOTT, C.J. (1981): On the validation of models. *Physical Geography* **2**, 184-194.

WILLMOTT, C.J. (1982): Some comments on the evaluation of model performance. *Bulletin of the American Meteorological Society* **63**, 1309-1313.

WIRTSCHAFTLICHE VEREINIGUNG ZUCKER (ed.) (2007): Anbau und Erzeugung. In: *Zuckermarkt Deutschland*. (05.02.2007) <http://www.zuckerwirtschaft.de/>

WOLF, J. (2002): Comparison of two soya bean simulation models under climate change. I. Model calibration and sensitivity analysis. *Climate Research* **20**, 55-70.

WOLF, J. & M. VAN OIJEN (2003): Model simulation of effects of changes in climate and atmospheric CO_2 and O_3 on tuber yield potential of potato (cv. Bintje) in the European Union. *Agriculture, Ecosystems and Environment* **94**, 141-157.

WU, J., ZHANG, R. & S. GUI (1999): Modeling soil water movement with water uptake by roots. *Plant and Soil* **215**, 7-17.

WULLSCHLEGER, S.D. (1993): Biochemical limitations to carbon assimilation in C_3 plants - A retrospective analysis of the A/C_i curves from 109 species. *Journal of Experimental Botany* **44**, 907-920.

XUE, Q., WEISS, A. & P.S. BAENZIGER (2004): Predicting phenological development in winter wheat. *Climate Research* **25**, 243-252.

YAN, W. & L.A. HUNT (1999): An equation for modelling the temperature response of plants using only the cardinal temperatures. *Annals of Botany* **84**, 607-614.

YANG, H.S., DOBERMANN, A., LINDQUIST, J.L., WALTERS D.T., ARKEBAUER, T.J. & K.G. CASSMAN (2004): Hybrid-maize - a maize simulation model that combines two crop modeling approaches. *Field Crops Research* **87**, 131-154.

YIN, X., KROPFF, M.J., MCLAREN, G. & R.M. VISPERAS (1995): A nonlinear model for crop development as a function of temperature. *Agricultural and Forest Meteorology* **77**, 1-16.

YIN, X., SCHAPENDONK, A.H.C.M., KROPFF, M.J., VAN OIJEN, M. & P.S. BINDRABAN (2000): A generic equation for nitrogen-limited leaf area index and its application in crop growth models for predicting leaf senescence. *Annals of Botany* **85**, 579-585.

YIN, X., GOUDRIAAN, J., LANTINGA, E.A., VOS, J. & H.J. SPIERTZ (2003a): A flexible sigmoid function of determinate growth. *Annals of Botany* **91**, 361-371.

YIN, X., LANTINGA, E.A., SCHAPENDONK, A.H.C.M. & X. ZHONG (2003b): Some quantitative relationships between leaf area index and canopy nitrogen content and distribution. *Annals of Botany* **91**, 893-903.

YIN, X. & A.H.C.M. SCHAPENDONK (2004): Simulating the partitioning of biomass and nitrogen between roots and shoot in crop and grass plants. *NJAS–Wageningen Journal of Life Sciences* **51**, 407-426.

YIN, X., STRUIK, P.C. & M.J. KROPFF (2004a): Role of crop physiology in predicting gene-to-phenotype relationships. *Trends in Plant Science* **9**, 426-432.

YIN, X., VAN OIJEN, M. & A.H.C.M. SCHAPENDONK (2004b): Extension of a biochemical model for the generalized stoichiometry of electron transport limited C_3 photosynthesis. *Plant, Cell and Environment* **27**, 1211-1222.

YIN, X. & H.H. VAN LAAR (2005): Crop Systems Dynamics. An ecophysiological simulation model for genotype-by-environment interactions. Wageningen Academic Publishers, Wageningen, 155 p.

YIN, X., STRUIK, P.C., TANG, J., QI, C. & T. LIU (2005): Model analysis of flowering phenology in recombinant inbred lines of barley. *Journal of Experimental Botany* **56**, 959-965.

ZADOKS, J.C., CHANG, T.T. & C.F. KONZAK (1974): A decimal code for the growth stages of cereals. *Weed Research* **14**, 415-421.

ZIMMERMANN, G. (1998): Getreidebau - Weizen. In: *Die Landwirtschaft. Band 1: Pflanzliche Erzeugung.* (eds Munzert, M. & H. Hüffmeier), p. 261-281. BLV Verlagsgesellschaft München, Landwirtschaftsverlag Münster-Hiltrup, 11th edition, München.

APPENDIX

Appendix A: Calculations referred to in the description of the simulated processes in the DANUBIA crop growth model (see chapter 2.2: *Simulated processes)*

Appendix B: List of symbols (with units) used in the text

Appendix C: Partitioning of global incident radiation into direct and diffuse components

Appendix D: Values of crop-specific parameters

Appendix E: Assignment of phenological stage to development stage and BBCH stage

Appendix F: Equations of model performance statistics

Appendix G: Field measurement data

Appendix A

Calculations referred to in the description of the simulated processes in the DANUBIA crop growth model (see chapter 2.2: *Simulated processes)*

All following calculations and descriptions are taken from the model GECROS (YIN & VAN LAAR 2005).

Calculation of photoperiodic day-length

Calculation of photoperiodic day-length D_{lp} uses the coefficients a and b (see eq. C-2a-c in Appendix C), and α, the sun angle below the horizon for including civil twilight:

$$D_{lp} = 12 \{1 + 2/\pi) \arcsin[(-\sin(\alpha \pi/180) + a)/b]\} \quad \text{(A–1)}$$

According to the model GECROS, a default value of -2° for α is assumed.

Resistances and net absorbed radiation

Leaf boundary layer resistance to heat is a function of the crop-specific leaf width w and wind speed u (above the canopy):

$$r_{bh} = 100 \sqrt{w/u} \quad \text{(A–2)}$$

Leaf boundary layer resistance to water is approximated as:

$$r_{bw} = 0.93 \; r_{bh} \quad \text{(A–3)}$$

because of the dissimilar velocity of boundary layer transport regarding heat and water vapour (GOUDRIAAN & VAN LAAR 1994). In terms of turbulence resistance, no distinction exists between the transfer of heat, water vapour and CO_2:

$$r_t = 0.74 \left\{ \ln\left[(2 - 0.7H)/(0.1H) \right] \right\}^2 / (0.16u) \quad \text{(A–4)}$$

where H denotes crop height.

The difference between total absorbed short-wave radiation (see chapter 2.2.3: *Scaling of canopy parameters*) and outgoing long-wave radiation $R^{\uparrow}$ gives the net absorbed radiation by leaves (R_n). According to GECROS, leaf temperature T_l, vapour pressure in the atmosphere V, and sky clearness f_{clear} are used to estimate $R^{\uparrow}$ (equations from VAN KEULEN *et al.* 1997).

$$R^{\uparrow} = B_z \left(T_l + 273.15 \right)^4 \; f_{vap} \; f_{clear} \; f_i \tag{A–5}$$

where B_z represents the Stefan-Boltzmann constant (5.668×10^{-8} J m^{-2} s^{-1} K^{-4}), T_l is leaf temperature, and f_i is the sunlit or shaded, respectively, fraction of a leaf class. The factors for the effect of vapour pressure (f_{vap}), and for the effect of sky clearness (f_{clear}) on $R^{\uparrow}$ are:

$$f_{vap} = 0.56 - 0.079 \sqrt{10\,V} \tag{A–6}$$

$$f_{clear} = 0.1 + 0.9 \; \max\left\{ 0, \; \min\left[1, \left(\tau - 0.2 \right) / \; 0.5 \right] \right\} \tag{A–7}$$

where V is vapour pressure and τ is atmospheric transmissivity.

Derivation of equation 2.2.2-22 (actual leaf stomatal resistance $r_{sw,a}$)

Substituting $r_{sw,p}$ by $r_{sw,a}$ in eq. 2.2.2-16 (for potential leaf transpiration), actual leaf transpiration is calculated as:

$$E_a = \frac{s\,R_n + \rho c_p\,D_a \,/\left(r_{bh} + r_t\right)}{\lambda\left\{ s + \gamma\left[\left(r_{bw} + r_t + r_{sw,a}\right)/\left(r_{bh} + r_t\right)\right]\right\}} \tag{A–8}$$

Although the parameters s and R_n are influenced by the modified leaf temperature due to reduced transpiration, their values are not recalculated. This simplification is considered to cause a negligible difference in calculating E_a.

Combining both the equations for E_p and E_a gives:

$$\frac{E_p}{E_a} = \frac{s\left(r_{bh} + r_t\right) + \gamma\left(r_{bw} + r_t + r_{sw,a}\right)}{s\left(r_{bh} + r_t\right) + \gamma\left(r_{bw} + r_t + r_{sw,p}\right)} \tag{A–9}$$

which is the basis for eq. 2.2.2-22.

Boundary layer conductances

Wind speed is assumed to attenuate exponentially in a canopy. According to eq. (A-2), boundary layer conductance for heat in the *i*-th layer of a canopy ($g_{\mathrm{bl},i}$) is estimated as:

$$g_{\mathrm{bl},i} = 0.01\sqrt{u_i / w} = 0.01\sqrt{u \exp\left(-k_{\mathrm{w}} L_i\right)/ w} \tag{A–10}$$

where k_{w} is the extinction coefficient for wind speed.

Leaf width w is assumed to be constant over the depth of a canopy. The boundary layer conductance for the entire canopy g_{bc} is defined as:

$$g_{\mathrm{bc}} = \int_0^L g_{\mathrm{bl},i}\,\mathrm{d}L_i = \int_0^L 0.01\sqrt{u \exp\left(-k_{\mathrm{w}} L_i\right) / w}\;\;\mathrm{d}L_i \tag{A–11}$$

$$= 0.01\sqrt{u / w}\left(1 - \exp\left(-0.5\,k_{\mathrm{w}} L\right)\right) / \left(0.5\,k_{\mathrm{w}}\right)$$

For the sunlit fraction of the canopy, the boundary layer conductance is:

$$g_{\mathrm{bc,sun}} = \int_0^L g_{\mathrm{bl},i}\;\varphi_{\mathrm{sun},i}\;\mathrm{d}L_i = \int_0^L g_{\mathrm{bl},i}\;\exp\left(-k_{\mathrm{b}} L_i\right)\mathrm{d}L_i \tag{A–12}$$

$$= 0.01\sqrt{u / w}\;\left[1 - \exp\left(-\left(0.5\,k_{\mathrm{w}} + k_{\mathrm{b}}\right)L\right)\right] / \left(0.5\,k_{\mathrm{w}} + k_{\mathrm{b}}\right)$$

For the shaded fraction, the boundary layer conductance can be simply given as difference:

$$g_{\mathrm{bc,shade}} = g_{\mathrm{bc}} - g_{\mathrm{bc,sun}} \tag{A–13}$$

Leaf nitrogen profile

Scaling of leaf nitrogen content with canopy depth is modelled according to GECROS (YIN & VAN LAAR 2005). YIN *et al.* (2000b) present the following equation for the exponential decline of leaf nitrogen content per unit leaf area:

$$n_i = n_0\;\exp\left(-k_{\mathrm{n}} L_i\right) \tag{A–14}$$

where n_i is the leaf nitrogen of the i-th layer of the canopy (counted from the top) with the corresponding leaf area index L_i. Leaf nitrogen content at the top of the canopy is represented by n_0, and k_n stands for the nitrogen extinction coefficient. Photosynthetically active nitrogen at the i-th layer ($n_{p,i}$) is defined as the difference between leaf nitrogen content at the i-th layer n_i and n_b, the crop-specific minimum leaf nitrogen content needed for photosynthesis:

$$n_{p,i} = n_i - n_b = n_0 \exp(-k_n L_i) - n_b \tag{A–15}$$

For the whole canopy, photosynthetically active nitrogen can be solved as:

$$\begin{aligned} N_c &= \int_0^L n_{p,i}\, dL_i = \int_0^L (n_0 \exp(-k_n L_i) - n_b)\, dL \\ &= n_0 (1 - \exp(-k_n L)) / k_n - n_b L \end{aligned} \tag{A–16}$$

Photosynthetically active nitrogen for the sunlit section of the canopy is:

$$\begin{aligned} N_{c,sun} &= \int_0^L n_{p,i}\, f_{sun,i}\, dL_i = \int_0^L (n_0 \exp(-k_n L_i) - n_b) \exp(-k_b L_i)\, dL_i \\ &= n_0 [1 - \exp(-(k_n + k_b) L)] / (k_n + k_b) \\ &\quad - n_b (1 - \exp(-k_b L)) / k_b \end{aligned} \tag{A–17}$$

Root depth

According to the model GECROS (YIN & VAN LAAR 2005), the following theory is used for the derivation of eq. 2.2.5-3 and eq. 2.2.5-4 (chapter 2.2.5: *Root growth*).

The distribution of root mass between soil surface and depth D can be described by an exponential equation (GERWITZ & PAGE 1974, cited by YIN & VAN LAAR 2005):

$$w_{RT,i} = w_{RT,0} \exp(-k_R D_i) \tag{A–18}$$

where $w_{RT,i}$ is root weight at the i-th soil depth (D_i) counted from the soil surface layer and $w_{RT,0}$ is root weight at the soil surface ($D_i = 0$). Entire root depth over the soil depth is:

$$W_{RT} = \int_0^D w_{RT,i}\, dD_i = w_{RT,0} (1 - \exp(-k_R D)) / k_R \tag{A–19}$$

If eq. (A–19) is solved for $w_{RT,0}$ and the term inserted into eq. (A–18), $w_{RT,i}$ is calculated as:

$$w_{RT,i} = k_R \; W_{RT} \; \exp\left(-k_R \, D_i \right) \; / \; \left(1 - \exp\left(-k_R \, D \right) \right) \tag{A–20}$$

A critical base value w_{Rb} for the effectiveness of absorption is assumed. The effective rooted depth is expressed as the distance from the soil surface to the depth at which root weight reaches this critical (base) value:

$$w_{Rb} = k_R \; W_{RT} \; \exp\left(-k_R \, D \right) \; / \; \left(1 - \exp\left(-k_R \, D \right) \right) \tag{A–21}$$

Consequently, D is:

$$D = \left(1 / k_R \right) \ln\left(1 + k_R \, W_{RT} \; / \; wRb \right) \tag{A–22}$$

Assuming a constant k_R over time, the differential form of eq. (A–22) gives the second part of equation 2.2.5-3 (chapter 2.2.5: *Root growth*). The percentage p of root mass between soil surface and depth D_i is:

$$p = 100 \left(1 - \exp\left(-k_R \, D_i \right) \right) \; / \; \left(1 - e^{-k_R \, D} \right) \tag{A–23}$$

The denominator can be approximated to 1.0, which gives root distribution over soil depth:

$$p = 100 \left(1 - \exp\left(-k_R \, D_i \right) \right) \tag{A–24}$$

Rooting depth is defined as the depth from which the roots effectively extract water and nutrients. Assuming that 95 % of the total root mass is located above this depth, gives following relationship to derive k_R:

$$95 = 100 \left(1 - \exp\left(-k_R \, D_{max} \right) \right) \tag{A–25}$$

Derivation of equation 2.2.8-3

The derivation of equation (chapter 2.2.8: *Nitrogen demand*, eq. 2.2.8-3) is presented as given by YIN & VAN LAAR (2005).

Corresponding to the study on relative growth rate (increase in biomass per unit biomass in a defined time-step) by HILBERT (1990), the optimization criterion is derived

for maximum relative carbon gain. Relative carbon gain is formulated as (see eq. 2.2.8-5):

$$\left(\Delta C \;/\; \Delta t \right) / \; C \; = \; C_S \; \sigma_C \;/\; C \; = \; f_S \; \sigma_C \tag{A–26}$$

where σ_C denotes relative shoot activity and f_S is the fraction of carbon in the shoot relative to total carbon in the plant. Thus root carbon fraction f_R is 1 - f_S. In order to retrieve the optimum plant nitrogen-carbon ratio for maximum relative growth rate, the derivative of relative carbon gain with respect to plant nitrogen-carbon ratio κ is set to zero:

$$f_S \; \frac{\mathrm{d}\,\sigma_C}{\mathrm{d}\,\kappa} \; + \; \sigma_C \; \frac{\mathrm{d}\,f_S}{\mathrm{d}\,\kappa} \; = \; 0 \quad \text{or} \quad f_S \; \frac{\mathrm{d}\,\sigma_C}{\mathrm{d}\,\kappa} \; = \; - \; \sigma_C \; \frac{\mathrm{d}\,f_S}{\mathrm{d}\,\kappa} \tag{A–27}$$

To obtain the derivative of relative carbon gain with respect to κ, a function for deriving $\mathrm{d}f_S/\mathrm{d}\kappa$ is needed. To determine f_S as a function of κ, conditions of balanced growth are assumed. According to HILBERT (1990), under balanced growth conditions, relative root and shoot activities are constant as well as root-shoot ratio, and nitrogen-carbon ratio in the tissue (N/C = $\Delta N/\Delta C$). The nitrogen-carbon ratio κ can then be formulated as:

$$\kappa \; = \; \frac{N}{C} \; + \; \frac{\Delta N}{\Delta C} \; = \; \frac{C_R \; \sigma_N}{C_S \; \sigma_C} \; = \; \frac{f_R \; \sigma_N}{f_S \; \sigma_C} \; = \; \frac{\left(1 - f_S\right) \sigma_N}{f_S \; \sigma_C} \tag{A–28}$$

Consequently, f_S is:

$$f_S = \sigma_N \; / \left(\kappa \sigma_C + \sigma_N \right) \tag{A–29}$$

The derivative of f_S with respect to κ, $\mathrm{d}f_S / \mathrm{d}\kappa$, is determined as:

$$\frac{\mathrm{d}\,f_S}{\mathrm{d}\,\kappa} \; = \; \frac{\left(\kappa \sigma_C + \sigma_N \right) \; \frac{\mathrm{d}\,\sigma_N}{\mathrm{d}\,\kappa} \; - \; \sigma_N \left(\sigma_C + \kappa \frac{\mathrm{d}\,\sigma_C}{\mathrm{d}\,\kappa} + \frac{\mathrm{d}\,\sigma_N}{\mathrm{d}\,\kappa} \right)}{\left(\kappa \sigma_C + \sigma_N \right)^2} \tag{A–30}$$

As stated by HILBERT (1990), it is assumed that σ_N is not a function of κ because root relative activity in natural conditions is most often controlled by the quantity of accessible soil nitrogen and its rate of diffusion to the root system, rather than by intrinsic root physiological function. Therefore, $\mathrm{d}\sigma_N/\mathrm{d}\kappa$ is set to zero and allows the simplification of equation (A–30) to:

$$\frac{\mathrm{d}f_S}{\mathrm{d}\kappa} = -\frac{\sigma_N\left(\sigma_C + \kappa\frac{\mathrm{d}\sigma_C}{\mathrm{d}\kappa}\right)}{\left(\kappa\sigma_C + \sigma_N\right)^2} \tag{A–31}$$

Based on equations (A–29) and (A–31), the following equation is obtained:

$$\frac{\mathrm{d}f_S}{\mathrm{d}\kappa}\frac{1}{f_S} = -\frac{\sigma_C + \kappa\frac{\mathrm{d}\sigma_C}{\mathrm{d}\kappa}}{\kappa\sigma_C + \sigma_N} \tag{A–32}$$

Replacing equation (A–34) into equation (A–27) results in:

$$\frac{\mathrm{d}\sigma_C}{\mathrm{d}\kappa}\frac{1}{\sigma_C} = \frac{\sigma_C + \kappa\frac{\mathrm{d}\sigma_C}{\mathrm{d}\kappa}}{\kappa\sigma_C + \sigma_N} = \frac{\sigma_C}{\kappa\sigma_C + \sigma_N} + \frac{\kappa\frac{\mathrm{d}\sigma_C}{\mathrm{d}\kappa}}{\kappa\sigma_C + \sigma_N} \tag{A–33}$$

By multiplying both sides of equation (A–33) by σ_C, and assembling the two terms including $\mathrm{d}\sigma_C/\mathrm{d}\kappa$ gives:

$$\frac{\mathrm{d}\sigma_C}{\mathrm{d}\kappa}\left(\frac{\sigma_N}{\kappa\sigma_C + \sigma_N}\right) = \frac{\sigma_C^{\,2}}{\kappa\sigma_C + \sigma_N} \tag{A–34}$$

which after further simplification results in equation (2.2.8-3).

Appendix B

List of symbols (with units) used in the text

Unless declared otherwise, weight in g refers to weight of dry matter (biomass) and m² denotes ground area. Crop-specific input parameters are marked with an asterisk.

Symbol		Definition	Unit
A		net assimilation rate	g CO_2 m^{-2} leaf s^{-1}
B_z		Stefan-Boltzmann constant	J m^{-2} s^{-1} K^{-4}
c_0		empirical coefficient	-
c_1		empirical coefficient	kPa^{-1}
C_a		CO_2 concentration in the air	µmol mol^{-1}
C_c		CO_2 concentration at carboxylation site of chloroplasts	µmol mol^{-1}
C_i		intercellular CO_2 concentration	µmol mol^{-1}
C_{LV}		carbon in living leaf	g C m^{-2}
C_{max}		maximum C content of seed at the end of its growth	g C m^{-2}
c_{Nfix}		carbon cost of symbiotic N fixation	g C g^{-1} N
C_R		carbon in living root	g C m^{-2}
C_R		carbon in living root (including root reserves)	g C m^{-2}
C_S		carbon in living shoot	g C m^{-2}
CS_R		daily C supply from photosynthesis for root growth	g C m^{-2} d^{-1}
CS_S		daily C supply from photosynthesis for shoot growth	g C m^{-2} d^{-1}
c_t	*	curvature factor for temperature response	-
$C_{\varphi i}$		C demand for growth of seed or stem	g C m^{-2} d^{-1}
D		rooting depth	cm
D_a		water vapour pressure saturation deficit of air	kPa
D_{al}		air-to-leaf vapour pressure deficit	kPa
D_J		energy of deactivation for J_{max}	J mol^{-1}
D_{lp}		photoperiodic day-length	h
D_{max}	*	maximum rooting depth	cm
d_p	*	plant density	plants m^{-2}
D_s	*	sowing depth	cm
E_a		actual leaf transpiration	mm s^{-1}
E_{Jmax}	*	activation energy for J_{max}	J mol^{-1}
E_{KmC}		activation energy for K_{mC}	J mol^{-1}
E_{KmO}		activation energy for K_{mO}	J mol^{-1}

Symbol		Definition	Unit
$E_{m,a}$	*	coefficient for determining threshold for emergence	-
$E_{m,b}$	*	factor for determining threshold for emergence	-
$E_{m,th}$		threshold for emergence	-
E_p		potential leaf transpiration	mm s^{-1}
E_{Rd25}		activation energy for R_d	J mol^{-1}
$E_{Rub,k}$		proxy for activation energies E_{KmC}, E_{KmO}, E_{Rd} and E_{Vcmax}	J mol^{-1}
$e_{s(Ta)}$		saturated vapour pressure of air	kPa
$e_{s(Tl)}$		saturated vapour pressure of leaf	kPa
E_{Vcmax}		activation energy for V_{cmax}	J mol^{-1}
f(P)		photoperiod response	-
f(T)		temperature response	-
f(V)		vernalization response	-
$f_{C,ini}$	*	initial fraction of C allocated to shoot	-
$f_{c,S}$		fraction of C in seed biomass	g C g^{-1}
$f_{c,V}$	*	fraction of C in vegetative-organ biomass	g C g^{-1}
f_{car}		fraction of carbohydrates in biomass of organs	g carbohydrate g^{-1}
f_{clear}		factor for effect of sky clearness on $R^{\uparrow}$	
f_{cyc}		fraction of cyclic electron transport around photosystem I	-
f_d		fraction of diffuse component in incoming radiation	-
$F_{H2O,Ni}$		soil water factor affecting N uptake	-
f_{ht}		integral factor of stresses on plant height growth	-
f_{lig}	*	fraction of lignin in biomass of organs	g lignin g^{-1}
f_{lip}	*	fraction of lipids in biomass of organs	g lipid g^{-1}
$f_{N,ini}$	*	initial fraction of N allocated to shoot	-
$f_{N,S}$		factor for dynamics of seed N concentration during seed fill	-
$f_{N,S,fin}$	*	factor for final N concentration of seed fill	-
$f_{N,S,ini}$	*	factor for initial N concentration of seed fill	-
F_{NH4i}		soil ammonium supply factor in soil layer *i*	-
F_{Nmin}	*	critical value of N supply factors	-
F_{NO3i}		soil nitrate supply factor in soil layer *i*	-
f_{Npre}	*	fraction of seed N that comes from remobilizable vegetative-organ N accumulated before t_e	-
f_{oac}	*	fraction of organic acids in biomass of organs	g organic acid g^{-1}
f_{pro}		fraction of proteins in biomass of organs	g protein g^{-1}
f_{pseudo}		fraction of pseudocyclic electron transport	-

Symbol		Definition	Unit
F_{PW}		plant water stress factor	
f_{Q}		fraction of electron transport that follows the Q-cycle	-
F_{RH}		root hospitality factor	-
F_{RLDi}		factor for root length density in layer i	-
F_{RLDP}		factor for root length density in the soil profile	-
F_{RS}		root senescence factor	-
f_{shade}		fraction of shaded leaves in a canopy	-
F_{SNi}		factor describing mineral N availability in layer i	-
F_{SNmin}	*	minimum value of F_{SN}	-
f_{sun}		fraction of sunlit leaves in a canopy	-
$f_{sun,i}$		sunlit fraction of leaves at canopy depth with L_i	-
F_{SW}		factor describing soil water deficit	-
f_{vap}		factor for effect of vapour pressure on $R\uparrow$	-
$F_{\Delta D,em}$	*	factor for root depth increase before emergence	-
g_{bc}		total boundary layer conductance in canopy	m s^{-1}
$g_{bc,\ shade}$		boundary layer conductance for shaded fraction of canopy	m s^{-1}
$g_{bc,\ sun}$		boundary layer conductance for sunlit fraction of canopy	m s^{-1}
$g_{c,p}$		potential conductance for CO_2	m s^{-1}
h		number of protons required to produce 1 mol ATP	mol mol^{-1}
H		plant height	m
H_{max}	*	maximum plant height	m
I		leaf chloroplasts-absorbed PAR	µmol m^{-2} leaf s^{-1}
$I_{b,top}$		incident direct-beam radiation above canopy	W m^{-2}
I_{beam}		absorbed direct-beam radation	W m^{-2}
I_{c}		absorbed radiation by canopy	W m^{-2}
$I_{c,shade}$		absorbed radiation by shaded leaves of canopy	W m^{-2}
$I_{c,sun}$		absorbed radiation by sunlit leaves of canopy	W m^{-2}
$I_{d,top}$		incident diffuse radiation above canopy	W m^{-2}
$I_{diffuse}$		absorbed diffuse radiation	W m^{-2}
$I_{m,seed}$	*	fraction of sigmoid curve inflexion in entire seed growth period	-
$I_{m,stem}$	*	fraction of sigmoid curve inflexion in entire plant height growth period	-
$I_{scat\ beam}$		absorbed scattered beam radiation	W m^{-2}
J_2		rate of linear electron transport through photosystem II	µmol electron m^{-2} leaf s^{-1}

Symbol		Definition	Unit
J_{max}		maximum rate of J_2	µmol electron m^{-2} leaf s^{-1}
J_{max25}		J_{max} at 25 °C	µmol electron m^{-2} leaf s^{-1}
k'_b		extinction coefficient for beam and scattered-beam radiation	m^2 ground m^{-2} leaf
k'_d		extinction coefficient for diffuse and scattered-diffuse radiation (for standard overcast sky conditions)	m^2 ground m^{-2} leaf
k_b		direct beam extinction coefficient	m^2 ground m^{-2} leaf
K_{mC}		Michaelis-Menten constant for CO_2	µmol mol^{-1}
K_{mC25}		Michaelis-Menten constant for CO_2 at 25°C	µmol mol^{-1}
K_{mO}		Michaelis-Menten constant for O_2	mmol mol^{-1}
K_{mO25}		Michaelis-Menten constant for O_2 at 25°C	mmol mol^{-1}
k_n		N extinction coefficient	m^2 ground m^{-2} leaf
k_r		diffuse PAR extinction coefficient	m^2 ground m^{-2} leaf
k_R		extinction coefficient of root weight density over soil depth	cm^{-1}
k_{Rn}		extinction coefficient of root N concentration	m^2 ground g^{-1}
k_w		wind speed extinction coefficient	m^2 ground m^{-2} leaf
L		green leaf area index of canopy	m^2 leaf m^{-2} ground
L_C		carbon-determined L	m^2 leaf m^{-2} ground
L_i		L counted from top to the i-th layer of canopy	m^2 leaf m^{-2} ground
L_N		nitrogen-determined L	m^2 leaf m^{-2} ground
L_T		total (green and senescent) leaf area index	m^2 leaf m^{-2} ground
M_{op}		optimum photoperiod	h
n		leaf N content	g N m^{-2} leaf
n_0		canopy top-leaf N	g N m^{-2} leaf
n_{act}		actual N concentration in living shoot	g N g^{-1}
n_b	*	minimum leaf N for photosynthesis	g N m^{-2} leaf
n_{bot}		canopy bottom-leaf N	g N m^{-2} leaf
n_{botE}		n_{bot} calculated from exponential N profile	g N m^{-2} leaf
N_c		total photosynthetically active N in canopy	g N m^{-2} ground
$N_{c,shade}$		photosynthetically active N in shaded leaves of canopy	g N m^{-2} ground
$N_{c,sun}$		photosynthetically active N in sunlit leaves of canopy	g N m^{-2} ground
n_{cri}		critical shoot N concentration	g N g^{-1}
n_{cri0}	*	initial critical shoot N concentration	g N g^{-1}
N_{dem}		crop N demand	g N m^{-2} d^{-1}
N_{demA}		activity-driven crop N demand	g N m^{-2} d^{-1}
N_{demD}		deficiency-driven crop N demand	g N m^{-2} d^{-1}

Symbol		Definition	Unit
N_{ex}		exuded N from roots	g N m^{-2} d^{-1}
N_{fix}		symbiotically fixed N	g N m^{-2} d^{-1}
n_{L}		N concentration in living leaf	g N g^{-1}
n_{Lmin}		minimum N concentration in leaf	g N g^{-1}
N_{LV}		N in living leaf	g N m^{-2}
N_{LVres}		amount of N in leaves available for remobilization	g N m^{-2} d^{-1}
N_{maxup}	*	maximum crop N uptake rate	g N m^{-2} d^{-1}
N_{NH4i}		ammonium N in layer *i*	mg N kg^{-1}
N_{NO3i}		nitrate N in soil layer *i*	mg N kg^{-1}
N_{R}		N in living root	g N m^{-2}
N_{res}		estimated vegetative-organ N remobilizable for seed growth	g N m^{-2}
n_{Rmin}	*	minimum N concentration in root	g N g^{-1}
N_{RTres}		amount of N in roots available for remobilization	g N m^{-2} d^{-1}
N_{S}		N in living shoot	g N m^{-2}
n_{Smin}	*	minimum N concentration in stem	g N g^{-1}
n_{SO}	*	standard N concentration in seed	g N g^{-1}
$n_{SO,ex}$		expected seed-N concentration dynamics during seed fill	g N g^{-1} N
Ns_{R}		daily N supply for root growth	g N m^{-2} d^{-1}
N_{SR}		N in living structural root	g N m^{-2}
Ns_{S}		daily N supply for shoot growth	g N m^{-2} d^{-1}
N_{T}		total N in living shoot and root	g N m^{-2}
N_{totali}		sum of ammonium and nitrate in layer *i*	mg elemental N kg^{-1} soil
O_{av}		average projection of leaves in the direction of a solar beam	m^2 ground m^{-2} leaf
O_{i}		intercellular oxygen concentration	mmol mol^{-1}
P_{a}		actual gross leaf photosynthesis	g CO_2 m^{-2} leaf s^{-1}
P_{C}		daily gross canopy photosynthesis	g CO_2 m^{-2} d^{-1}
P_{Cnet}		daily net canopy photosynthesis	g CO_2 m^{-2} d^{-1}
P_{p}		potential gross leaf photosynthesis	g CO_2 m^{-2} leaf s^{-1}
p_{sen}	*	photoperiod sensitivity	h^{-1}
R		universal gas constant	J K^{-1} mol^{-1}
$R^{\uparrow}$		net long-wave radiation	J m^{-2} leaf s^{-1}
r_{bh}		leaf boundary layer resistance to heat	s m^{-1}
r_{bw}		leaf boundary layer resistance to water vapour	s m^{-1}
R_{d}		leaf dark respiration	g CO_2 m^{-2} leaf s^{-1}

Symbol		Definition	Unit
R_{d25}		R_d at 25 °C	g CO_2 m^{-2} leaf s^{-1}
R_G		growth respiration	g CO_2 m^{-2} d^{-1}
$RG_{\varphi i}$		expected relative growth rate of seed or stem	d^{-1}
R_{HT}		rate of change in plant height	m d^{-1}
R_k		proxy for K_{mC}, K_{mO}, R_d and V_{cmax} in eq. (2.2.2–10)	various
R_{LDi}		root length density of soil layer i	cm root cm^{-3} soil
R_{LM}	*	root length to mass ratio	cm root length g^{-1} root
R_M		non-growth components of respiration (excluding the cost of N-fixation)	g CO_2 m^{-2} d^{-1}
$R_{M,min}$		respiratory cost of minerals uptake	g CO_2 m^{-2} d^{-1}
$R_{M,NH4}$		respiratory cost of ammonium-N uptake	g CO_2 m^{-2} d^{-1}
$R_{M,NO3}$		respiratory cost of nitrate-N uptake and reduction	g CO_2 m^{-2} d^{-1}
$R_{M,phl}$		respiratory cost due to phloem loading of C assimilates to roots	g CO_2 m^{-2} d^{-1}
$R_{M,res}$		residual maintenance respiration	g CO_2 m^{-2} d^{-1}
$R_{M,UP}$		total respiration for uptake and phloem loading	g CO_2 m^{-2} d^{-1}
R_{max}		maximum daily development rate	d^{-1}
$R_{max,r}$	*	R_{max} in the reproductive (seed fill) phase	d^{-1}
$R_{max,v}$	*	R_{max} in the vegetative phase	d^{-1}
$R_{max,v1}$	*	R_{max} in the emergence till terminal spikelet initiation phase	d^{-1}
$R_{max,v2}$	*	R_{max} in the terminal spikelet initiation till start of seed fill phase	d^{-1}
R_n		net leaf absorbed radiation	J m^{-2} leaf s^{-1}
R_{Nfix}		respiratory cost of N_2 fixation	g CO_2 m^{-2} d^{-1}
$r_{sw,a}$		leaf stomatal resistance to water in the presence of water stress	s m^{-1}
$r_{sw,p}$		leaf stomatal resistance to water in the absence of water stress	s m^{-1}
r_t		turbulence resistance	s m^{-1}
s		slope of the curve relating saturation vapour pressure to temperature	kPa $°C^{-1}$
s^*		proxy for s in eq. (2.2.2–21)	kPa $°C^{-1}$
S_c		solar constant	W m^{-2}
S_f		number of seeds	seeds m^{-2}
S_J		entropy term	J K^{-1} mol^{-1}
s_{la}	*	specific leaf area constant	m^2 leaf g^{-1} leaf
S_o		instantaneous global radiation	W m^{-2}

Symbol		Definition	Unit
S_w	*	seed weight	g seed^{-1}
T_a		air temperature	°C
T_b	*	base temperature for phenological development	°C
$T_{b,em}$	*	base temperature for emergence	°C
T_c	*	ceiling temperature	°C
t_d		Julian daynumber	d
t_e	*	development stage for the end of seed-number determining period	-
t_h		time of the day (solar time)	h
T_l		leaf temperature	°C
T_o	*	optimum temperature for phenological development	°C
T_{sm}		daily mean soil temperature	°C
TT_{em}		daily thermal time for emergence	°C day
u		wind speed	m s^{-1}
U_N		actual N uptake rate from the soil profile	kg N ha^{-1} d^{-1}
U_{NH4i}		actual ammonium uptake in soil layer i	kg N ha^{-1} d^{-1}
U_{NH4pi}		potential uptake rate of ammonium in soil layer i	kg N ha^{-1} d^{-1}
U_{NO3i}		actual nitrate uptake in soil layer i	kg N ha^{-1} d^{-1}
U_{NO3pi}		potential uptake rate of nitrate in soil layer i	kg N ha^{-1} d^{-1}
U_{Np}		potential N uptake rate from the soil profile	kg N ha^{-1} d^{-1}
U_{NRmax}	*	maximum N uptake rate per unit length of root	kg N ha^{-1} cm^{-1} root
U_{Wai}		actual water uptake from soil layer i	cm h^{-1}
U_{WaP}		actual water uptake from soil profile	cm h^{-1}
U_{Wpi}		potential water uptake from soil layer i	cm h^{-1}
U_{WpP}		potential water uptake from soil profile	cm h^{-1}
U_{Wri}		water uptake per unit of root length	cm^3 cm^{-1} d^{-1}
V		vapour pressure	kPa
V_c		rate of carboxylation limited by Rubisco activity	µmol CO_2 m^{-2} leaf s^{-1}
V_{cmax}		maximum rate of carboxylation limited by Rubisco activity	µmol CO_2 m^{-2} leaf s^{-1}
V_{cmax25}		V_{cmax} at 25 °C	µmol CO_2 m^{-2} leaf s^{-1}
VD		effective vernalization days	d
$VD_{0.5}$		VD when plants are 50 % vernalized	d
V_j		rate of carboxylation limited by electron transport	µmol CO_2 m^{-2} leaf s^{-1}
w	*	leaf blade width	m
W_{LV}		dry weight of living leaves	g m^{-2}

Symbol		Definition	Unit
W_R		dry weight of living roots	g m^{-2}
w_{Rb}		critical root weight density	g m^{-2} cm^{-1}
W_S		weight of living shoot	g m^{-2}
W_{SR}		weight of living structural root	g m^{-2}
$W_{SR,N}$		nitrogen-determined W_{SR}	g m^{-2}
X_{NH4}	*	supply coefficient for ammonium	-
X_{NO3}	*	supply coefficient for nitrate	-
$Y_{G,S}$		storage organ (seed) growth efficiency	g C g^{-1} C
$Y_{G,V}$	*	vegetative-organ (leaf, stem, root) growth efficiency	g C g^{-1} C
z_i		thickness of soil layer i	cm
a		inclination of sun angle for including civil twilight	degrees
a_2		quantum efficiency for electron transport of PS II based on absorbed light	mol mol^{-1}
β		solar elevation	degrees
β_L	*	leaf angle inclination in canopy	degrees
Γ		CO_2 compensation point in the presence of dark respiration	µmol mol^{-1}
γ		psychrometric constant	kPa $°C^{-1}$
Γ_*		CO_2 compensation point in the absence of dark respiration	µmol mol^{-1}
δ		declination of the sun	radians
$\Delta C/\Delta t$		net rate of shoot C fixation	g C m^{-2} d^{-1}
ΔC_{LV}		rate of change in living-leaf C	g C m^{-2} d^{-1}
ΔD		rate of change in rooting depth	cm d^{-1}
ΔL_C		rate of change of L_C	m^2 leaf m^{-2} d^{-1}
$\Delta N/\Delta t$		rate of root N uptake	g N m^{-2} d^{-1}
Δn_{bot}		rate of change of n_{bot}	g N m^{-2} leaf d^{-1}
$\Delta N_{\bar{LV}}$		loss rate of leaf N because of senescence	g N m-2 d-1
ΔN_{LV}		rate of change of N_{LV}	g N m^{-2} d^{-1}
$\Delta N_{\bar{R}}$		loss rate of root N because of senescence	g N m^{-2} d^{-1}
ΔR_L		root length increase	cm root cm^{-2} ground
ΔT		leaf-to-air temperature difference	°C
Δt		time step of dynamic simulation	d
$\Delta W_{\bar{LV}}$		loss rate of leaf weight because of senescence	g m^{-2} d^{-1}
$\Delta W_{\bar{R}}$		loss rate of root weight because of senescence	g m^{-2} d^{-1}
ΔW_{RT}		rate of change in total root weight	g m^{-2} d^{-1}
$\Delta\kappa$		increment in κ	g N g^{-1} C

Symbol		Definition	Unit
ε_g		efficiency of germination	g g^{-1}
ζ		latitude	degrees
Θ	*	convexity factor for response of J_2 to PAR	-
θ_{FCi}		θ in layer i at field capacity	cm^3 water cm^{-3} soil
θ_i		volumetric soil water content in layer i	cm^3 water cm^{-3} soil
θ_{SATi}		volumetric soil water content at saturation in layer i	cm^3 water cm^{-3} soil
θ_{WPi}		θ in layer i at wilting point	cm^3 water cm^{-3} soil
κ		nitrogen-carbon ratio in crop	g N g^{-1} C
λ		latent heat of water vaporization	J kg^{-1}
$\lambda_{C,leaf}$		fraction of newly assimilated shoot C partitioned to leaf	g C g^{-1} C
$\lambda_{C,R}$		fraction of newly assimilated C partitioned to root	g C g^{-1} C
$\lambda_{C,S}$		fraction of newly assimilated C partitioned to shoot	g C g^{-1} C
$\lambda_{C,seed}$		fraction of newly assimilated shoot C partitioned to seed	g C g^{-1} C
$\lambda_{C,Sres}$		fraction of newly assimilated shoot C partitioned to stem reserve pool	g C g^{-1} C
$\lambda_{C,stem}$		fraction of newly assimilated shoot C partitioned to structural stem	g C g^{-1} C
$\lambda_{N,R}$		fraction of newly absorbed N partitioned to root	g N g^{-1} N
$\lambda_{N,S}$		fraction of newly absorbed N partitioned to shoot	g N g^{-1} N
ρ	*	proportion factor between stem biomass and plant height	g m^{-2} m^{-1}
ρ_b		soil bulk density	g soil cm^{-3} soil
ρ_{cb}		canopy reflection coefficient for direct-beam radiation	-
ρ_{cd}		canopy reflection coefficient for diffuse radiation	-
ρc_p		volumetric heat capacity	J m^{-3} °C^{-1}
ρ_h		canopy reflection coefficient for horizontal leaves	-
ς		leakage of CO_2 back to the mesophyll as a fraction of the PEP carboxylation	-
σ		leaf scattering coefficient	-
σ_C		relative shoot activity	g C g^{-1} C d^{-1}
σ_N		relative root activity	g N g^{-1} C d^{-1}
τ		atmospheric transmissivity	-
φ		development stage	-
φ_1	*	development stage at which photoperiod sensitivity starts	-
φ_2	*	development stage at which photoperiod sensitivity ends	-
Φ_{2m}		maximum electron transport efficiency of PS II	mol mol^{-1}
φ_e		development stage at the end of growth of stem or seed	-

Appendix B

Symbol		Definition	Unit
φ_i		development stage during the growth of stem or seed	-
φ_m		development stage at the time of maximal growth rate of stem or seed	-
φ_{tr}	*	development stage when transition from $f_{N,S,ini}$ to $f_{N,S,fin}$ is fastest	-
χ_{jn}	*	proportion factor for the relation of J_{max} to leaf N	µmol electron g^{-1} N s^{-1}
χ_{vcn}	*	proportion factor for the relation of V_{cmax} to leaf N	µmol CO_2 g^{-1} N s^{-1}
ω_i		daily development rate	d^{-1}

Appendix C

Partitioning of global incident radiation into direct and diffuse components

For modelling canopy photosynthesis and energy exchange, it is essential to differentiate between the diffuse and direct components of the incoming global radiation. The diffuse flux arises from scattering (reflection and transmission) in the atmosphere. The fraction reaching the earth´s surface is modified by clouds and aerosols and therefore related to atmospheric transmissivity. While the incoming global radiation is a standard quantity measured in many weather stations, records of direct sunlight and diffuse skylight are rare.

According to the model GECROS (YIN & VAN LAAR 2005), the method presented by SPITTERS *et al.* (1986) and modified by GOUDRIAAN & VAN LAAR (1994) is used to estimate the diffuse fraction of measured incoming global radiation. This algorithm derives the portion of the diffuse component from the ratio between calculated extraterrestrial radiation outside the atmosphere and measured global radiation at the earth´s surface.

Table C-1: Symbols, definitions and units used for calculation of direct and diffuse radiation

Symbol	Definition	Unit
f_d	diffuse light fraction	-
S_c	solar constant	W m^{-2}
S_o	instantaneous global radiation	W m^{-2}
t_d	Julian daynumber	d
t_h	time of the day (solar time)	h
β	solar elevation	degrees
δ	declination of the sun	radians
ζ	latitude	degrees
τ	atmospheric transmissivity	-

The declination of the sun (δ) related to the equator varies with day of year (t_d) (SPITTERS *et al.* 1986):

$$\delta = -\arcsin\{ \sin(23.45\,\pi/180)\cos[2\,\pi\,(t_d+10)/365] \} \quad \text{(C–1)}$$

Using solar time (t_h), Julian day of year (t_d) and latitude (ζ), the diurnal course of the sine of solar elevation ($\sin\beta$) is calculated (GOUDRIAAN & VAN LAAR 1994):

$$\sin\beta = a + b\cos[2\,\pi\,(t_h-12)/24] \quad \text{(C–2a)}$$

$$a = \sin(\pi\zeta / 180)\ \sin\delta \quad \text{(C-2b)}$$

$$b = \cos(\pi\zeta / 180)\ \cos\delta \quad \text{(C-2c)}$$

The incoming solar radiation at the outer surface of the atmosphere, the solar constant (S_c, 1 367 W m^{-2}), on day t_d is corrected for the eccentricity of the sun´s orbit (GOUDRIAAN & VAN LAAR 1994):

$$S_c = 1367\ \{1 + 0.033\ \cos[2\pi(t_d - 10)/365]\} \quad \text{(C–3)}$$

The atmospheric transmissivity (τ) depends on the degree of cloudiness and is given by (GOUDRIAAN & VAN LAAR 1994):

$$\tau = \frac{S_o}{S_c\ \sin\beta} \quad \text{(C–4)}$$

The diffuse light fraction (f_d) as a function of atmospheric transmissivity can then be calculated as (SPITTERS *et al.* 1986):

$$\tau \le 0.22 \qquad f_d = 1 \quad \text{(C–5a)}$$

$$0.22 < \tau \le 0.35 \qquad f_d = 1 - 6.4\ (\tau - 0.22)^2 \quad \text{(C-5b)}$$

$$\tau < 0.35 \qquad f_d = 1.47 - 1.66\tau \quad \text{(C-5c)}$$

The diffuse light fraction is limited to a minimum by the following value:

$$0.15 + 0.85\ \left(1 - \exp(-0.1 / \sin\beta)\right) \quad \text{(C–6)}$$

The coefficients are based on literature data and radiation measurements taken in the Netherlands but the relationships are stable over climates and latitudes (SPITTERS *et al.* 1986).

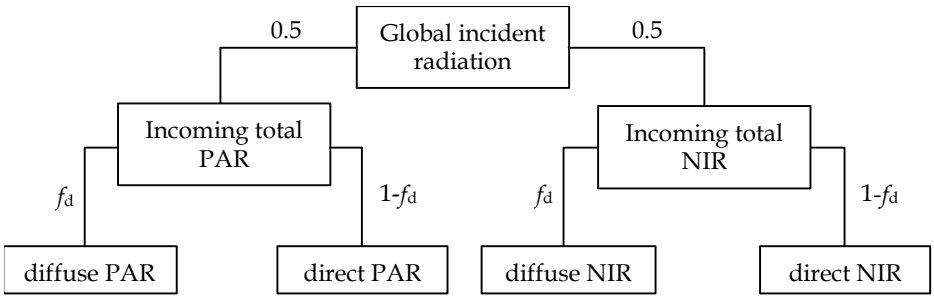

Fig. C-1: Division of global incident radiation into direct and diffuse components.

Photosynthetically active radiation (PAR) designates the spectral range of solar light from 400 to 700 nm and represents about one half (45 % under sunny conditions to 55 % under overcast conditions) of the amount of global radiation (approx. 350 to 2000 nm) (GOUDRIAAN & VAN LAAR 1994). In GECROS, global radiation is divided equally between PAR and near-infrared radiation (NIR). Therefore, to obtain the share of diffuse PAR, half of the incident global radiation is multiplied with the diffuse light fraction (f_d). In this way the measured incident global radiation can be divided into four components needed by the crop growth model: direct and diffuse PAR as well as direct and diffuse NIR.

Comparison with measurements

For validating the partitioning of radiation into its direct and diffuse components, measurements taken with the "*Beam Fraction Sensor BF2*" from *Delta-T Devices* (*Delta-T Devices Ltd.*, Cambridge, UK) were analyzed. This device uses seven cosine-corrected photodiodes under a special "shading pattern" to record total incident PAR and diffuse PAR with an accuracy of ± 15 % (DELTA-T DEVICES LTD 1999).

Table C-2: Characteristics of analyzed data

number of pair of variates	range of total incident PAR	range of diffuse PAR	range of solar zenith angle
281	264 - 2075 µmol m^{-2} s^{-1}	258 - 988 µmol m^{-2} s^{-1}	27.1° - 71.9°

A total of 281 measurements recorded on 12 days in the years 2003 and 2004 in the Sieg catchment area were compared with calculated diffuse PAR. Table C-2 shows characteristics of the analyzed data. To convert the modelled PAR data from W m^{-2} to measured photosynthetically active photon flux density in µmol m^{-2} s^{-1}, a factor of 4.56 µmol J^{-1} is used (YIN & VAN LAAR 2005).

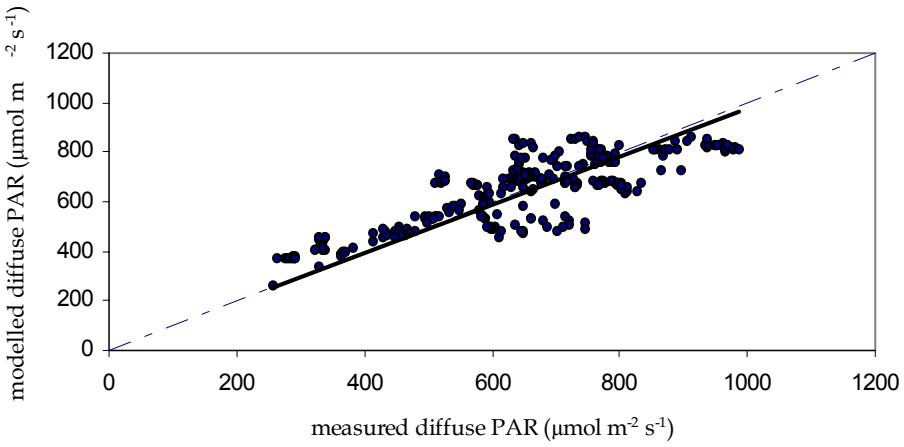

Fig. C-2: Scatter diagram of measured and modelled diffuse PAR
The dashed line refers to 1:1 relationship whereas the solid line shows the linear regression relationship (y = 0.977x)

The scatter diagram of measured and modelled diffuse PAR (Fig. C-2) shows that the diffuse radiation can be estimated with reasonable accuracy (Pearson´s correlation coefficient: 0.747, RMSE: 95.7 µmol m^{-2} s^{-1}).

As Fig. C-3 indicates, an apparently strong relationship exists between model performance and total incident PAR. Measured diffuse PAR from total incident radiation data lower than approx. 1 350 µmol m^{-2} s^{-1} is generally underestimated by the model, whereas higher values result in an overestimation. Further analysis would be needed to interpret this correlation. However, for the given purpose the results are satisfying and are derived with an acceptable complexity.

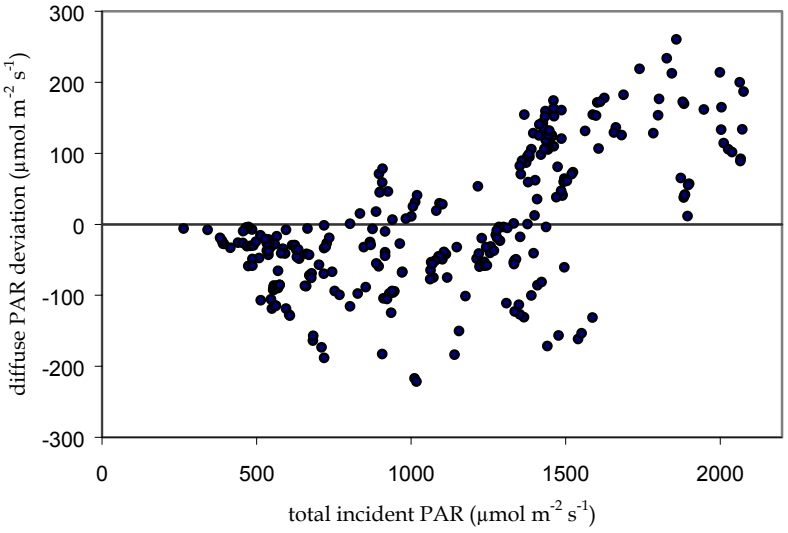

Fig. C-3: Diffuse PAR deviation in relation to total PAR

Appendix D

Values of crop-specific parameters

for sugar beet, spring barley, maize, winter wheat and potato

The references of the mentioned models are:

CERES:	JONES & KINIRY, eds, (1986), RITCHIE & GODWIN (2000)
CERES-BEET:	LEVIEL (2000), LEVIEL *et al.* (2003)
GECROS:	YIN & VAN LAAR (2005)
PROMET-V:	SCHNEIDER (1999)

Sugar beet

Symbol			Value	Unit	Source
			biomass composition		
$f_{C,ini}$			0.5	-	GECROS
$f_{c,V}$			0.48	g C g^{-1}	GECROS
f_{lig}			0.05	g lignin g^{-1}	GECROS
f_{lip}			0	g fat g^{-1}	GECROS
$f_{N,ini}$			0.62	-	GECROS
f_{oac}			0.04	g organic acid g^{-1}	GECROS
$Y_{G,V}$			0.81	g C g^{-1} C	GECROS
ε_g			0.25	g g^{-1}	GECROS
			leaf photosynthesis		
E_{Jmax}			39600	J mol^{-1}	derived from measurements
n_b			0.25	g N m^{-2} leaf	GECROS
θ			0.67	-	derived from measurements
χ_{jn}			100.61	µmol electron g^{-1} N s^{-1}	twice the value of χ_{vcn}
χ_{vcn}			50.31	µmol CO_2 g^{-1} N s^{-1}	derived from measurements
			root growth and nitrogen uptake		
F_{Nmin}			0.03	-	CERES-BEET
F_{SNmin}			0.01	-	CERES-BEET
$F_{\Delta D,em}$			0.15	-	CERES-BEET
N_{maxup}	(+)	~	0.8	g N m^{-2} d^{-1}	estimated
R_{LM}			0.8	cm root length g^{-1} root	CERES-BEET
U_{NRmax}			0.008	kg N ha^{-1} cm^{-1} root	CERES-BEET
X_{NH4}			-0.025	-	CERES-BEET
X_{NO3}			-0.0275	-	CERES-BEET
			morphology		
D_{max}	(+)		120	cm	GECROS
f_{Npre}		~	0.7	-	estimated
H_{max}	+		0.5	m	estimated
$I_{m,seed}$		~	0.4	-	estimated
$I_{m,stem}$		~	0.9	-	estimated
s_{la}			0.02	m^2 leaf g^{-1} leaf	GECROS
w			0.08	m	GECROS
β_L	+		52.5 (45-60)	degrees	GUERIF & DUKE (2000)
ρ			150	g m^{-2} m^{-1}	GECROS
			phenology		
c_t	+	~	1	-	GECROS
$E_{m,a}$			sowing date	Julian day	CERES-BEET
$E_{m,b}$			5.9	-	CERES-BEET
p_{sen}	+		0	h^{-1}	*(no photosensitivity)*
$R_{max,r}$	+		0.012	d^{-1}	estimated
$R_{max,v}$	+		0.033	d^{-1}	estimated
T_b			0	°C	GECROS
$T_{b,em}$			3	°C	CERES-BEET
T_c			37	°C	GECROS
t_e	(+)	~	1.5	-	estimated
T_o			25	°C	GECROS
φ_1	+	~	-	-	*(no photosensitivity)*
φ_2	+	~	-	-	*(no photosensitivity)*
			biomass nitrogen content		
$f_{N,S,ini}$			0.75	-	GECROS
$f_{N,S,fin}$			1	-	GECROS
n_{cri0}			0.05	g N g^{-1}	GECROS
n_{Rmin}			0.005	g N g^{-1}	GECROS
n_{Smin}			0.01	g N g^{-1}	GECROS
φ_{tr}			1.5	-	GECROS
			seed characteristics		
n_{SO}	+		0.00175 (0.0015-0.002)	g N g^{-1}	KTBL, ed., (2005)
S_w	+		0.0285 (0.027-0.03)	g $seed^{-1}$	KTBL, ed., (2005)
			management		
D_s			3 (2-4)	cm	KTBL, ed., (2005)
d_p			13.5 (9-18)	plants m^{-2}	KTBL, ed., (2005)

Spring barley

Symbol			Value	Unit	Source
			biomass composition		
$f_{C,ini}$			0.50	-	GECROS
$f_{c,V}$			0.48	g C g^{-1}	GECROS
f_{lig}			0.04	g lignin g^{-1}	GECROS
f_{lip}			0.01	g fat g^{-1}	GECROS
$f_{N,ini}$			0.62	-	GECROS
f_{oac}			0.02	g organic acid g^{-1}	GECROS
$Y_{G,V}$			0.81	g C g^{-1} C	GECROS
ε_g			0.25	g g^{-1}	GECROS
			leaf photosynthesis		
E_{Jmax}			30200	J mol^{-1}	GECROS
n_b			0.30	g N m^{-2} leaf	GECROS
θ			0.70	-	GECROS
χ_{jn}			120	µmol electron g^{-1} N s^{-1}	GECROS
χ_{vcn}			60	µmol CO_2 g^{-1} N s^{-1}	GECROS
			root growth and nitrogen uptake		
F_{Nmin}			0.03	-	CERES
F_{SNmin}			0.01	-	CERES
$F_{\Delta D,em}$			0.10	-	CERES
N_{maxup}	(+)	~	0.40	g N m^{-2} d^{-1}	estimated
R_{LM}			1.05	cm root length g^{-1} root	CERES
U_{NRmax}			0.006	kg N ha^{-1} cm^{-1} root	CERES
X_{NH4}			-0.025	-	CERES
X_{NO3}			-0.0275	-	CERES
			morphology		
D_{max}	(+)		130	cm	GECROS
f_{Npre}		~	0.8	-	estimated
H_{max}	+		0.7	m	estimated
$I_{m,seed}$		~	0.4	-	estimated
$I_{m,stem}$		~	0.8	-	estimated
s_{la}			0.031	m^2 leaf g^{-1} leaf	GECROS
w			0.01	m	GECROS
β_L	+		50	degrees	estimated
ρ			450	g m^{-2} m^{-1}	GECROS
			phenology		
c_t	+	~	1	-	GECROS
$E_{m,a}$			50	-	CERES
$E_{m,b}$			10.4	-	CERES
p_{sen}	+		-0.082	h^{-1}	derived from PROMET-V
$R_{max,r}$	+		0.0331	d^{-1}	derived from PROMET-V
$R_{max,v}$	+		0.0431	d^{-1}	derived from PROMET-V
T_b			0	°C	GECROS
$T_{b,em}$			2	°C	CERES
T_c			37	°C	GECROS
t_e	(+)	~	1.2	-	estimated
T_o			25	°C	GECROS
φ_1	+	~	0.4285	-	YIN *et al.* (2005)
φ_2	+	~	0.8	-	derived from PROMET-V
			biomass nitrogen content		
$f_{N,S,ini}$			0.75	-	GECROS
$f_{N,S,fin}$			1	-	GECROS
n_{cri0}			0.05	g N g^{-1}	GECROS
n_{Rmin}			0.005	g N g^{-1}	GECROS
n_{Smin}			0.01	g N g^{-1}	GECROS
φ_{tr}			1.5	-	GECROS
			seed characteristics		
n_{SO}	+		0.017 (0.013-0.021)	g N g^{-1}	KTBL, ed., (2005)
S_w	+		0.045 (0.04-0.05)	g $seed^{-1}$	KTBL, ed., (2005)
			management		
D_s			3 (2-4)	cm	KTBL, ed., (2005)
d_p			310 (220-400)	plants m^{-2}	KTBL, ed., (2005)

Maize

Symbol			Value	Unit	Source
			biomass composition		
$f_{C,ini}$			0.50	-	GECROS
$f_{c,V}$			0.48	g C g^{-1}	GECROS
f_{lig}			0.11	g lignin g^{-1}	GECROS
f_{lip}			0.05	g fat g^{-1}	GECROS
$f_{N,ini}$			0.62	-	GECROS
f_{oac}			0.04	g organic acid g^{-1}	GECROS
$Y_{G,V}$			0.81	g C g^{-1} C	GECROS
ε_g			0.25	g g^{-1}	GECROS
			leaf photosynthesis		
E_{Jmax}			70890	J mol^{-1}	GECROS
n_b			0.25	g N m^{-2} leaf	GECROS
θ			0.70	-	GECROS
χ_{jn}			124	µmol electron g^{-1} N s^{-1}	twice the value of χ_{vcn}
χ_{vcn}			62	µmol CO_2 g^{-1} N s^{-1}	derived from measurements
			root growth and nitrogen uptake		
F_{Nmin}			0.04	-	CERES
F_{SNmin}			0.10	-	CERES
$F_{\Delta D,em}$			0.15	-	CERES
N_{maxup}	(+)	~	0.50	g N m^{-2} d^{-1}	estimated
R_{LM}			0.80	cm root length g^{-1} root	CERES
U_{NRmax}			0.006	kg N ha^{-1} cm^{-1} root	CERES
X_{NH4}			-0.03	-	CERES
X_{NO3}			-0.03	-	CERES
			morphology		
D_{max}	(+)		145	cm	GECROS
f_{Npre}		~	0.7	-	estimated
H_{max}	+		2.0	m	estimated
$I_{m,seed}$		~	0.4	-	estimated
$I_{m,stem}$		~	0.9	-	estimated
s_{la}			0.022	m^2 leaf g^{-1} leaf	GECROS
w			0.05	m	GECROS
β_L	+		50	degrees	estimated
ρ			570	g m^{-2} m^{-1}	GECROS
			phenology		
c_t	+	~	1	-	GECROS
$E_{m,a}$			15	-	CERES
$E_{m,b}$			6	-	CERES
p_{sen}	+		0	h^{-1}	*no photoperiod sensitivity*
$R_{max,r}$	+		0.0450	d^{-1}	derived from PROMET-V
$R_{max,v}$	+		0.0365	d^{-1}	derived from PROMET-V
T_b			8	°C	GECROS
$T_{b,em}$			10	°C	CERES
T_c			42	°C	GECROS
t_e	(+)	~	1	-	*determinate plant*
T_o			30	°C	GECROS
φ_1	+	~	-	-	*no photoperiod sensitivity*
φ_2	+	~	-	-	*no photoperiod sensitivity*
			biomass nitrogen content		
$f_{N,S,ini}$			0.75	-	GECROS
$f_{N,S,fin}$			1	-	GECROS
n_{cri0}			0.05	g N g^{-1}	GECROS
n_{Rmin}			0.005	g N g^{-1}	GECROS
n_{Smin}			0.008	g N g^{-1}	GECROS
φ_{tr}			1.5	-	GECROS
			seed characteristics		
n_{SO}	+		0.014 (0.012-0.016)	g N g^{-1}	KTBL, ed., (2005)
S_w	+		0.325 (0.2-0.4)	g $seed^{-1}$	KTBL, ed., (2005)
			management		
D_s			6 (4-8)	cm	KTBL, ed., (2005)
d_p			9 (8-10)	plants m^{-2}	KTBL, ed., (2005)

Winter wheat

Symbol			Value			Unit	Source
			biomass composition				
$f_{C,ini}$			0.50			-	GECROS
$f_{c,V}$			0.48			g C g^{-1}	GECROS
f_{lig}			0.06			g lignin g^{-1}	GECROS
f_{lip}			0.02			g fat g^{-1}	GECROS
$f_{N,ini}$			0.62			-	GECROS
f_{oac}			0.02			g organic acid g^{-1}	GECROS
$Y_{G,V}$			0.81			g C g^{-1} C	GECROS
ε_g			0.25			g g^{-1}	GECROS
			leaf photosynthesis				
E_{Jmax}			48270			J mol^{-1}	GECROS
n_b			0.35			g N m^{-2} leaf	GECROS
θ			0.70			-	GECROS
χ_{jn}			120			µmol electron g^{-1} N s^{-1}	GECROS
χ_{vcn}			60			µmol CO_2 g^{-1} N s^{-1}	GECROS
			root growth and nitrogen uptake				
F_{Nmin}			0.03			-	CERES
F_{SNmin}			0.01			-	CERES
$F_{\Delta D,em}$			0.10			-	CERES
N_{maxup}	(+)	~	0.50			g N m^{-2} d^{-1}	estimated
R_{LM}			1.05			cm root length g^{-1} root	CERES
U_{NRmax}			0.009			kg N ha^{-1} cm^{-1} root	CERES
X_{NH4}			-0.025			-	CERES
X_{NO3}			-0.0275			-	CERES
			morphology				
D_{max}	(+)		130			cm	GECROS
f_{Npre}		~	0.8			-	estimated
H_{max}	+		0.8			m	estimated
$I_{m,seed}$		~	0.4			-	estimated
$I_{m,stem}$		~	0.9			-	estimated
s_{la}			0.028			m^2 leaf g^{-1} leaf	GECROS
w			0.01			m	GECROS
β_L	+		50			degrees	estimated
ρ			460			g m^{-2} m^{-1}	GECROS
			phenology				
c_t	+	~	1			-	GECROS
$E_{m,a}$			40			-	CERES
$E_{m,b}$			10.2			-	CERES
p_{sen}	+		-0.088			h^{-1}	derived from PROMET-V
$R_{max,r}$	+		0.02857			d^{-1}	derived from PROMET-V
$R_{max,v}$	+		0.03731			d^{-1}	derived from PROMET-V
T_b			0 (1)	4 (2)	8 (3)	°C	PORTER & GAWITH (1999)
$T_{b,em}$			2			°C	CERES
T_c			30 (1)	35 (2)	35 (3)	°C	PORTER & GAWITH (1999)
t_e	(+)	~	1			-	*determinate plant*
T_o			19 (1)	24 (2)	24 (3)	°C	PORTER & GAWITH (1999)
φ_1	+	~	0.2			-	estimated
φ_2	+	~	0.783			-	derived from PROMET-V
T_b, T_o, T_c			for vernalization effect: -1.3, 4.9, 15.7			°C	PORTER & GAWITH (1999)
			biomass nitrogen content				
$f_{N,S,ini}$			0.75			-	GECROS
$f_{N,S,fin}$			1			-	GECROS
n_{cri0}			0.05			g N g^{-1}	GECROS
n_{Rmin}			0.005			g N g^{-1}	GECROS
n_{Smin}			0.01			g N g^{-1}	GECROS
φ_{tr}			1.5			-	GECROS
			seed characteristics				
n_{SO}	+		0.02 (0.015-0.025)			g N g^{-1}	KTBL, ed., (2005)
S_w	+		0.0475 (0.04-0.055)			g $seed^{-1}$	KTBL, ed., (2005)
			management				
D_s			2.5 (2-3)			cm	KTBL, ed., (2005)
d_p			300 (200-400)			plants m^{-2}	KTBL, ed., (2005)

(1) for the phase between emergence and terminal spikelet initiation

(2) for the phase between terminal spikelet initiation and start of seed fill

(3) for the phase between start of seed fill and physiological maturity

Potato

Symbol			Value	Unit	Source
			biomass composition		
$f_{C,ini}$			0.50	-	GECROS
$f_{c,V}$			0.48	g C g^{-1}	GECROS
f_{lig}			0.03	g lignin g^{-1}	GECROS
f_{lip}			0	g fat g^{-1}	GECROS
$f_{N,ini}$			0.62	-	GECROS
f_{oac}			0.04	g organic acid g^{-1}	GECROS
$Y_{G,V}$			0.81	g C g^{-1} C	GECROS
ε_g			0.25	g g^{-1}	GECROS
			leaf photosynthesis		
E_{Jmax}			84180	J mol^{-1}	derived from measurements
n_b			0.35	g N m^{-2} leaf	GECROS
θ			0.72	-	derived from measurements
χ_{jn}			117.72	µmol electron g^{-1} N s^{-1}	twice the value of χ_{vcn}
χ_{vcn}			58.86	µmol CO_2 g^{-1} N s^{-1}	derived from measurements
			root growth and nitrogen uptake		
F_{Nmin}			0.03	-	HODGES (1997)
F_{SNmin}			0.01	-	value adopted from sugar beet
$F_{\Delta D,em}$			0.15	-	value adopted from sugar beet
N_{maxup}	(+)	~	0.80	g N m^{-2} d^{-1}	estimated
R_{LM}			0.80	cm root length g^{-1} root	RENWICK (1999)
U_{NRmax}			0.008	kg N ha^{-1} cm^{-1} root	value adopted from sugar beet
X_{NH4}			-0.025	-	HODGES (1997)
X_{NO3}			-0.0275	-	HODGES (1997)
			morphology		
D_{max}	(+)		100	cm	GECROS
f_{Npre}		~	0.7	-	estimated
H_{max}	+		0.4	m	estimated
$I_{m,seed}$		~	0.6	-	estimated
$I_{m,stem}$		~	0.6	-	estimated
s_{la}			0.033	m^2 leaf g^{-1} leaf	GECROS
w			0.025	m	GECROS
β_L	+		60	degrees	estimated
ρ			170	g m^{-2} m^{-1}	GECROS
			phenology		
c_t	+	~	1	-	GECROS
$E_{m,a}$			60	-	estimated
$E_{m,b}$			5.9	-	value adopted from sugar beet
p_{sen}	+		0	h^{-1}	*(no photosensitivity)*
$R_{max,r}$	+		0.021	d^{-1}	estimated
$R_{max,v}$	+		0.0357	d^{-1}	estimated
T_b			0	°C	GECROS
$T_{b,em}$			3	°C	value adopted from sugar beet
T_c			37	°C	GECROS
t_e	(+)	~	1.35	-	estimated
T_o			25	°C	GECROS
φ_1	+	~	-	-	*(no photosensitivity)*
φ_2	+	~	-	-	*(no photosensitivity)*
			biomass nitrogen content		
$f_{N,S,ini}$			0.75	-	GECROS
$f_{N,S,fin}$			1	-	GECROS
n_{cri0}			0.05	g N g^{-1}	GECROS
n_{Rmin}			0.005	g N g^{-1}	GECROS
n_{Smin}			0.01	g N g^{-1}	GECROS
φ_{tr}			1.5	-	GECROS
			seed characteristics		
n_{SO}	+		0.0035 (0.003-0.004)	g N g^{-1}	KTBL, ed., (2005)
S_w	+		10	g $seed^{-1}$	estimated
			management		
D_s			6 (4-8)	cm	KTBL, ed., (2005)
d_p			4.5 (3.5-5.5)	plants m^{-2}	KTBL, ed., (2005)

Appendix E

Assignment of phenological stage to development stage and BBCH stage

(based on HOOGENBOOM *et al.* (2003), MEIER (ed., 2001), STRECK *et al.* (2003b), WANG & ENGEL (1998))

Wheat and barley

Start of stage	development stage	BBCH stage
sowing	-	00
germination	-	05
emergence	0.00	09
floral initiation	0.20	14-22
terminal spikelet initiation	0.40	-
terminal spikelet (wheat) maximum primordia (barley)	0.45	30
flag leaf	0.65	41
heading	0.90	51
anthesis	1.00	61
milk development	1.15	71
dough development	1.50	81
ripening	1.95	90
maturity	2.00	92

Maize

Start of stage	development stage	BBCH stage
sowing	-	00
germination	-	05
emergence	0.00	09
anthesis	1.00	61
milk development	1.15	73
dough development	1.50	83
ripening	1.95	87
maturity	2.00	89

Sugar beet

Start of stage	development stage	BBCH stage
sowing	-	00
germination	-	01-07
emergence	0.00	09
start of beet root development	1.00	40
maturity	2.00	49

Potato

Start of stage	development stage	BBCH stage
planting	-	00
sprouting/germination	-	01-07
emergence	0.00	09
start of tuber formation	1.00	40
maturity	2.00	49

Appendix F

Equations of model performance statistics

The formulas of the model performance statistics are listed according to WALLACH (2006).

The root mean squared error (RMSE) is given by:

$$\mathrm{RMSE} = \sqrt{\frac{1}{n}\sum_{i=1}^{n}\left(Y_i - X_i\right)^2} \tag{F–1}$$

where n stands for the number of samples and Y_i and X_i are the i^{th} measured and modelled values, respectively. The relative root mean squared error is given by:

$$\mathrm{RRMSE} = \frac{\mathrm{RMSE}}{\overline{Y}} \tag{F–2}$$

where $\overline{Y}$ is the mean of the measured values. The mean absolute error (MAE) is calculated as:

$$\mathrm{MAE} = \frac{1}{n}\sum_{i=1}^{n}\left|Y_i - X_i\right| \tag{F–3}$$

The index of agreement (IA) expresses the average relative error and is calculated as:

$$\mathrm{IA} = 1 - \frac{\sum_{i=1}^{n}\left(Y_i - X_i\right)^2}{\sum_{i=1}^{n}\left(\left|X_i - \overline{Y}\right| + \left|Y_i - \overline{Y}\right|\right)^2} \tag{F–4}$$

The numerator is the mean squared error and the denominator represents the variability of the measured and modelled data. In a perfect fit, IA would result in the value of 1.

The modelling efficiency statistic (MEF) is calculated as:

$$\mathrm{MEF} = 1 - \frac{\sum_{i=1}^{n}\left(Y_i - X_i\right)^2}{\sum_{i=1}^{n}\left(Y_i - \overline{Y}\right)^2} \tag{F–5}$$

Were the model perfect, MEF would likewise be 1.

Appendix G

Field measurement data

Biomass weight is given in dry matter (DM).

Sugar beet
Feienberg 2004

	green LAI	living leaf			dead leaf			taproot			phenology
date	(m^2 m^{-2})	(g DM m^{-2})	C (%)	N (%)	(g DM m^{-2})	C (%)	N (%)	(g DM m^{-2})	C (%)	N (%)	BBCH-stage
19.05.04	0.02	1	37.2	4.4	0	0	0	0	0.0	0.0	15
26.05.04	0.06	4	36.2	4.8	0	0	0	0	0.0	0.0	16
09.06.04	0.46	34	36.4	4.6	0	0	0	0	0.0	0.0	19
23.06.04	1.69	195	35.2	3.9	0	0	0	54	38.9	1.6	33
07.07.04	2.59	379	39.1	2.9	6	16.2	1.2	178	34.8	1.3	36
21.07.04	2.97	360	40.1	2.4	11	29.2	1.7	257	45.2	0.8	39
03.08.04	2.45	316	42.7	2.3	5	26.5	1.2	266	49.0	0.8	39
17.08.04	5.57	809	39.7	1.8	26	23.2	1.1	911	40.8	0.6	39
07.09.04	5.90	1077	40.7	1.9	45	32.6	1.6	1501	41.3	0.6	49

Sugar beet
Feienberg 2005

	green LAI	living leaf			dead leaf			taproot			phenology
date	(m^2 m^{-2})	(g DM m^{-2})	C (%)	N (%)	(g DM m^{-2})	C (%)	N (%)	(g DM m^{-2})	C (%)	N (%)	BBCH-stage
17.05.05	-	1	27.6	3.7	0	0	0	0	0	0	11-12
08.06.05	0.28	27	32.8	4.1	0	0	0	0	0	0	19
22.06.05	1.10	100	40.6	4.1	0	0	0	38	-	-	19
08.07.05	2.93	241	42.1	3.2	4	24.62	1.46	127	43.54	1.07	19
20.07.05	3.22	330	42.6	2.6	18	31.88	1.73	248	39.63	1.35	34
10.08.05	5.60	725	41.4	2.6	18	28.23	1.67	851	44.83	0.83	39
31.08.05	5.78	994	42.9	2.7	23	30.00	1.69	1211	46.21	0.73	39
14.09.05	5.72	983	44.6	2.6	46	32.56	1.55	1436	45.06	0.62	49

Appendix G

Potato

Hofferhof 2004

	green LAI	living leaf			dead leaf			stem			tuber			phenology
date	(m^2 m^{-2})	(g DM m^{-2})	C (%)	N (%)	(g DM m^{-2})	C (%)	N (%)	(g DM m^{-2})	C (%)	N (%)	(g DM m^{-2})	C (%)	N (%)	BBCH-stage
09.06.04	0.93	52	38.7	6.5	0	0.0	0.0	10	30.8	5.1	0	0.0	0.0	107
23.06.04	2.34	145	37.4	4.5	1	-	-	51	31.4	2.6	67	41.6	2.0	509
07.07.04	2.58	158	38.5	3.6	9	26.4	1.9	72	38.4	1.9	150	40.0	1.5	700
21.07.04	3.35	172	34.4	2.7	19	26.7	1.4	93	36.3	0.8	488	41.7	1.0	709
03.08.04	0.28	18	33.2	2.6	54	37.5	2.4	116	38.4	1.0	712	42.3	1.3	709

Potato

Hofferhof 2005

	green LAI	living leaf			dead leaf			stem			tuber			phenology
date	(m^2 m^{-2})	(g DM m^{-2})	C (%)	N (%)	(g DM m^{-2})	C (%)	N (%)	(g DM m^{-2})	C (%)	N (%)	(g DM m^{-2})	C (%)	N (%)	BBCH-stage
08.06.05	0.09	6	37.8	5.8	0	0	0	2	28.8	5.8	0	0.0	0.0	104
22.06.05	0.59	30	42.4	4.9	0	0	0	17	34.3	4.0	4	41.0	2.3	204
08.07.05	2.14	104	39.5	4.7	4	23.2	1.8	46	34.3	3.5	35	39.2	2.2	602
20.07.05	2.59	132	41.2	3.8	7	31.9	1.6	73	38.7	1.4	129	41.8	1.6	608
10.08.05	2.98	171	39.5	2.8	26	27.1	1.4	103	40.2	0.8	645	39.7	1.3	709

Maize
Feienberg 2004

	green LAI	living leaf			brown leaf			stem			ear			phenology
date	(m^2 m^{-2})	(g DM m^{-2})	C (%)	N (%)	(g DM m^{-2})	C (%)	N (%)	(g DM m^{-2})	C (%)	N (%)	(g DM m^{-2})	C (%)	N (%)	BBCH-stage
26.05.04	-	-	-	-	-	-	-	-	-	-	-	-	-	13
21.07.04	3.21	140	-	-	0	-	-	426	-	-	0	-	-	53
17.08.04	4.91	287	-	-	0	-	-	774	-	-	646	-	-	71
07.09.04	4.57	378	-	-	3	-	-	854	-	-	938	-	-	88

Maize
Feienberg 2005

	green LAI	living leaf			brown leaf			stem			ear			phenology
date	(m^2 m^{-2})	(g DM m^{-2})	C (%)	N (%)	(g DM m^{-2})	C (%)	N (%)	(g DM m^{-2})	C (%)	N (%)	(g DM m^{-2})	C (%)	N (%)	BBCH-stage
28.06.05	0.92	32	44.6	2.4	0	0.00	0.00	35	43.7	1.9	0	0.0	0.0	18
07.08.05	-	-	-	-	-	-	-	-	-	-	-	-	-	32
10.08.05	1.20	76	41.7	2.5	0	0.00	0.00	228	43.7	0.8	319	46.5	2.4	75
05.10.05	1.32	135	-	-	16	-	-	533	-	-	879	-	-	89

Winter wheat
Feienberg 2004

	green LAI	brown LAI	living leaf			dead leaf			stem			ear			phenology
date	(m^2 m^{-2})	(m^2 m^{-2})	(g DM m^{-2})	C (%)	N (%)	(g DM m^{-2})	C (%)	N (%)	(g DM m^{-2})	C (%)	N (%)	(g DM m^{-2})	C (%)	N (%)	BBCH-stage
25.03.04	0.08	0.00	35	33.5	4.4	0	0	0	0	0.0	0.0	0	0	0	21
08.04.04	1.08	0.00	71	39.2	4.9	0	0	0	0	0.0	0.0	0	0	0	23
22.04.04	2.56	0.00	172	44.2	4.1	0	0	0	56	41.6	2.9	0	0	0	31
05.05.04	4.70	0.15	200	43.1	4.3	0	0	0	182	40.3	3.1	0	0	0	33
19.05.04	6.15	0.54	260	42.6	3.5	24	37.5	1.5	405	40.7	1.0	0	0	0	34
26.05.04	5.57	0.84	205	43.0	3.4	38	38.5	1.4	479	41.9	0.6	0	0	0	43
09.06.04	6.15	1.26	259	43.5	3.4	84	38.9	1.2	828	43.0	1.0	214	44.8	1.7	61
23.06.04	4.57	1.39	230	44.1	3.5	88	39.3	1.4	1156	44.5	0.8	472	44.6	1.8	71
07.07.04	3.40	1.58	146	42.9	3.0	97	39.2	1.1	837	43.3	1.5	906	43.7	1.6	75
21.07.04	0.56	1.73	42	41.3	1.7	141	41.4	1.2	535	45.4	0.6	958	44.4	1.5	83
03.08.04	0.00	1.74	0	0.0	0.0	177	40.5	1.0	613	43.9	0.4	1146	44.2	1.7	89

Erklärung

Ich versichere, dass ich die von mir vorgelegte Dissertation selbständig angefertigt, die benutzten Quellen und Hilfsmittel vollständig angegeben und die Stellen der Arbeit – einschließlich Tabellen, Karten und Abbildungen –, die anderen Werken im Wortlaut oder dem Sinn nach entnommen sind, in jedem Einzelfall als Entlehnung kenntlich gemacht habe; dass diese Dissertation noch keiner anderen Fakultät oder Universität zur Prüfung vorgelegen hat; dass sie noch nicht veröffentlicht worden ist sowie, dass ich eine solche Veröffentlichung vor Abschluss des Promotionsverfahrens nicht vornehmen werde. Die Bestimmungen der Promotionsordnung sind mir bekannt. Die von mir vorgelegte Dissertation ist von Prof. Dr. Karl Schneider betreut worden.

Köln, 29. April 2007 Victoria Lenz